Investigations on Shear Including the Development of a Material Model for the FE Analysis of Cracked RC Structures

A thesis submitted for the degree of Doctor of Philosophy in the Faculty of Engineering of the University of Sheffield

by

Martin Haas, Dipl.-Ing. (TU Munich)

Department of Civil and Structural Engineering
University of Sheffield

May 1996

Abstract

This dissertation reports investigations on shear in cracked reinforced concrete (RC) elements including the development and implementation of a material subroutine for the commercial finite element (FE) program ABAQUS. The material subroutine UMAT is intended to substantially improve the shear behaviour of the standard concrete options of ABAQUS.

At first the important shear theories are reviewed in detail and their advantages and drawbacks are summarised. The modified compression field theory (MCFT) is identified as a suitable shear theory worth being coded for its application in FE analysis.

A comprehensive check on the MCFT confirms its suitability in a slightly modified form for the investigation of a variety of cracked structural RC elements. This check is conducted on a section analysis level by means of a developed program called LAYER which is coded according to the MCFT.

The main part of the work is the implementation and testing of the material subroutine UMAT which is added to the source code of ABAQUS via an interface provided by the commercial FE program.

Finally, the UMAT is utilised for examining the ductility of RC walls. It is concluded that shear deflections can influence the displacement and curvature ductility of squat structures in a substantial way, even though a flexural type of failure might prevail.

Acknowledgements

This dissertation was prepared in the Department of Civil and Structural Engineering of the University of Sheffield. From the many persons who contributed to the work the author is first of all indebted to Dr. Kypros Pilakoutas who served as an inspiring supervisor.

Gratitude is also owed to Prof. Peter Waldron, the Head of Department, for his support as a second supervisor.

My very private gratitude, however, belongs to my wife Dagmar and my daughter Sophie who suffered from the years of absence of their 'Papa'.

Table of Contents

List of Tables

Page

List of Figures

Page

Notation

A_s	Area of reinforcing bars
A_l	Area of longitudinal reinforcement
A_t	Area of transverse reinforcement
C	Force in compression zone
N	Normal force in cross section
M	Section Moment
P	Load
P_u	Ultimate load
T	Tension force in longitudinal reinforcement or tension chord
V	Shear force in cross section
E_M	Stress energy due to bending
E_V	Stress energy due to shear
E_T	Total stress energy
E_s	Young's modulus for steel
E_c	Young's modulus for concrete
a	Shear span
b	Beam width
b_w	Width of web
d	Effective beam height
h	Beam height
l	Span of beam
s	Stirrup spacing
z	Lever arm
σ_1 , σ_2	Principal stress state
σ_{c1} , σ_{c2}	Principal stress state in concrete
σ_x , σ_y , τ_{xy}	Stress state in xy direction
σ_ξ , σ_η , $\tau_{\xi\eta}$	Stress state in $\xi\eta$ direction
σ_d , σ_r , τ_{dr}	Stress state in dr direction (crack direction in Kupfer's theory)
σ_{cx} , σ_{cy} , τ_{xy}	Stress state in concrete in xy direction
σ_1	Principal tensile stress
σ_2	Principal compressive stress

σ_{c1}	Principal tensile stress of concrete
σ_{c2}	Principal compressive stress of concrete
$\sigma_{c2\ max}$	Maximum compressive stress due to lateral strain
σ_{ci} , τ_{ci}	Crack stresses (MCFT)
σ_{sx}	Steel stress in x direction
σ_{sy}	Steel stress in y direction
f_c	Cylinder strength of concrete
f_{ct}	Tensile strength of concrete
f_{yl}	Yielding stress of longitudinal reinforcement
f_{yt}	Yielding stress of transverse reinforcement
ε_1 , ε_2	Principal strain state
ε_x , ε_y , γ_{xy}	Strain state in xy direction
ε_1	Principal tensile strain
ε_2	Principal compressive strain
ε_{cr}	Cracking strain of concrete in tension
ε_c'	Concrete compressive strain at peak stress
θ	Angle of principal compressive strain of concrete
θ'	Crack angle of concrete
θ_c	Angle of principal compressive stress of concrete
δ_M	Deflection due to bending
δ_V	Deflection due to shear
δ_T	Total deflection
δ_{pl}	Plastic deflection
ν	Poisson's ratio
μ	Reduction factor due to tension stiffening
β	Shear retention factor
μ_Δ	Displacement ductility
μ_Φ	Curvature ductility
Φ	Curvature

1 Introduction

The earthquake resistant design of reinforced concrete structures is mainly based on principles which are known as the capacity design method (Paulay/Priestley, 1992), incorporated in nearly all modern codes of practice. In 1993 the second draft of the Eurocode 8 was released and its introduction as a standard for seismic design in Europe is considered to be not far off. With this development, the capacity design philosophy has emerged in European design practice and it is worthwhile considering its implications. The philosophy is founded on the fact that severe seismic action is by nature a rare event and we, therefore, accept higher risks of damage than under other comparable loads. This enables the method to take advantage of the knowledge that a structure can sustain large deflections far into the post elastic range, provided it is detailed in a sufficiently ductile manner. Consequently, seismic design loads may be substantially reduced if the corresponding ductility demand is accounted for. Therefore, a crucial point in capacity design is the evaluation of deflections which is necessary for the determination of the ductility μ_Δ, the ratio of displacement at the ultimate limit to displacement at the onset of yielding.

Until recently, the calculation of deformations was considered to be necessary only at the serviceability level and, hence, little research was carried out up to now for the exact determination of deformations at the ultimate limit. This means that the displacement ductility μ_Δ cannot be calculated in a reliable fashion using the traditional design rules derived in many RC text books and lecture notes. Roughly speaking, these traditional procedures are based on section analysis and till recently they have been virtually the only possible method of designing reinforced concrete structures. However, an intrinsic disadvantage of section analysis is that its focus is confined to local areas making it incapable of describing the overall behaviour of a structure. Since the development of the finite element method (FEM) a powerful tool has become available for the calculation of global values which are not easily attainable by section analysis procedures. Therefore, it is obvious that predicting quantities like the displacement ductility of a complex reinforced concrete structure is only possible by means of a finite element calculation.

However, the method is far from being perfect and much work has to be conducted till the non-linear material behaviour of cracked reinforced concrete, subjected to high shear stresses, can be modelled in a reasonably accurate manner. Unfortunately, the advantage of section analysis, which is the proper treatment of local effects, is a main disadvantage of the FEM and that shortcoming becomes significant when trying to implement phenomena like aggregate interlock, dowel action or the size effect, which are all features connected with the shear transfer in a cracked reinforced concrete member.

The main objective of the capacity design method is to avoid shear failure at all costs and, hence, shear is treated in a more conservative way which makes the aforementioned shortcomings less dominant, especially when dealing with highly ductile framed skeleton structures, consisting of slabs, columns and beams. However, particularly in central and northern Europe, stiff shear walls are often used in reinforced concrete buildings to carry the lateral loads generated by seismic action. In this case, deflections due to shear are no longer negligible and a procedure is necessary for the proper evaluation of the influence of shear action on the displacement ductility of a structure.

Usually, in FE programs cracks are treated as smeared over the element and secondary shear carrying actions are accounted for by the introduction of a shear retention factor. No guidelines are available for the realistic evaluation of this factor and, hence, an arbitrary value between zero and one must be chosen to care for shear transfer in a crack. However, aggregate interlock influences the shear response in a significant way and therefore, it is desirable to improve the shear behaviour of existing FE programs by implementing a shear model, in which aggregate interlock is an intrinsic feature of the constitutive equations.

In recent years, various theories on cracked reinforced concrete were developed which treated shear in a more physical fashion. In the early sixties Walther, then a co-worker of Leonhardt, published his shear failure theory (1964). Almost concurrently Kani in Toronto (1964) and Fenwick/Paulay (1968) in New Zealand established the tooth model which was later refined by Reineck (1991), a researcher of Schlaich in Stuttgart. Important work was conducted in Canada by Collins/Mitchell (1980), known as the compression field theory (CFT), which was later extended to the modified compression field theory (MCFT) by Vecchio/Collins (1986). In Munich Kupfer and his researchers (1983) developed a similar theory with a more sophisticated approach to aggregate interlock.

Thürlimann (1989) in Zurich and Nielsen (1984) in Copenhagen developed limit analysis procedures based on the plasticity theory for concrete. All the above mentioned theories are reviewed in Chapter 2 in a state-of-the-art report in some detail, however, for the sake of completeness it should be mentioned that many other researchers have contributed to the better understanding of shear action in the last few decades.

One of the objectives of this work is to clarify the influence of shear deflections on the displacement ductility of reinforced concrete structures. It is therefore intended to improve the shear behaviour of RC elements in the FE program ABAQUS (1994) by adding a user defined material based on the MCFT to the source code of the package. The purpose of the procedure is to fit ABAQUS with a facility which enables the program to calculate the global response of a cracked reinforced concrete structure in a realistic way. This goal will be achieved in two steps, the first of which can be described as a check on the MCFT (Chapter 3) to prove that the theory, which is based on a rather simple but reasonable compatibility condition, provides good results on a local level and is by nature suitable to be implemented in an FE program. The second step (Chapter 4) includes a comprehensive description of the coded user subroutine and its verification by means of comparisons with test data given in the literature. Numerous calculations reported in Chapter 5 are carried out to scrutinise the influence of shear on ductility. Finally, the provisions of the EC8 have been checked and recommendations on their practical application conclude the work.

2 Shear Theories: A State-of-the-Art Report

2.1 The Shear Failure Theory

In 1962 Walther published his shear failure theory. This theory focused mainly on the flexural shear behaviour of a reinforced concrete beam and was based on the following assumptions:

- Shear failure occurs when the concrete has crushed above the tip of a shear crack. Therefore, the stress state in a section perpendicular to the beam axis is investigated.
- In the shear span of a beam, the plane section hypothesis of Bernoulli must be abandoned and replaced by a compatibility relation which accounts for the shear deformation in a cracked cross section.
- The stress in transverse direction σ_y in the compression zone is taken to be zero and in the vicinity of concentrated loads special considerations may apply.

Walther (1964) used a Mohr failure criterion to evaluate the strength of the compression zone. The criterion and the relevant equations are given in Fig.2.1. The failure criterion consists of an ellipse for $\sigma_x / f_c \leq -0.25$ and of a parabola for $\sigma_x / f_c \geq -0.25$, while the failure envelope is modelled as a parabola, taking the ratio of compression and tension strength of the concrete to be *0.125*.

Failure of the concrete occurs when the Mohr's stress circle touches the failure envelope. If the stress distribution in the compression zone is considered to be homogeneous for both the compression and the shear stress, then one particular stress circle is valid for all points in the cross section. However, when the stresses are distributed in a more uneven way, eg as shown in Fig.2.2, then for each point in the compression zone another set of stresses applies and the respective Mohr's circles vary from point to point along the cross section.

$$\text{Failure circles: } \left(\frac{\sigma_\xi}{f_c}-\frac{\sigma_x}{2f_c}\right)^2+\left(\frac{\tau_{\xi\eta}}{f_c}\right)^2=\left(\frac{\sigma_x}{2f_c}\right)^2+\left(\frac{\tau_{xy}}{f_c}\right)^2 \quad (2.1)$$

$$\text{Failure envelope: } \left(\frac{\tau_{\xi\eta}}{f_c}\right)^2+\frac{\sigma_\xi}{2f_c}-\frac{1}{16}=0 \quad (2.2)$$

$$\text{Abscissa point A: } \frac{\sigma_\xi}{f_c}=\frac{\sigma_x}{2f_c}+\frac{1}{4}\pm\sqrt{\left(\frac{\sigma_x}{2f_c}+\frac{1}{4}\right)^2+\left(\frac{\tau_{xy}}{f_c}\right)^2-\frac{1}{16}} \quad (2.3)$$

$$\text{Failure criterion for } \sigma_x/f_c \le -0.25\text{: } \left(\frac{\sigma_x}{f_c}\right)^2+\frac{\sigma_x}{f_c}+\left(\frac{2\tau_{xy}}{f_c}\right)^2=0 \quad (2.4)$$

$$\sigma_x/f_c \ge -0.25\text{: } 1-8\frac{\sigma_x}{f_c}-\left(8\frac{\tau_{xy}}{f_c}\right)^2=0 \quad (2.5)$$

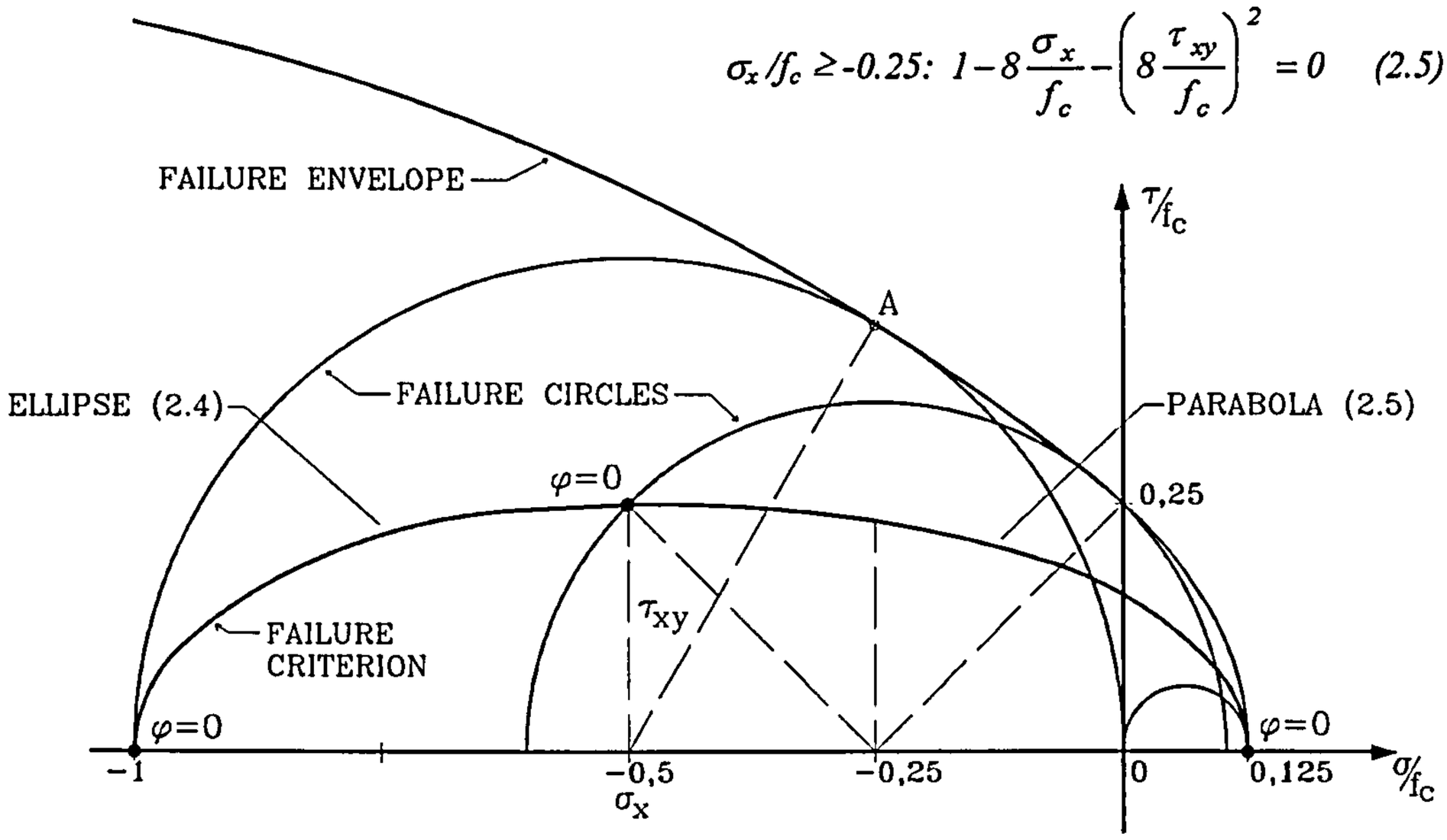

Fig.2.1 Failure Envelope and Failure Criterion for Compression Zone of an RC Beam

Fig.2.1 shows some Mohr's stress circles and as they all touch the failure envelope they can additionally be regarded as failure circles. This means that each point along the perimeter of a circle represents a stress state causing failure in a plane inclined under the angle φ. As Walther investigates the cross section perpendicular to the beam axis, only the stress state with σ_x, $\sigma_y=0$ and τ_{xy} is used for further scrutiny. From Fig.2.1 it can be seen that all points representing a failure stress state in the xy direction are located on a curve which is an ellipse for $\sigma_x/f_c \le -0.25$ and a parabola for $\sigma_x/f_c \ge -0.25$. Eqs.(2.4) and (2.5), describing the above explained failure criterion, can be derived by calculating the contact point A of the failure envelope with the failure circle from Eqs.(2.1) and (2.2). This yields Eq.(2.3) for the abscissa of the contact point A. The mathematical discussion of Eq.(2.3) reveals that for $\sigma_x/f_c \le -0.25$ Eq.(2.4) is obtained by setting the root to zero. For values $\sigma_x/f_c \ge -0.25$ the abscissa of the contact point A is always 0.125. Hence Eq.(2.5) is derived from Eq(2.3) with $\sigma_\xi/f_c=0.125$.

After the failure criterion is established it is possible to check whether a stress state with σ_x, $\sigma_y=0$ and τ_{xy} leads to failure or not. From Fig.2.1 it is clear that at failure $\sigma_x=f_{c\tau}$ is always less than the compression strength of plain concrete provided the shear stress acting simultaneously is other than zero. It is therefore desirable to derive a relationship which shows how the concrete strength in the compression zone depends on the applied shear force. This equation was found by Walther using the expressions given in Fig.2.2 together with the failure criterion represented by Eq.(2.4).

It can be seen from this equation that $f_{c\tau}$ is a function of the shear ratio M/Vd which might be replaced by a/d in the case of a beam subjected to concentrated loads. In Fig.2.3 the shear ratio M/Vd is plotted against the normalised reduced compression strength of the concrete $\psi=f_{c\tau}/f_c$. For this graph Walther used a slightly modified equation to account for the transverse reinforcement in the beam. This was accomplished by adding the parameter η giving the ratio of the yielding force of the transverse reinforcement to the total shear force in the cross section as depicted in Fig.2.2. η becomes 0 for a beam without stirrups and 1 if all shear is carried by shear reinforcement. Additionally, the influence of the vertical stresses $\sigma_y \neq 0$ in the vicinity of a concentrated load is accounted for by shifting the curves towards $\psi=1$ at a shear ratio of about 1.5. This measure can be regarded to be reasonable, because the transverse stresses enhance the compression strength of the concrete.

Although Walther gives only a more qualitative explanation for the length of the region under a concentrated load where σ_y stresses are substantial, it is possible to verify his value of about 2 to $2.5d$ with Schleeh's method (1973). It is obvious from Fig.2.3 that the extension of the St.Venant disturbances is as long as the height of the beam. This means that the correct value becomes $a/d=2$ when both the concentrated load at the support and in the beam span are considered. This can be regarded to be in line with the value given by Walther.

a) Free Body Diagram

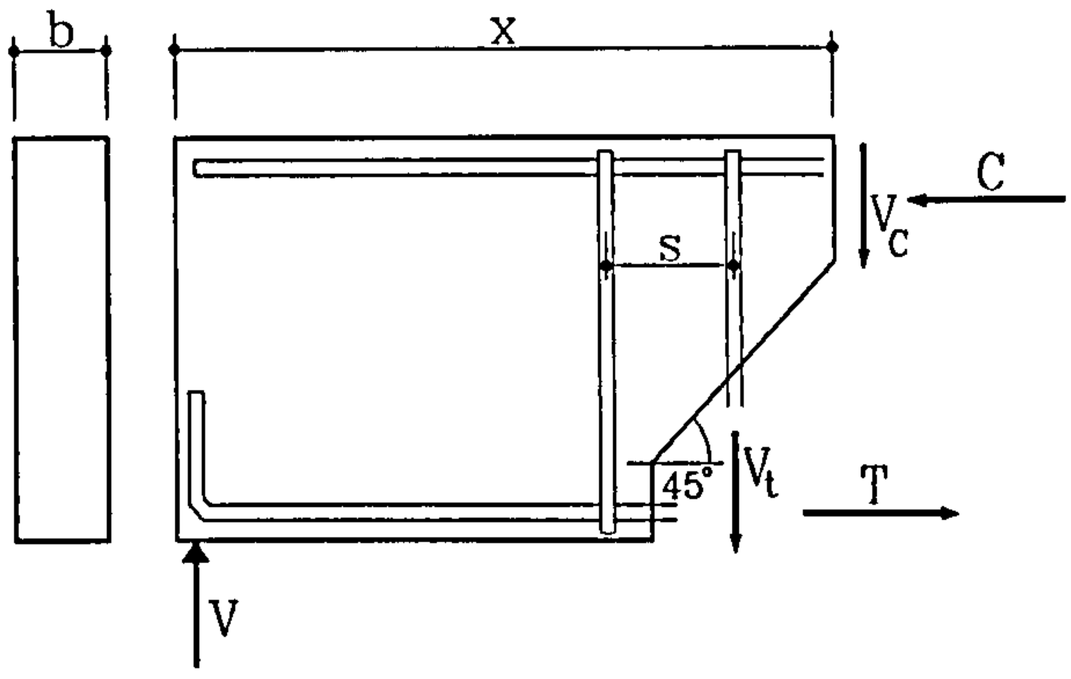

b) Possible Stress Distributions

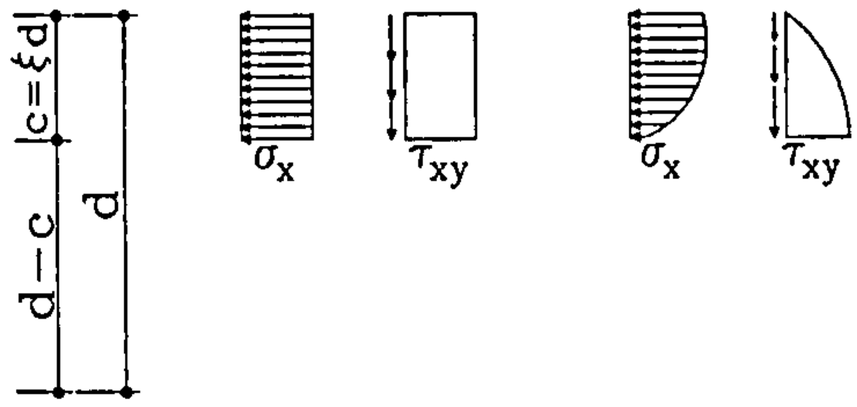

$$V_t = A_v f_y \ (d\text{-}c)/s$$

$$\eta = V_t/V = V_t/(V_t + V_c)$$

$$\sigma_x = f_{c\tau} = \frac{C}{bc} = \frac{M}{bc(d - c/2)} \cong \frac{M}{0.9bcd}$$

$$\tau_{xy} = \frac{V}{bc} \quad for\ \eta = 0$$

$$\psi = \frac{f_{c\tau}}{f_c} = \frac{1}{1 + 3.2\left(\frac{Vd}{M}\right)^2} \qquad (2.6)$$

c) Concrete Law

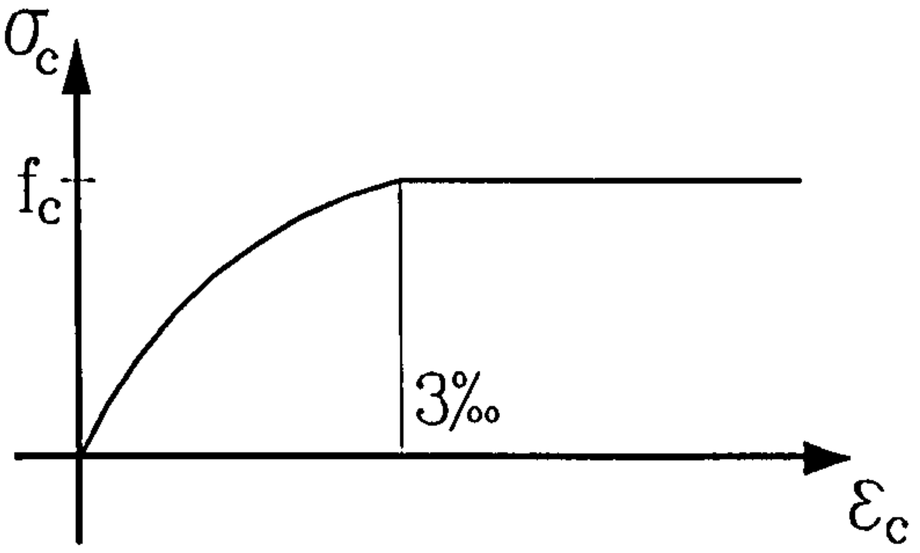

$$\frac{\varepsilon_c}{max.\varepsilon_c} = \left(\frac{\sigma_c}{f_c}\right)^2 = \left(\frac{f_{c\tau}}{f_c}\right)^2 = \psi^2 \qquad (2.7)$$

$f_{c\tau}$ = *reduced concrete strength in compression zone of shear span*

Fig.2.2 Free Body Diagram, Stress Distribution and Concrete Law

Up to this point only equilibrium has been taken into account by Walther, but now compatibility considerations will be introduced. When a beam consisting of an isotropic material is loaded in the elastic range, its flexural and shear resistance can be calculated applying the technical bending theory with Bernoulli's plane section hypothesis. However, when a reinforced concrete beam cracks it develops a highly anisotropic behaviour. In particular, in regions with inclined shear cracks the plane section hypothesis is no longer valid. This means that the depth of the compression zone in the shear span, which is needed to calculate the shear resistance, cannot be calculated using the simplifications of the technical bending theory.

Walther considered the deformations of a beam under a load to occur mainly in the vicinity of the inclined cracks. When a crack opens, the two separated parts are distorted around the centre of rotation which is assumed to be at the tip of the crack. Two different parts contribute to the total deformation, as can be seen from Fig.2.4. The upper part of the sketch shows the rotation of the beam due to moderate shear forces, which Walther called the shear rotation. From the geometry of this deformation Eq.(2.8) can be derived and its evaluation reveals the similarity with the relation for the plane section hypothesis $\varepsilon_c = \varepsilon_s \xi/(1-\xi)$. However, Bernoulli's equation is an infinitesimal description of the strain state all over the cross section, while Eq.(2.8) gives a finite formulation for the deformations concentrated in the vicinity of a crack.

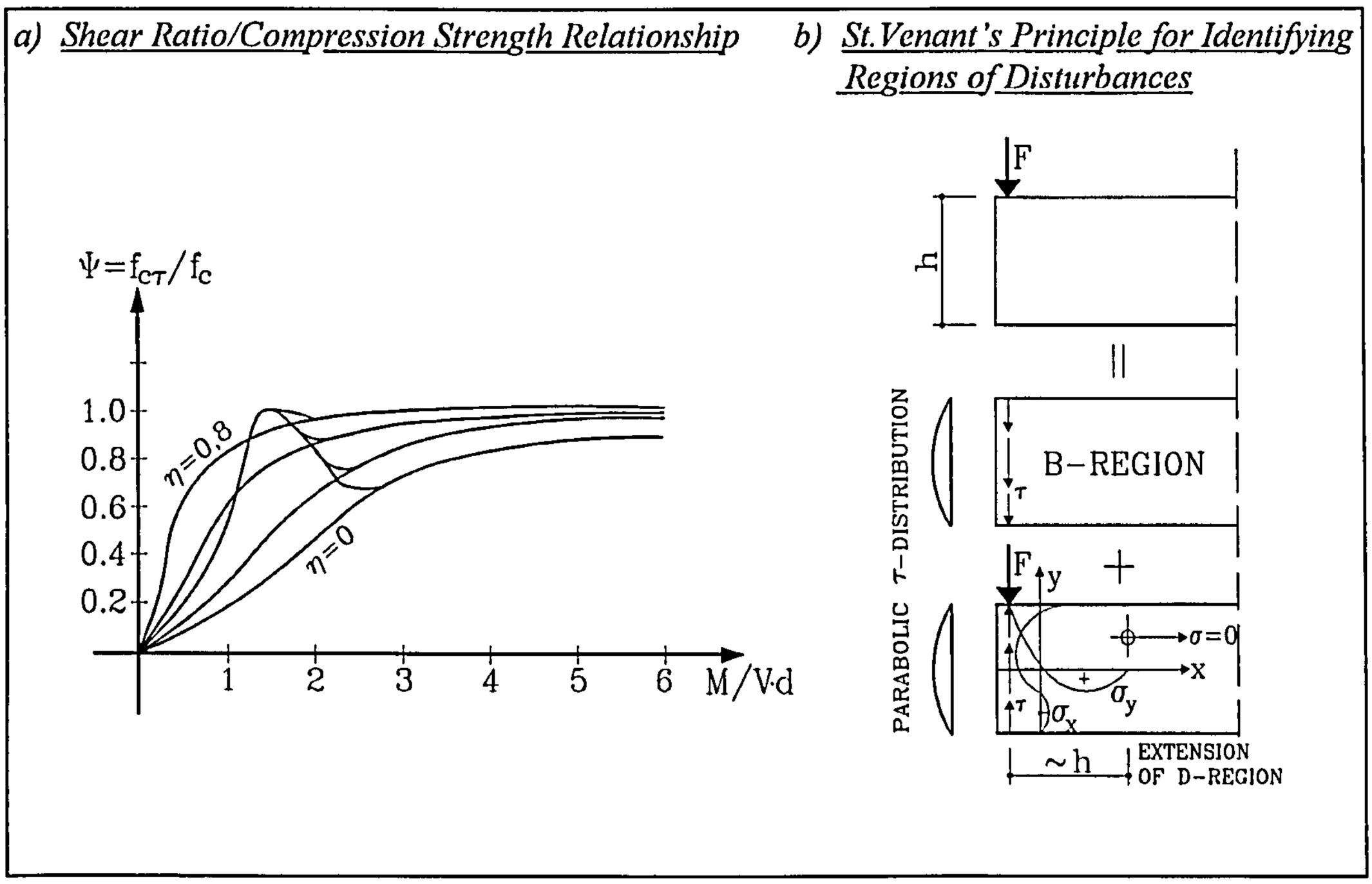

Fig.2.3 Shear Ratio/Compression Strength Relationship and St.Venant's Principle

At a further load stage near the ultimate limit, additional rotation occurs which increases the crack width at the top of the beam but not that at its bottom, because the longitudinal reinforcement restrains it. As a result of this restraint the concrete tooth tends to bend and hence, the crack opens in the middle part of the web. Walther named this the deformation of the web. The geometry of the total deformation including the shear rotation is given by Eq.(2.9) and shown in the lower sketch of Fig.2.4. Comparison of both equations shows that the deformations at high shear are accounted for by a factor k_τ which is always equal to or greater than *1* and depends mainly on the shear stress at the ultimate limit.

It is obvious that the next step in the theory must be the transition to an infinitesimal description which means that Δs_o and Δs_u are to be replaced by the concrete and steel strain respectively. Walther, therefore, assumes Δs_o to be proportional to the depth of the compression zone increased by a factor $1/\sqrt{\xi}$, and Δs_u to be mainly dependent on the crack length and the shear ratio. The two compatibility equations which connect the quantities Δs_o and Δs_u with the strains ε_c and ε_s, respectively, are given in Fig.2.4 as Eqs.(2.10) and (2.11). Elimination of Δs_o and Δs_u and rearranging finally yields the crucial compatibility equation of Walther's shear theory, which is also shown in Fig.2.4 as Eq.(2.12). Eqs.(2.10) and (2.11) seem to be established in a rather arbitrary way, although Walther gives some reasonable explanations for the determination of the various relationships. Nevertheless, it seems that some parameters may have been chosen arbitrarily for the sake of simplicity.

a) Geometry of Deformations

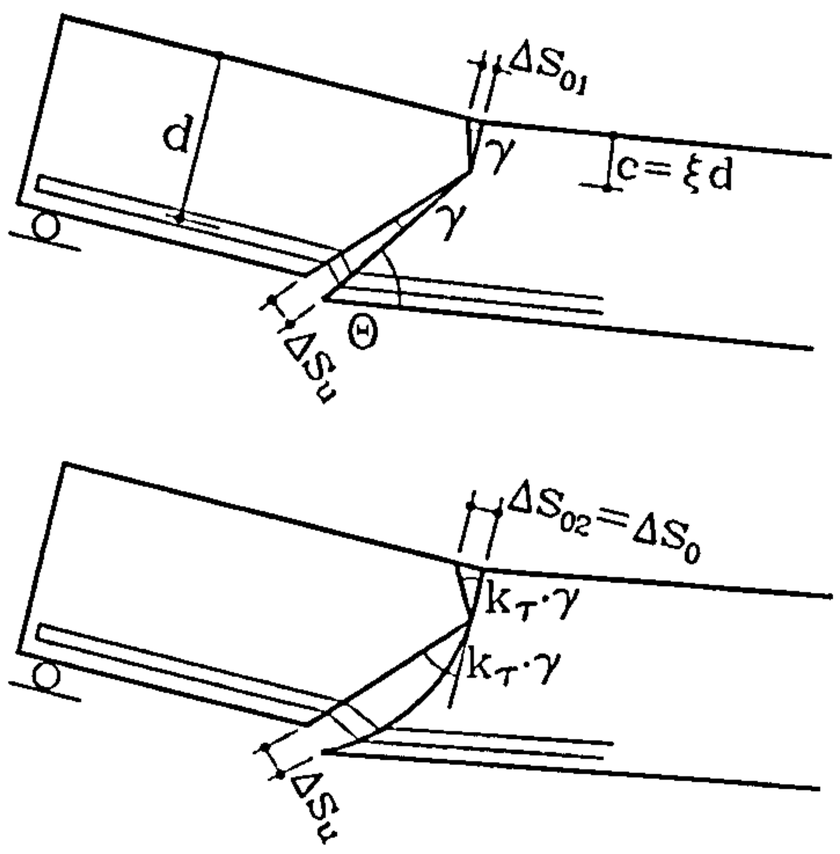

b) Compatibility Equations

$$\Delta s_{o1} = \Delta s_u \frac{\xi}{1-\xi} \sin\theta \qquad (2.8)$$

$$\Delta s_o = \Delta s_u k_\tau \frac{\xi}{1-\xi} \sin\theta \qquad (2.9)$$

$$\Delta s_o = \varepsilon_c d \sqrt{\xi} \qquad (2.10)$$

$$\Delta s_u = \varepsilon_s \frac{d-c}{\sin\theta} k_c \frac{1}{\psi^2} \qquad (2.11)$$

$$\frac{max.\varepsilon_c}{\varepsilon_s} = \frac{k_\tau k_c}{\psi^4} \sqrt{\xi} \qquad (2.12)$$

k_τ = magnification factor due to web deformation
k_c = reduction factor due to bond slip

Fig.2.4 Deformations in a Crack and Corresponding Compatibility Equations

Eq.(2.12), which replaces the plane section hypothesis in Walther's shear failure theory incorporates the special case of pure bending, when k_τ and consequently ψ is set to unity. Fig.2.5 depicts an evaluation of Walther's calculations using both theories for pure flexure. As Eq.(2.12) is dependent on the bond factor k_c, the normalised moment at the ultimate limit m_u is a function of the diameter of the steel bars. Therefore, the values calculated by using Eq.(2.12) are scattered over a certain range, which is shown in the graph by the shaded area, while the results obtained with the plane section assumption, are represented by the dashed line. Eq.(2.12) also reveals that the shear theory allows a smooth transition from pure flexure to flexure with shear.

As mentioned before, the factor k_τ, representing the deformation in the web, is a function of the shear stress. Therefore, equation $k_\tau=\tau_u/\tau_c \geq 1$ might apply, where τ_u denotes the shear stress at the ultimate limit and τ_c the shear stress at the onset of cracking. If $k_\tau=1$, then $\tau_u=\tau_c$ which means that at a load stage where cracking commences, no web deformation in terms of tooth bending can occur. In the presence of transverse reinforcement the relationship would read $k_\tau=(\tau_u-\tau'_s)/\tau_c \geq 1$ with $\tau'_s = \tau_s-\tau_c$, where τ_s is equivalent to that portion of the shear force which is resisted by the stirrups. The final equation for k_τ derived by Walther (1964) was found to be wrong. Therefore, here only the correct formulation is given:

$$k_\tau = \frac{\tau_u(1-\alpha\eta)}{\tau_c} + \eta \qquad (2.13)$$

In Eq.(2.13) α represents a factor which is *1.0* for inclined stirrups and *0.75* for vertical transverse reinforcement. This is a conservative measure which accounts for Walther's observation of a certain amount of tooth bending when using vertical stirrups even when $\eta=1$. For $\eta=0$ Eq.(2.13) yields $k_\tau=\tau_u/\tau_c \geq 1$, and for $\eta=1$ it yields $k_\tau=1$ for inclined stirrups $(\alpha=1)$ and $k_\tau=1+0.25\tau_u/\tau_c \geq 1$ for vertical stirrups $(\alpha=0.75)$. This trial proves that Eq.(2.13) is correct, while the equation for k_τ derived by Walther is not.

The equation for the ultimate moment resisted by the cross section was derived by Walther from the equilibrium of the free body of Fig.2.2 and is given in Fig.2.5 in a normalised form. The flexural resistance is dependent on the relevant parameters of the shear failure theory and yields lower values when a structure fails in shear. The shear failure theory of Walther uses a Mohr failure criterion to calculate the concrete strength in the compression zone of a beam. To account for the decreased depth of the compression zone in the shear span of a structure he introduced a compatibility relationship describing the deformations due to shear which are concentrated in the vicinity of a crack. His shear deformation relationship includes the influence of the longitudinal reinforcement on the deformations in the web and can manage the transition from pure flexure to flexure with shear.

$$m_u = \frac{M_u}{f_c\, bd^2} = \psi\xi\left(1-\frac{\xi}{2}\right)\left(1+\frac{\eta}{2\dfrac{M}{Vd}}\right) \qquad (2.14)$$

m_u = *normalised ultimate flexural resistance of cross section*

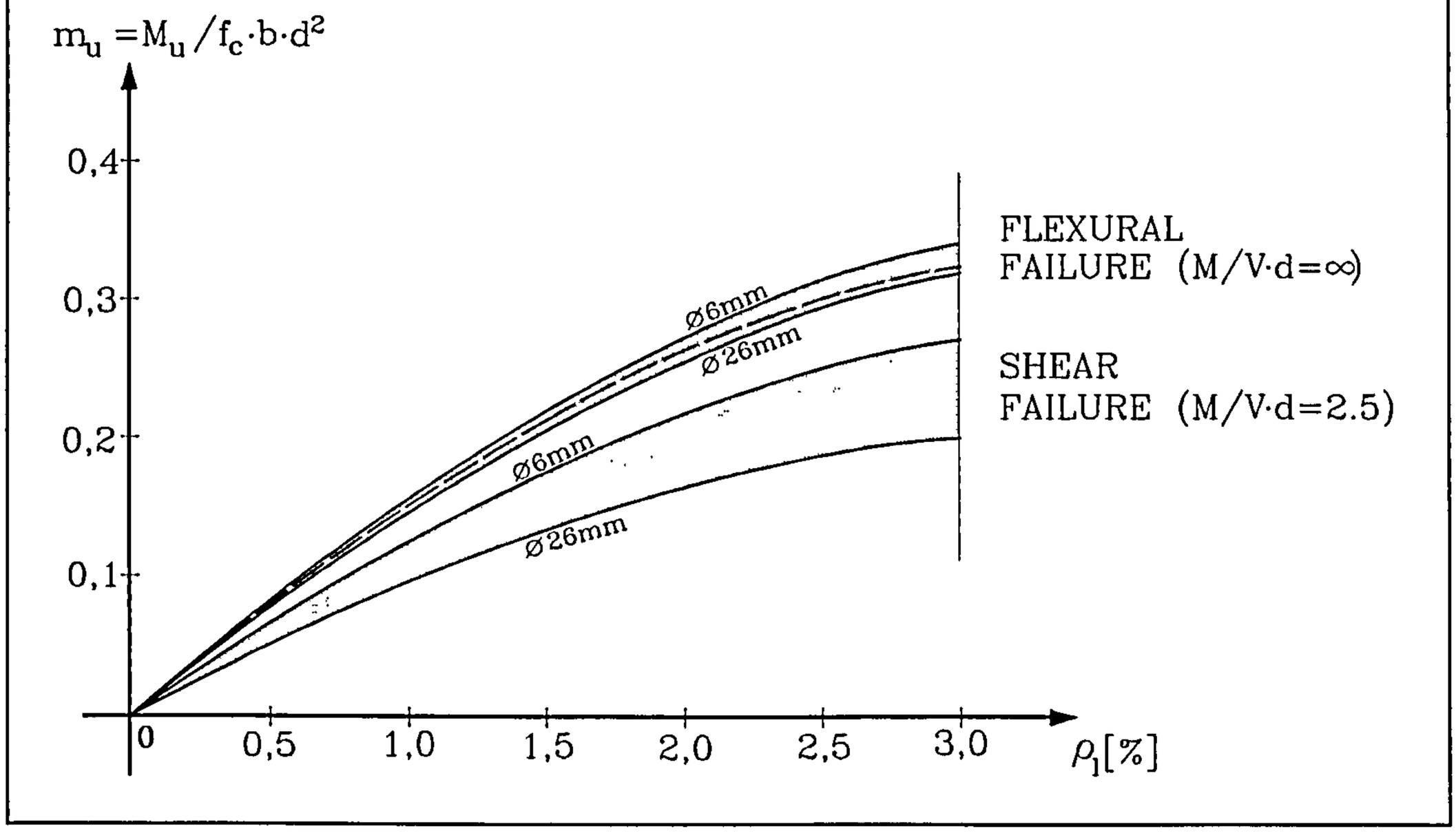

Fig.2.5 Normalised Moment m_u against Longitudinal Reinforcement Ratio ρ_l

With this theory Walther became the first researcher to describe the shear behaviour of reinforced concrete beams based on a physical model. However, his theory has also shortcomings. The main disadvantage is that at a certain stage, Walther was forced to introduce rather arbitrary assumptions which he could only explain in a more qualitative way. Therefore, his theory lost a part of its elegance and credibility and in the end became a semi empirical approach to shear design. Nevertheless, Walther's shear failure theory was in 1962 a great step forward and started a development into shear research which is not yet successfully concluded.

2.2 The Tooth Model of Kani refined by Fenwick / Paulay

In this section the tooth model of Kani (1964) and Fenwick/Paulay (1968) is briefly reviewed in a more qualitative fashion, because it was later improved by Reineck, whose model will afterwards be presented in detail.

In 1964 Kani published a paper in which he developed a new theory for the shear transfer in an RC beam without transverse reinforcement. Since the early fifties, the use of deformed steel bars had become increasingly common in RC design and it soon emerged that the enhanced steel bond of ribbed bars changed the performance of an RC beam in a substantial way. The visible sign of this new behaviour was a regular crack pattern which developed when a beam was loaded beyond yielding of the flexural reinforcement to failure. Kani compared a heavily cracked beam with a comb and referred to the body between two adjacent cracks as a concrete cantilever or tooth.

When deformed steel bars are used in an RC beam the tension force in the steel decreases towards the support by generating bond stresses which act on the surrounding concrete and tries to bend the concrete tooth anchored in the compression zone of the beam. Kani assumed that after the resistance of a cantilever is reached it will break off dropping the bond stresses acting on it to zero. This procedure would lead to a steady transition from beam to arch action as the concrete teeth may gradually fail at their clamped ends. However, arch action would only increase the shear resistance of a beam if the aspect ratio is below a significant value *a/d* which is usually between *2* and *3*, otherwise a sudden shear failure would occur.

In Kani's theory all bond stresses are resisted at the clamped ends of the concrete cantilevers. However, Fenwick and Paulay recognised that the main proportion of the shear is carried by aggregate interlock and dowel action. In their paper, published in 1968, they concluded from their intensive investigations that some *60%* of the shear in a beam without transverse reinforcement is carried by aggregate interlock, while tooth bending and dowel action might contribute to the shear resistance by about *20%* each. Fenwick/Paulay also confirmed that appreciable arch action occurs only when the shear ratio is less than *2.5* and extensive cracking ensures the bond slip of the longitudinal reinforcement necessary for the development of arch action. Fenwick/Paulay did not try to give a physical explanation of aggregate interlock and dowel action but established empirical formulae, with which they achieved good results compared with their testing. It was the work of Walraven on aggregate interlock in the early eighties which enabled many researchers to include aggregate interlock in their models in a less empirical manner.

2.3 The Shear Model of Reineck

The mechanism of force transfer across cracks was not described in a satisfying manner until Walraven (1981) succeeded in developing a model which explained the friction between two adjacent crack surfaces. After that development, it was possible to improve the tooth model of Kani and Fenwick/Paulay by adding aggregate interlock to the model. It soon turned out that aggregate interlock was, besides stirrups, the most important mechanism of shear transfer in reinforced concrete elements.

In his dissertation Reineck (1990) tried to treat the shear transfer along beams in a physically consistent way. The following pages introduce the work of Reineck on the shear resisting mechanisms of RC elements without transverse reinforcement. The significance of this work is the introduction of kinematics to the model, which, together with constitutive relations and equilibrium considerations on free body diagrams, yields the various proportions of a shear force which are assigned to the different mechanisms of shear transfer, such as aggregate interlock or dowel action. When Reineck derived his mechanical model for RC members without transverse reinforcement, he mainly focused on slabs, the most widespread structural element in everyday design practice. As little is known about their shear behaviour, it was desirable to establish a model which should be able to describe the load transfer to the supports at every load stage up to the ultimate limit.

The basis of Reineck's model is the tooth model which was already mentioned earlier. Fig.2.6 shows the shear region of a beam without stirrups. A discrete crack pattern was adopted with the first crack developing at a distance of h from the support, a crack spacing of $s_{cr} = 0.7(d\text{-}c)$, and a crack inclination angle θ of $60°$.

The following shear carrying actions were identified:

- Aggregate interlock
- Flexure at the clamped end of the concrete tooth
- Dowel action of the longitudinal reinforcement

a) Free Body Diagram and Concrete Tooth

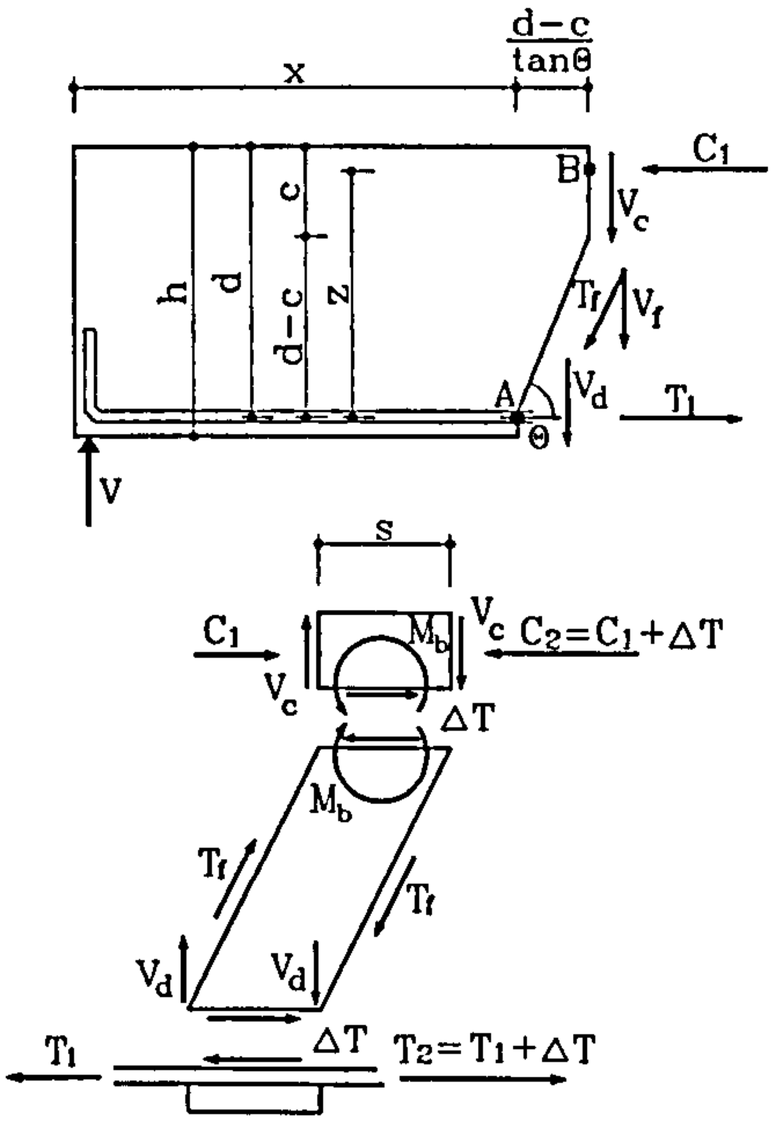

$$V = V_c + V_f + V_d$$

$$\frac{\Delta T}{b\,s} = \frac{V}{b z} = \tau_n$$

$$V_c = \frac{2}{3} c b \tau_n = \frac{2}{3}\frac{c}{z} \quad V = V_{cf} + V_{cb} + V_{cd}$$

$$V = \frac{z}{d-c}(V_f + V_d)$$

$$V\left(x + \frac{d-c}{\tan\theta}\right) - \sigma_s A_s z - V_d \frac{d-c}{\tan\theta} + V_f \frac{2c}{3\tan\theta} = 0$$

$$\varepsilon_s = \frac{1}{E_s A_s z}\left[V\left(x + \frac{d-c}{\tan\theta}\left(1 + \frac{2}{3}\frac{c}{z}\right)\right) - V_d \frac{z}{\tan\theta}\right]$$

$$\varepsilon_c = \frac{2d}{c E_c}\left[\frac{V}{b z}\left(\frac{x}{d} + \frac{2}{3}\left(1 - \frac{c}{d}\right)\frac{c}{z\tan\theta}\right)\right]$$

V_c = shear force in compression zone
V_d = shear force due to dowel action
V_f = shear force due to aggregate interlock

s = crack spacing
b = beam width
τ_n = average shear stress
V_{cd}, V_{cb}, V_{cf} = proportions of V_c due to dowel action, tooth bending and aggregate interlock, respectively

b) Independent Shear Carrying Actions

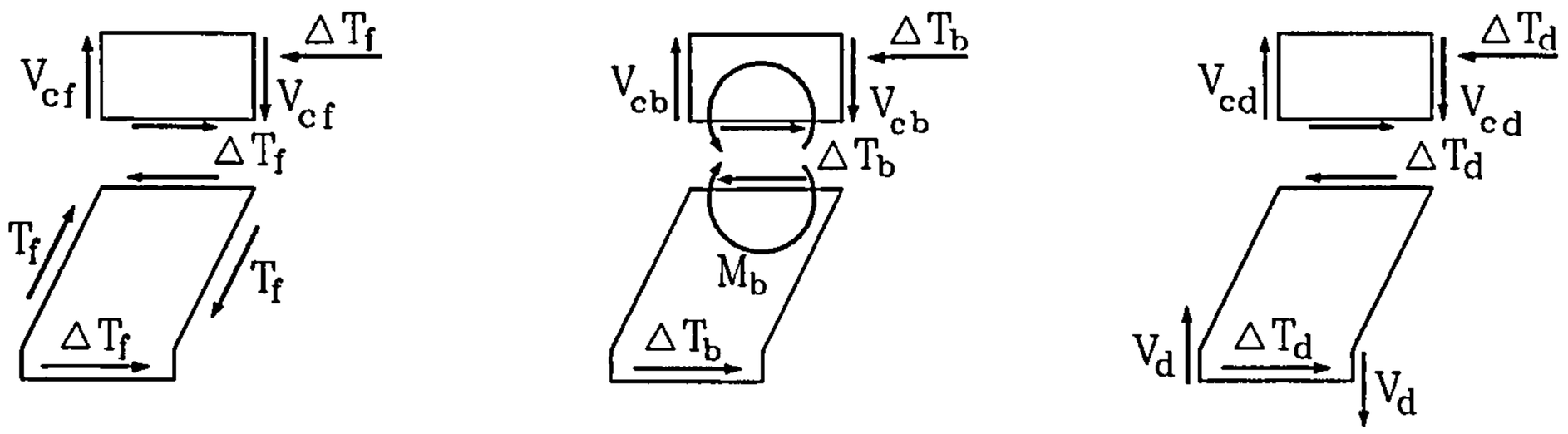

Aggregate interlock *Tooth bending* *Dowel action*

Fig.2.6 Free Body Diagram, Concrete Tooth and Shear Carrying Actions.

According to Reineck's assumptions, each shear carrying action will generate shear stresses in the compression zone of the cross section, which are added together to the shear force V_c. In the literature V_c has often been referred to as the contribution of the concrete to the shear force, and Reineck shows with his model, as Kupfer has done before him, that V_c is triggered by secondary shear carrying actions in the web and not by arch action, which has to be ignored in B-regions of a beam where the plane section hypothesis of Bernoulli applies. Moreover, it was recognised that tooth bending cannot be assigned to the web below the neutral axis, but provides a certain amount of shear in the compression zone, however small it may be.

As depicted in Fig.2.6, each shear carrying action is treated separately and the total amount of shear, transferred through a cross section, is always the sum of the shear generated by the various independent shear carrying actions. This is an important feature of Reineck's model because it ensures the ongoing shear transfer even in the case of the loss of a single shear carrying action. For instance, the tooth bending mechanism is considered to be failing long before the ultimate limit is reached, in which case aggregate interlock and dowel action have to take over the proportion of the lost mechanism.

Fig.2.6 shows a set of equilibrium equations which can be derived from the provided sketches. Reineck assumed that the depth of the compression zone c can be at most $0.5z$, where z denotes the internal lever arm. Then the shear force carried in the compression chord can be a maximum of one third the total shear force, resisted in the cracked section. With these equations, the stress and strain state in the chords are easily calculated. The derivation of the final equilibrium equation requires assumptions to be made concerning the distribution of the friction forces along the cracked surface. Reineck recognised that the dowel forces generated in the crack by the longitudinal reinforcement counteract the friction forces in the lower part of the crack. This is accounted for in his final equation of equilibrium:

$$V = b\,z\tau_f + \frac{3}{4}\frac{z}{d-c}\,V_d$$

where τ_f are the friction stresses at mid-depth of the crack.

Up to now, only the equilibrium in a cross section has been considered. However, the derived equations are not sufficient for the solution of the statically indeterminate problem. Other equations are necessary to determine the still redundant quantities c, z, V_d, and τ_f. Constitutive laws and kinematic relations are now needed to yield the still missing equations.

For concrete in compression and steel in tension, simple bilinear *stress/strain* relations were adopted, because the concrete in chord and web is only under little stress. Fig.2.7 shows the material laws used, including that for the tensile strength of concrete. Reineck modelled aggregate interlock using a law which is based on the work of Walraven. When keeping the crack width constant at a level below *0.9 mm* the friction is considered to be dependent on the relative displacement of the crack surfaces. However, until a slip of Δm_0 is overcome, no friction stresses can be developed at all.

The friction is assumed to increase linearly until the maximum value τ_{fu} is reached at a displacement of Δm_u. A further increase of friction stresses beyond τ_{fu} is only possible in the presence of normal stresses σ_n which are not considered to be generated in members without transverse reinforcement. Reineck restricted the friction stress τ_{fu} to a value of less than *50%* of the tensile strength of concrete and he further assumed, according to Walraven, that no friction occurs beyond a crack width of *0.9 mm*. With the $\tau_f/\Delta m$-relationship of Fig.2.7 it is now possible to calculate the crack friction as a function of the crack width and the mutual displacement of the crack surfaces. The material law for the dowel action was taken from Vintzeleou / Tassios (1986) and Baumann / Rüsch (1970), and the *force/displacement* relationship was derived by Hamadi/Regan (1980).

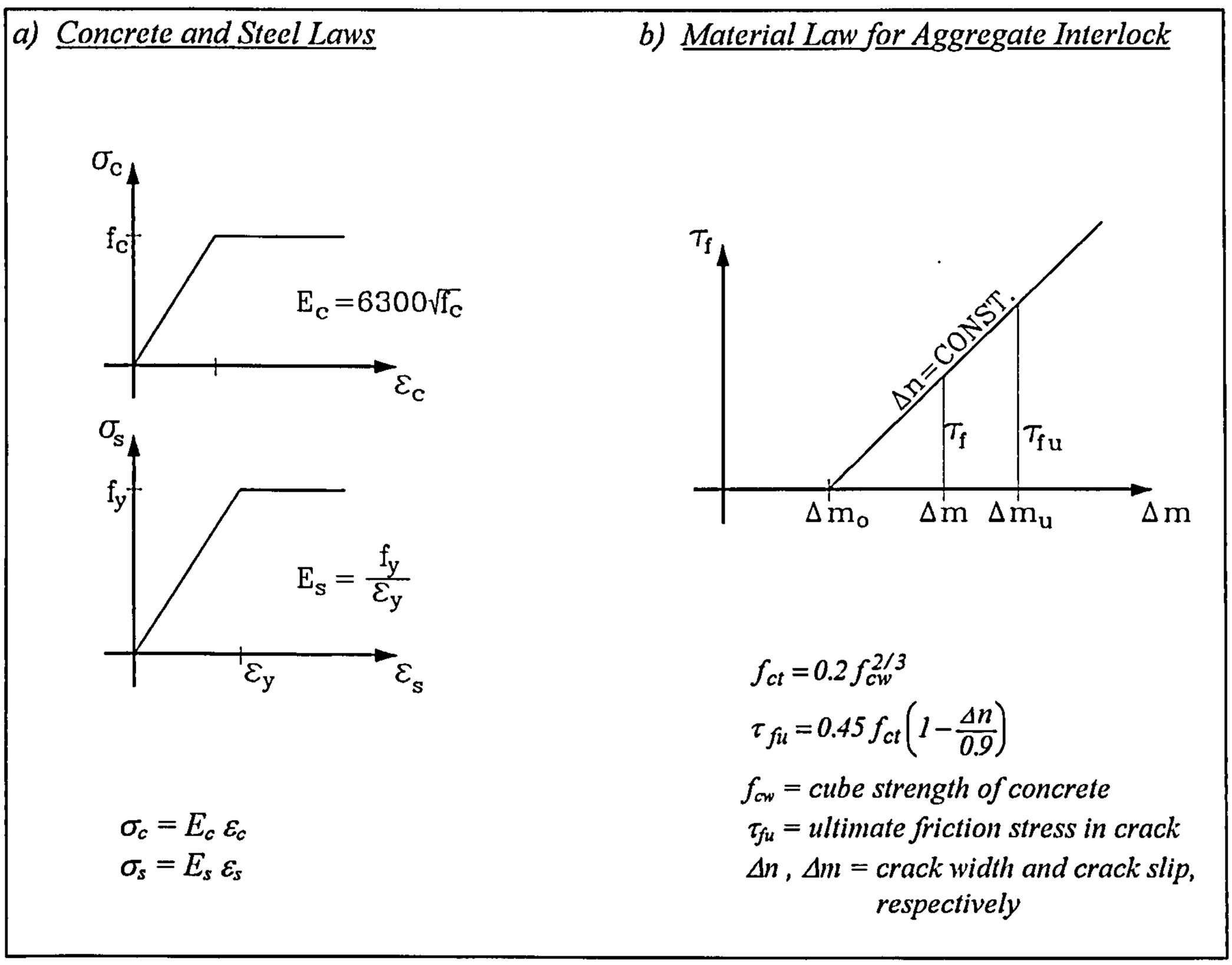

Fig.2.7 Material Laws for Concrete and Steel and Constitutive Relations for Aggregate Interlock

Fig.2.8 shows the equations and the $V_d/\Delta w$ graph. The second part of Fig.2.8 depicts the kinematic relationship between the crack surface displacements Δm and Δn on the one hand, and the crack displacements in horizontal and vertical direction Δu and Δw, respectively, on the other hand. Δu and Δw are made from deformations of the compression and tension zone under the various shear carrying actions described in Fig.2.6.

a) $V_d/\Delta w$-Relationship

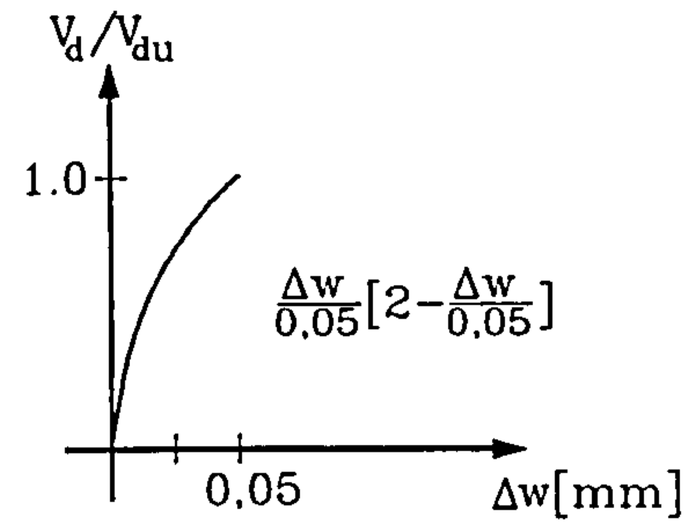

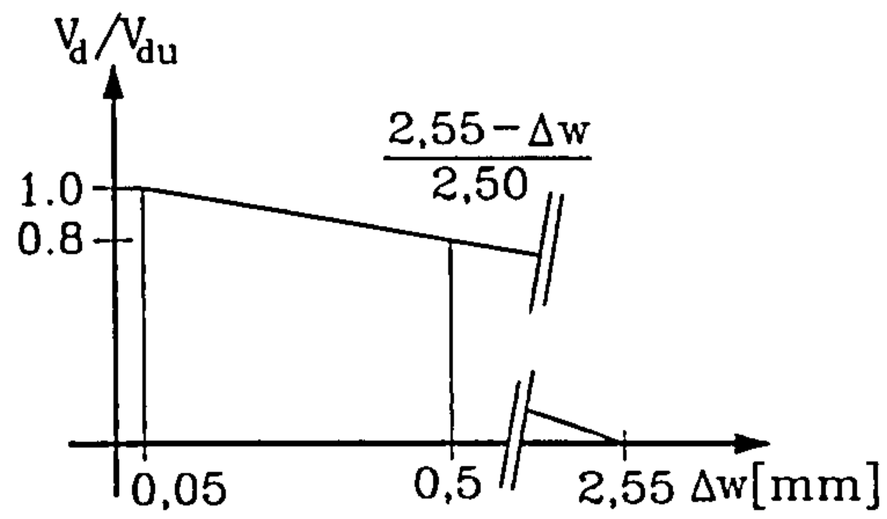

b) Geometry of Relative Crack Displacements

$$\Delta u = \Delta n \sin\theta - \Delta m \cos\theta$$
$$\Delta w = \Delta n \cos\theta + \Delta m \sin\theta$$
$$\Delta n = \Delta u \sin\theta + \Delta w \cos\theta$$
$$\Delta m = -\Delta u \cos\theta + \Delta w \sin\theta$$

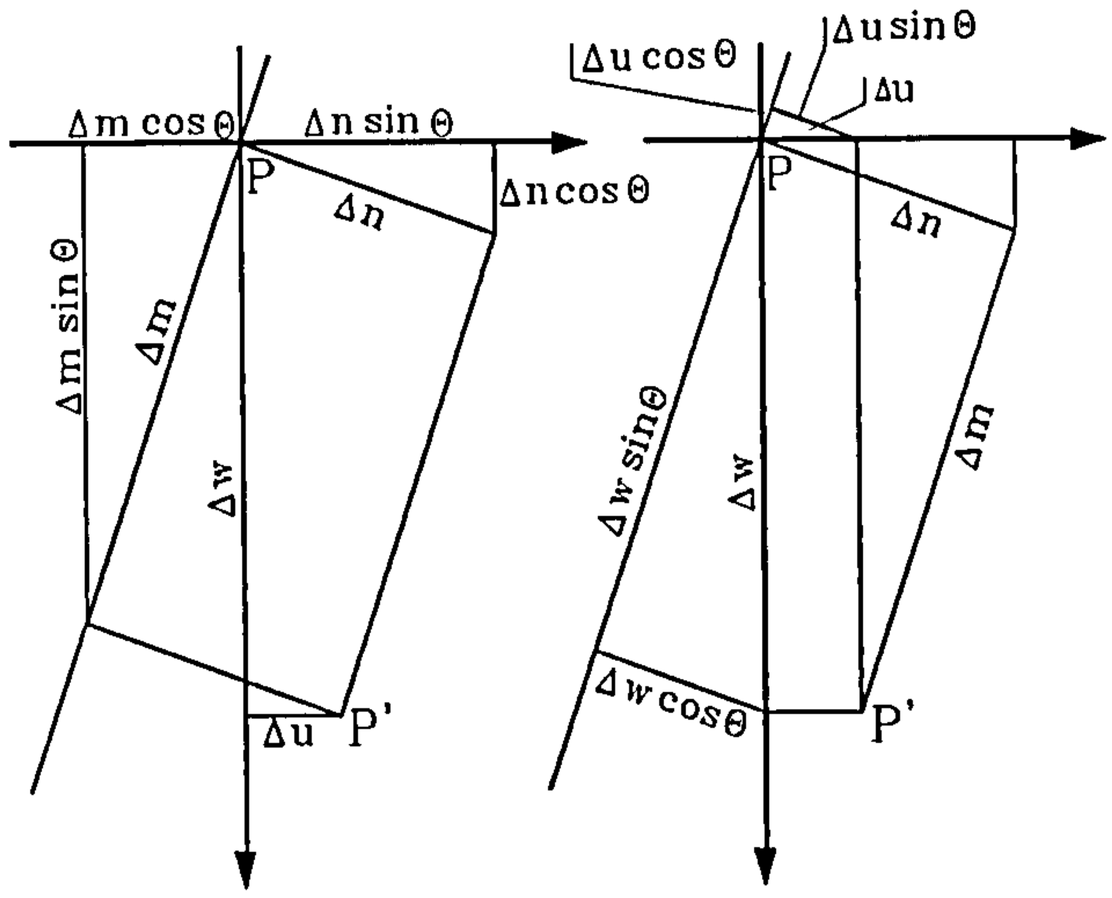

Δn = *crack width*
Δm = *crack slip*
Δu = *horizontal relative crack displacement*
Δw = *vertical relative crack displacement*

$$V_{du} = \frac{6}{f_c^{1/3}} b_n d_b f_{ct}$$

V_{du} = *ultimate shear resistance due to dowel action*

$$b_n = b - \sum d_b$$

b_n, d_b = *beam net width and bar diameter of longitudinal reinforcement, respectively*

Fig.2.8 Material Law for Dowel Action and Kinematics of Crack Displacements

Reineck calculated the deformations for a unit force using FE analysis and this gave equations for the displacements Δu and Δw in mid-depth of a crack, dependent on the parameters c, z, V_d and ε_c.

In the last step Reineck formulated compatibility equations to match crack width at reinforcement level with steel bar elongation. Fig.2.9 shows the geometrical conditions and the equation which was derived from them. For B-regions of an RC beam (see Schlaich/Schäfer/Jennewein, 1987) without transverse reinforcement Reineck's model should now be able to predict both the ultimate shear force V_u and, at every load stage below the ultimate limit, each proportion of the shear force connected with its respective shear carrying action.

When Reineck established his theory he tried to approach the structural behaviour of an RC member in an as realistic way as possible. Therefore, he abandoned assumptions which are normally introduced in shear theories for the sake of simplicity. For instance, Reineck dropped the simplification of a uniform stress and strain state in the web. With this his shear theory became rather complicated and it was no surprise that the verification of its supposed features revealed some shortcomings.

Reineck described three different load stages, two of which are at service load level, while the third can be referred to as ultimate limit. He tried to prove his theory by recalculating numerous tests described in the literature. One of these tests was carried out by Leonhardt/Walther (1964) and was part of a programme known as the Stuttgart shear tests. Reineck recalculated beam 7 and 8 at all three load levels and the results are given in his dissertation in various tables.

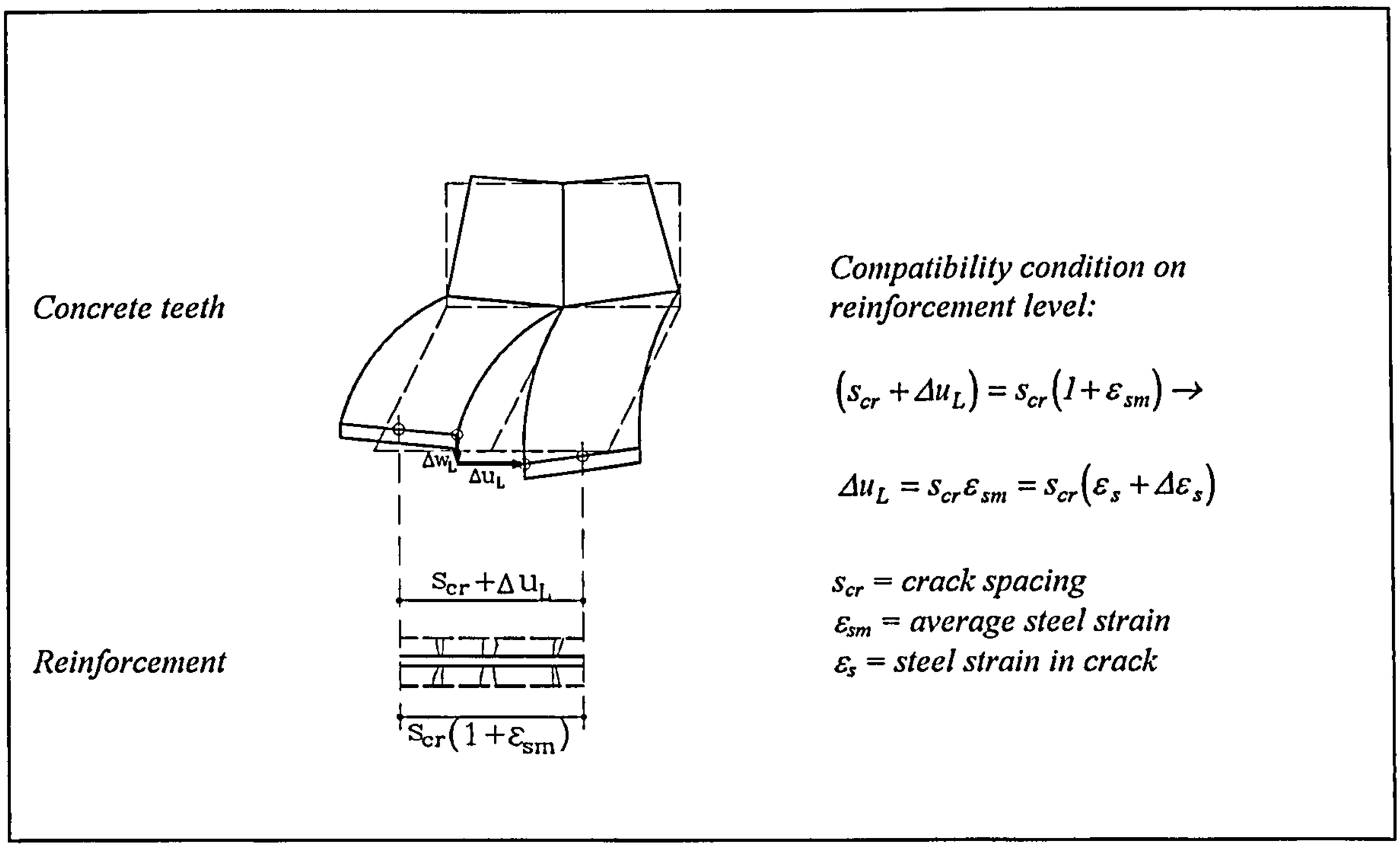

Fig.2.9 Conditions of Compatibility

It turned out that Reineck's theory is able to predict the ultimate limit of the above mentioned beams in an accurate fashion. However, the main feature of the theory should be its ability to predict the various proportions of the shear force which might be attributed to the different shear carrying actions and this objective was only partly reached. While the results of Reineck's calculations on a load level slightly below the ultimate limit could be verified in a cross check in a satisfying manner, the results of his calculations on a load stage before the failure of the concrete cantilevers are simply wrong.

$q = 0.01$	$k_x = 0.44$	$\varepsilon_s = 0.00034$	$\varepsilon_c = 0.00023$	$q_f = -0.0034$	$q_d = 0.0051$	$\sigma_1/f_c =$
$x/h = 4.04$		*Mutual displacements [m]*				*0.080*
		Δu	Δw	Δn	Δm	$\Delta m/\Delta n$
	L	*0.000030*	*0.000013*	*0.000032*	*-0.000004*	*-0.125*
	f/2	*0.000012*	*0.000010*	*0.000016*	*0.000002*	*0.125*
$q = 0.016$	$k_x = 0.42$	$\varepsilon_s = 0.00054$	$\varepsilon_c = 0.00038$	$q_f = -0.0063$	$q_d = 0.0087$	$\sigma_1/f_c =$
$x/h = 4.04$		*Mutual displacements [m]*				*0.134**
		Δu	Δw	Δn	Δm	$\Delta m/\Delta n$
	L	*0.000057*	*0.000026*	*0.000062*	*-0.000006*	*-0.097*
	f/2	*0.000024*	*0.000018*	*0.000030*	*0.000004*	*0.133*
$q = 0.023$	$k_x = 0.41$	$\varepsilon_s = 0.00077$	$\varepsilon_c = 0.00055$	$q_f = -0.0080$	$q_d = 0.0113$	$\sigma_1/f_c =$
$x/h = 4.04$		*Mutual displacements [m]*				*0.194**
		Δu	Δw	Δn	Δm	$\Delta m/\Delta n$
	L	*0.000089*	*0.000048*	*0.000100*	*-0.000003*	*-0.030*
	f/2	*0.000039*	*0.000030*	*0.000049*	*0.000006*	*0.123*

*$\sigma_1 > f_{ct}$ → failure of the tooth bending mechanism

Tab.2.1 Recalculation of Leonhardt's Tests (see Reineck, 1990, Fig.3.7.3, Page 112)

In Tab.2.1 the correct values are depicted and it can be seen that Reineck's theory delivers negative friction stresses in the crack which is in contrast to the physical reality. It is easy to verify that Reineck's results do not represent an equilibrium set of values. The reason for the problems at low load stages is that Reineck's equations are rather sensitive to some parameters, for instance the tensile strength of the concrete or the crack spacing, which are quantities of uncertain nature and therefore, difficult to estimate.

Although section analysis normally provides an easier access to modelling of more sophisticated features than FE procedures do, the above discussed shear model turns out to be too complicated to deliver correct results at all load stages.

2.4 The Compression Field Theory

The compression field theory was developed in the seventies by Collins/Mitchell (1980) as a model to describe the behaviour of reinforced concrete members in pure torsion. When a beam is subjected to torsion the torque T is resisted by the shear flow q. Assuming a truss model it can be seen that chords and posts are under tension while the diagonal struts are under compression (see Fig.2.10). As the concrete is considered not to resist any tension, the tensile members must consist of reinforcing steel, while compression is carried by the concrete.

To investigate the deformations of the truss members it is convenient to isolate a truss section as shown in Fig.2.12.(a). Due to their respective stress state the truss members will undergo deformations, which means that members in tension are elongated and those in compression are shortened. Both chords carry the same tension force and hence their elongation Δl is the same as well. As this also applies to the posts, a truss section may be replaced by a structural member, the stress and strain state of which can be described by Mohr's circles (see Fig.2.11). This transition from truss model to structural member is possible, because the strain and stress state in the web is regarded to be uniform.

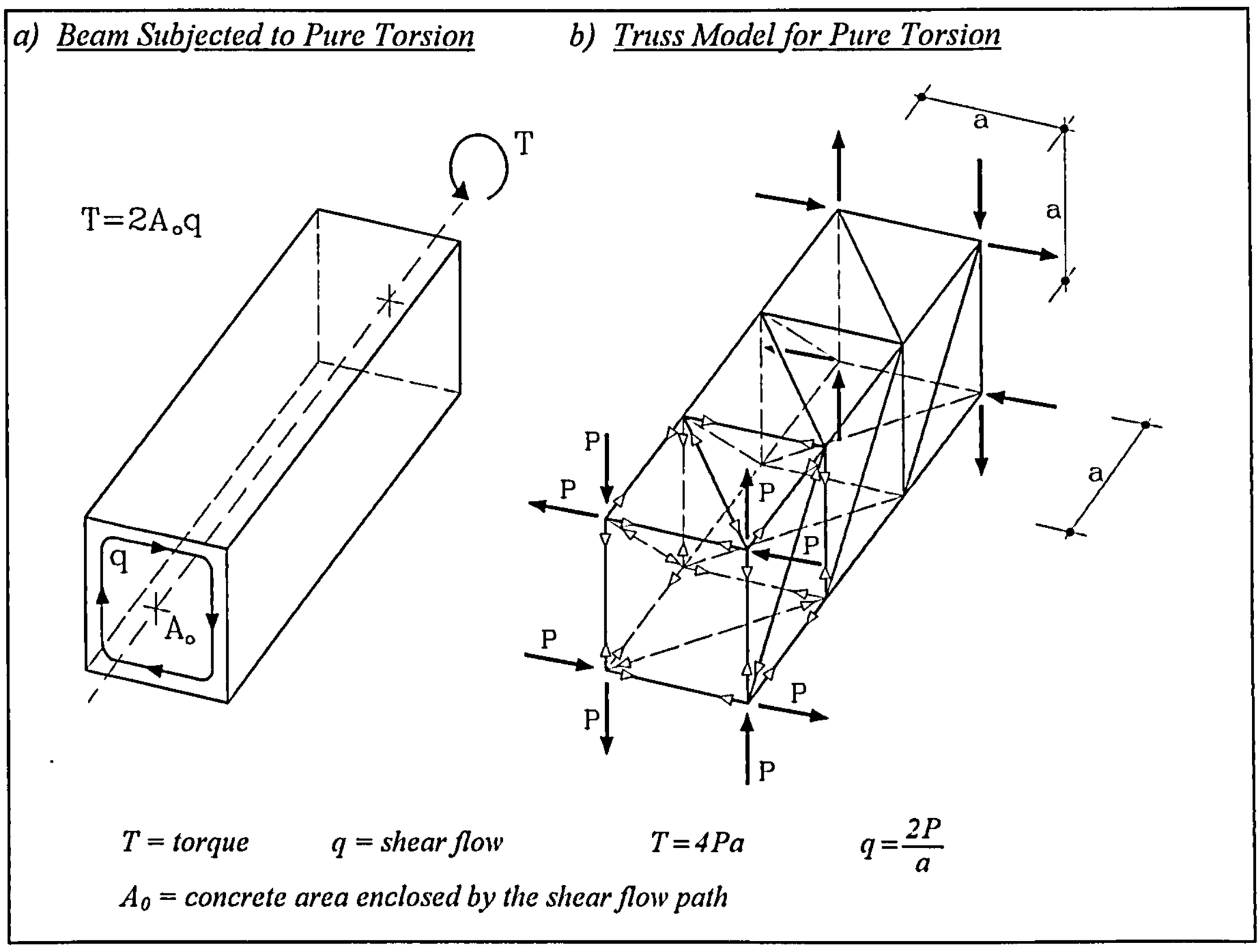

Fig.2.10 RC Beam Subjected to Pure Torsion and Associated Truss Model

a) Structural Member

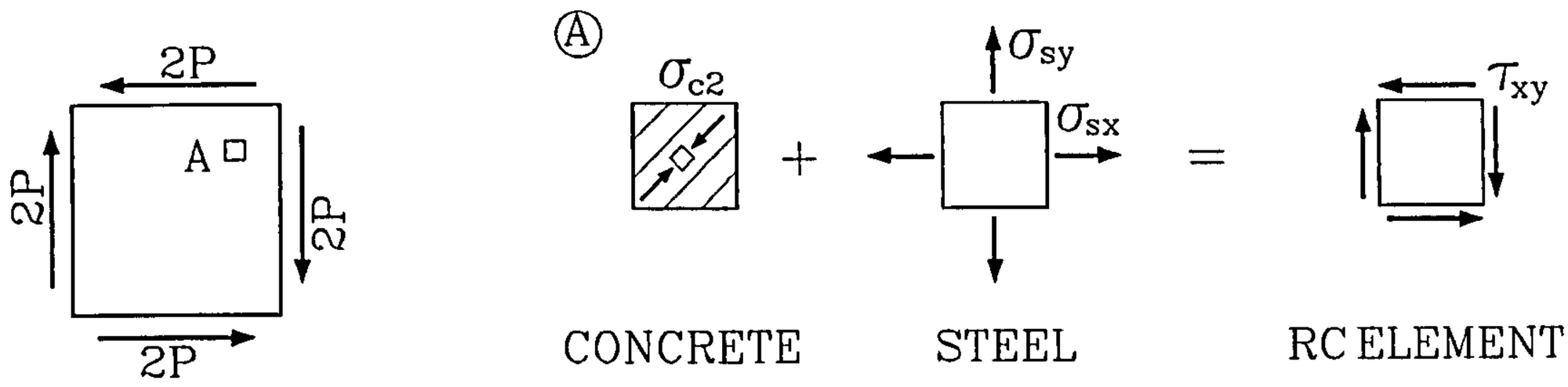

b) Stress State

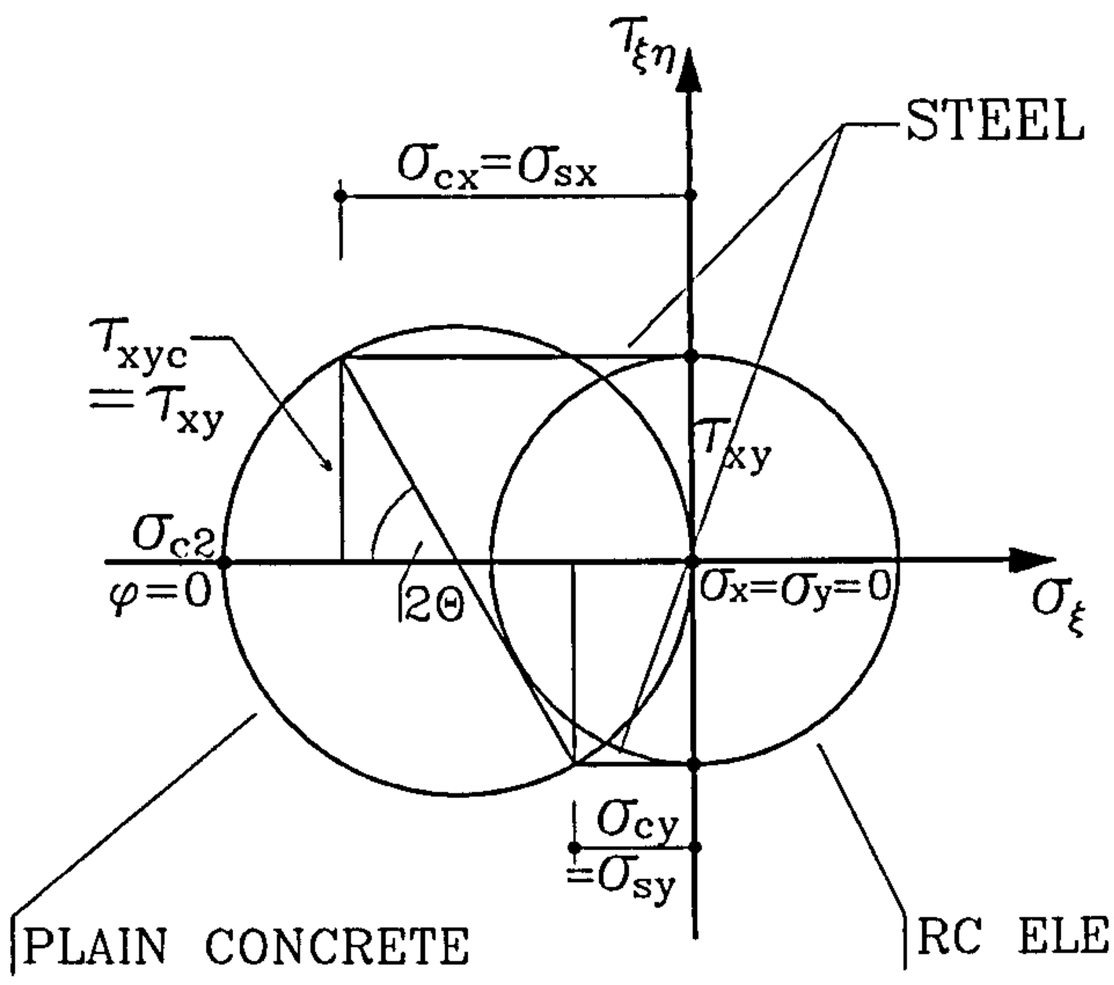

c) Strain State

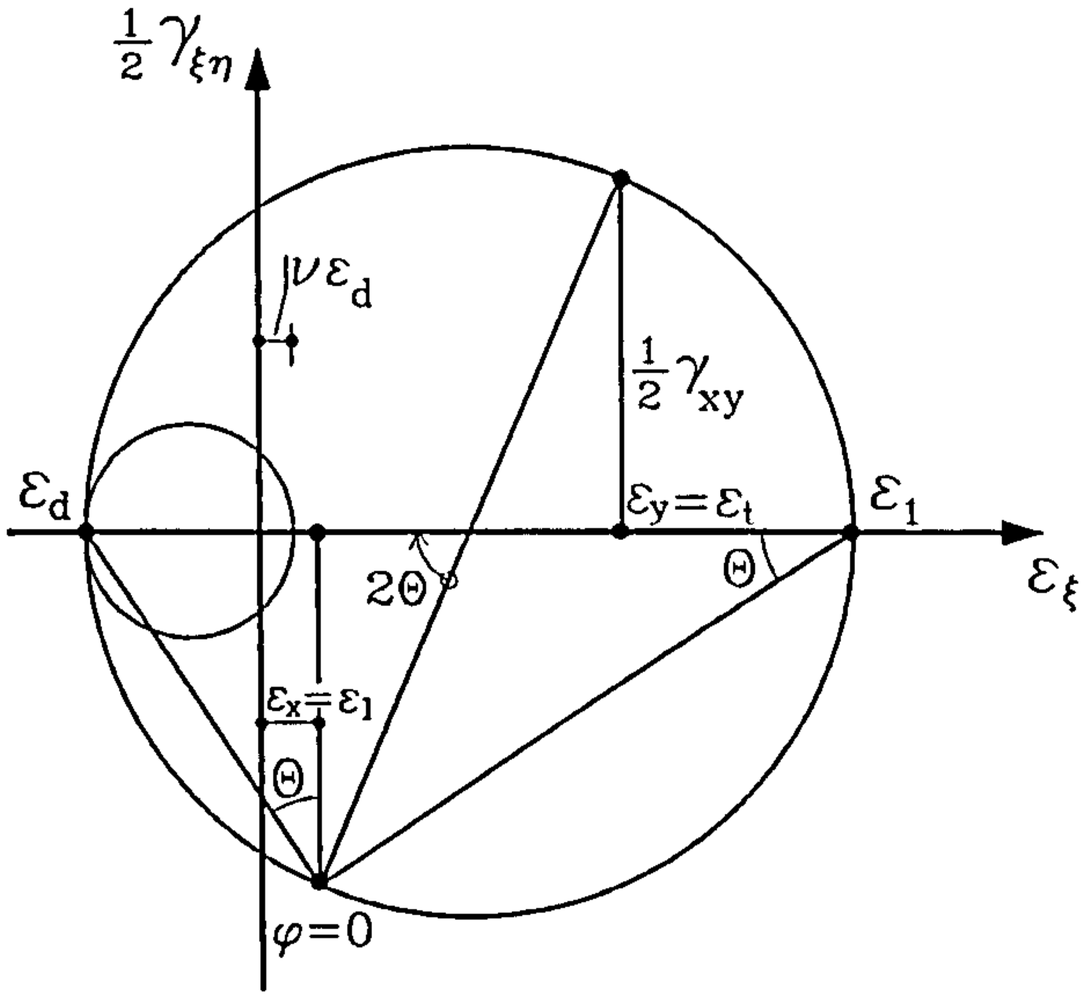

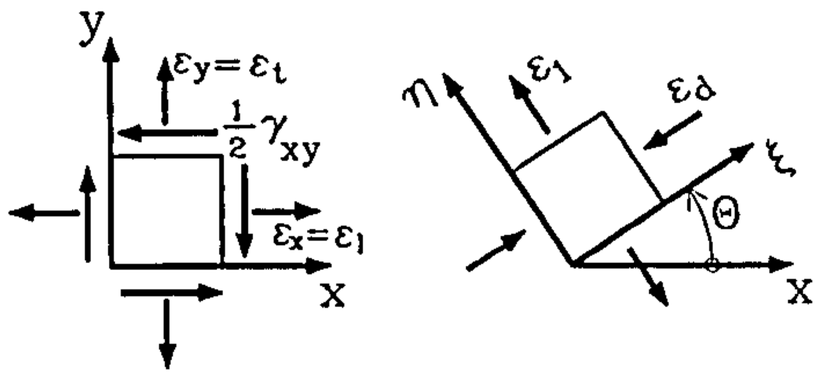

ν = Poisson's ratio

$$\tan\theta=\frac{\gamma}{2}/\left(\varepsilon_d-\varepsilon_y\right)$$

$$\tan\theta=\frac{2}{\gamma}\left(\varepsilon_d-\varepsilon_x\right)$$

$$\tan^2\theta=\frac{\varepsilon_d-\varepsilon_x}{\varepsilon_d-\varepsilon_y} \qquad (2.15)$$

Fig.2.11 Uniform Stress and Strain State in an RC Member under Pure Torsion

The stress state itself could be described as consisting of two parts: The stress state of the concrete and that of the steel providing it is smeared over the element. Fig.2.11.(b) shows the stress state of the structural member and the Mohr's circle describing it. As the steel does not resist any shear, its stress state cannot be modelled with a Mohr's circle. The Mohr's circle of the RC member is therefore obtained by adding the steel stress in the x and y direction to the respective points of the Mohr's circle for the plain concrete. This procedure yields $\sigma_x = \sigma_y = 0$, and τ_{xy} is taken from the concrete circle. Thus the circle of an infinitesimal element of the structural member is found and with it a complete description of its stress state.

Fig.2.11.(c) also shows the strain state of the RC member. The CFT regards the principal stresses as having the same inclination as the principal strains. This assumption is correct as the tensile strength of the concrete is neglected and, with it, aggregate interlock. The principal compression strain ε_d is the same for both the plain concrete and the structural member and coincides with the principal compression stress σ_{c2} in the concrete. The second principal strain ε_l is the total strain in the direction perpendicular to the strain ε_d and consists mainly of the smeared cracks. For the purpose of comparison, the transverse strain of the plain concrete $\nu\varepsilon_d$ is also depicted, and it is obvious that ε_l must be much bigger than $\nu\varepsilon_d$.

By rotating the strain state in the xy direction of the beam axis, we receive the strain values ε_x and ε_y which are the strains of the longitudinal and shear reinforcement, respectively. As already mentioned the strain circle is valid everywhere in the beam, which means that ε_x and ε_y have constant values and this is in line with statements on a truss model for pure torsion given earlier in this section. Eq.(2.15) is the compatibility equation of the CFT and can be directly read from the strain circle in Fig.2.11. This means that for each strain state the inclination angle θ is fixed and cannot be chosen at random as was stated in earlier shear theories. Fig.2.12 reveals the impact of the compatibility equation on the equivalent truss model: An arbitrarily fixed set of deformations does not meet Eq.(2.15), while a compatible set complies with it.

Collins/Mitchell (1980) derived the CFT by investigating a reinforced concrete beam in pure torsion. However, it was desirable to manage the transition to shear due to flexure. When modelling shear due to flexure with the truss analogy, it is obvious that the top chord is no longer in tension. The linear strain distribution along the depth of the structural member which now replaces the constant strain value ε_x prevents the compression field theory from being applied without additional specifications.

a) Isolated Truss Member

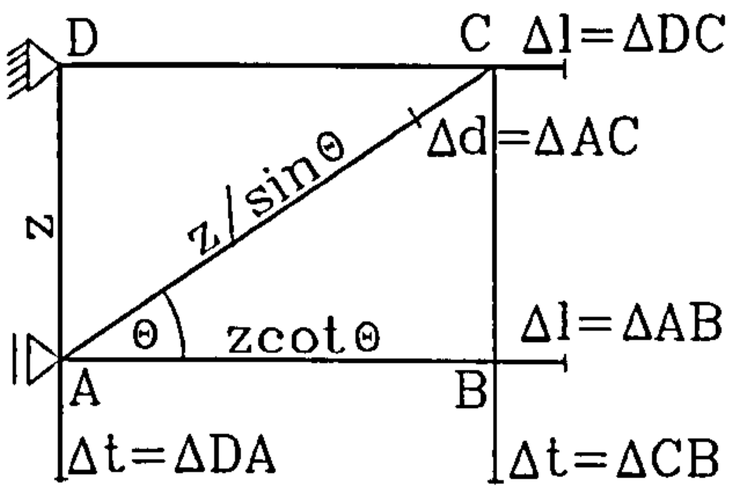

$$\Delta l = \varepsilon_l z \cot\theta$$
$$\Delta t = \varepsilon_t z$$
$$\Delta d = \varepsilon_d z / \sin\theta$$

b) Displacement Plan for an Arbitrary Set of Deformations

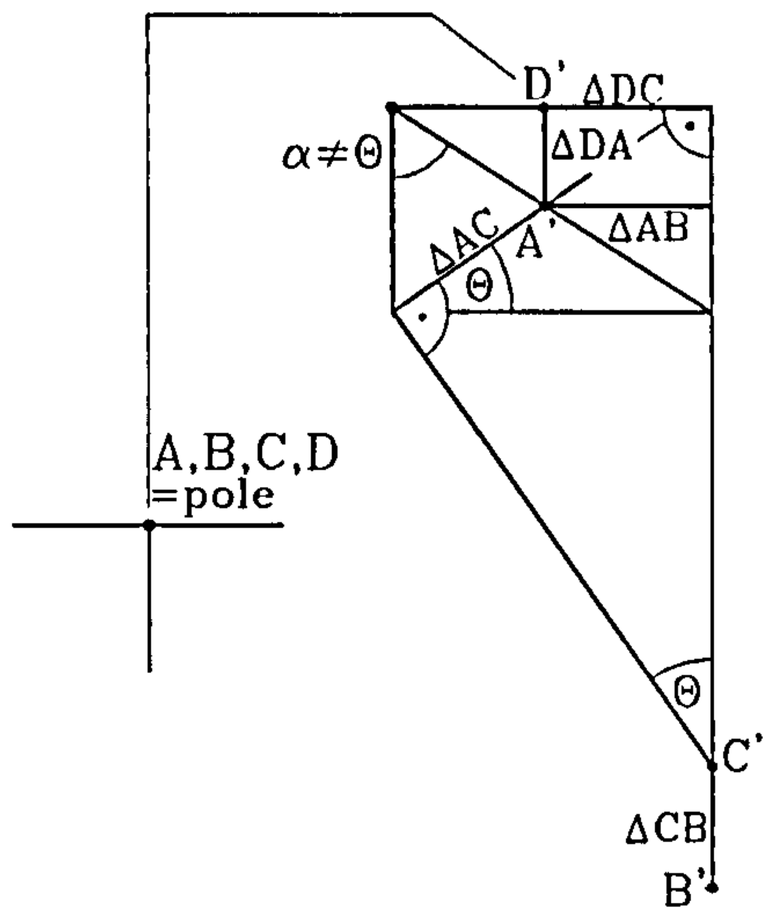

c) Strain Distribution for a Beam with Shear from Flexure

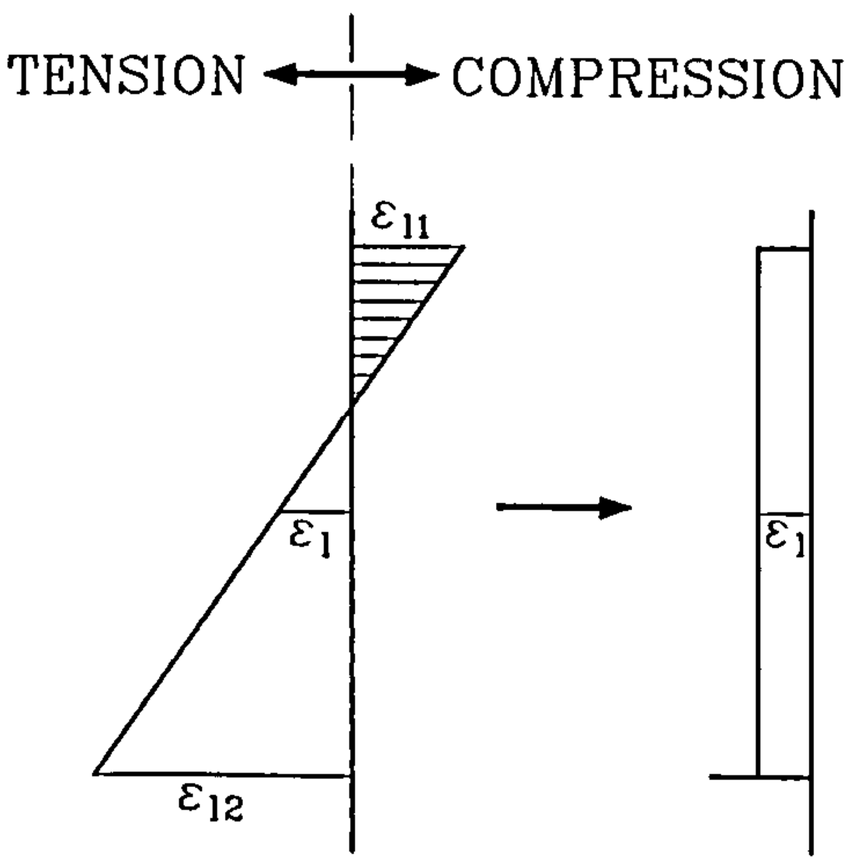

d) Displacement Plan for a Compatible Set of Deformations

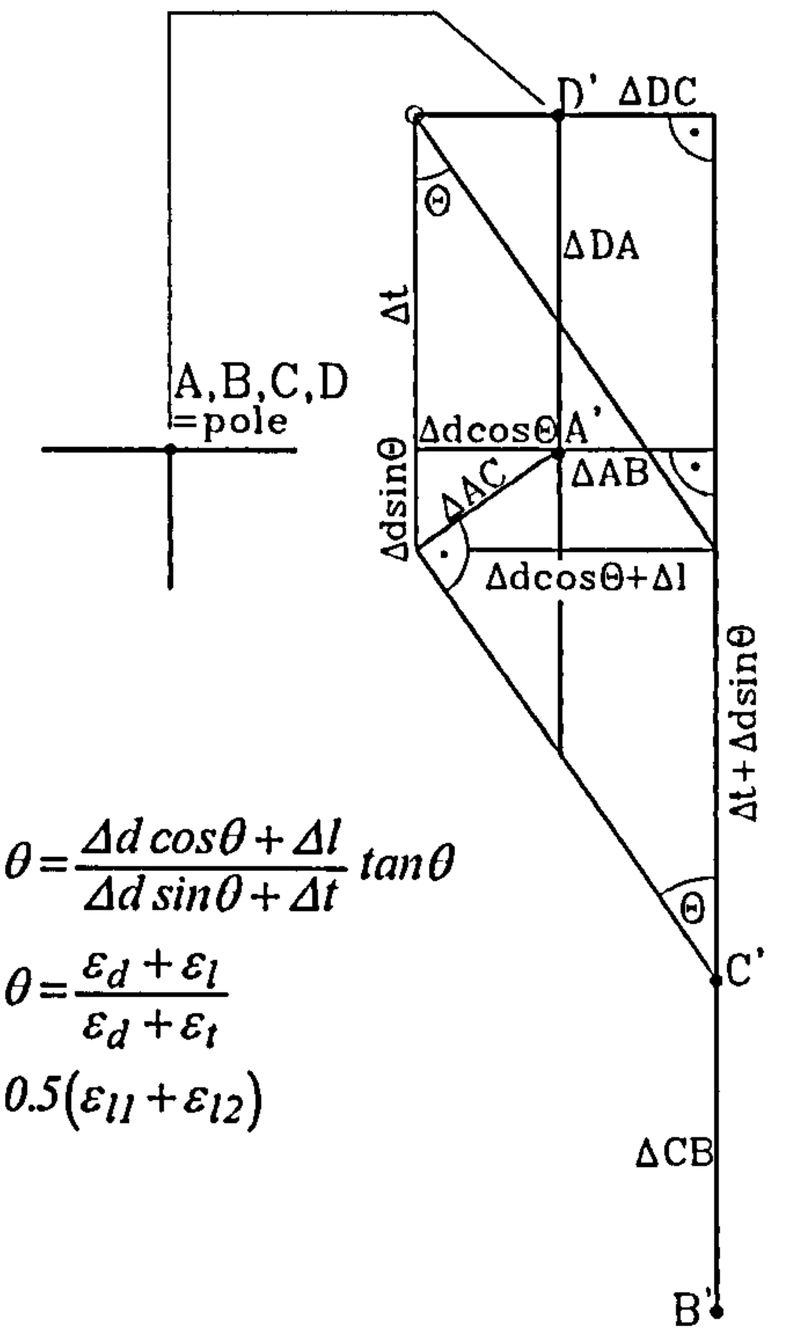

$$\tan^2\theta = \frac{\Delta d\cos\theta + \Delta l}{\Delta d\sin\theta + \Delta t}\tan\theta$$

$$\tan^2\theta = \frac{\varepsilon_d + \varepsilon_l}{\varepsilon_d + \varepsilon_t}$$

$$\varepsilon_l = 0.5(\varepsilon_{l1} + \varepsilon_{l2})$$

ε_l = *strain in longitudinal direction*
ε_t = *strain in transverse direction*
ε_d = *strain in principal compressive direction*

Fig.2.12 Williot's Displacement Plan for Torsion, and Strain Distribution due to Flexure

Collins/Mitchell replaced the strain in beam axis direction ε_l by the mean value of compression strain ε_{l1} in the top chord and tension strain in the bottom chord ε_{l2} as shown in Fig.2.12.(c). At least for T or I shaped beams this is an acceptable measure as usually ε_{l2} is much bigger than ε_{l1}, in which case ε_l is always a tensile strain and this complies with the basic assumptions of the CFT.

The advantage of the compression field theory is the introduction of a compatibility relation with the simple assumption of a homogeneous stress and strain state in the web of an RC member. The theory is rather accurate for its application on pure shear due to torsion and gives good results for shear from flexure and all combined actions at the ultimate limit level.

2.5 The Modified Compression Field Theory

The modified compression field theory of Vecchio/Collins (1986) is a further development of the CFT. The main difference is the utilisation of the tensile strength of concrete. Initially, the CFT was conceived as a multiple truss model, smearing its members more or less over the structure. The basic assumption postulated a uniform stress state represented by a compression field inclined under a certain angle θ_c to the horizontal. This angle θ_c can be calculated using Eq.(2.15) (see Fig.2.11). It will be shown later in Chapter 3, that with the tensile strength of the concrete, an additional truss member has emerged making the truss indeterminate. Therefore, the constitutive laws had to be extended to include the tensile strength of the concrete. Vecchio/Collins (1986) derived the material laws for the MCFT from extensive testing on membrane elements. By evaluating measured stress and strain circles they recognised that the concrete carries a substantial amount of stress in its principal tensile direction, despite the fact that the tested specimens were heavily cracked. The CFT included a further assumption: It was claimed that the principal direction of the concrete stresses should coincide with the principal strain direction of the cracked structure. This assumption was retained in the MCFT and once again it will be shown later in Chapter3 that this deprived the theory from treating the mechanism of shear transfer over a crack in an appropriate way.

a) Membrane Element and Equilibrium Conditions

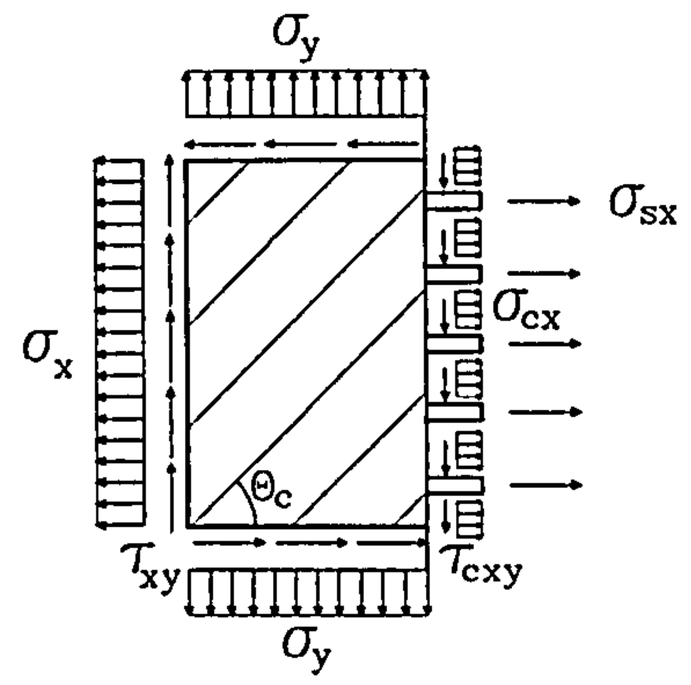

$$\sigma_x = \sigma_{cx} + \rho_{sx}\sigma_{sx}$$
$$\sigma_y = \sigma_{cy} + \rho_{sy}\sigma_{sy}$$
$$\tau_{xy} = \tau_{cxy}$$
$$\sigma_{cx} = \sigma_{c1} - \tau_{xy} / \tan\theta_c$$
$$\sigma_{cy} = \sigma_{c1} - \tau_{xy}\tan\theta_c$$
$$\sigma_{c2} = \sigma_{c1} - \tau_{xy}(\tan\theta_c + 1/\tan\theta_c)$$

b) Constitutive Equations

Steel:

$$\sigma_{sx} = E_s\varepsilon_x$$
$$\sigma_{sy} = E_s\varepsilon_y$$

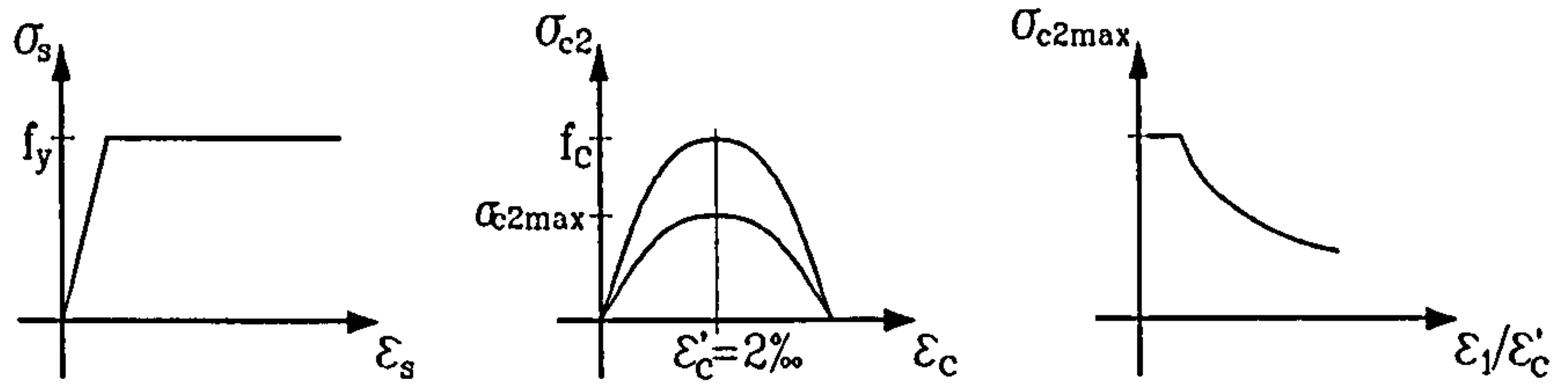

Concrete:

$$\sigma_{c2} = \sigma_{c2max}\left[2\frac{\varepsilon_2}{\varepsilon_c'} - \left(\frac{\varepsilon_2}{\varepsilon_c'}\right)^2\right]$$

$$\sigma_{c2\max} = f_c\,\frac{1}{0.8 - 0.34\,\varepsilon_1/\varepsilon_c'} \le f_c$$

$$\sigma_{c1} = E_c\varepsilon_1 \qquad for\ \ \varepsilon_1 \le \varepsilon_{cr}$$

$$\sigma_{c1} = \frac{\sigma_{cr}}{1+\sqrt{200\varepsilon_1}} \qquad for\ \ \varepsilon_1 \ge \varepsilon_{cr}$$

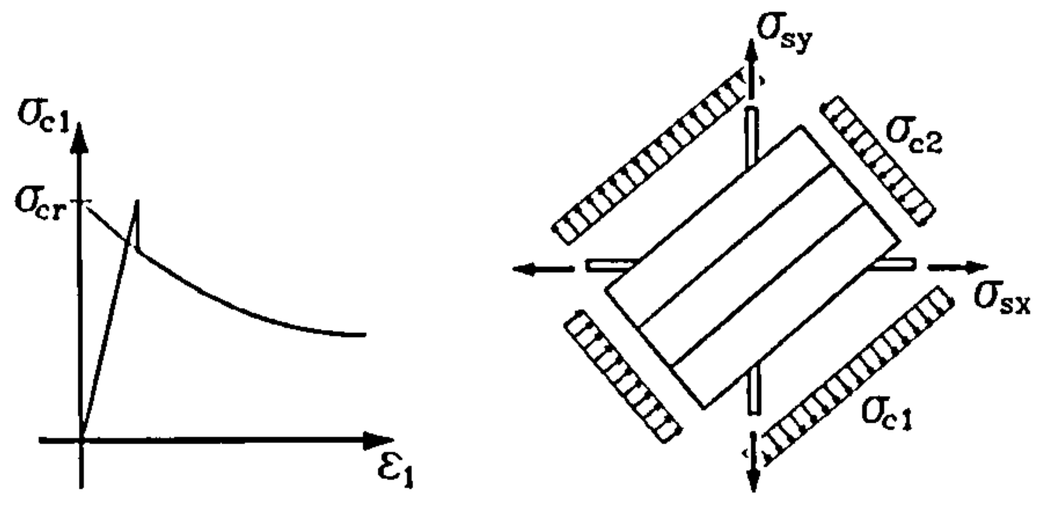

Fig.2.13 Equilibrium Conditions and Material Laws according to the MCFT

Fenwick/Paulay (1968), and later various other researchers, described aggregate interlock as an independent shear mechanism and Kupfer et al (1983) showed, that when aggregate interlock occurs, the principal direction of the concrete stresses must always deviate to a certain degree from the principal strain direction. Due to this fact, the MCFT could not treat aggregate interlock as an independent shear carrying action, but only as a mechanism which provides friction and compression stresses in the crack to enable the redistribution of tensile stresses from the concrete to the steel. Consequently, aggregate interlock was dealt with in a sort of postprocessing, which represents a check as to whether the stirrups were capable of carrying the additional load.

However, the increase of stirrup stresses in a crack is due to the loss of bond rather than the aggregate interlock action. This treatment of aggregate interlock restricted the MCFT to its application on reinforced concrete elements, which was not necessary, as shear transfer by aggregate interlock is not dependent on the presence of stirrups, as will be seen in Section 3.3.

Fig.2.13 shows a membrane element subjected to inplane stresses with the equilibrium conditions and also the material laws derived by Vecchio/Collins from their testing. It is assumed that shear forces are carried by the concrete alone, while normal forces are resisted by concrete and steel.

2.6 Kupfer's Shear Theory for Slender RC Beams

In 1983 Kupfer, Mang and Karavesyroglou published a paper in which they introduced a shear theory for slender RC beams similar to the MCFT, and in 1987 Kirmair and Mang released a companion paper treating the same theory in greater detail. The theory is based on the same assumption of a uniform stress and strain state in the web of an RC beam, but includes hook slip, loss of bond and shrinkage, and treats aggregate interlock in a more physical way. However, two major simplifications had to be introduced: The crack angle θ' was made an input quantity and has to be fixed before the start of each calculation and the strain in the horizontal beam axis direction ε_x was assumed to be constant over the web height. The aforementioned features restricted Kupfer's theory to distinctly T and I shaped cross sections, as will be seen later in Chapter 3 in more detail. In the following, for simplicity the theory will be referred to as Kupfer's shear theory, although it is well-known that his co-workers contributed to the theory in a substantial fashion. In contrast to the MCFT, Kupfer's theory dealt with aggregate interlock as an independent shear carrying action.

Fig.2.14 shows the truss model and an element of unit length with the forces acting on it and from the equilibrium of this element the given equations can be derived. The work of Walraven (1981) revealed that aggregate interlock depends largely on the mutual displacements of the surfaces of a crack. Therefore, to account for shear friction it was necessary to evaluate both v and w, which are the displacements in the crack direction and perpendicular to it, respectively. Kupfer was dealing with a truss model and assumed a uniform stress state, which means that the mutual crack displacements had to be smeared over the shear zone. The compatibility relations between the displacements v and w, and the strains ε_x, ε_y and γ_{xy} were derived by using Mohr's strain circle as depicted in Fig.2.15. The resulting strain state in the web was then obtained as the sum of the strain states of plain concrete and smeared cracks.

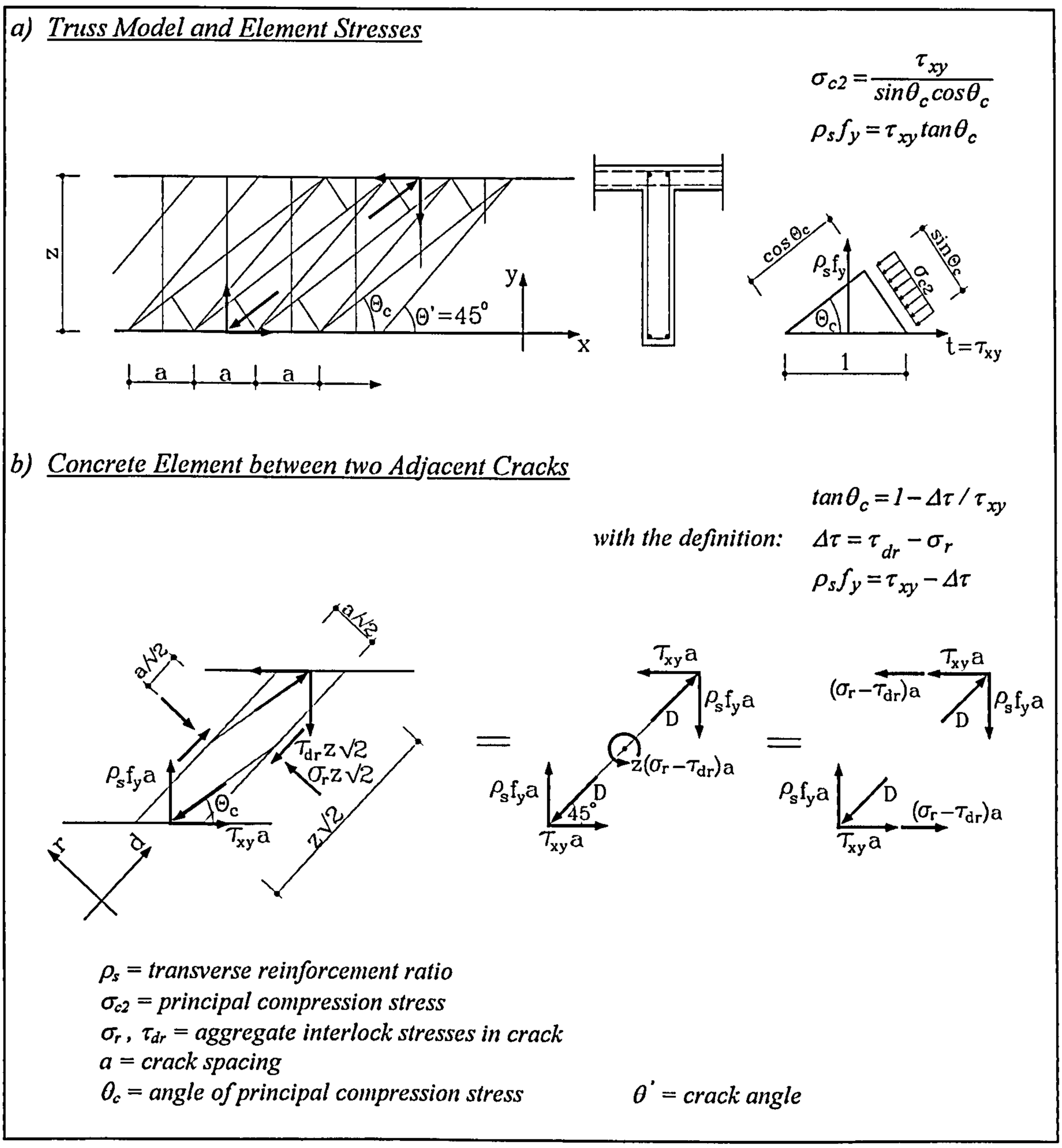

Fig.2.14 Truss Model according to Kupfer's Theory

For the special case of $\varepsilon_x = 0$ the equations for v and w were derived and are given in Fig.2.16. $\varepsilon_x = 0$ might be an acceptable simplification for non-prestressed reinforced concrete beams as in that case the strain in the compression chord has the same order of magnitude as the strain in the tension chord. Also in Fig.2.16 the Mohr's circles for the concrete strut and the web including the smeared cracks are depicted. In the equations for v and w, a is the crack spacing which is considered to have a constant value depending on the reinforcement ratio ρ_s and the diameter of the steel bars d_s. It is worth noting that Kupfer's approach explicitly needs the crack spacing a while the modified compression field theory does not. As already mentioned, this is because Vecchio/Collins did not treat aggregate interlock as an independent shear carrying action.

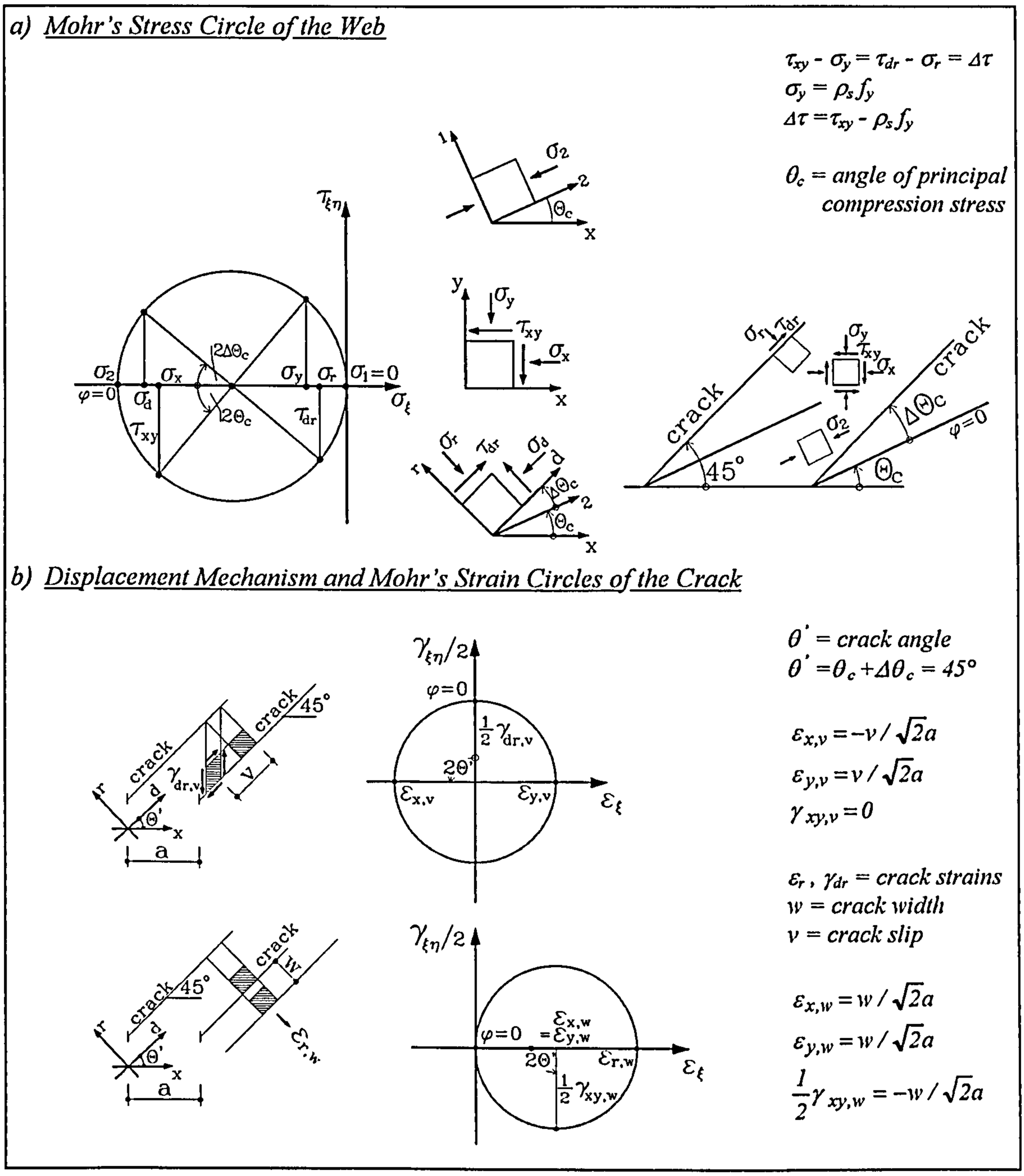

Fig.2.15 Stress State of Web and Strain State of Crack

The objective of Kupfer's theory is to calculate that proportion of shear which is not carried by stirrups. It was named $\Delta\tau$ and consists mainly of friction stresses τ_{dr} and compressive stresses σ_r perpendicular to them. Kupfer used the work of Walraven to calculate $\Delta\tau$. The constitutive equations for aggregate interlock as well as those for the concrete in compression are given in Fig.2.16.

a) Strain States of Plain Concrete and Complete Element

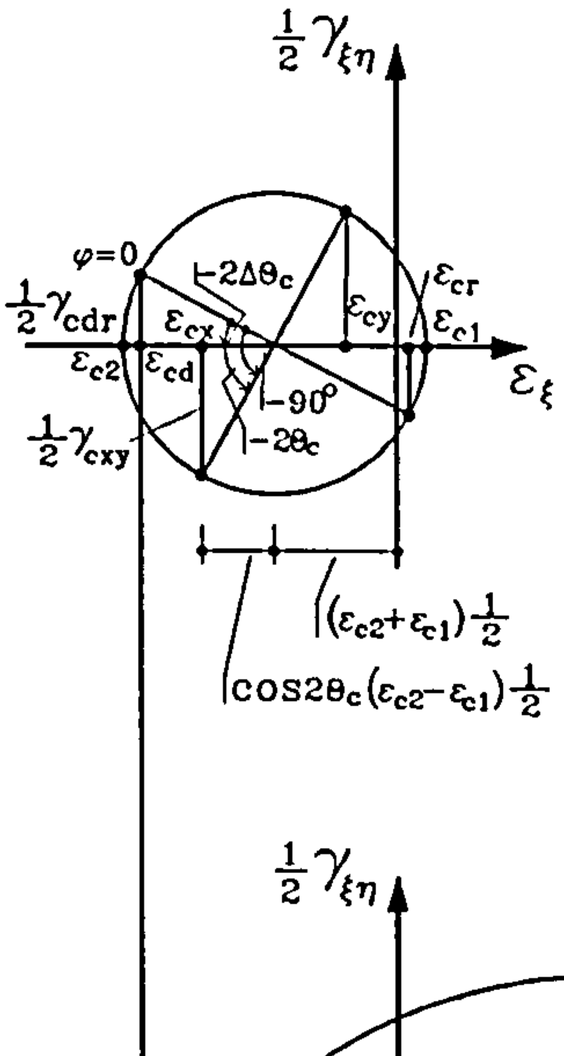

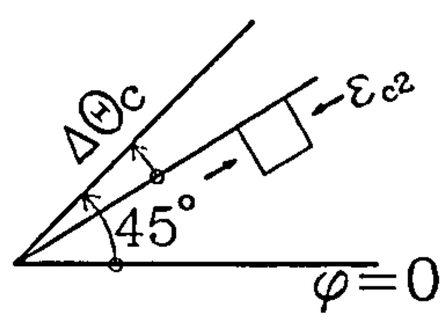

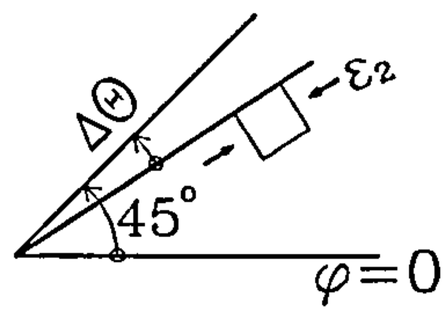

$$v = a/\sqrt{2}\left(\varepsilon_y + \varepsilon_{cx} - \varepsilon_{cy}\right)$$

$$w = a/\sqrt{2}\left(\varepsilon_y - \varepsilon_{cx} - \varepsilon_{cy}\right)$$

θ' = *crack angle* = 45°
θ_c = *angle of principal compr. stress* = *angle of principal compr. strain of plain concrete*
θ = *angle of principal compr. strain of complete element*

$$\varepsilon_d = \varepsilon_{cd} + \varepsilon_{d,v} + \varepsilon_{d,w}$$
$$\varepsilon_{d,v} = \varepsilon_{d,w} = 0$$
$$\varepsilon_d = \varepsilon_{cd}$$

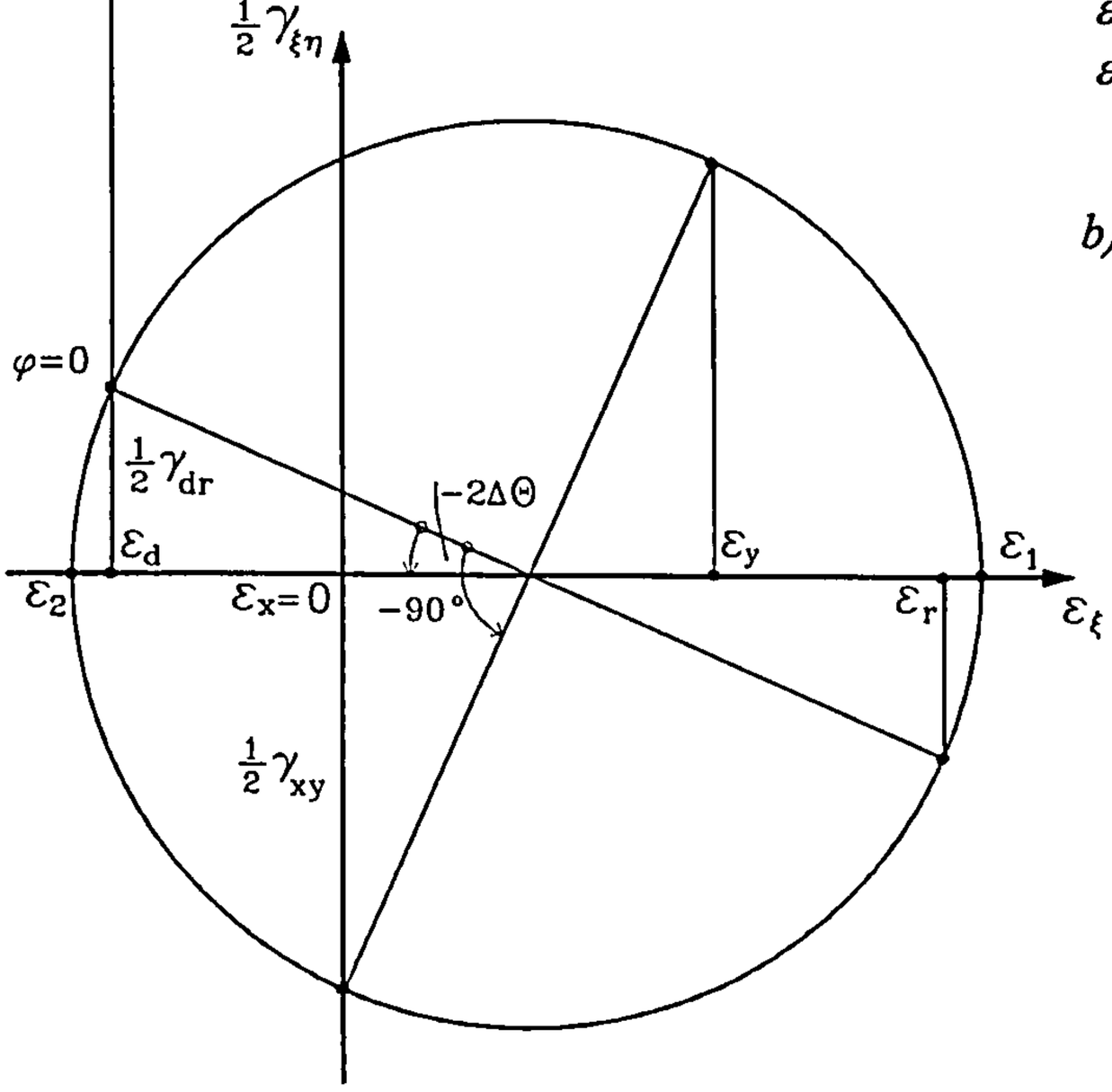

b) Crack Spacing

$$a = 0.15\frac{d_s}{\rho_s} \le 0.75z$$

c) Constitutive Equations

$$\frac{\Delta\tau}{f_c} = \left(0.017 + 0.1v/w\right) - 0.085v$$

$$\varepsilon_{c2} = \varepsilon_c'\left(1 - \sqrt{1 - \sigma_{c2}/0.67f_c}\right)$$

with $\varepsilon_c' = -0.002$

w = *crack width*
v = *crack slip*
$\Delta\tau$ = *shear stress not carried by stirrups*

$$\varepsilon_x = \varepsilon_{cx} + \varepsilon_{x,v} + \varepsilon_{x,w} = \varepsilon_{cx} - v/\sqrt{2}a + w/\sqrt{2}a = 0$$

$$\varepsilon_y = \varepsilon_{cy} + \varepsilon_{y,v} + \varepsilon_{y,w} = \varepsilon_{cy} + v/\sqrt{2}a + w/\sqrt{2}a$$

Fig.2.16 Strain State of Plain Concrete and Complete Element Including Cracks

Abandoning the assumption that the principal compression stress direction of the concrete coincides with the principal direction of the compressive strains in the web generates three different angles in Kupfer's theory, which in the MCFT are altogether the same: The crack angle θ', the angle of the principal compression stress in the concrete θ_c and the angle of the principal compression strain in the web θ. It becomes obvious from this fact alone that Kupfer's theory is a rather complicated one and, therefore, θ' was treated as an input quantity making the theory more attractive, but also detracting from a part of its sophistication. It will be seen later in Chapter 3 that the complexity of the shear model triggered out by the dropping of simplifications leads to further problems, not yet solved in a satisfying way.

2.7 Limit Analysis

In this chapter a shear theory which has become known as limit analysis will be briefly reviewed. It was promoted by Thürlimann in Zurich and Nielsen in Copenhagen. The teams around both researchers developed design procedures based on concrete plasticity, but introduced slightly different compatibility considerations. Therefore, the summary given in this report includes both derivations, which have been taken from papers published by Grob/Thürlimann in 1976 and Nielsen/Braestrup/Bach in 1978. For the sake of simplicity the limit analysis procedures are here referred to as Thürlimann's or Nielsen's approach, although it is well-known that many other researchers have contributed to the development of the plasticity theory for concrete.

In precisely the same way as the CFT or Kupfer's shear theory, the limit analysis was derived from considerations of a multiple truss smearing its stirrups over the web and assuming a principal compressive stress state inclined at a certain angle θ_c. Fig.2.17.(a) shows a shear wall element with the forces acting on it. According to the lower bound theorem, Thürlimann calculated the shear resistance of the cross section and the resistance of the tensile reinforcement by assuming yielding of the transverse and longitudinal reinforcement. Substituting θ_c in Eqs.(2.16) and (2.17) leads to a bending-shear interaction relationship, which is depicted in Fig.2.17.(c).

Thürlimann assumed the strain state in the web as shown in Fig.2.18.(a). The deformations were considered to stem from the elongation of the reinforcement, while the concrete was expected to be rigid. For $\varepsilon_2 = \varepsilon_d = 0$ this yielded the well-known compatibility equation $tan^2\theta_c = \varepsilon_x/\varepsilon_y = \varepsilon_L/\varepsilon_B$. The principal tensile strain $\varepsilon_1 = \varepsilon_R$ is linked to the strain in x and y direction through equations $\varepsilon_1 sin^2\theta_c = \varepsilon_R sin^2\theta_c = \varepsilon_x = \varepsilon_L$ and $\varepsilon_1 cos^2\theta_c = \varepsilon_R cos^2\theta_c = \varepsilon_y = \varepsilon_B$. In Fig.2.18.(b) these relations are illustrated for yielding of each reinforcement.

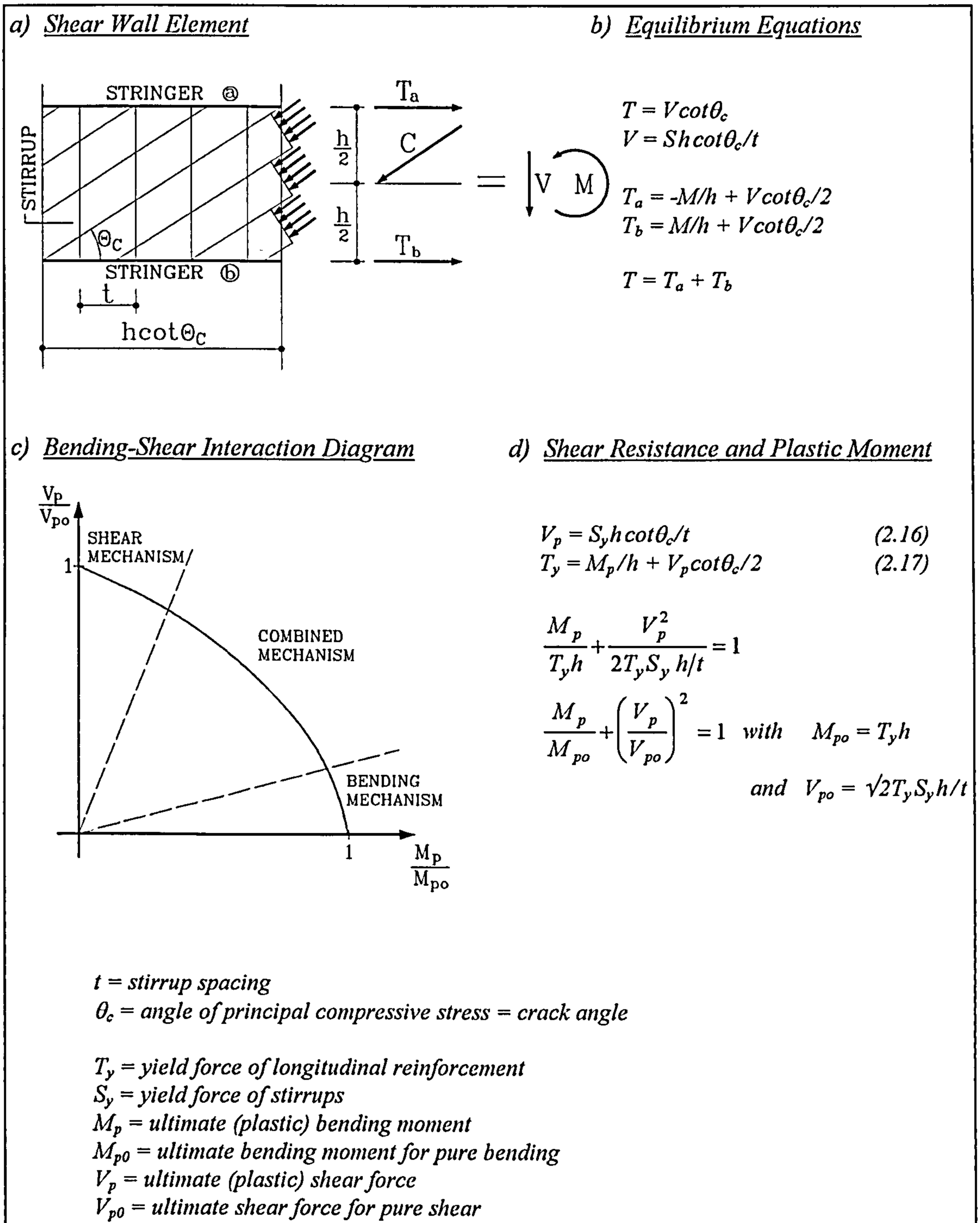

Fig.2.17 Shear Wall Element according to Grob/Thürlimann (1976)

Thürlimann restricted the angle of the compression field to values in the range of $0.5 \leq \tan\theta_c \leq 2.0$, derived by testing and he gave a physical explanation by means of the crack model depicted in Fig.2.18.(c). It can be seen from this model that for values $\tan\theta_c \leq 0.5$ and for yielding of the stirrups no aggregate interlock can occur. The same is valid for high values $\tan\theta_c \geq 2.0$ and for yielding of the longitudinal reinforcement. Both features were referred to as shear and bending mechanism, respectively.

a) Strain State in the Web of a Shear Wall Element

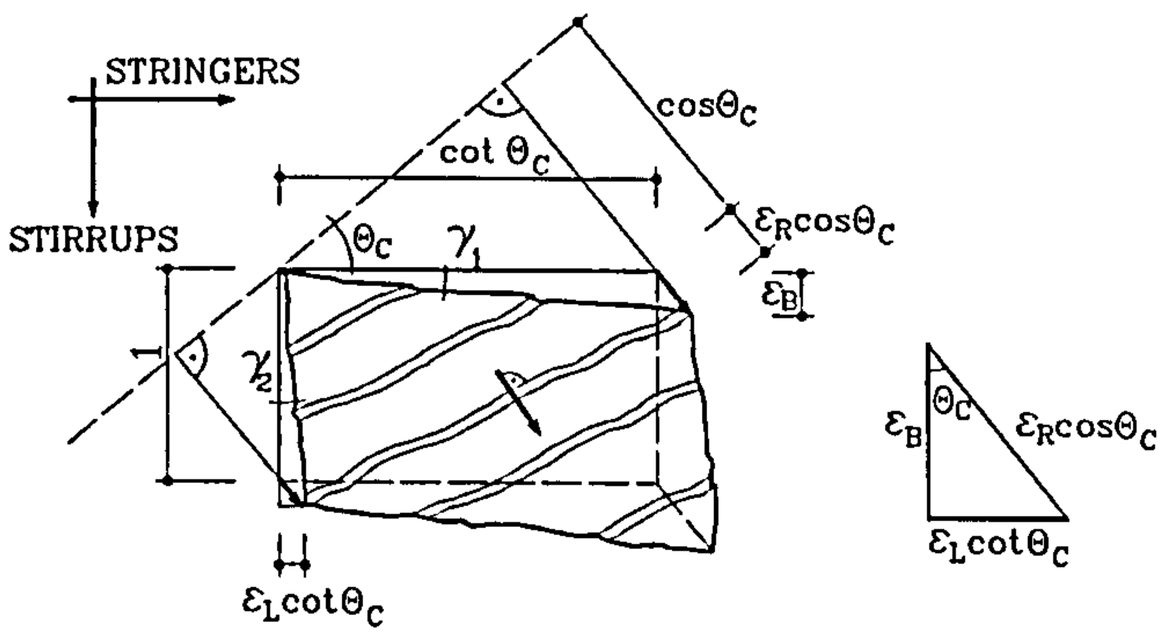

$$\gamma = \gamma_1 + \gamma_2 = \varepsilon_L \cot\theta_c + \varepsilon_B \tan\theta_c$$

$$\varepsilon_B = \varepsilon_L \cot^2\theta_c \rightarrow \tan^2\theta_c = \varepsilon_L/\varepsilon_B$$

$$\varepsilon_R \sin^2\theta_c = \varepsilon_L \qquad \varepsilon_R \cos^2\theta_c = \varepsilon_B \rightarrow$$
$$\varepsilon_R = \varepsilon_L + \varepsilon_B = 1.\ Inv.\ of\ strain\ tensor$$

b) Principal Strain ε_R Depending on the Inclination Angle θ_c

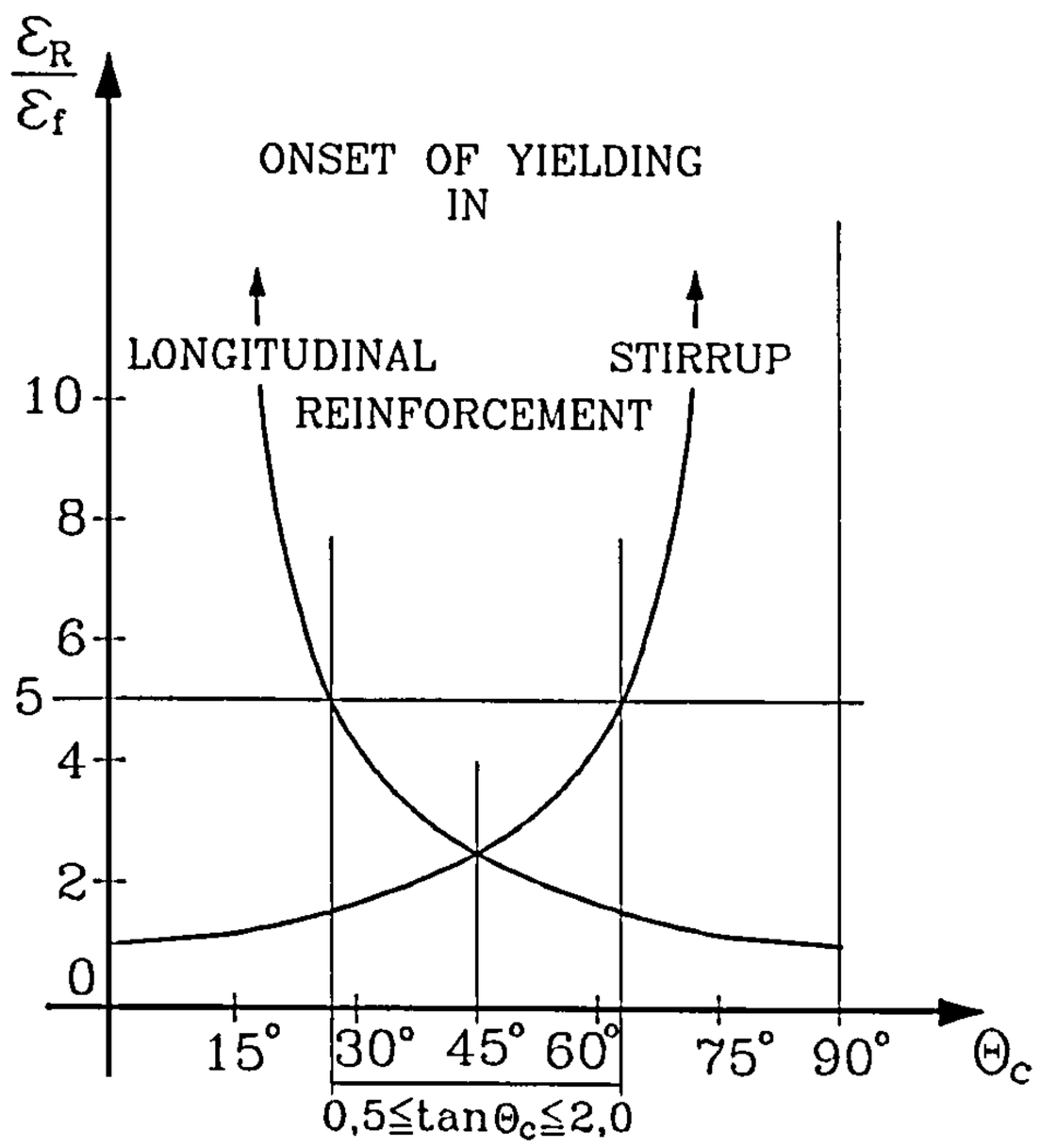

c) Crack Model for Various Angles θ_c

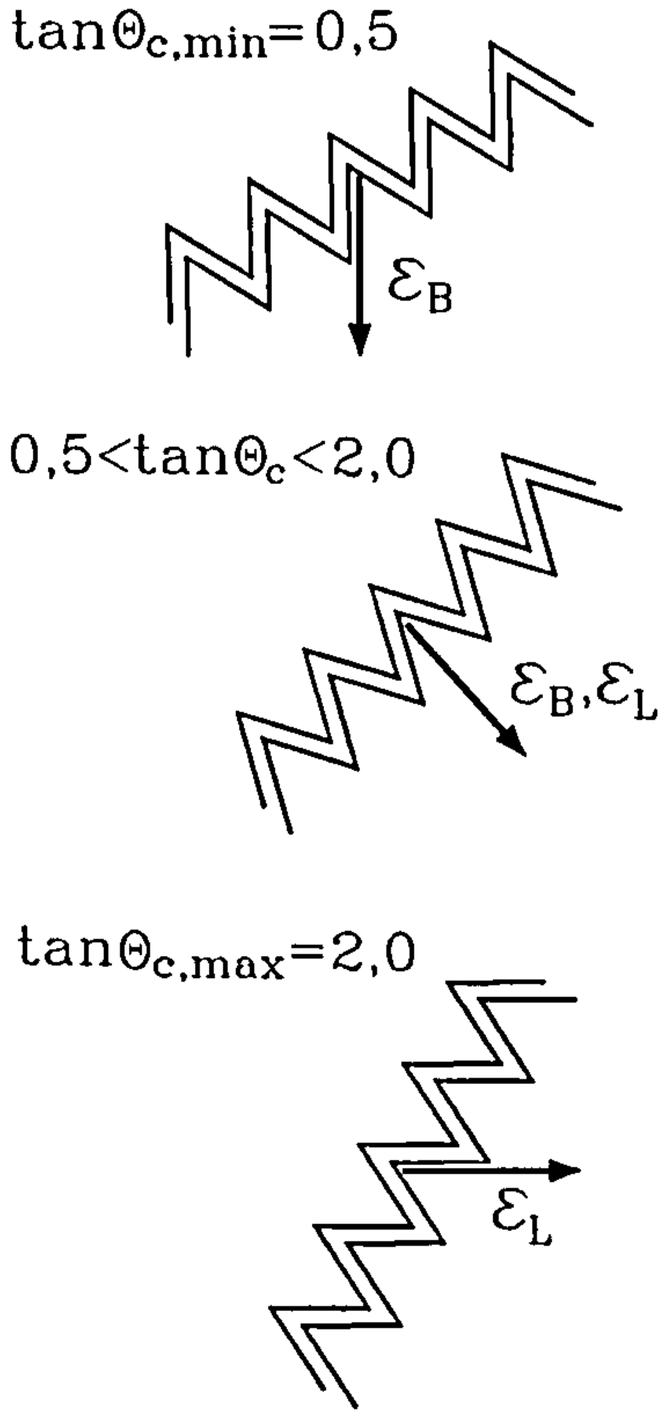

Yielding of longitudinal reinforcement: $\varepsilon_R = \varepsilon_f (1+\cot^2\theta_c)$
Yielding of transverse reinforcement: $\varepsilon_R = \varepsilon_f (1+\tan^2\theta_c)$

ε_R = *principal tensile strain = displacement parameter*
ε_f = *yield strain of reinforcing steel*
ε_L , ε_B = *stringer and stirrup strain, respectively*

Fig.2.18 Strain State and Limitation for the Crack Angle

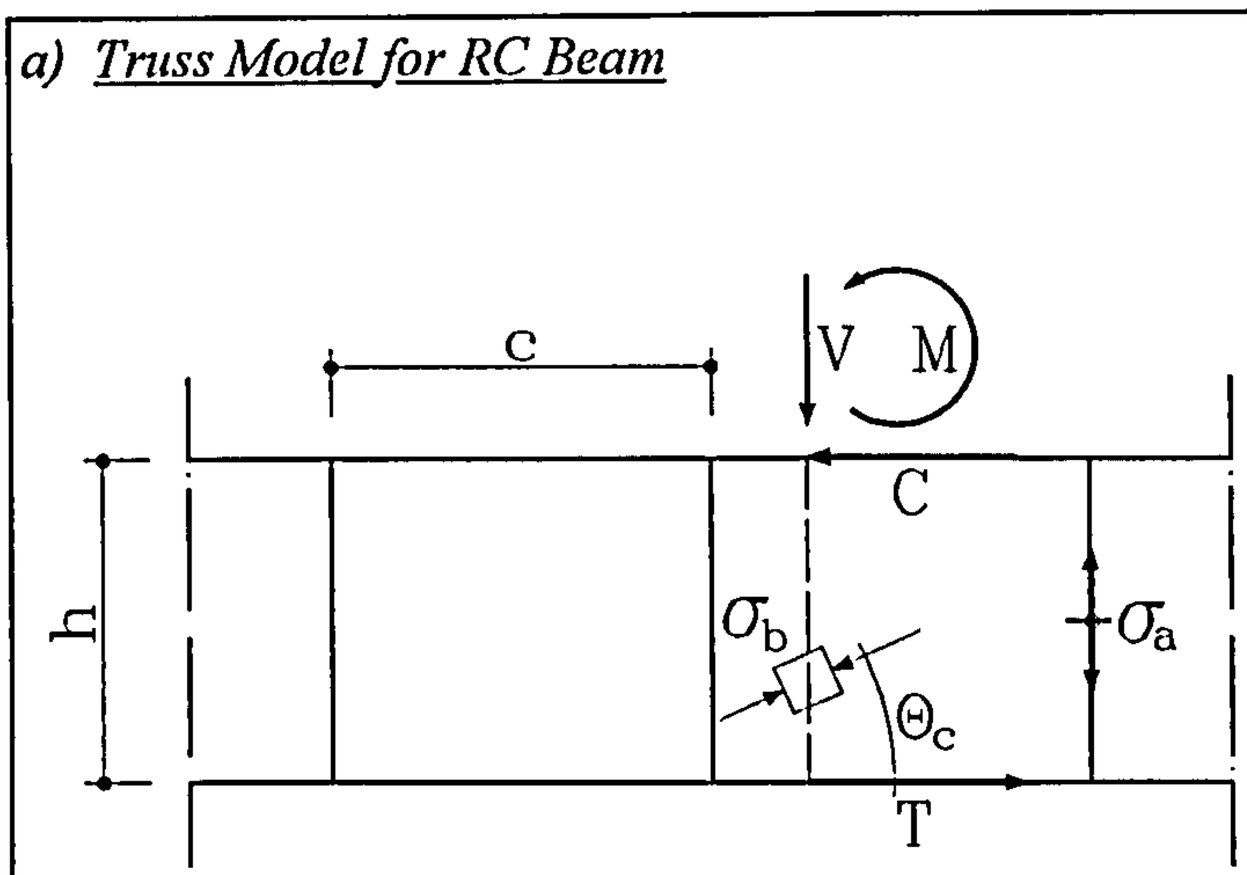

Fig.2.19 Truss Model and Shear Resistance according to Nielsen et al (1978)

If $\tan\theta_c$ is in the given range of $0.5 \div 2.0$ yielding of both reinforcements is necessary for the occurrence of a combined mechanism. However, if only one of both reinforcements yields, then the crack surfaces will interlock and hence, friction stresses can be generated, thus avoiding a premature shear failure. All three regions are distinguished in Figure 2.17.(c), separated from each other by dashed lines.

From the limit analysis procedures briefly reviewed here simple design rules were derived and incorporated in the Swiss standard SIA 162, making it, at that time, a modern code based on a realistic, physical model.

Nielsen used the same truss model as Thürlimann for his approach to limit analysis. Fig.2.19.(a) shows the truss model consisting of a top and bottom chord, an inclined compression field and smeared stirrups, and Fig.2.19.(b) the equilibrium equations derived from it. For simplicity the transverse reinforcement here is assumed to be vertically arranged. By introducing material properties according to the theory of plasticity the shear strength is given by Eqs.(2.18) or (2.19). From Eq.(2.18) one can read that the shear resistance increases with decreasing values of θ_c. This is illustrated in Fig.2.19.(c) and it is obvious that cross section *II* gives a higher stirrup yield force than cross section *I*. However, the increase in shear resistance is at the cost of higher forces in stringers and compression struts. This feature can also be interpreted as the ability of an RC structure to sustain an increase in load by adjusting the inclination angle θ_c, provided the stringers and compression struts are not exhausted. This is in line with the lower bound of the theory of plasticity and was utilised by Nielsen to establish his web failure criterion, which was used instead of a compatibility equation to determine θ_c.

Eliminating θ_c from Eqs.(2.19) and (2.20) yields Nielsen's web failure criterion, which is given by Eq.(2.21) for stirrup yielding and Eq.(2.22) when the transverse reinforcement does not reach f_y. The inclination angle for stirrup yielding becomes $cot\theta_c = \sqrt{\nu f_c/\rho_{sy} f_y} - 1$ while $cot\theta_c = 1$ is valid for $\sigma_{sy} < f_y$. Nielsen verified the web failure criterion with the upper bound method of the plasticity theory by assuming a failure mechanism with yield lines inclined at an angle $\beta = 2\theta_c$. By adjusting the web effectiveness ratio of the concrete under compression to a value of $0.75 \leq \nu \leq 0.85$ he successfully recalculated shear tests described in the literature. However, the specimens were all moderately reinforced in shear. For beams with weak or no shear reinforcement the inclination angle of the compression struts becomes very small and the truss degenerates to a strut and tie mechanism. Nevertheless, Nielsen applied his theory on RC beams without transverse reinforcement. His statement that 'beams without stirrups fail in shear by diagonal tension without any apparent truss action' should obviously provide evidence for strut and tie action and the suitability of his theory, but was a misinterpretation of diagonal tension failure. Evidence for this criticism of Nielsen's statement is provided hereafter in a qualitative manner.

It has been well-known since the work of Fenwick/Paulay (1968) that the shear resistance of an RC beam without stirrups depends strongly on the tensile strength of the concrete. Walraven (1981) showed how tension is transferred across cracks and Reineck (1991) modelled a beam without shear reinforcement qualitatively with a truss, the ties of which are provided by the tensile strength of the concrete. The capacity of these tensile ties is given by aggregate interlock stresses dependent on the crack width. Once the deterioration of the web concrete has progressed and the failure crack has formed the aggregate interlock mechanism will fail, resulting in the sudden collapse of the beam.

It will be seen later in Chapter 3, where arch action is briefly investigated, that in beams without stirrups ribbed longitudinal steel bars force the web to build a truss mechanism by activating the tensile strength of the concrete. Series EA to GB of the Stuttgart shear tests (1964) provide evidence for this truss although this was not explicitly stated in Leonhardt's test evaluation.

3 Investigations on the Local Element Level

3.1 Some Basic Remarks

As already mentioned in the introduction to this work, shear theories usually describe the behaviour of cracked reinforced concrete on a local element level and it is on this local level where effectiveness and reliability of a shear theory have to be checked. Intrinsically, the CFT was conceived as a multiple truss model by smearing struts and ties over the structure, creating a uniform stress state in the web, which is represented by a compression field, inclined under a certain angle. This approach was further developed in the MCFT by additionally smearing the chords, thereby generating a membrane element with equal compatibility characteristics. Changing stress and strain conditions, for instance in a flexural member due to bending, can be modelled by splitting up the structure into elements of any necessary size.

It is obvious that this concept is similar to the way in which the FE method approaches the analysis of a structure. Therefore, the MCFT provides basic features, necessary for the implementation of a shear model in an FE program, in a quite natural fashion. Moreover, as will be seen later, the MCFT incorporates secondary shear carrying actions, like aggregate interlock or dowel action, in an intrinsic manner, thus avoiding a conceptual weakness of the FEM, which is the proper treatment of local effects connected with the behaviour of cracked reinforced concrete.

For the above reasons it was intended to implement the MCFT in an FE package (see Section 4.2), providing the theory covers the main features of shear transfer in a reasonable way. Therefore, in the following sections of Chapter 3, checks on the MCFT are described which should reveal whether the MCFT is a reliable theory on a local section analysis level. These checks are supplemented by comparisons with other shear theories and by some general investigations on mechanisms like arch action or the size effect, which are not implicitly covered by the material laws of the MCFT.

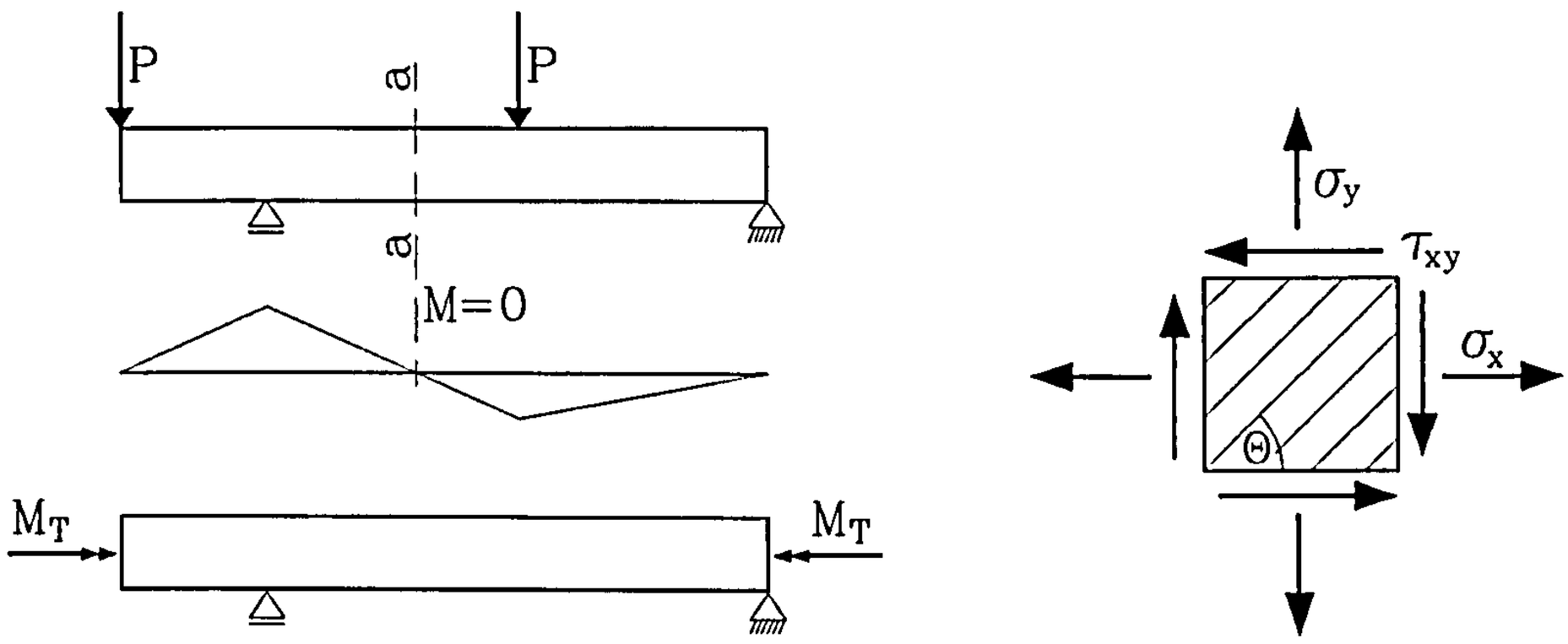

Fig.3.1 Comparison of Features of CFT and MCFT

3.2 CFT and MCFT Trusses

It was stated earlier that the CFT and the MCFT were derived from multiple trusses and it is desirable for the understanding of the theories to get to know what sort of trusses these are and how they react under load. Therefore, a cross section was subjected to a shear force and the response calculated at various load levels according to both theories.

Fig.3.2.(c) shows the system data of the beam and Fig.3.2.(a) and (b) two sets of equations, one according to each theory. The CFT set consists of *4* equilibrium, *1* compatibility and *3* constitutive equations. These *8* equations match the *8* unknowns N, θ_c, σ_{c2}, σ_{sx}, σ_{sy}, ε_2, ε_x *and* ε_y. The MCFT set, however, consists of *4* equilibrium, *2* compatibility and *5* constitutive equations and these *11* equations match the *11* unknowns N, θ_c, σ_{c1}, σ_{c2}, σ_{c2max} σ_{sx}, σ_{sy}, ε_1, ε_2, ε_x *and* ε_y. It is obvious that the number of equilibrium equations remained the same, while the constitutive set had to be extended because of the introduction of the tensile strength of the concrete. The second compatibility equation is only the first invariant of the strain tensor and was not needed in the CFT set. The introduction of the tensile strength of the concrete can be interpreted as an additional tensile tie in the truss model for the MCFT. Fig.3.3 shows both the determinate CFT and the indeterminate MCFT truss and the calculations carried out with these two shear models are summarised in Tab.3.1.

a) Set of Equations According to CFT

$N = V/\tan\theta_c$

$\sigma_{c2} = V/(b\ d \sin\theta_c \cos\theta_c)$

$A_t\ \sigma_{sy} = V\ s\ \tan\theta_c/d$

$\sigma_{sx} = N/(A_1+A_1')$

$$\tan^2\theta_c = \frac{\varepsilon_2 - \varepsilon_x}{\varepsilon_2 - \varepsilon_y}$$

$$\sigma_{c2} = f_c\left[2\frac{\varepsilon_2}{\varepsilon_c'} - \left(\frac{\varepsilon_2}{\varepsilon_c'}\right)^2\right]$$

$\sigma_{sx} = E_s\ \varepsilon_x \quad , \quad \sigma_{sy} = E_s\ \varepsilon_y$

N = *normal force in concrete triggered by* V

b) Set of Equations According to MCFT

Equilibrium:

$V = \sigma_{c2}\ b\ d \sin\theta_c \cos\theta_c + \sigma_{c1}\ b\ d \sin\theta_c \cos\theta_c$

$N = \sigma_{c2}\ b\ d \cos^2\theta_c - \sigma_{c1}\ b\ d \sin^2\theta_c$

$V = A_t\ \sigma_{sy}\ d/(\tan\theta_c\ s) + \sigma_{c1}\ b\ d/\tan\theta_c$

$\sigma_{sx} = N/(A_1+A_1')$

Compatibility:

$$\tan^2\theta_c = \frac{\varepsilon_2 - \varepsilon_x}{\varepsilon_2 - \varepsilon_y} \quad , \quad \varepsilon_x+\varepsilon_y = \varepsilon_1+\varepsilon_2$$

Material:

$$\sigma_{c2} = \sigma_{c2max}\left[2\frac{\varepsilon_2}{\varepsilon_c'} - \left(\frac{\varepsilon_2}{\varepsilon_c'}\right)^2\right]$$

$$\sigma_{c2max} = f_c\frac{1}{0.8 - 0.34\varepsilon_1/\varepsilon_c'}$$

$$\sigma_{c1} = \frac{f_{ct}}{1+\sqrt{200\varepsilon_1}} \quad or \quad \sigma_{c1} = E_c\ \varepsilon_1$$

$\sigma_{sx} = E_s\ \varepsilon_x \quad , \quad \sigma_{sy} = E_s\ \varepsilon_y$

c) System Data

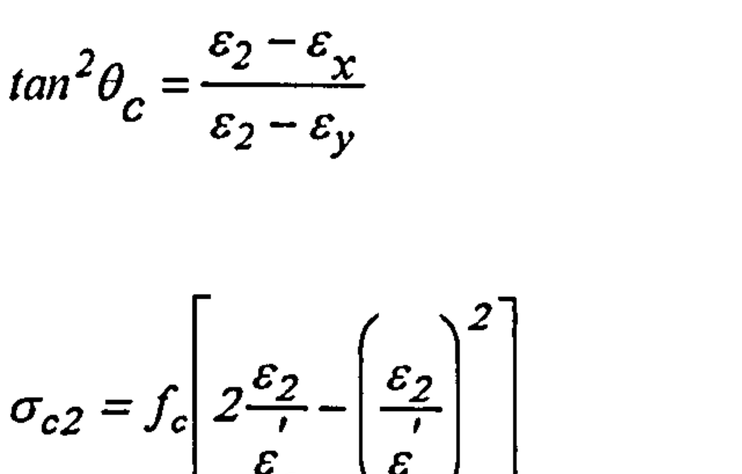

$b = 200\ mm \quad d = 283\ mm \quad f_c = 20\ MPa$

$h = 400\ \text{“} \quad s = 100\ \text{“} \quad f_y = 400\ \text{“}$

$A_1 = A_1' = 500\ mm^2$

Fig.3.2 Comparison of CFT and MCFT

The calculations according to the MCFT were performed using two different values for the tensile strength of the concrete. At first f_{ct} was set to $1.5MPa$ which is equal to a value of $0.33\sqrt{f_c}$. This value was used by Vecchio/Collins (1982) for the recalculation of their PV panel tests and in fact, they calibrated their material laws for concrete in tension on this value which is the provision of the ACI, although they did not explicitly comment on that. However, it will be seen later in Section 3.4 that a tensile strength of $0.33\sqrt{f_c}$ is not suitable in all cases were structural members are analysed with the MCFT. For instance, RC beams with stirrups which are subjected to flexure with shear need a higher value for the tensile strength of the concrete. It was found that a value of $f_{ct} = 0.75\sqrt{f_c}$ yields reasonable results and was, therefore, taken for a second set of calculations also depicted in Tab.3.1.

	V [kN]	50	100	150	200	250	300
CFT	θ_c [°]	27.5	33	37	39.5	41.5	43.2
	ε_1 [‰]	2.6	3.0	3.3	3.6	3.9	4.2
	ε_2 "	-0.1	-0.2	-0.3	-0.4	-0.5	-0.6
	σ_{c1} [MPa]	0.0	0.0	0.0	0.0	0.0	0.0
	σ_{c2} "	-2.2	-3.9	-5.5	-7.2	-8.9	-10.6
	σ_{sx} "	95	155	200	245	285	320
	σ_{sy} "	400	400	400	400	400	400
MCFT $f_{ct} = 1.5\,MPa$	θ_c [°]	45	43.8	43.3	43.2	43.2	43.2
	ε_1 [‰]	0.045	0.6	1.4	2.2	3.1	4.1
	ε_2 "	-0.045	-0.1	-0.2	-0.4	-0.6	-1.0
	σ_{c1} [MPa]	0.9	1.1	1.0	0.9	0.8	0.8
	σ_{c2} "	-0.9	-2.5	-4.4	-6.2	-8.0	-9.8
	σ_{sx} "	0.0	40	105	165	220	280
	σ_{sy} "	0.0	50	125	195	270	340
MCFT $f_{ct} = 3.4\,MPa$	θ_c [°]	45	45	45	43.8	43.5	43.4
	ε_1 [‰]	0.045	0.09	0.14	1.1	2.1	3.0
	ε_2 "	-0.045	-0.09	-0.14	-0.3	-0.5	-0.7
	σ_{c1} [MPa]	0.9	1.8	2.7	2.3	2.0	1.9
	σ_{c2} "	-0.9	-1.8	-2.7	-4.8	-6.9	-8.7
	σ_{sx} "	0.0	0.0	0.0	80	150	210
	σ_{sy} "	0.0	0.0	0.0	90	180	250

Tab.3.1 Comparative Calculations with CFT and MCFT

For the calculations described in Tab.3.1 the stirrup reinforcement was not kept constant but was increased from load stage to load stage. For the analyses carried out according to the CFT ρ_{sy} was taken to that value which for each load level ensured the onset of stirrup yielding. The MCFT calculations were then performed with the same transverse steel ratio ρ_{sy}.

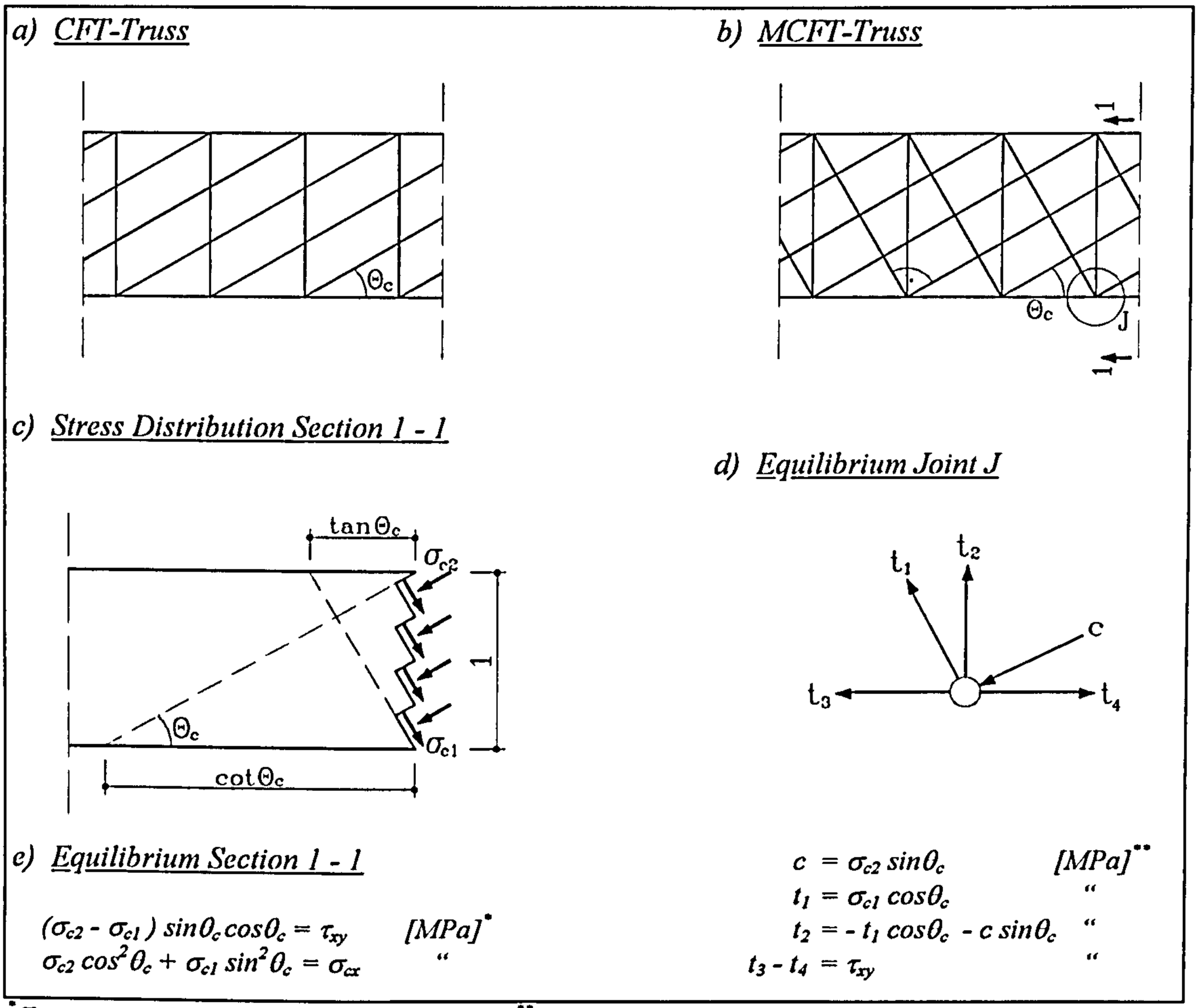

* Force per mm beam height h and beam width b; ** Force per mm beam length l and beam width b

Fig.3.3 Truss Models for CFT and MCFT

Some conclusions can be drawn by examining Tab.3.1. When applying the MCFT at low load levels the structure remains uncracked and behaves like an elastic isotropic material. For a tensile strength of *3.4 MPa* it will even respond elastically nearly throughout the whole serviceability range, while the CFT analysis gives the response of a heavily cracked beam with yielding of the stirrup reinforcement at every load level. However, with increasing load the differences in the results reduce.

At the ultimate limit, which (for the CFT calculation) was reached slightly above *300kN*, the CFT and the MCFT results with the lower tensile strength showed a rather similar structural behaviour although some differences remained. For the MCFT runs with a high, but reasonable, tensile strength of *3.4 MPa* the differences with the CFT results remained more distinct. Ultimate limit was attained for $f_{ct} = 1.5\ MPa$ at a load stage of *340 kN* and for $f_{ct} = 3.4\ MPa$ at *370 kN*, which is *10%* and *20%* more than the CFT value, respectively. This shows that the introduction of the tensile strength of the concrete relieves the stirrups and increases the section resistance. This is in line with the interpretation of the tensile strength as an additional truss member.

The above investigation provides evidence for the earlier statement that the significance of the MCFT seems to be more on the serviceability level than at the ultimate limit and in fact, this level is important for the evaluation of the ductility as the displacement at the onset of yielding is governed by the tensile strength of concrete.

3.3 The Treatment of Aggregate Interlock in the MCFT

When a reinforced concrete beam is subjected to a slowly increasing load, it will initially behave like an elastic, isotropic material carrying its internal forces by means of principal compression and tension stresses. Once cracks have started occurring a redistribution of forces takes place which goes on until the ultimate limit is reached. This redistribution mainly happens in cracks by transferring concrete stresses to the steel, and is possible because a cracked reinforced concrete beam can be considered as being an extremely indeterminate structure. In addition, in cracks friction forces are often generated, which are part of the redistribution process that transforms a beam, step by step, into a truss like structure. Fenwick/Paulay (1968) recognised that crack friction is an important and independent shear carrying mechanism and that it takes place when, due to the mutual displacement of the crack surfaces, the aggregate particles of the concrete are forced to interlock in each other. Kupfer et al (1983) showed that due to this aggregate interlocking, the principal concrete stresses always deviate to a certain degree from the principal strain direction.

a) Unreinforced Element

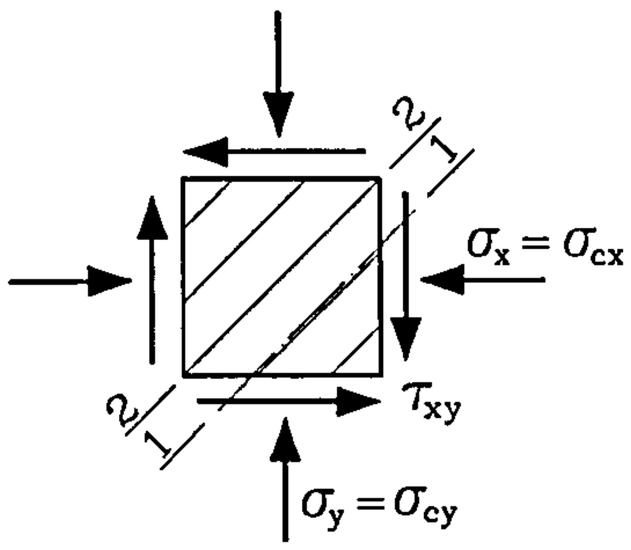

b) Stress Distribution in an Unreinforced Element for $\theta' \neq \theta_c$

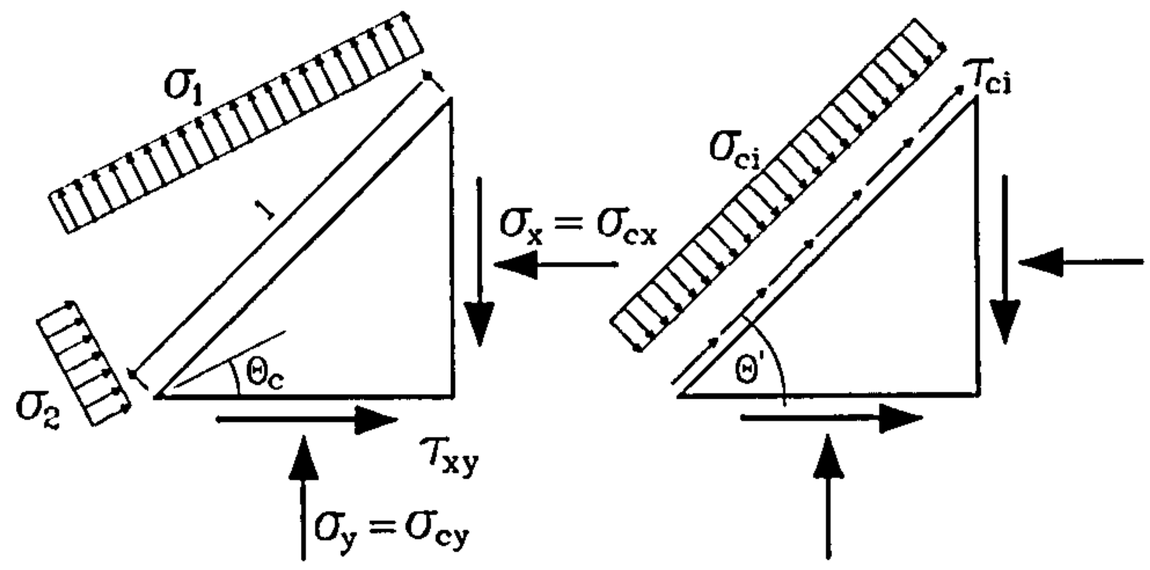

c) Stress Distribution in an Unreinforced Element for $\theta' = \theta_c$

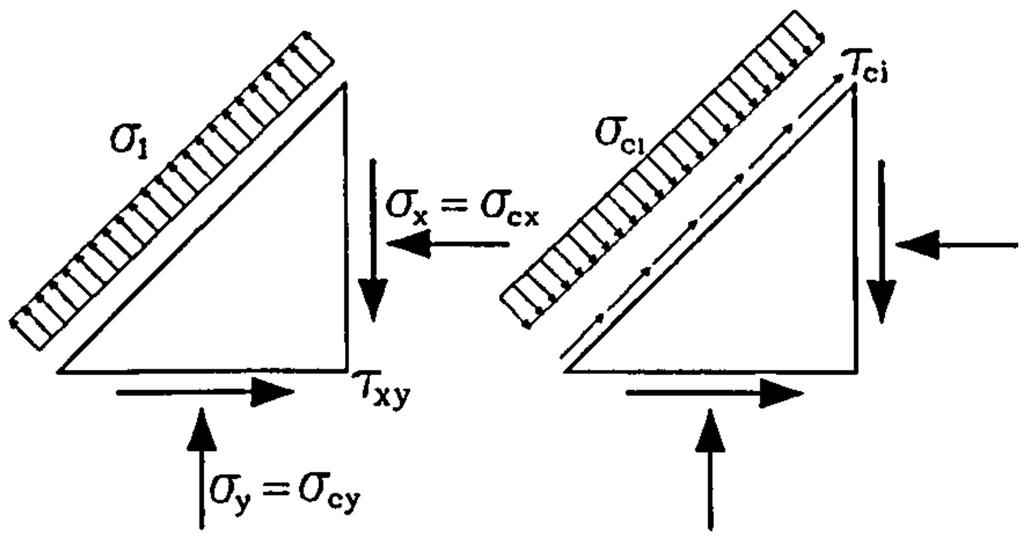

d) Equilibrium in an Unreinforced Element for $\theta' \neq \theta_c$

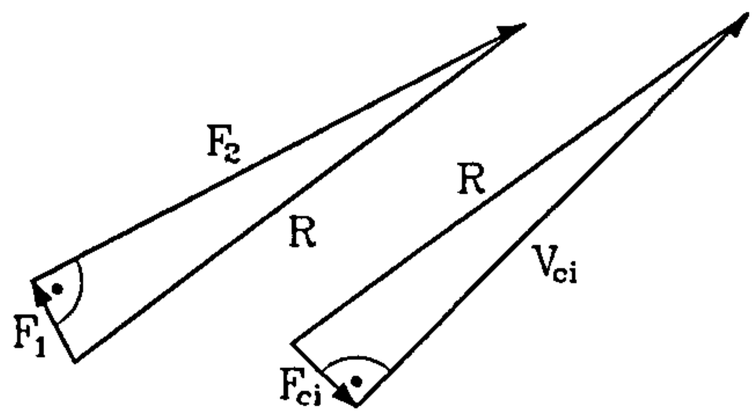

$F_1 = \sigma_1 \cos(\theta' - \theta_c) \cdot 1$
$F_2 = \sigma_2 \sin(\theta' - \theta_c) \cdot 1$
$F_{ci} = \sigma_{ci} \cdot 1 \cdot 1 \qquad V_{ci} = \tau_{ci} \cdot 1 \cdot 1$
R = resultant of section forces

e) Transversely Reinforced Element

f) Stress Distribution in an Tranversely Reinforced Element for $\theta' = \theta_c$

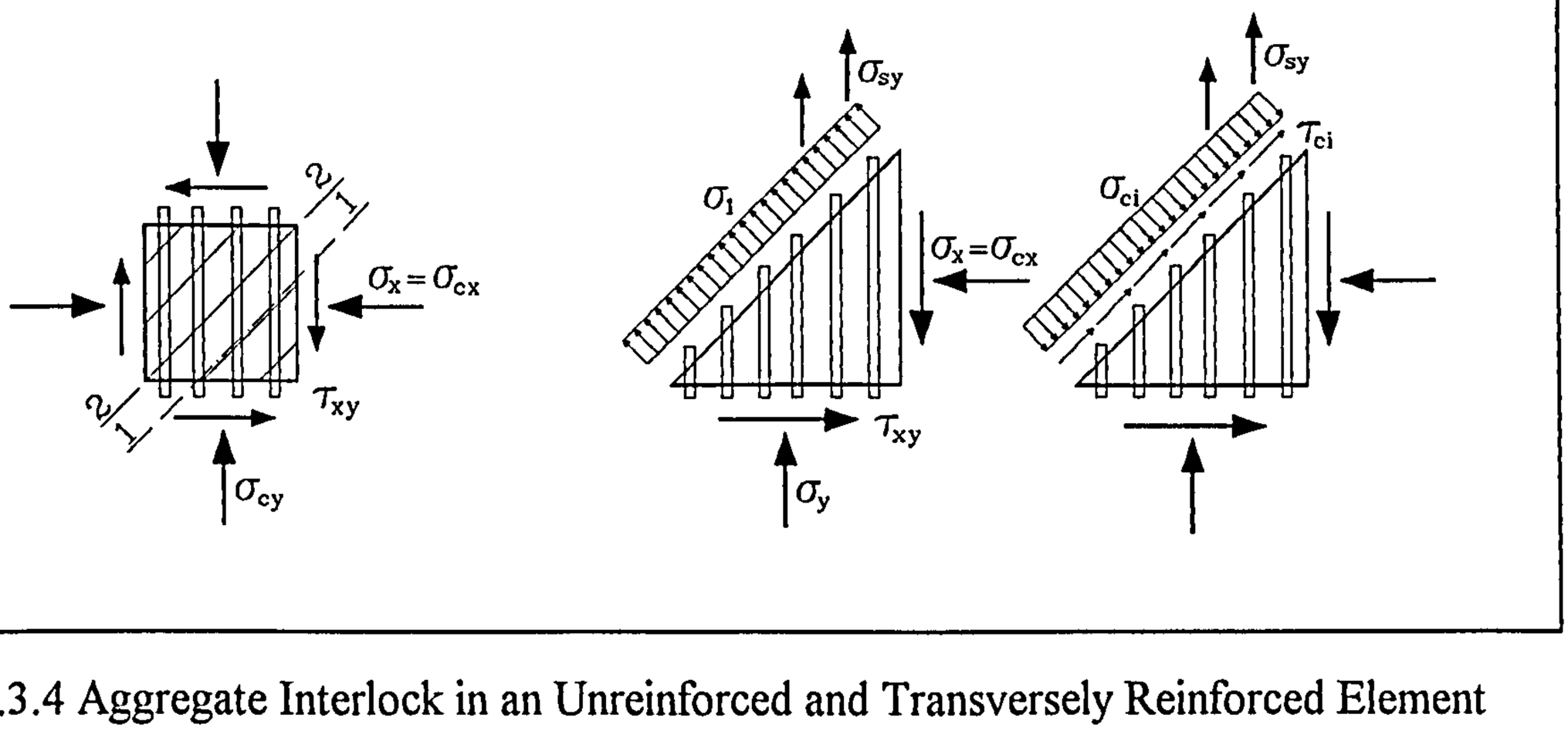

Fig.3.4 Aggregate Interlock in an Unreinforced and Transversely Reinforced Element

It was stated earlier that the MCFT assumes the principal stress direction of the concrete being coincident with the principal strain direction of the structural member and this is why Vecchio/Collins could not treat aggregate interlock as an independent shear mechanism. An investigation of the aggregate interlock procedure in the MCFT, briefly described below, reveals that for the equilibrium in a crack, both transverse and longitudinal reinforcement is necessary. However, this is against the nature of aggregate interlock as an original shear carrying action which is not dependent on the presence of reinforcement, as was proved by the work of Walraven (1981). For that reason, in the MCFT the aggregate interlock forces could not be part of the statically indeterminate section analysis process.

This will now be explained using an unreinforced and a transversely reinforced element, typically found in the web of a beam. Fig.3.4 gives details of both elements under investigation. The free body diagrams belonging to cross sections *1-1* reveal the stress state between two adjacent cracks, while the free body diagrams which belong to cross sections *2-2* show the stress state in a crack. Assuming that the free bodies *1-1* are all in equilibrium, then the free bodies *2-2* must also be in equilibrium, as the distance between the two cross sections can be infinitely small and the applied element load is for both the same. It is obvious that only for $\theta' \neq \theta_c$ equilibrium of the free bodies *2-2* can be achieved. This proves that in the absence of either longitudinal or any other reinforcement, equilibrium cannot be ensured, as long as the friction stresses τ_{ci} are assumed to act as depicted. However, a change of the direction of τ_{ci} would violate the physical reality. Therefore, Fig.3.4 gives evidence that, even though the element is unreinforced, aggregate interlock is able to transfer a certain amount of shear over a crack, provided the crack angle deviates to a certain amount from the angle of the principal stress direction of the concrete. Fig.3.4 clearly reveals that the main assumption of the MCFT prevents the theory from a physically correct treatment of aggregate interlock. However, it will be seen later in this chapter that aggregate interlock, as well as all other secondary shear carrying actions, are an intrinsic feature of the MCFT which do not need any explicit treatment.

It should be mentioned here that later in Section 4.1 (see Fig.4.6) an additional explanation is given for the inability of the MCFT to treat aggregate interlock in a physically correct fashion.

3.4 The Layered Approach to Flexure with Shear

3.4.1 Program LAYER

In their 1982 Publication, Vecchio/Collins reported a comprehensive set of shear tests on RC panels which was named the Toronto PV series. These tests served to calibrate the material laws of the MCFT. However, the constitutive model for cracked reinforced concrete so derived could not directly be applied on members subjected to combined flexure with shear, such as simple RC beams, as the MCFT assumes a uniform stress and strain state in the structural member under investigation.

a) General Truss Model for Flexure with Shear

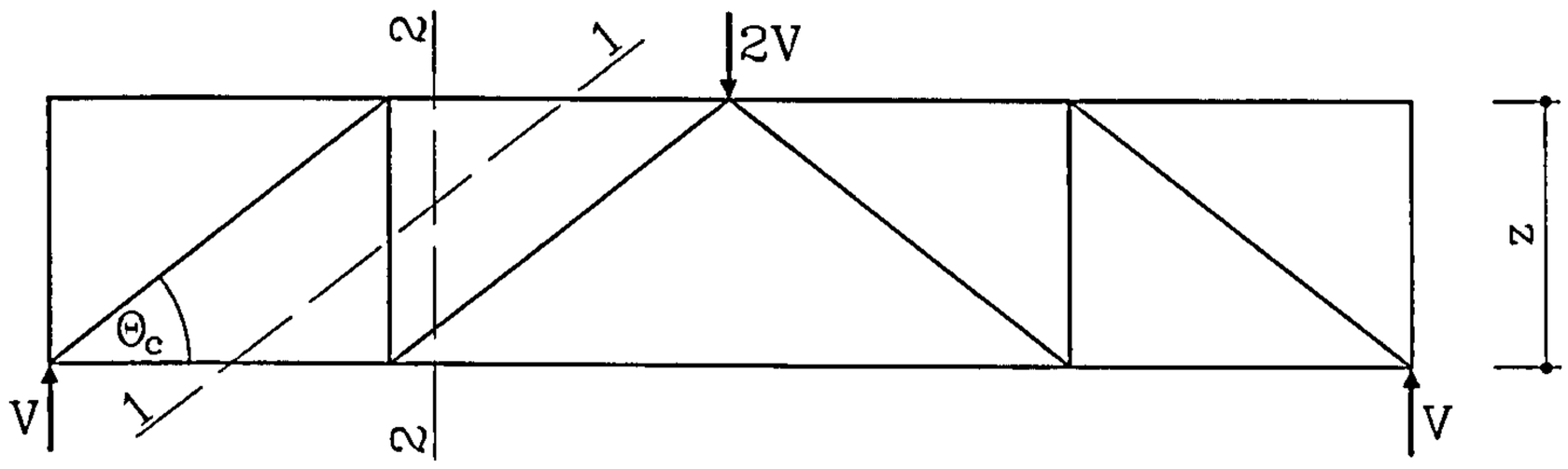

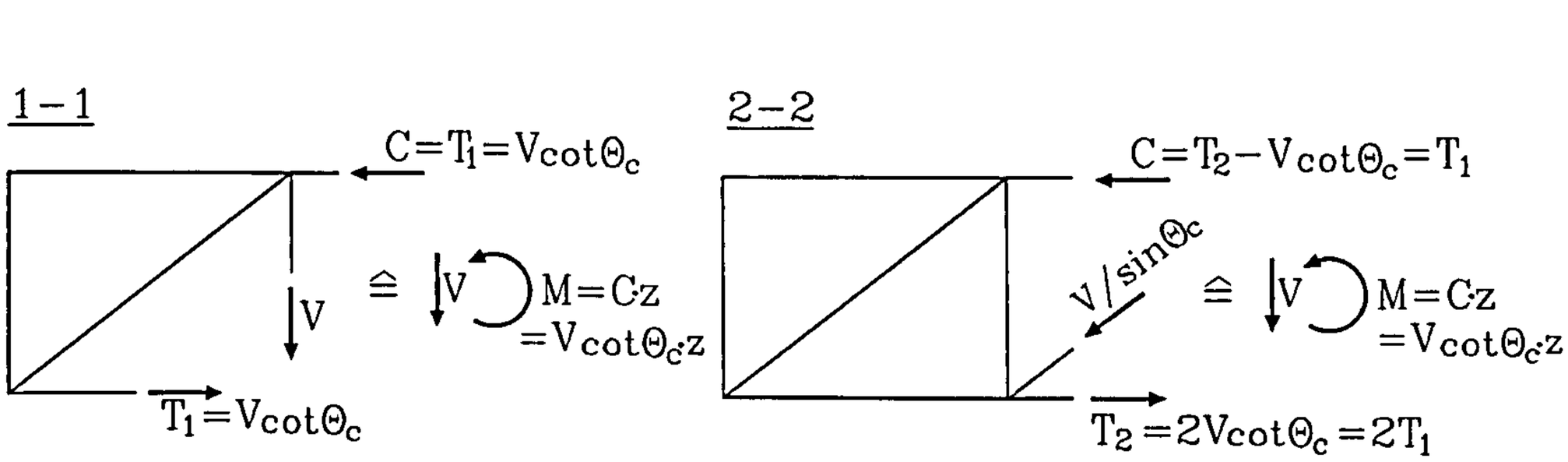

b) MCFT Truss Model for Flexure with Shear

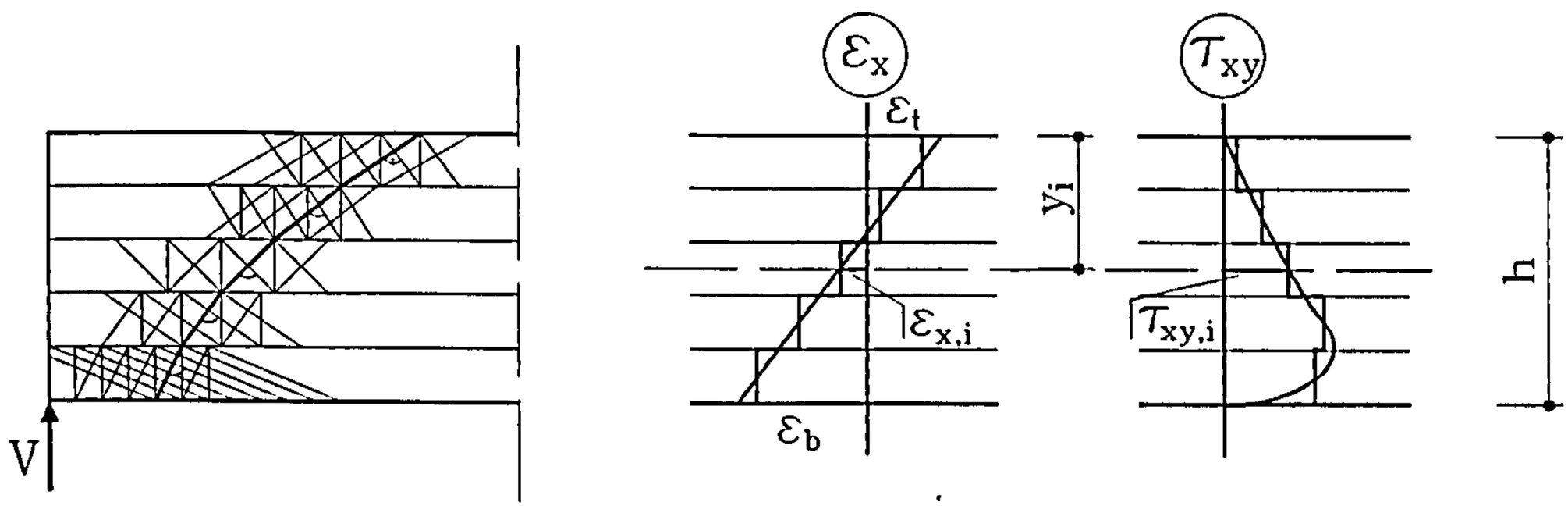

ε_t = *strain in x direction in top layer*

ε_b = *strain in x direction in bottom layer*

$$\varepsilon_{x,i} = \varepsilon_t + \frac{\varepsilon_b - \varepsilon_t}{h} y_i$$

Fig.3.5 Truss Model and Cross Section of an RC Beam

Fig.3.5.(a) shows a truss model of a simply supported RC beam with a concentrated load in mid-span. It is obvious from the free bodies *1-1* and *2-2* that the section moment is carried by the chords and the shear force either by the vertical tensile tie or the inclined compression strut, depending on the cross section under consideration. Two important features of this truss should be mentioned here. At first, the truss model does not yield any shear distribution in the cross section which, therefore, has to be regarded as uniform; an assumption against the physical reality. Second, the moment generates tensile stresses in the bottom chord and compression stresses in the top stringer. Smearing out of the truss members would not yield a uniform stress and strain state as required from the MCFT. This clearly shows that the MCFT cannot be applied on flexural members without additional considerations.

a) Layered Cross section with Notation

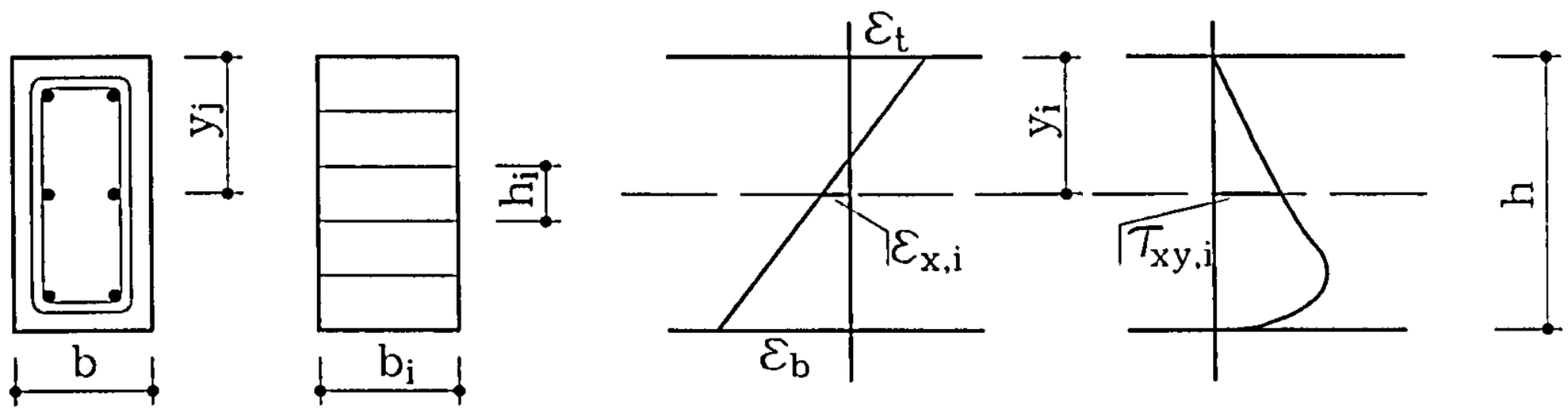

b) Equations for Section Equilibrium

$$N = \sum_{i=1}^{m} \sigma_{cx,i} b_i h_i + \sum_{j=1}^{n} \sigma_{sx,j} A_{s,j} \qquad (3.1)$$

$$V = \sum_{i=1}^{m} \tau_{xy,i} b_i h_i \qquad (3.2)$$

$$M = \sum_{i=1}^{m} \sigma_{cx,i} b_i h_i y_i + \sum_{j=1}^{n} \sigma_{sx,j} A_{s,j} y_j \qquad (3.3)$$

Fig.3.6 Cross Section and Section Equilibrium of the Layered Model

A general possibility to overcome the problems is to divide the structure into discrete horizontal layers. In such a model each layer represents its own truss. Once the normal strain distribution is considered to be constant in a layer, then both chords of a layer truss carry equal forces and hence, smearing out of the truss members would deliver a uniform stress and strain state as required by the MCFT. The accuracy of the method now only depends on the discretisation. Fig 3.5.(b) shows the model according to the layered ap-

proach. The various trusses are indicated as well as the horizontal strain gradient and the shear stress distribution.

Vecchio/Collins (1982) incorporated the MCFT in a layered model for the analysis of RC beams under shear and flexure and the procedure was coded in a program named SMAL. Calculations with program SMAL revealed drawbacks some of which are summarised here. Good results with SMAL were only achieved when the analysed beams were well reinforced in both longitudinal and transverse direction. Beams without stirrups could not be investigated. However, the main disadvantage of SMAL is that the material laws are not capable of being modified. The tensile strength of the concrete is an input quantity, but tension stiffening at high strains cannot be modified.

a) Equilibrium of Individual Layer

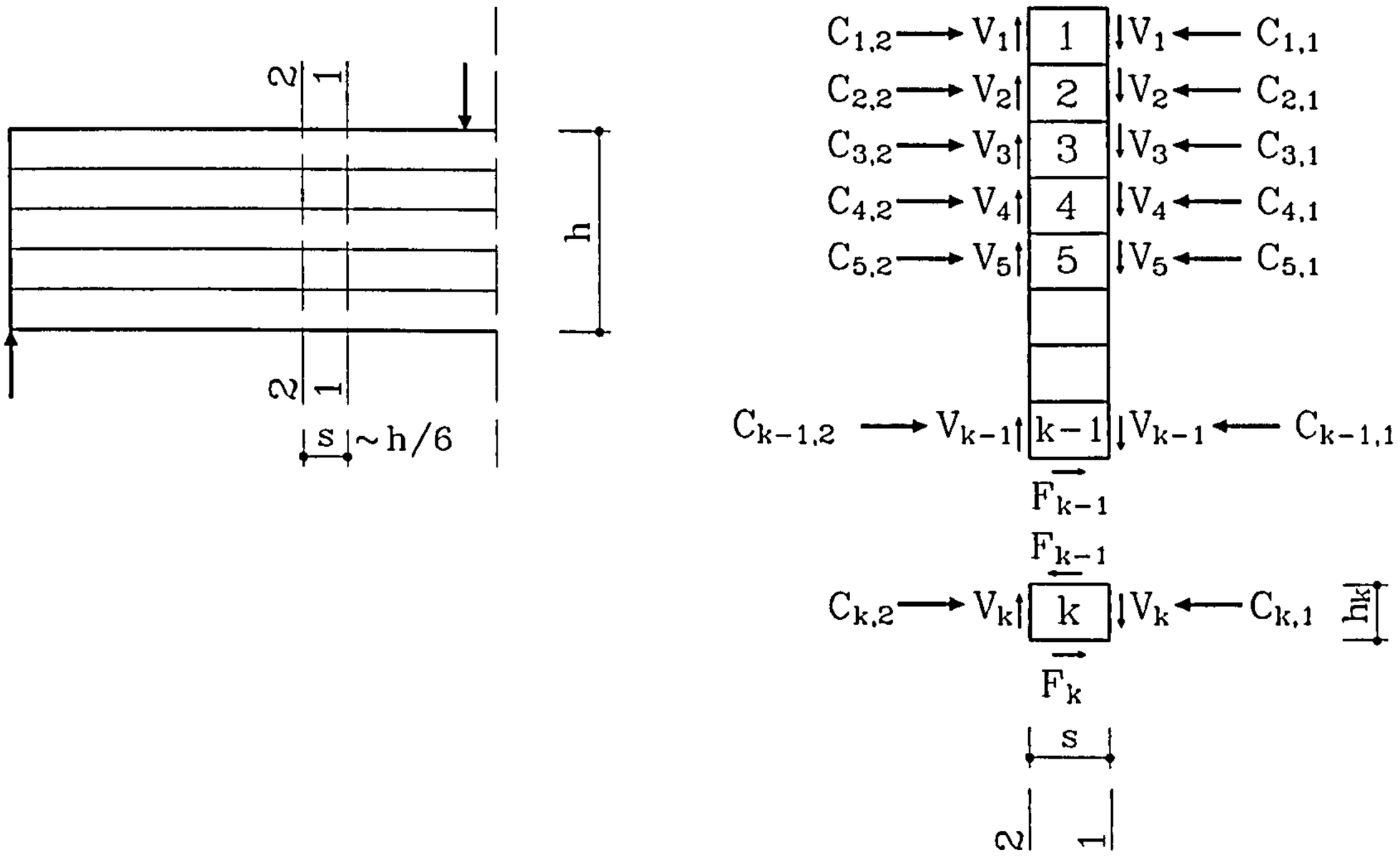

b) Equations for Equilibrium of Layer

$$F_{k-1} = \sum_{i=1}^{k-1} \left(C_{i,1} - C_{i,2} \right) \qquad (3.4)$$

$$F_k = F_{k-1} + C_{k,1} - C_{k,2} \qquad (3.5)$$

$$V_k = \frac{F_k + F_{k-1}}{2} \frac{h_k}{s} \qquad (3.6)$$

$$\tau_{xy,k} = \frac{V_k}{b_k h_k} \qquad (3.7)$$

Fig.3.7 Individual Layer with Equilibrium Equations for Layered Model

In Section 4.2.3 a modification of the material laws of the MCFT is proposed and justified, and it was intended to carry out all calculations with the same constitutive model. As this is not possible with SMAL, it was decided to code a completely new program for section analysis based on the MCFT, but with adapted material laws. This program was named LAYER and it revealed a much better performance than SMAL, especially when analysing RC beams with only little or no transverse reinforcement. Program LAYER, which was generally coded according to the procedure described in Vecchio / Collins (1982), will now be briefly introduced.

The basic assumption of the section analysis program LAYER is the plane section hypothesis of Bernoulli which postulates that sections remain plane throughout the entire loading process. Therefore, at the beginning of each analysis, the normal strain distribution of the investigated cross section has to be specified by estimating the top and bottom strain ε_t and ε_b , respectively. In addition, the shear stress distribution has to be specified, normally by assuming a constant shear flow which for rectangular beams is equivalent to a constant shear stress τ_{xy} . Once normal strain and shear stress distribution are fixed, then the *xy* stresses in concrete and steel can be calculated from the constitutive laws of the MCFT. Note that the constitutive laws are written in the principal direction and that all necessary rotations to the *xy* direction must be undertaken.

The next step is to check the section equilibrium which is easily achieved with Eqs.3.1 through to 3.3 (see Fig.3.6). If equilibrium is not satisfied, then the strain gradient has to be adjusted until section equilibrium is warranted. At that stage the shear stress distribution will still not be correct and, hence, this has to be fixed by first analysing a second section a short distance away from the first and then checking equilibrium of each layer. If equilibrium is not achieved, the shear stress distribution must be adjusted, which is a straightforward procedure consisting of setting the new shear stress distribution to that obtained at the end of the first run. A second run is then usually enough to obtain a sufficiently correct shear stress distribution in the cross section. Eqs.3.4 through to 3.7 of Fig.3.7.(b) depict the procedure with which equilibrium of each layer has to be checked. Finally, Fig.3.8 shows the flow chart of the complete program LAYER.

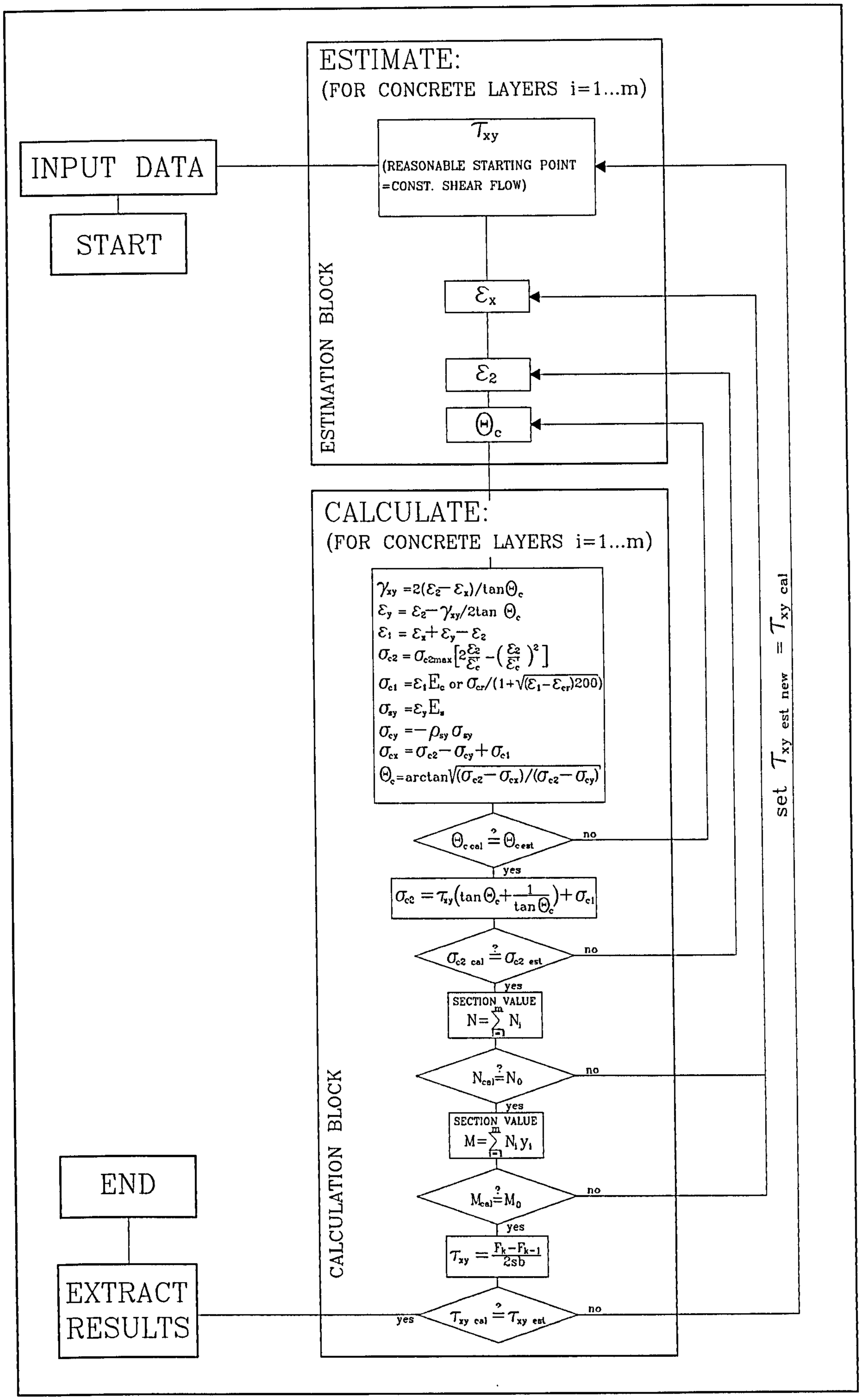

Fig.3.8 Flow Chart of Program LAYER

3.4.2 Calculations with the Layered Model

It was stated in the previous Section 3.4.1 that one of the reasons why program LAYER had to be coded was the fact that SMAL did not allow changes in the implemented constitutive model for the concrete.

a) Cross Sections of Beam

$f_y = 420\,MPa$

$f_c = 30\ MPa$

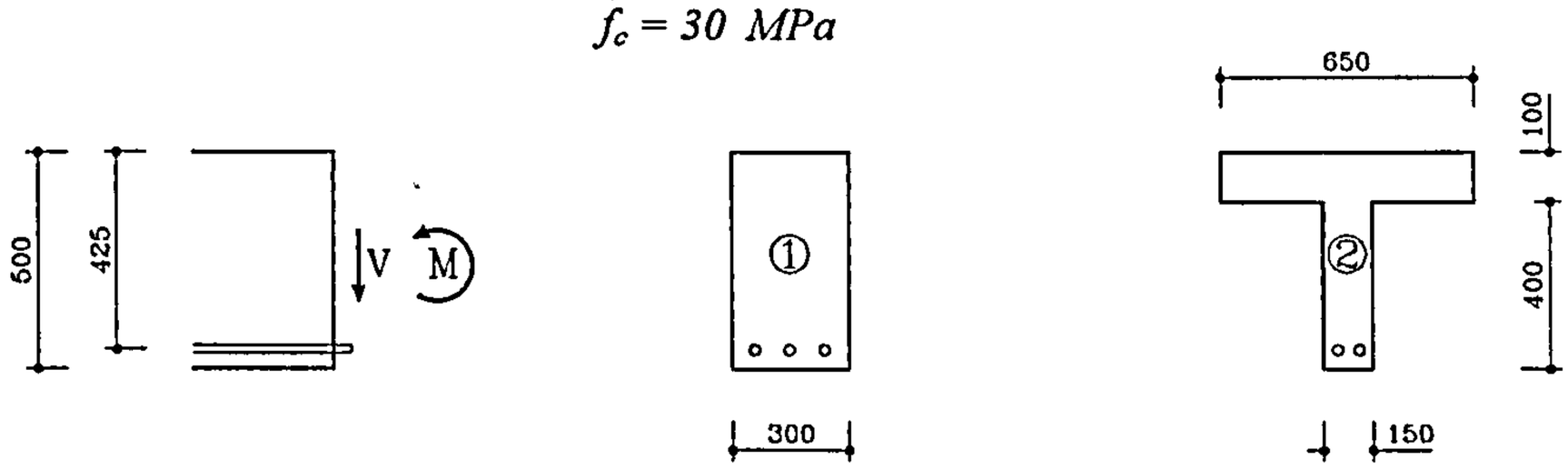

b) Modified Constitutive Model

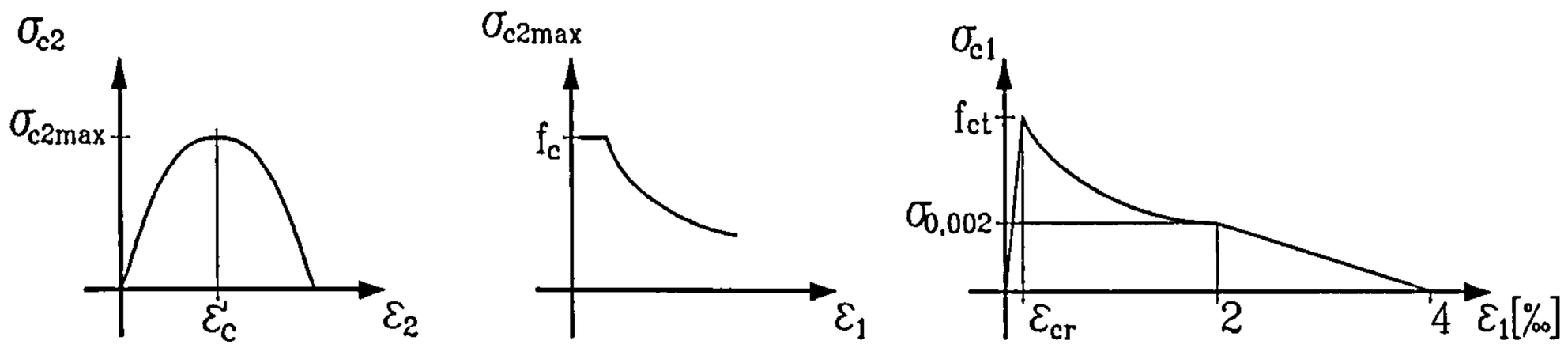

$$for \quad \varepsilon_1 < \varepsilon_{cr} \qquad \sigma_{c1} = E_c \varepsilon_1 \quad with \quad E_c = 2f_c / \varepsilon_c'$$

$$for \quad \varepsilon_{cr} < \varepsilon_1 < 0.002 \qquad \sigma_{c1} = \frac{f_{ct}}{1 + \sqrt{200\left(\varepsilon_1 - \varepsilon_{cr}\right)}} \qquad with \qquad f_{ct} = \alpha\sqrt{f_c}, \quad \alpha = 0.33 \div 0.75$$

$$for \quad 0.002 < \varepsilon_1 < 0.004 \qquad \sigma_{c1} = \sigma_{0.002}\left(2 - \frac{\varepsilon_1}{0.002}\right)$$

$$for \ 0.004 < \varepsilon_1 \qquad \sigma_{c1} = 0$$

$$\sigma_{c2} = \sigma_{c2max}\left[2\frac{\varepsilon_2}{\varepsilon_c'} - \left(\frac{\varepsilon_2}{\varepsilon_c'}\right)^2\right] \qquad \sigma_{c2max} = \frac{f_c}{0.8 - 0.24\varepsilon_1 / \varepsilon_c'}$$

Fig.3.9 Cross Section and Modified Constitutive Model for Calculations with LAYER

In Section 4.2 it is explained in some detail why it was desired to modify the material laws. The main reason is that the MCFT overestimates both the stiffness degradation of the concrete under compression and the tension stiffening of the concrete under tension. When dealing with structural elements subjected to pure shear both drawbacks will counter-act each other. This was the case with the PV panel tests of Vecchio / Collins (1982) with which they calibrated the material laws of the MCFT. However, for structural members with dominant tension and little compression, the overestimation of tension

stiffening leads to far too high values for the ultimate capacity of the analysed elements. For example, a simple RC beam under pure tension analysed with the original constitutive laws of the MCFT would give a section capacity much higher than the yield strength of the steel which is not acceptable. Therefore, the slightly modified constitutive laws of program LAYER are given in Fig.3.9.(b) while further explanations are provided in Section 4.2. Fig.3.9.(a) shows two different cross sections and the material properties of an RC beam with which calculations were carried out in order to demonstrate features of the layered model suitable to clarify general issues on the stress and strain state in a cracked reinforced concrete member. The calculations are summarised in Tab.3.2.

Nr.	ρ_{sx} *[%]*	ρ_{sy} *[%]*	*M [kNm]*	*V [kN]*	*a/d*	σ_{sx} *[MPa]*	σ_{sy} *[MPa]*	τ_{xy} *[MPa]*	ε_{sx} *[‰]*	ε_{sy} *[‰]*	*Cross Sect.*	*Failure Mode*
1	*2.7*	*0.3*	*525*	*250*	*5.0*	*420*	*420*	*3.1*	*2.0*	*4.0*	*1*	*Shear*
2	*2.7*	*0.3*	*500*	*325*	*3.6*	*420*	*420*	*3.7*	*2.0*	*5.5*	*1*	*Shear*
3	*2.7*	*0.13*	*500*	*250*	*4.7*	*420*	*420*	*2.9*	*2.0*	*14.8*	*1*	*Shear*
4	*2.5*	*0.3*	*500*	*250*	*4.7*	*420*	*420*	*2.9*	*2.0*	*2.9*	*1*	*Shear*
5	*2.4*	*0.3*	*500*	*200*	*5.9*	*420*	*410*	*2.3*	*2.0*	*1.95*	*1*	*Bending*
6	*0.84*	*0.05*	*200*	*150*	*3.1*	*390*	*420*	*1.6*	*1.9*	*2.5*	*1*	*Shear*
7	*0.84*	*0.05*	*220*	*75*	*6.9*	*420*	*135*	*0.7*	*2.1*	*0.6*	*1*	*Bending*
8	*4.0*	*0.6*	*600*	*400*	*3.5*	*415*	*420*	*4.6*	*1.95*	*2.4*	*1*	*Shear*
9	*4.7*	*0.6*	*600*	*400*	*3.5*	*295*	*420*	*5.9*	*1.4*	*2.8*	*1*	*Shear*
10	*3.2*	*0.6*	*530*	*500*	*2.5*	*420*	*400*	*5.5*	*2.3*	*1.9*	*1*	*Bending*
11	*3.2*	*0.9*	*585*	*250*	*5.5*	*420*	*420*	*5.3*	*2.0*	*4.3*	*2*	*Shear*
12	*3.2*	*0.6*	*500*	*330*	*3.6*	*420*	*420*	*6.2*	*2.0*	*6.5*	*2*	*Shear*

Tab.3.2 Calculations with the Layered Model of the MCFT

The shear stresses τ_{xy} varied between *0.7* and *6.2 MPa*, which means that the whole range from low to high shear was covered by the calculations. When the longitudinal reinforcement reached a strain of *2‰* after stirrup yielding, the program stopped converging and this was typically referred to as shear failure. When the longitudinal reinforcement yielded before the stirrups then a bending failure was encountered, in which case the program did not reach the specified moment and the run was terminated. In Section 3.7, where Leonhardt's tests were recalculated, two more shear failures which the program is able to recognise will be described. One occurs when the concrete strength in the inclined compression strut is reached in heavily reinforced T beams leading to web failure. The other occurs when the tensile strength of the concrete is exceeded in beams without any transverse reinforcement, thus announcing a shear tension failure.

3.4.3 Stress and Strain Distribution in RC Beams

It was stated earlier that when an RC beam is modelled by just one truss it is not possible to specify any stress distribution in the cross section: In fact, only theories which are based on discretisation like the FE method or the layered approach of the MCFT can provide a distribution of stresses according to the assumptions the theory is based on. Therefore, in Fig.3.10 the stress and strain distributions in the cross section according to some of the computer runs of Tab.3.2 are shown. One sample for each shear range was chosen and in addition, as an extreme example for high shear, the recalculation of Leonhardt's test beam T1 is also given. For calculations Nr. 1, 7 and 10 the distribution of concrete stresses σ_{cx}, shear stresses τ_{xy} and normal strains ε_x are depicted and for beam T1 two further graphs are plotted: The distribution of the shear flow and the corresponding quantity for the normal stresses.

It can be seen from Fig.3.10 that the shear stresses start increasing from *0* at the compression edge, reaching their highest values at the neutral axis where they remain nearly constant over the tension zone and then drop rapidly to *0* at the tension edge of the beam. The shear distribution reveals that most of the shear is carried in the tension zone and only a proportion of up to *30%* is transferred above the neutral axis. Despite the fact that the forces in the compression zone are usually high, their vertical component remains small as the struts are only little inclined, generating low amounts of shear. However, in the middle parts of the cross section, below the neutral axis where the inclination angle of the struts is in the range of *30°* to *50°*, high shear stresses can form although the compression forces are much smaller than above the neutral axis. It will be seen later in Section 3.9, where arch action is investigated, that in deep beams substantial shear is carried by a strut and tie mechanism and this proportion can be regarded as being evenly distributed for reasons given earlier. This means that shear is either more uniformly distributed in the cross section or concentrated in the tension zone depending on the transfer mechanism which applies in an RC beam. From considerations of the layered approach of the MCFT to date it can be stated that in a vertical cross section of an RC beam nominal shear stresses τ_{xy} can only be assigned to areas where the compression forces are distinctly inclined and this is mainly the case between the neutral axis and the longitudinal reinforcement. In the compression zone of a beam and below the longitudinal reinforcement only little shear stresses τ_{xy} can be generated.

a) Distribution for Low Shear
(see Tab.3.2, Row Nr.7)

b) Distribution for Medium Shear
(see Tab.3.2, Row Nr.1)

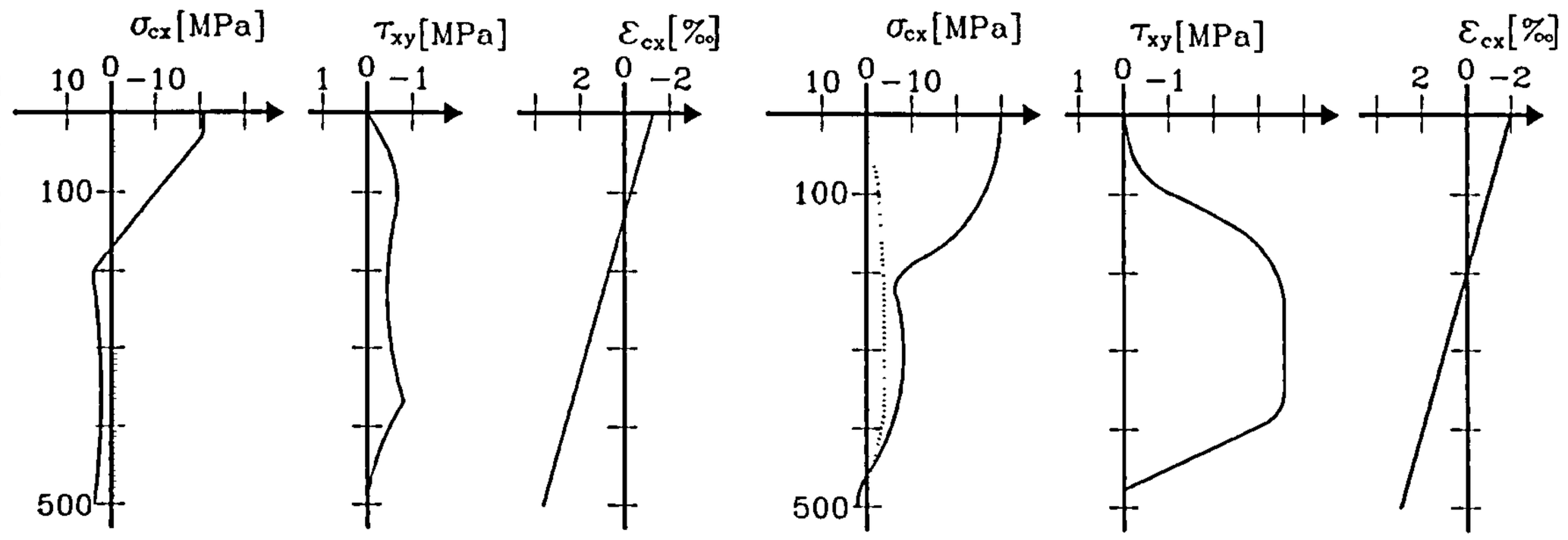

c) Distribution for High Shear
(see Tab.3.2, Row Nr.10)

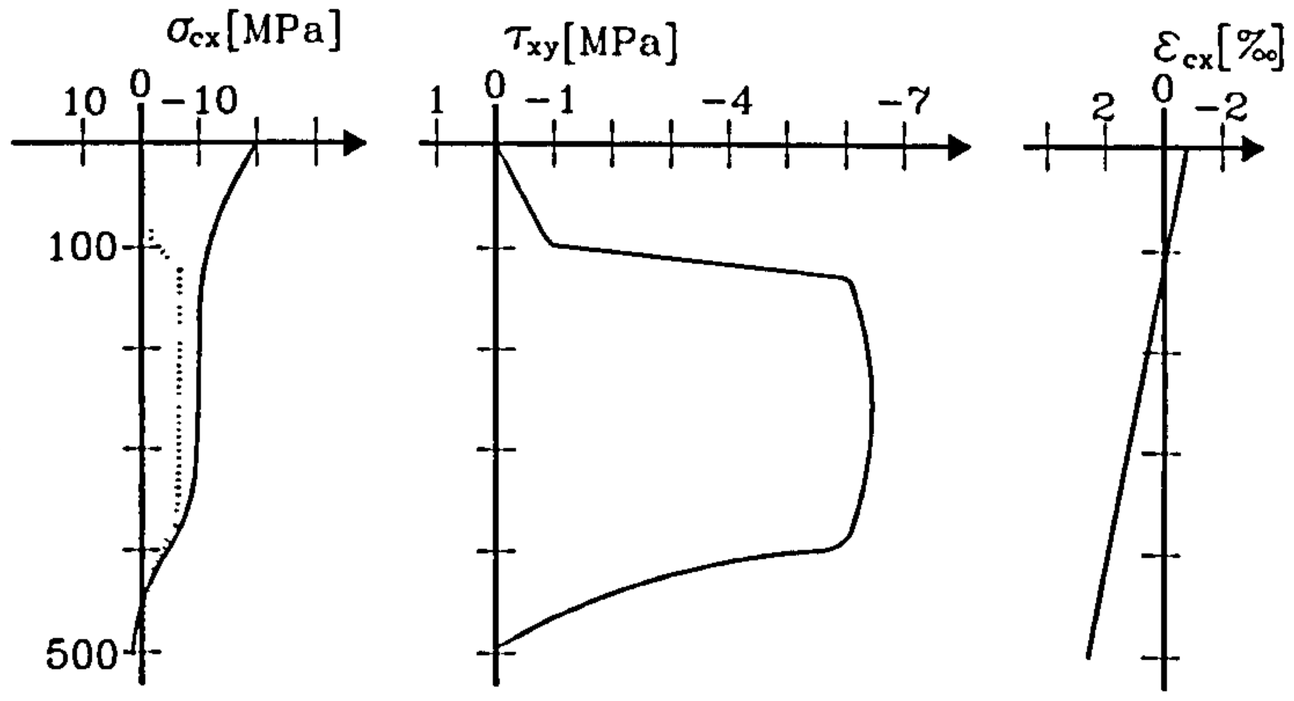

d) Distribution for Extremely High Shear
(see Recalculation of Leonhardt's Beam T1)

p_{xy} = *normal stress times beam width*
q_{xy} = *shear stress times beam width = shear flow*

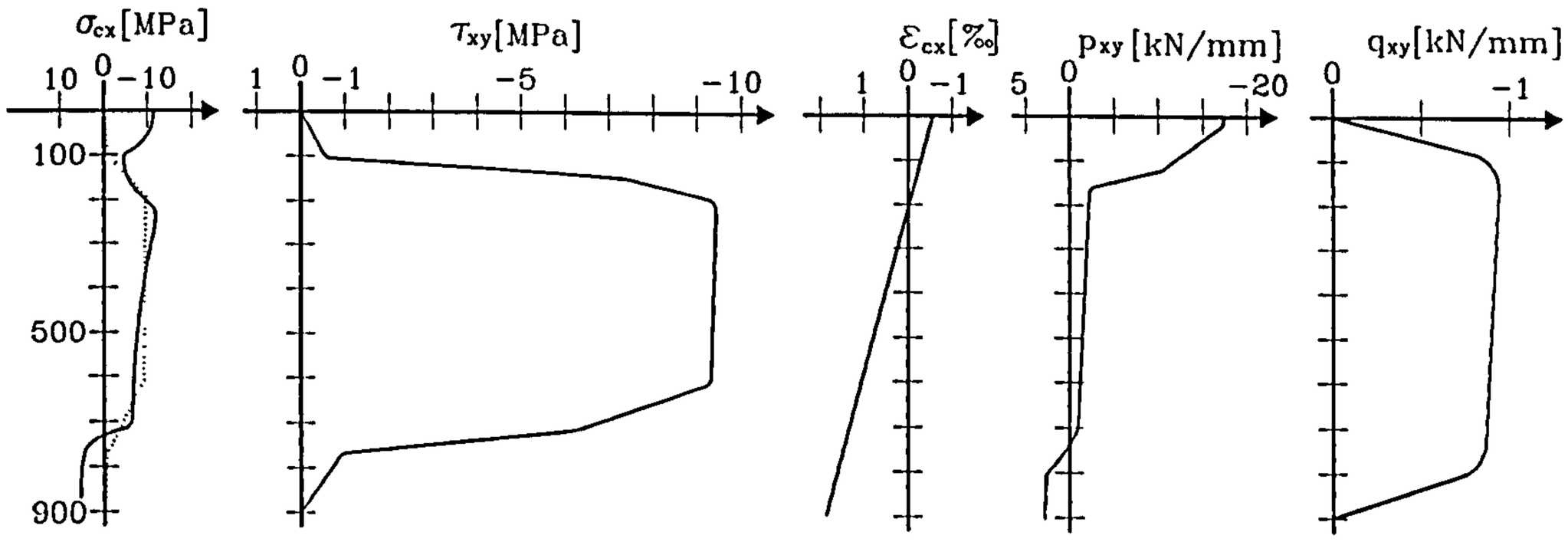

Fig.3.10 Stress and Strain Distribution in a Vertical Cross Section

Shear is either carried by compression struts or tensile ties depending on the free body under consideration (see Fig.3.5). Therefore, in a structural model where trusses with varying inclination angles are arranged in horizontal layers, not only the forces in the compression strut vary but also the tension forces in the ties. This means that the stress in the stirrups cannot be constant over the beam height and in fact, the calculations with LAYER confirmed this feature of the MCFT. Moreover, in 1967 a test report was published by Rüsch and Mayer (see Fig.21) in which they verified this prediction virtually 20 years in advance when they measured the stirrup strains of beams at various levels of height. The fact that shear is mainly carried in the tension zone of a beam was postulated by many researchers in the past like Fenwick/Paulay, Kupfer, Reineck and others. However, only the layered approach of the MCFT could visualise the shear distribution in a cross section in a striking way.

In Fig.3.10 the shear stresses τ_{xy} are depicted in an exaggerated manner compared with the normal stresses σ_{cx}. To show their real magnitude they are additionally indicated to scale in the graph for the σ_{cx} stresses. One can see that the normal stresses are in general much higher than the shear stresses, in particular in the compression zone of a beam. Moreover, at the tension edge the huge tensile stresses of the longitudinal reinforcement are not depicted in the graph (see also Fig.3.13). This provides evidence of the fact that the load of a beam is carried by normal stresses rather than shear action. From that point of view the question of the shear distribution in a cross section is rather academic.

From Fig.3.10.(a) we can see that the normal stresses are distributed as we normally expect them to be: High compression above the neutral axis and little tension below it in the tension zone of the beam. Surprisingly, when higher shear is involved, the tension below the neutral axis converts into compression and in extreme situations, when beams are subjected to very high shear, these compressive stresses can even become as high as in that region of a beam which is typically referred to as the compression zone. The MCFT provides a simple explanation for this unexpected behaviour.

In Fig.3.11.(a) the web of a beam is depicted as well as a membrane element which might be located somewhat below the neutral axis in the tension zone of the beam. Before cracking, the element can be considered as being under pure shear and its stress state could be as shown in Fig.3.11.(b). When the load is raised, cracking will start to occur, substantially increasing the compression in the principal direction and slightly lowering

the value for the tension perpendicular to it. This is equivalent to a certain shift of the $\tau_{\xi\eta}$ axis towards the tension side of the graph. The situation is qualitatively depicted in Fig.3.11.(c) and it is obvious that the vertical cross section undergoes substantial compression stresses once cracks have commenced to form. A second, clearer illustration is given in Fig.3.11.(d) where the compression in the tension zone is interpreted as the horizontal proportion of the compression force D in the concrete strut which has to counterbalance the tension force $V\,cot\theta_c$ generated by the shear force V.

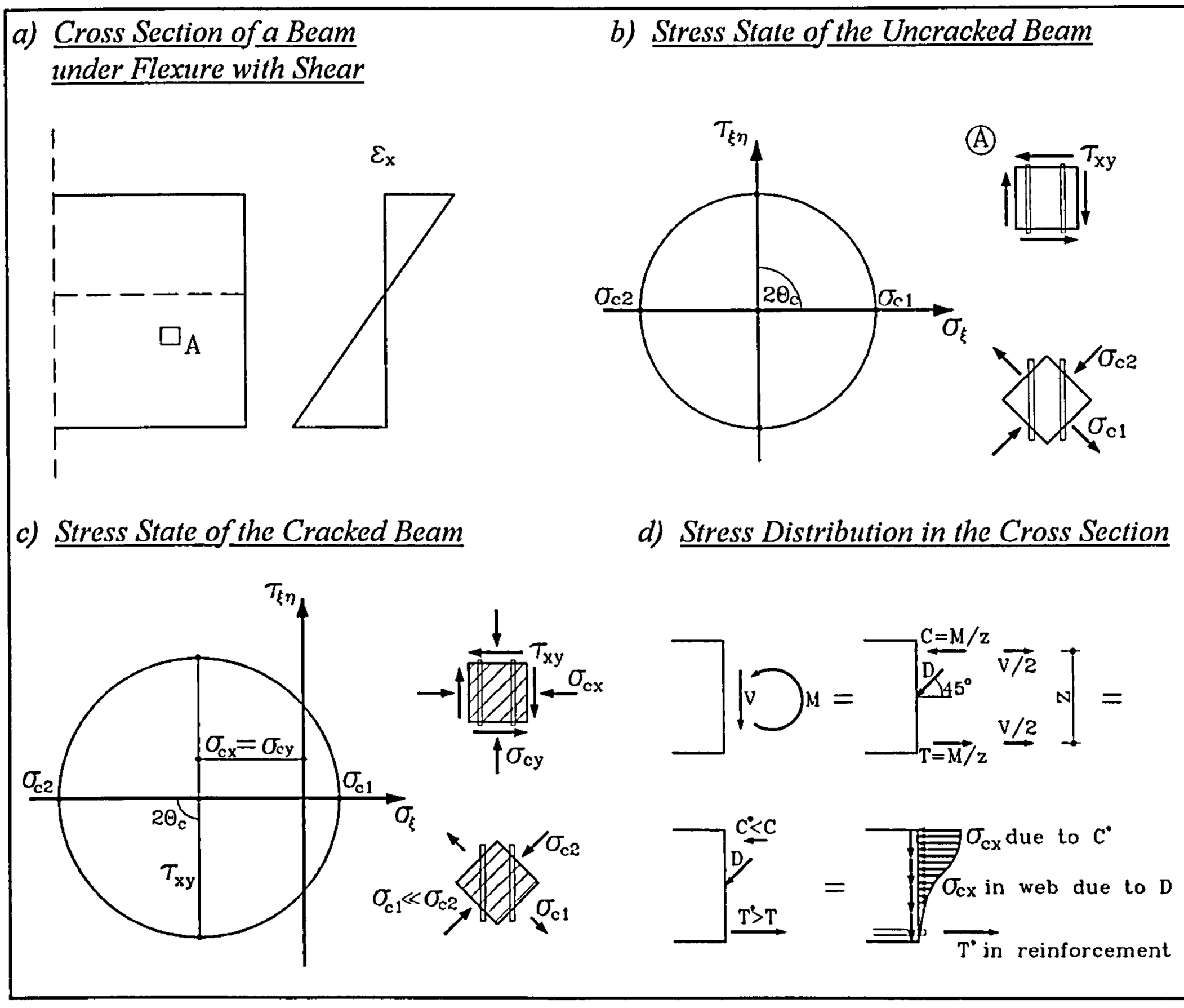

Fig.3.11 Compression Stresses in the Tension Zone of a Beam

The compression stresses in the vertical cross section as they have been described are accompanied by substantial tensile strains in x and y direction and this is even more surprising than the occurrence of compression stresses in the web itself. A short explanation for this phenomenon will be given here. It is assumed that the membrane element investigated earlier is in a state of pure shear, although it is well-known that this applies only roughly in the web below the neutral axis, and it was stated that after cracking the stress state in the concrete is as given in Fig.3.11.(c). In addition, Fig.3.12.(a) shows the membrane element both in xy position and rotated to its principal direction. After cracking,

the element will undergo a substantial elongation in the tensile direction. When we further assume, for simplicity, that the total deformation is caused by the cracks alone, then the loaded element might look as shown in Fig.3.12.(b).

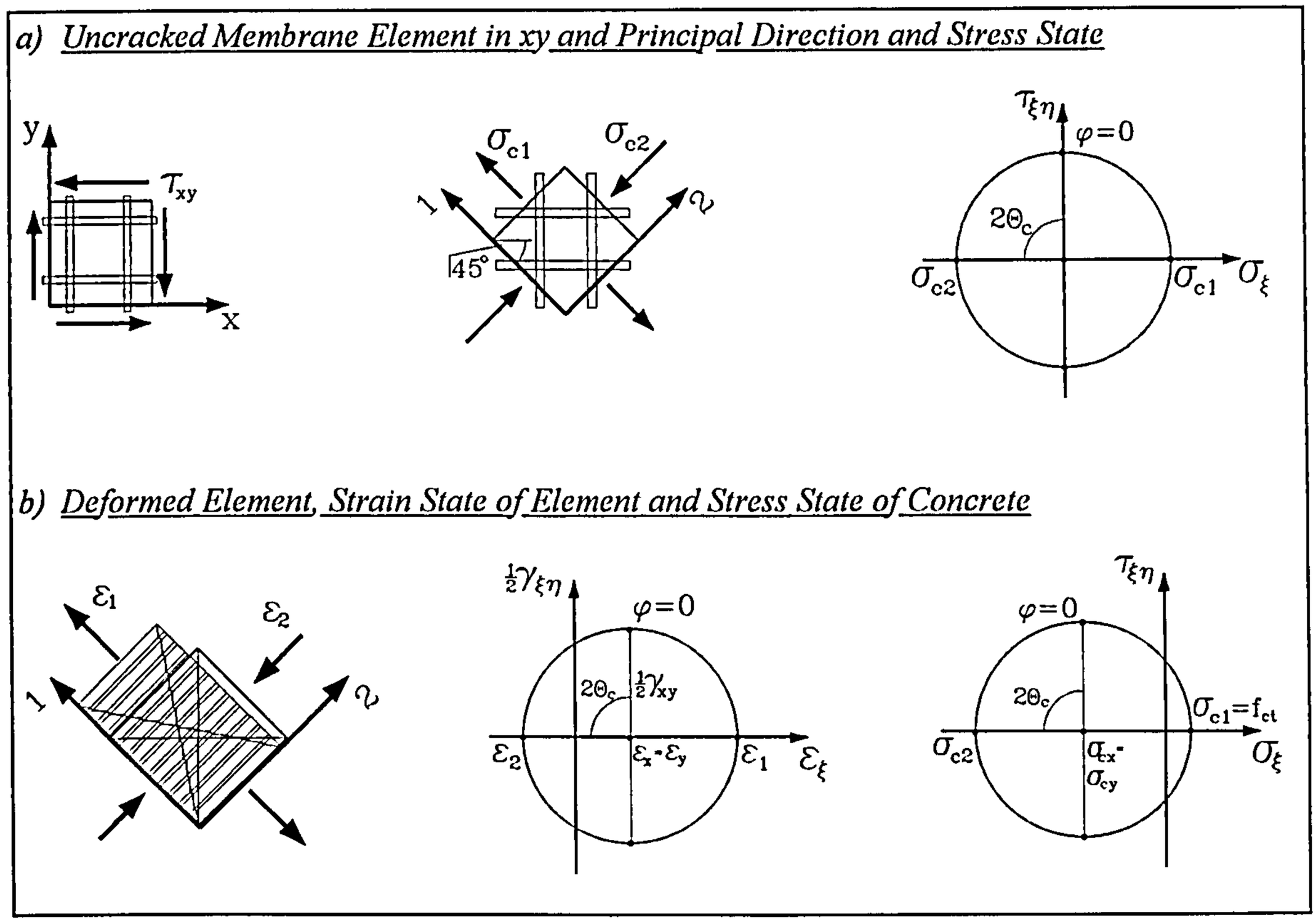

Fig.3.12 Tensile Strains in Element Causing Compression in Plain Concrete

It is obvious that both the transverse and, if available, also the horizontal reinforcement will be elongated by the deformation of the element. However, the stresses in the longitudinal reinforcement can only act in x direction and in the stirrups only in y direction. As no external normal forces are applied on the element, which is considered to be under pure shear, the stresses in the reinforcement must be balanced by the stresses in the concrete. Consequently, the concrete in the tension zone comes under compression in both directions.

3.4.4 Effect of the Tensile Strength of the Concrete

The comparison of results of CFT and MCFT calculations in Tab.3.1 revealed differences between both theories. The reason for this is the tensile strength of the concrete f_{ct} which influences the response of an RC structure in a significant manner. It should be mentioned that Vecchio/Collins referred to the introduction of f_{ct} as tension stiffening and this expression will be used here in the same way. An important observation was that the differences between CFT and MCFT become more distinct when f_{ct} is increased but tend to vanish when the ultimate limit is being approached. However, the results of Tab.3.1 were computed with a particular cross section to which no moment was applied. Therefore, to obtain a more comprehensive image of the influence of the concrete's tensile strength and to illustrate the order of magnitude of stresses and strains encountered in the web of an RC beam, additional investigations were employed. Figs.3.13 through to 3.15 depict Mohr's circles for the layers of the beam used for scrutiny throughout this section and the properties of which are given in Fig.3.9. The calculations were carried out with cross section *1* and section loads of $M = 500\ kNm$ and $V = 250\ kN$, which were the ultimate limit values for the run with $f_{ct} = 0$. The shear resistance of the cross section increased by about *30%* when the tensile strength was added providing that the moment was kept constant.

Fig.3.13.(a) shows stress circles according to the MCFT with $f_{ct} = 0$, and Fig.3.13.(b) the circles when the tensile strength was set to $f_{ct} = 0.75\sqrt{f_c}$. For layers *1* and *2* the stress circles for the plain concrete are identical with the stress circles for the entire RC element, however, for layers *3* through to *8* the differences are so small that they could not be depicted in the chosen scale. Therefore, for layer *6* the procedure of transition from the plain concrete circle to the RC element circle is shown in Fig.3.15 in a larger scale. As the layer is merely transversely reinforced, the stirrups have to balance the concrete stresses according to $\sigma_y = \sigma_{cy} + \sigma_{sy} = 0$. The unbalanced concrete stresses σ_{cx} are equilibrated by both the longitudinal reinforcement in layer *9* and the force in the compression zone above the neutral axis. The procedure shown in Fig.3.15 applies in general for each layer, but is of crucial importance here only in layer *9* which carries all the longitudinal reinforcement. Once again it becomes obvious that the section forces are mainly carried by normal stresses in the concrete of the compression zone and in the steel bars of the tension zone. This would be even more distinct if a T shaped beam was chosen for investigation.

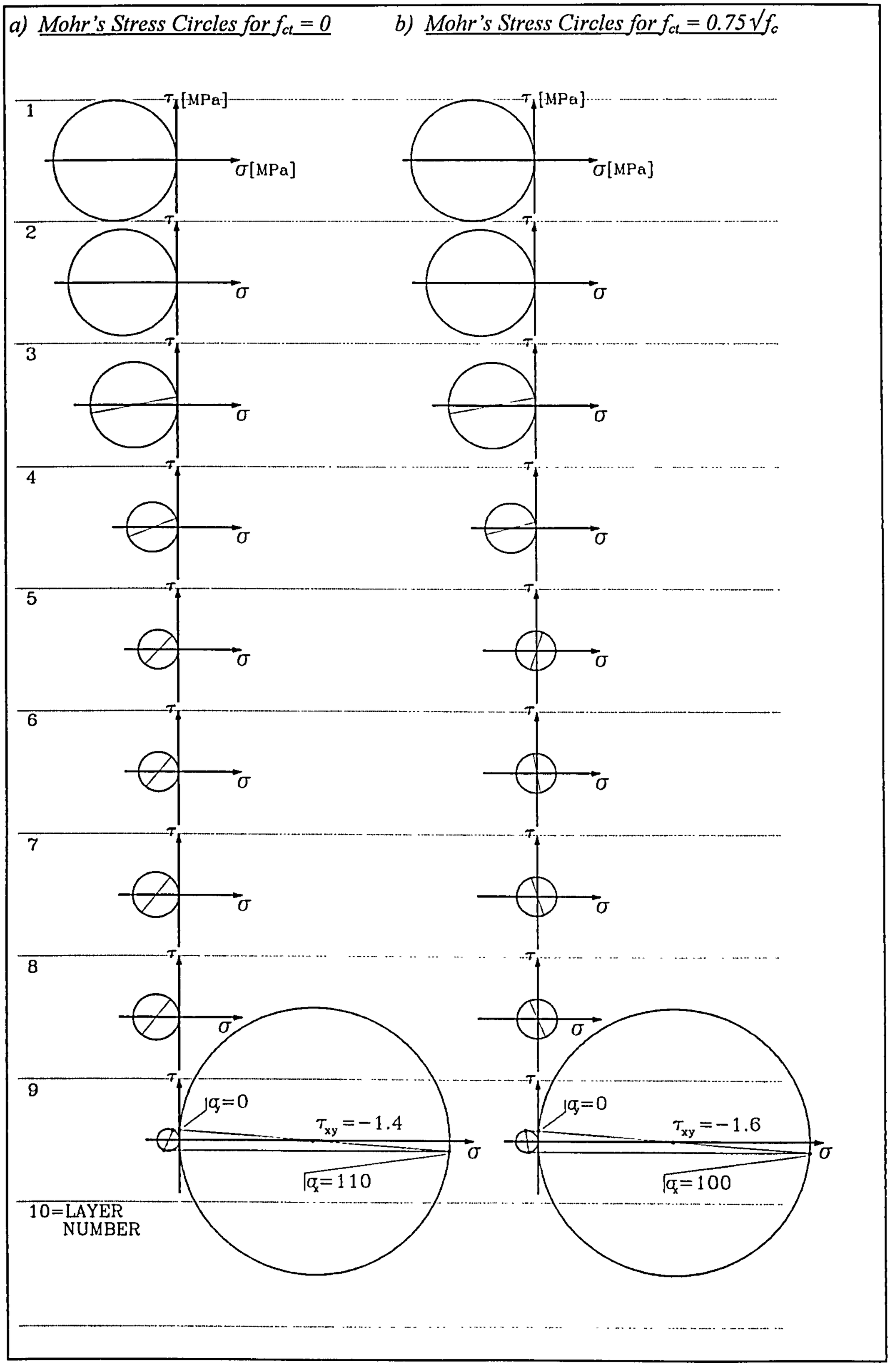

Fig.3.13 Mohr's Stress Circles for the Cross Section of an RC Beam

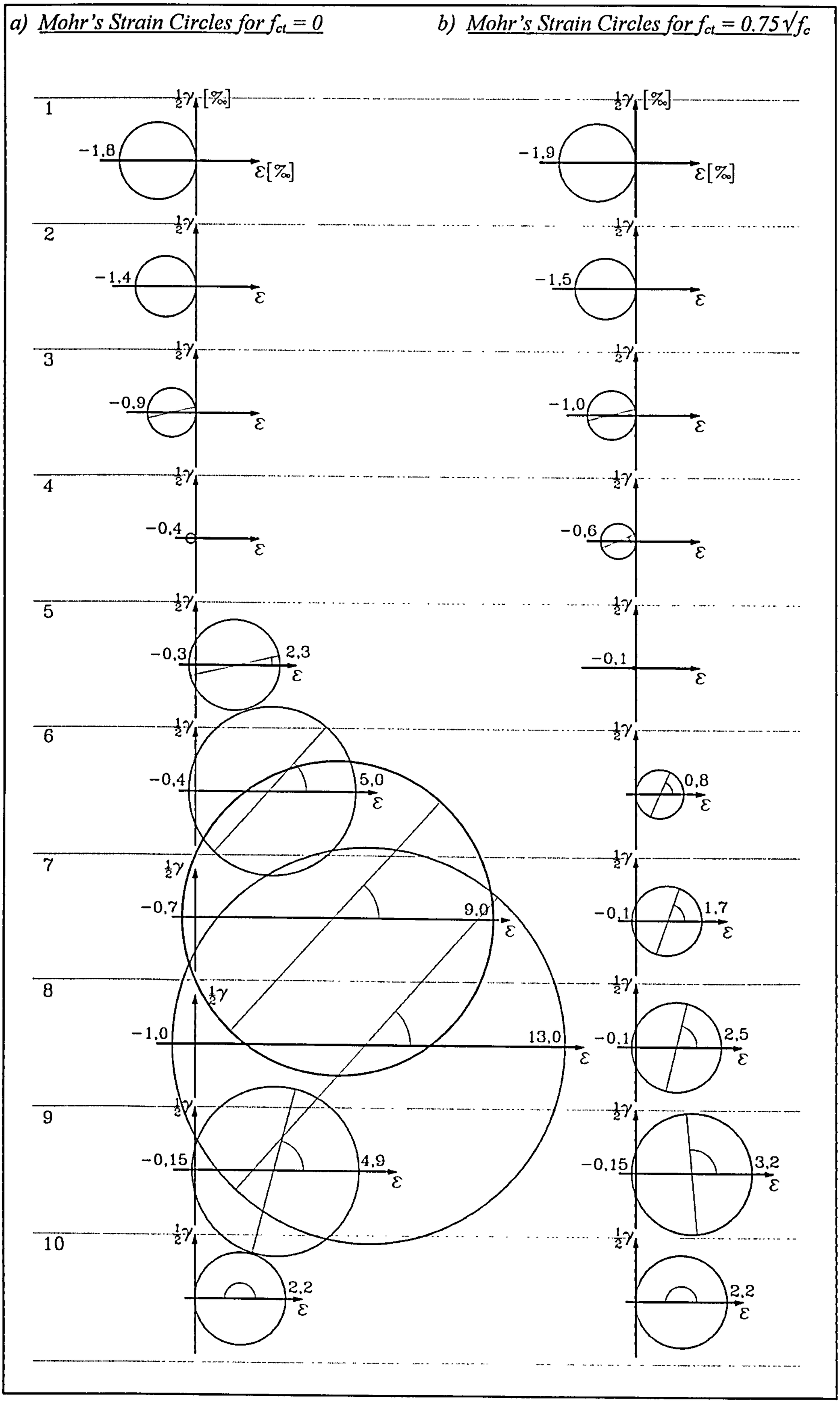

Fig.3.14 Mohr's Strain Circles for the Cross Section of an RC Beam

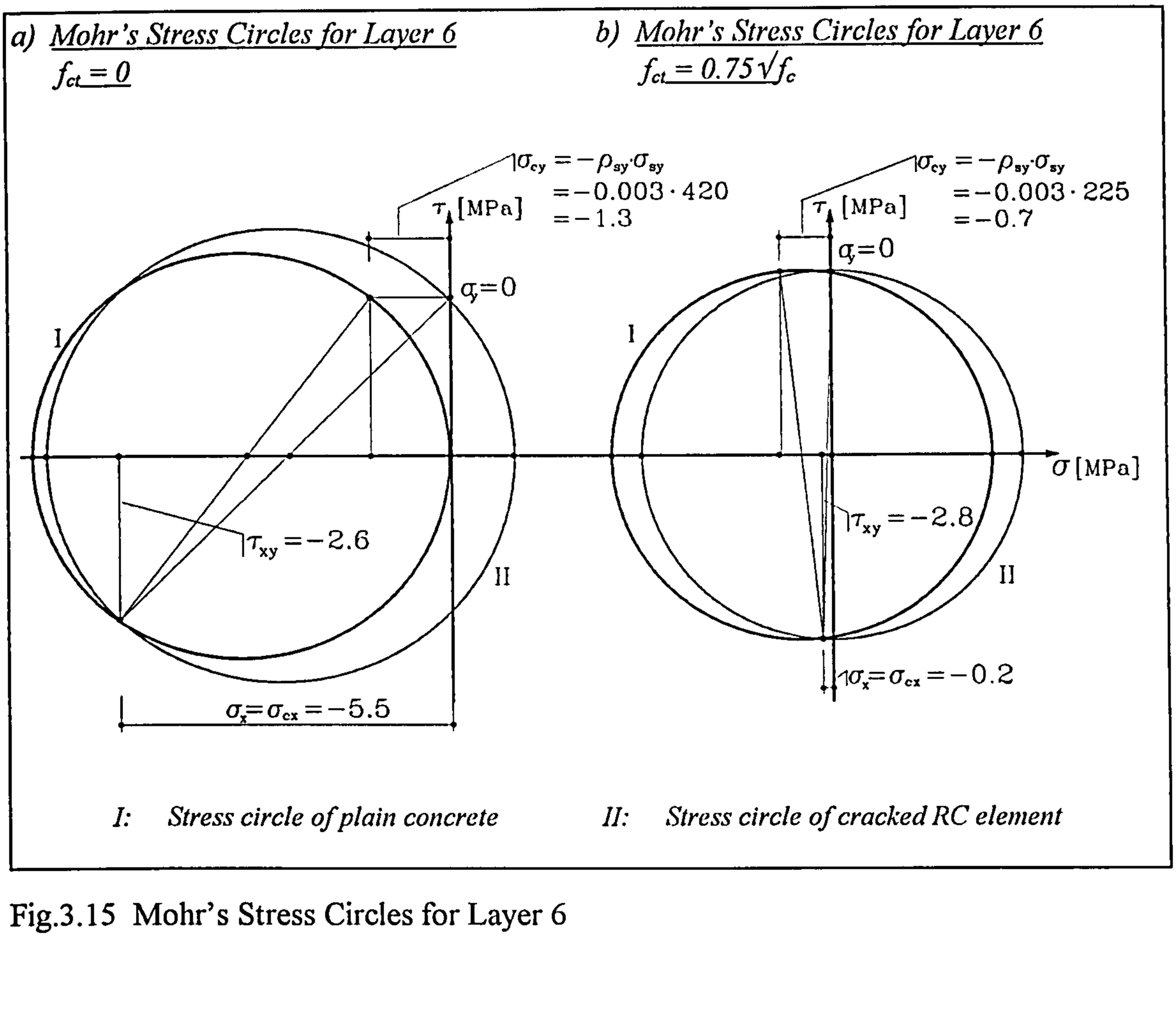

Fig.3.15 Mohr's Stress Circles for Layer 6

The only substantial difference between the two methods revealed in Figs.3.13 - 3.15 is the inclination angle θ_c, which is much bigger when tension stiffening is introduced. This becomes clear as the relieved stirrups carry less tension and, therefore, only slight concrete stresses are to be balanced, as is shown in Fig.3.15.(b). The assumption of a stress state of pure shear, which was postulated earlier for the web below the neutral axis, is verified by the circles of layers 5 through to 8 in Fig.3.13.(b). In addition, Fig.3.14 shows that the tensile strength has a considerable influence on the strain state of a structure. As a result it is obvious that without tension stiffening a reliable evaluation of deformations is not possible. Fig.3.14 gives evidence for the importance of reasonable constitutive laws which are particularly necessary for the calculation of deflections on the finite element level.

3.5 A Check on Kupfer's Shear Theory

As mentioned earlier in the state-of-the-art report, Kupfer's shear theory (1983) was further developed mainly by Kirmair and Mang (1987). For the subsequent investigations the theory was used as described in Kirmair's 1987 publication, a short form of which was summarised in a paper issued in the same year. According to this version of the theory, a computer program was coded and some simple calculations were carried out on a rectangular cross section of a beam, subjected to a shear force $V=300\ kN$. No moment was applied to meet exactly the assumption of a constant strain distribution ε_x, in the knowledge that such a situation only occurs in the case of pure shear or in the vicinity of a zero point in a bending beam, as shown in Fig.3.16.(a). The same cross section and material properties were chosen as in the calculation with the MCFT depicted in Fig.3.2 and the crack angle θ' was taken from the MCFT results of Tab.3.1.

a) Cross Section with M=0 and V=const. *b) Two Mohr's Stress Circles for the Web*

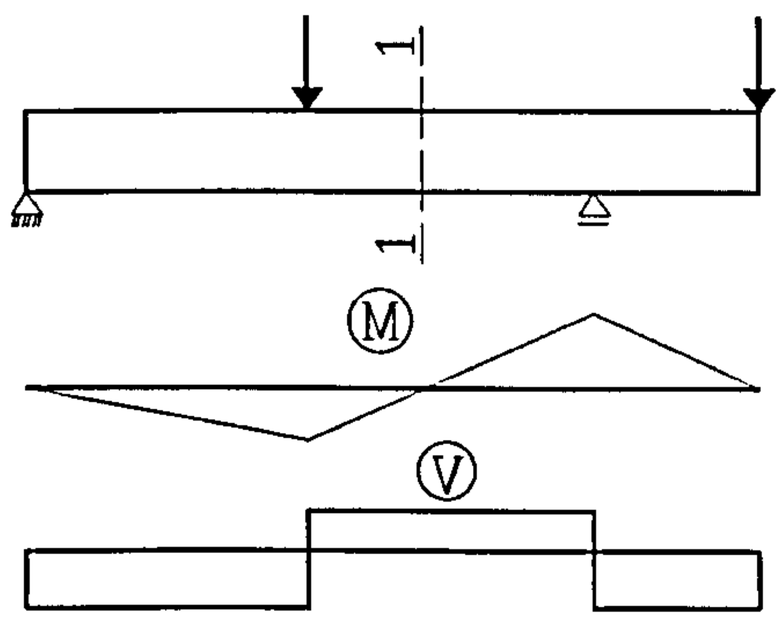

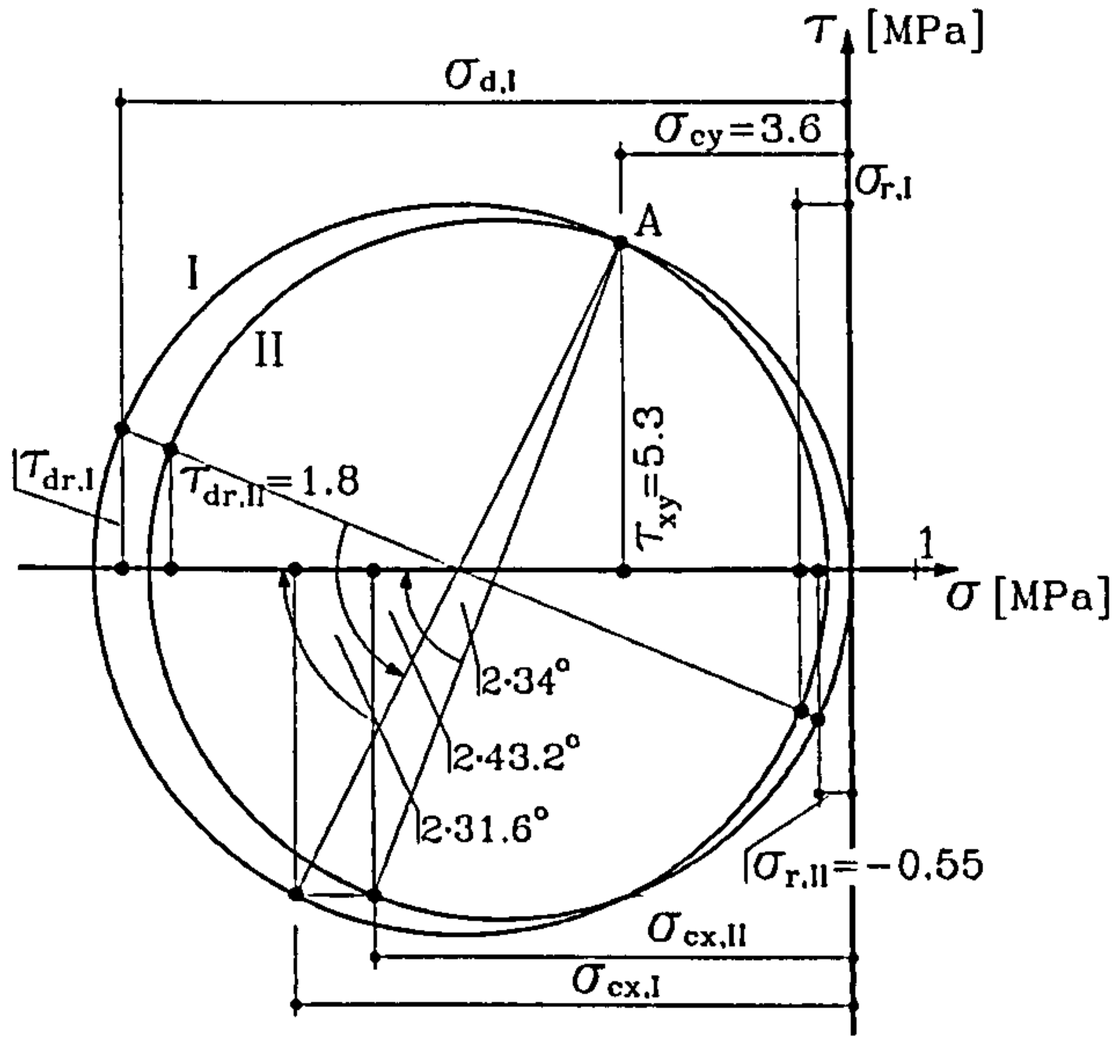

$$\tan\theta_c = \tan\theta'(1-\Delta\tau/\tau_{xy}) \qquad (3.8)$$

$$\theta_c = \theta' - \Delta\theta_c \quad \text{with} \qquad (3.9)$$

$$\tan(2\Delta\theta_c) = 2\tau_{dr}/(\sigma_d-\sigma_r)$$

$$\sigma_2 = \tau_{xy}/(\sin\theta_c \cos\theta_c) \qquad (3.10)$$

Circle I:

	$\sigma_{d,I}$	= -11.7 MPa		$\sigma_{1,I}$	= -0.3 MPa
p_1 =	$\sigma_{r,I}$	= - 0.8 "	=	$\sigma_{2,I}$	= -12.2 "
	$\tau_{dr,I}$	= 2.3 "		$\theta_{c,I}$	= 31.6°

Circle II:

	$\sigma_{1,II}$	= 0 MPa			
p_2 =	$\sigma_{2,II}$	= -11.4 "	*Aggregate interlock stresses:*	$\sigma_{r,II}$	= -0.55 MPa
	$\theta_{c,II}$	= 34°		$\tau_{dr,II}$	= 1.8 "

Fig.3.16 Stress State in Web of an RC Beam

It was stated earlier that Kupfer's shear theory includes hook slip, loss of bond of both longitudinal and transverse reinforcement, and shrinkage of the concrete. In Section 3.6, some explanation will be given on these features but for the time being they will be omitted. This means that the strains due to hook slip $\Delta\varepsilon_s$ and shrinkage ε_{cs} are set to zero, while the bond factors for the longitudinal and transverse reinforcement α_{sl} and α_{st}, respectively, are set to one. The calculation delivers a stress state p_1 and an angle $\theta_c = 34°$. This angle was calculated by the program with Eq.(3.8) which was derived from equilibrium considerations and this means that θ_c should be the principal direction of the stress state p_1. However, as Fig.3.16 reveals, $\theta_c = 34°$ does not match the transformation conditions of the stress state p_1. The correct value is $\theta_c = 31.6°$ and can be calculated with Eq.(3.9). With this value, the principal stresses become $\sigma_1 = -0.3$ and $\sigma_2 = -12.2\ MPa$. Surprisingly σ_1 is not found to be zero, as the equilibrium equations require. Assuming $\theta_c = 34°$ was the correct angle of the principal stress direction this would then yield a second stress state p_2 which is derived by the equilibrium equation for σ_2 given in Kupfer's theory. Eq.(3.10) and the stress state p_2 are shown in Fig.3.16.(a). In addition, Fig.3.16.(b) depicts Mohr's circles for both stress states. Noticeably, both circles have a common point A where they intersect each other, and in fact A determines the same shear stress τ_{xy} and transverse stress σ_{cy}, of which the latter is needed to design the stirrup reinforcement.

The conclusion of the calculation so far is that Kupfer's theory yields two different sets of stresses for the web. As the theory assumes a uniform stress state, only one stress set can represent the stress state in the tension zone of a beam. Admittedly, the difference in the stress circles is small and the vertical equilibrium is correct for both stress states as Fig.3.17 proves. However, the above investigation reveals a certain flaw in Kupfer's theory. From the Mohr's circle the transverse reinforcement can be designed, or in the case of a given reinforcement the stirrup stress might be calculated using the stress in y direction of the Mohr's stress circle. In the example, the transverse steel ratio is $\rho_{sy} = 1.235\ \%$ which yields a steel stress of $\sigma_{sy} = -\sigma_{cy}/\rho_{sy} = 3.6/0.01235 = 290\ MPa$. In a similar fashion one can calculate the steel stress of the longitudinal reinforcement. As there are two different values according to the different stress states p_1 and p_2 it is not clear which value to take.

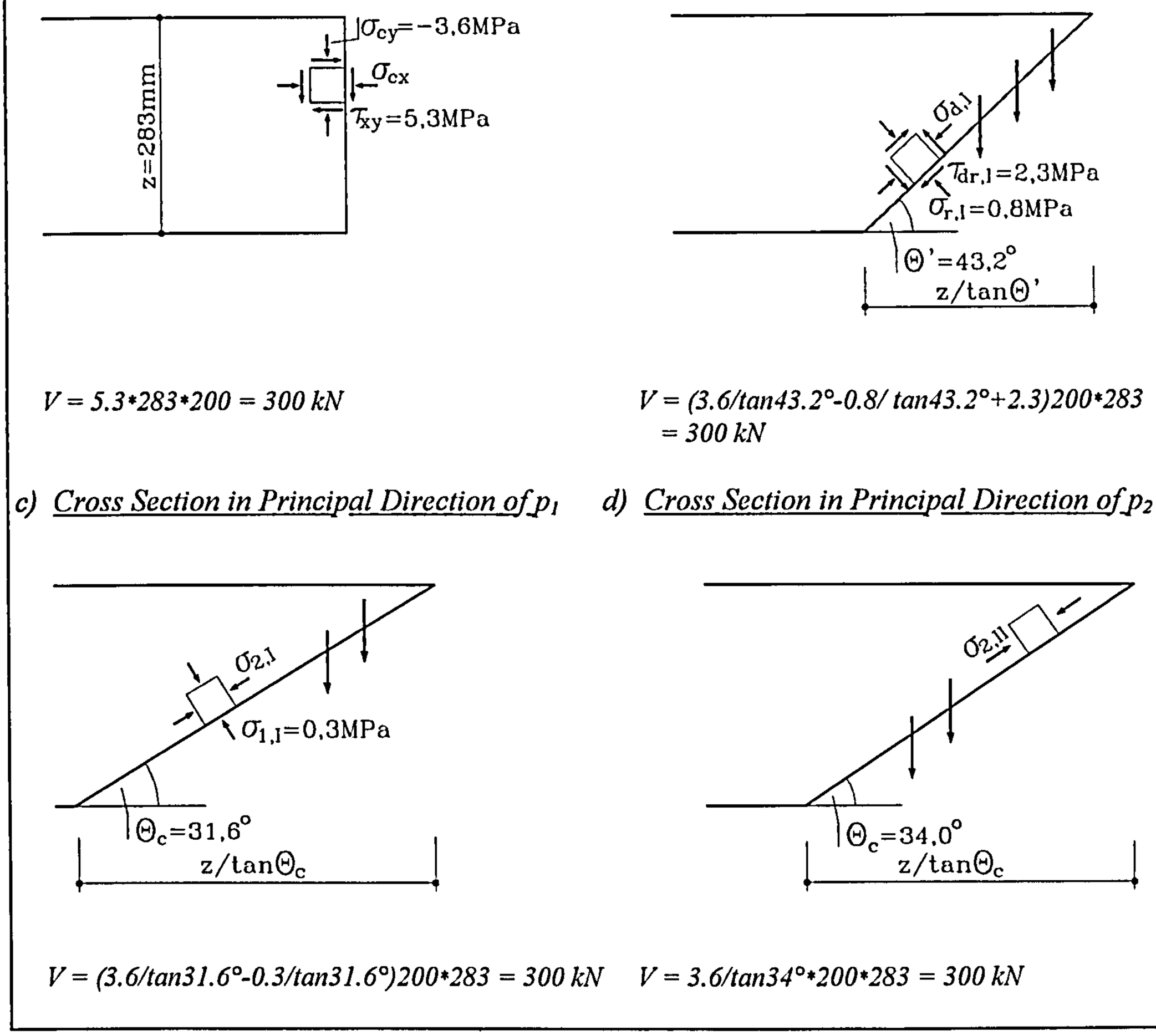

Fig.3.17 Vertical Equilibrium in Various Cross Sections

The longitudinal reinforcement ratio is $\rho_{sx} = 1.77\ \%$ and, therefore, p_1 gives $\sigma_{sx} = -\sigma_{cx}/\rho_{sx} = 9/0.0177 = 510\ MPa$ and p_2 yields $\sigma_{sx} = 7.7/0.0177 = 435\ MPa$. Both values are beyond yielding, which means that the horizontal equilibrium cannot be satisfied with the given amount of longitudinal reinforcement. A check of Kirmair's equation for the force in the chords reveals the core of the problem. Kirmair calculates the horizontal force in the web, which must be equilibrated by the longitudinal reinforcement, from Eq.(3.11) given in Fig.3.18 and this yields a value of $\sigma_{sx} = 3.27/0.0177 = 185\ MPa$, which is far below yielding. However, as we are dealing with a uniform stress state the shear stress at the edge of the web is not zero and must be taken into account. Fig.3.18 shows the proportion of the shear stress which has to be included in the horizontal equilibrium. The theoretical stress in the longitudinal reinforcement then becomes $\sigma_{sx} = 510\ MPa$, which is beyond yielding.

It is obvious that the calculated stress circles of Fig.3.16 are not correct, as the longitudinal reinforcement is not able to carry the load. Usually, the part of the tensile stress in the longitudinal reinforcement generated by the shear force is small when high moments are applied to the cross section. Indeed, in this case the overstrength of the steel bars may carry the additional load. However, the above investigations show that the theory is not free of shortcomings.

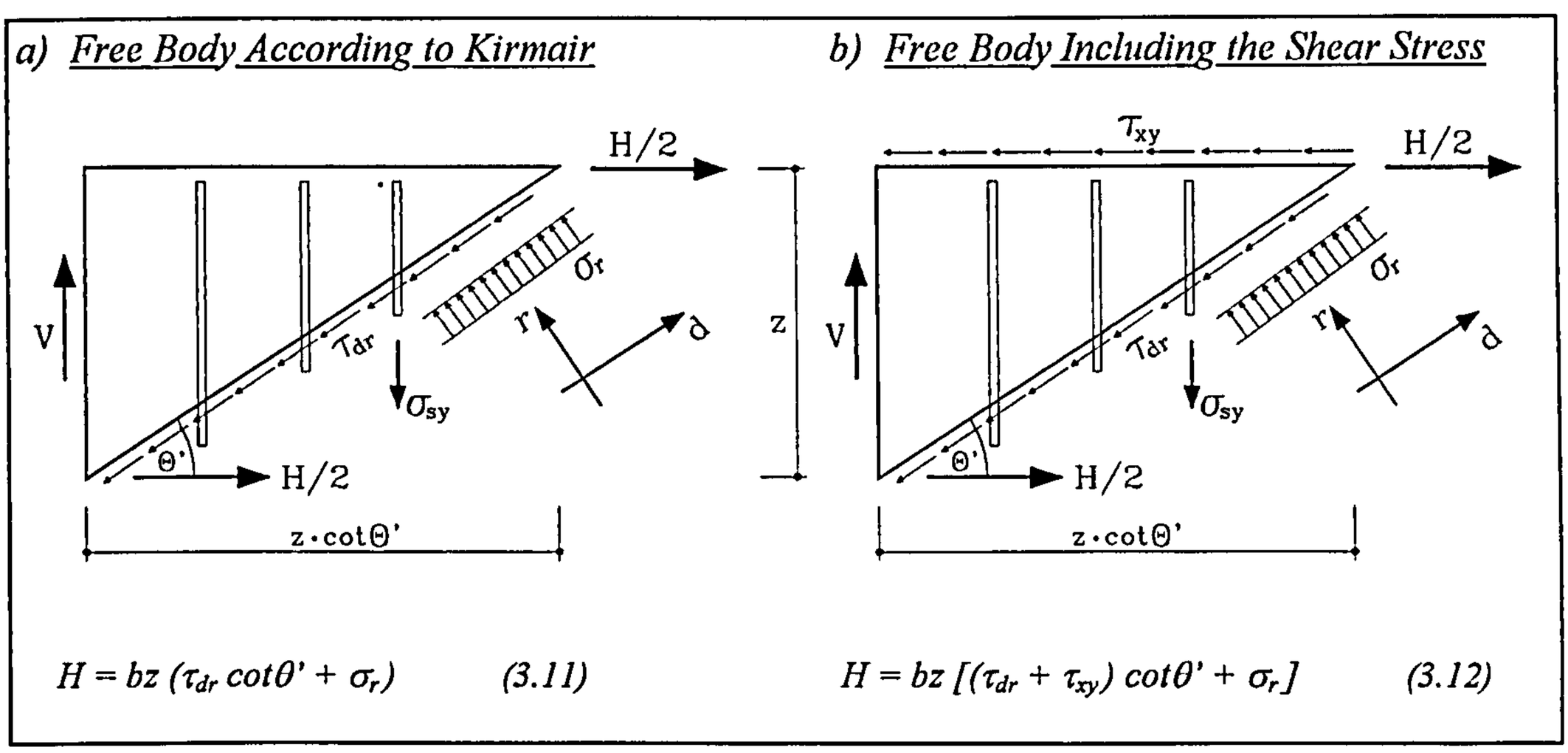

Fig.3.18 Horizontal Equilibrium in Web

3.6 Comparison of MCFT and Kupfer's Theory

In Sections 3.2 and 3.5 calculations were carried out on a rectangular cross section applying both the MCFT and Kupfer's shear theory. In this section, some of the results are compared allowing for the presentation of further evidence that Kupfer's theory does not yield the correct stress in the longitudinal reinforcement. In addition, strain circles delivered from calculations on the same cross section are investigated and compared in order to obtain an idea of the significance of features like hook slip, shrinkage and loss of bond, all of which are incorporated in Kupfer's theory.

For a shear force of $V=300\ kN$ the CFT delivers a compression stress in the concrete struts of $\sigma_2=-10.6\ MPa$, a stirrup stress of $\sigma_{sy}=400\ MPa$, and a stress in the longitudinal reinforcement of $\sigma_{sx}=320\ MPa$. The equivalent values for the MCFT calculation are $\sigma_2=-9.8\ MPa$, $\sigma_{sy}=340\ MPa$ and $\sigma_{sx}=280\ MPa$.

It is clear that the introduction of the tensile strength of the concrete relieves the various element members, which results in decreased stress values. The calculation using Kupfer's theory yields σ_2=*-11.4 MPa*, σ_{sy}=*290 MPa* and σ_{sx}=*140 MPa*. Obviously, the value σ_{sx} is not reasonable. As the angle of the principal stress direction decreases from *43.2°* to *34°*, it is correct that the stirrups are relieved and therefore, generate less tension stress. However, as a countermove the stress in the longitudinal reinforcement must increase and exceed the CFT and MCFT values, as the correct calculation with Eq.(3.12) in Section 3.5 clearly demonstrated.

Kupfer's theory includes hook slip, shrinkage and loss of bond for both reinforcements. These features are depicted in Fig.3.19 and some additional explanations on them will be given here. Hook slip occurs when high tension stresses are applied to a steel bar the hook of which is cast in concrete. Fig.3.19 shows the constitutive relationship for a bar with diameter *12 mm* and a concrete strength of f_c=*30 MPa*. It can be seen that the slip of the reinforcement bar depends strongly on whether the steel pull direction coincides with the cast direction of the specimen. This is because the concrete tends to settle below the hook and the tension force of the steel bar pushes it into the deteriorated concrete, thus causing a certain amount of relative displacement between steel and concrete. A longitudinal reinforcement bar which touches the hook at its highest point has a beneficial influence and prevents the hook from being completely pushed into the concrete. In Kupfer's theory the hook slip Δ is divided by the stirrup length giving the strain value $\Delta\varepsilon_s$ which is added to the overall strain ε_{sy} in the transverse direction. As will be seen later, $\Delta\varepsilon_s$ can become very high, depending on the beam depth and therefore the constitutive relations for the hook slip are to be handled carefully.

When the tensile strength of the concrete is exceeded in an RC member, a crack will occur causing a certain amount of bond loss along the steel bars. In a crack, the concrete stresses drop to zero, while in between them the concrete remains under tension. This is equivalent to the transfer of tensile stresses from steel to concrete between adjacent cracks, and decreases the strain in the transverse direction as the bulky concrete is much stiffer than the few slender steel bars. In Kupfer's theory this was taken into account by a factor α_{st} with which the stirrup strain was multiplied. Kirmair derived α_{st} from constitutive equations for loss of bond whose value is always less than *1*. In a similar fashion, the factor α_{sl} for the longitudinal reinforcement was introduced, but, in general, set to a value between *0.8-0.9*.

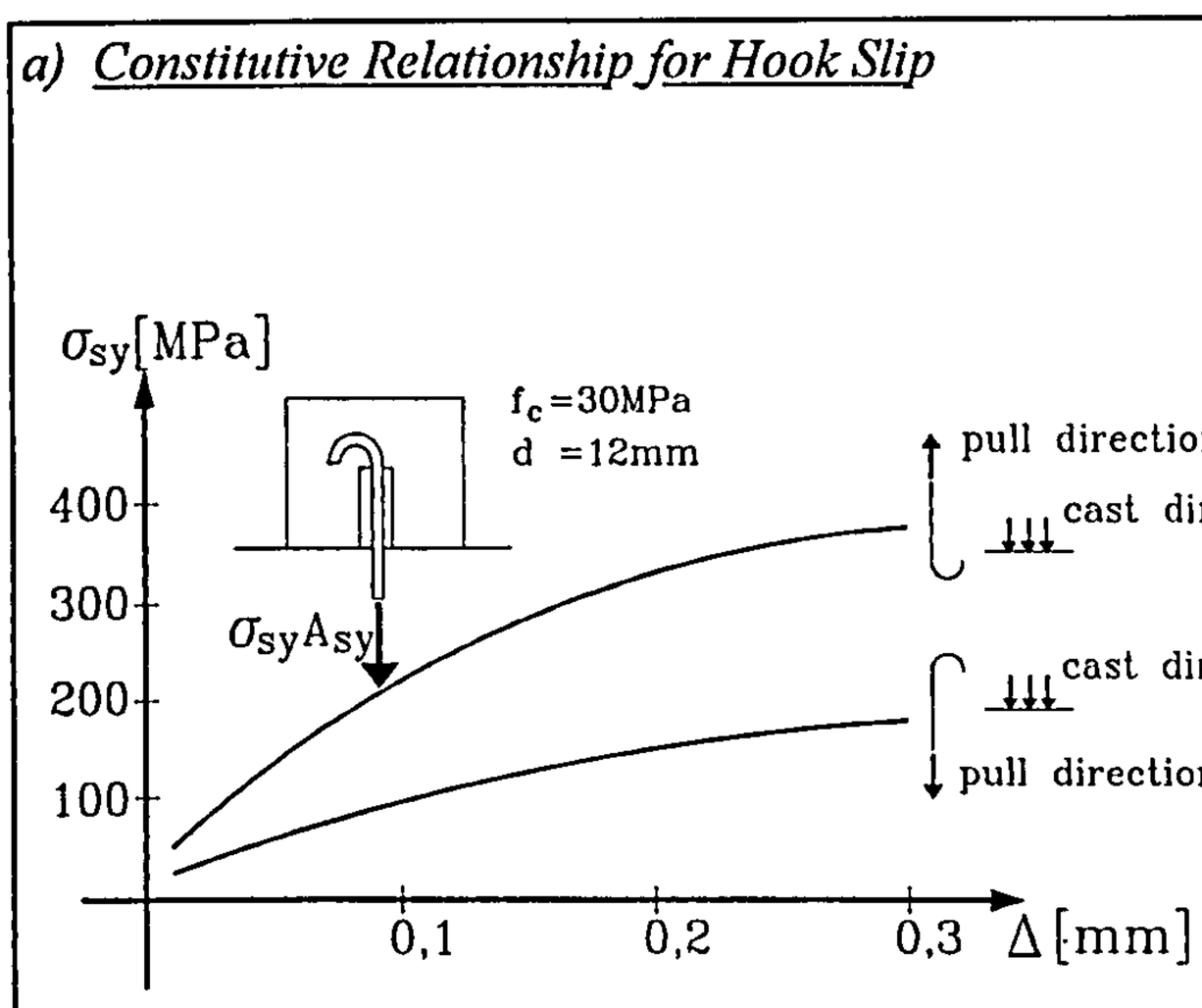

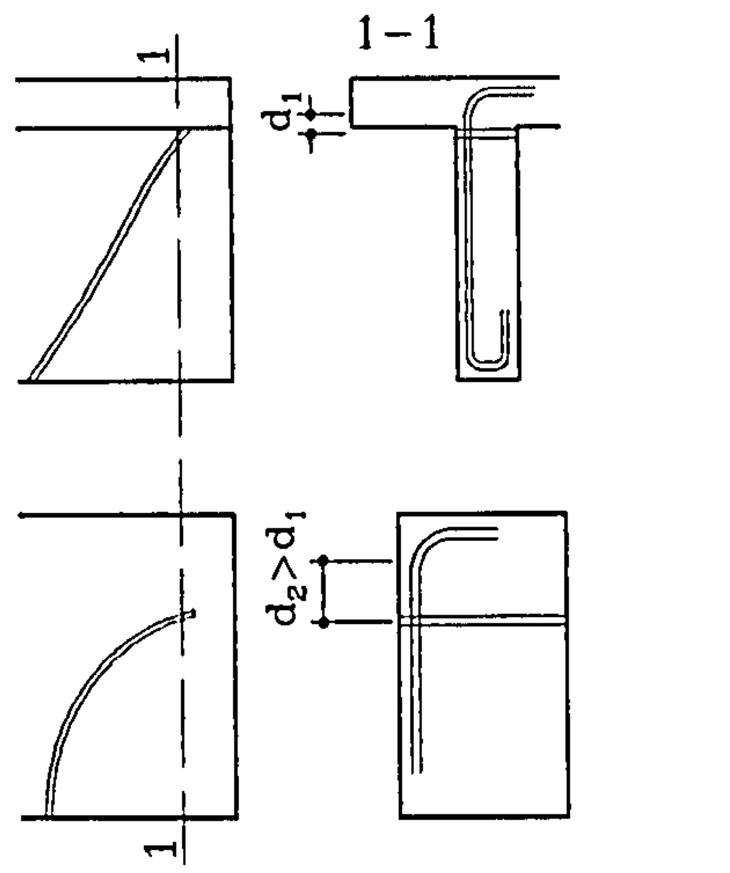

Δ = hook slip
d_1 = distance crack - hook in T beam
d_2 = distance crack - hook in rectangular beam

c) Stress State Caused by Stirrup Bond Stresses

Uniform stress state according to Kirmair:

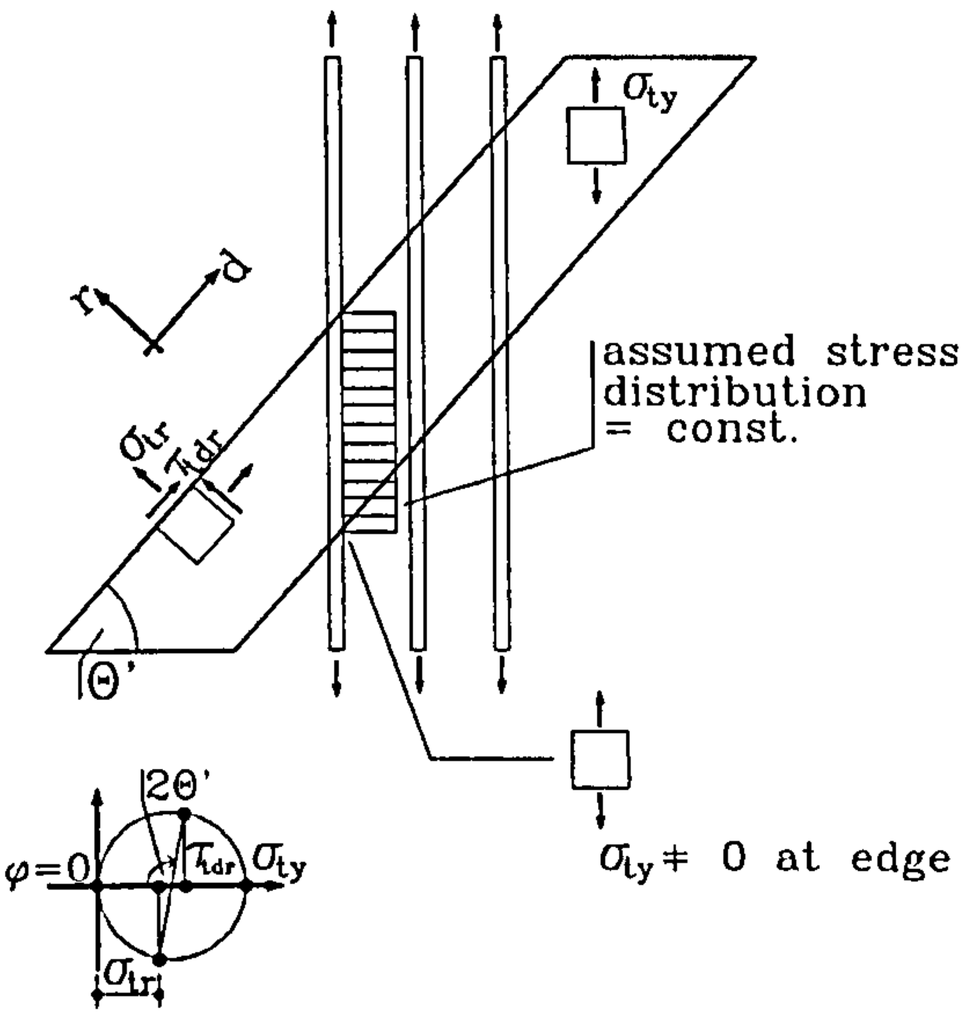

More physically correct stress state:

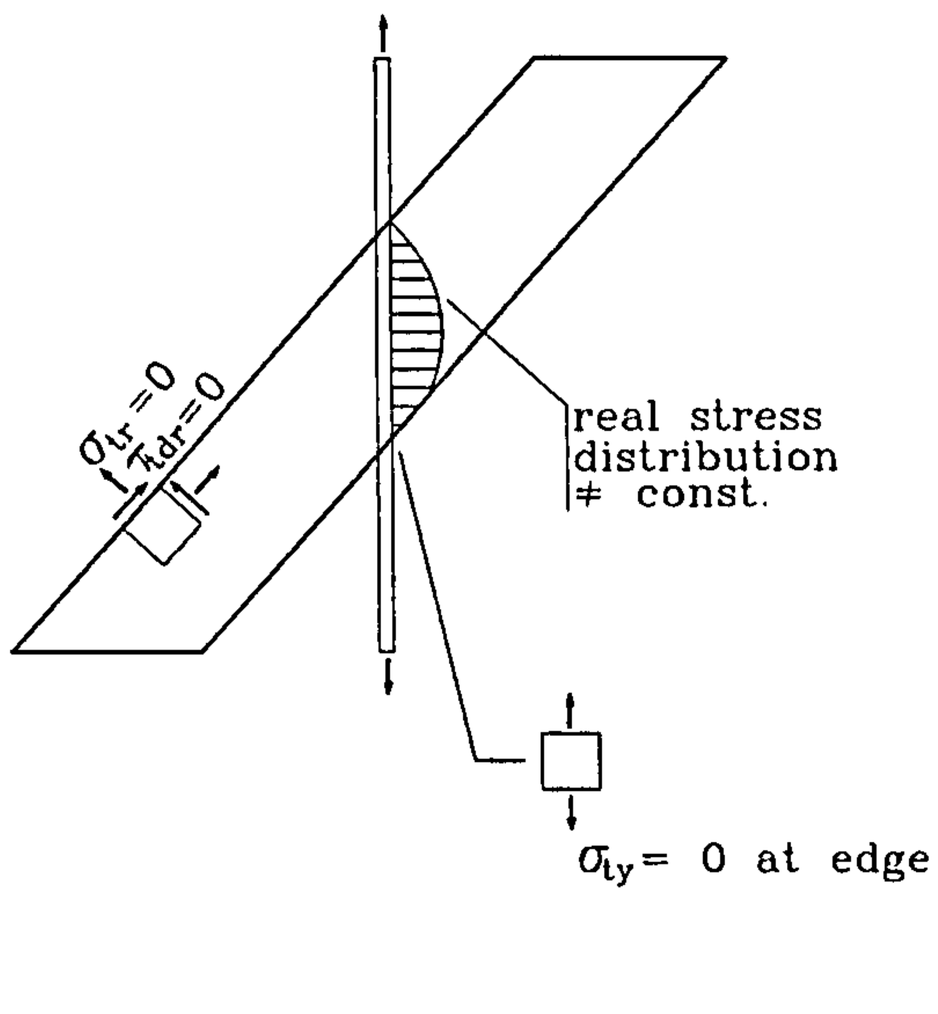

Final stress state in crack:

$\sigma_{cr} = \sigma_{tr} + \sigma_r$, $\tau_{cdr} = \tau_{tdr} + \tau_{dr}$

$\sigma_{cr} = \sigma_r$, $\tau_{cdr} = \tau_{dr}$

σ_{ty} = stress in y direction due to loss of stirrup bond
σ_{tr} , τ_{tdr} = stresses in crack due to loss of stirrup bond
σ_{cr} , τ_{cdr} = aggregate interlock stresses in crack including stresses due to loss of stirrup bond

Fig.3.19 Hook Slip and Loss of Stirrup Bond in Kupfer's Shear Theory

Kirmair assumed a uniform stress state in the concrete which is caused by bond stresses. This stress state is depicted in Fig.3.19.(c) in the left hand sketch whose principal tensile stress is σ_{ty} acting in the stirrup direction. This treatment of loss of bond generates nor-

mal and shear stresses along the crack edge which Kirmair added to the friction stresses σ_r and τ_{dr} to yield the final stress state of the web. He now calculates the mutual crack displacements v and w with σ_{cr} and τ_{cdr} using Walraven's constitutive equations for aggregate interlock. However, this is not appropriate as Walraven's equations require σ_r and τ_{dr} rather than σ_{cr} and τ_{cdr}. In fact, the assumption of a uniform stress state created by bond stresses is to blame for that flaw, as in reality the stress distribution along the stirrup bars is as shown in Fig.3.19.(c) in the right hand sketch. As can be seen from this the stresses at the crack edge are zero and no additional forces are generated in the crack which would be a physical contradiction anyway, since at a free edge no stresses of that manner can occur. Earlier in Section 3.5 it was stated that Kirmair's procedure yields two different sets of stresses for the stress state in the web. It is now obvious that the incorrect treatment of loss of stirrup bond caused this shortcoming.

Kupfer added a certain amount of strain to the total transverse strain in the web to account for shrinkage of the concrete. The reason for this is that shrinkage causes compression stresses in the reinforcement before an RC member is loaded. Once a force is applied the web must undergo deformations until zero stress is reached in the stirrups. This is equivalent to additional stirrup strains which increase the total transverse strain in the web. Typically the stirrup strain ε_{cs} due to shrinkage of the concrete is set to *0.2‰*. It should be noted that transverse strains $\Delta\varepsilon_s$ due to hook slip and ε_{cs} due to shrinkage do not increase any stirrup stress but only contribute to the strain state of the web.

In the following, results of calculations are discussed which have been carried out using the cross section and material properties of Fig.3.2.(c) and a shear force $V=300\ kN$ (see also Haas/Pilakoutas, 1995). Fig.3.20.(b) shows strain circles of the shear zone plotted from results of various computer runs with MCFT and Kupfer's theory. Strain circle I was obtained by Kupfer's theory using his constitutive equations for hook slip and loss of stirrup bond and circle II when hook slip, loss of bond and shrinkage was omitted. Circle III is the MCFT's circle and circle IV is the contribution of the concrete to the overall strain due to Kupfer's theory. Circle IV is depicted to give an idea of the order of magnitude of the strain in the web caused by cracking and bond slip. Initially, it is surprising that circle I, which is obtained by the standard procedure of Kupfer's theory, is much bigger than both the other circles. However, the evaluation of the data showed that the high value of the effective stirrup strain ε_y is mostly due to hook slip, which in the present case is highly overestimated.

In a rectangular beam shear cracks, causing loss of bond, pass through the stirrups at a relatively far distance from the upper hooks. However, for the occurrence of hook slip loss of bond is necessary in the vicinity of the hook.

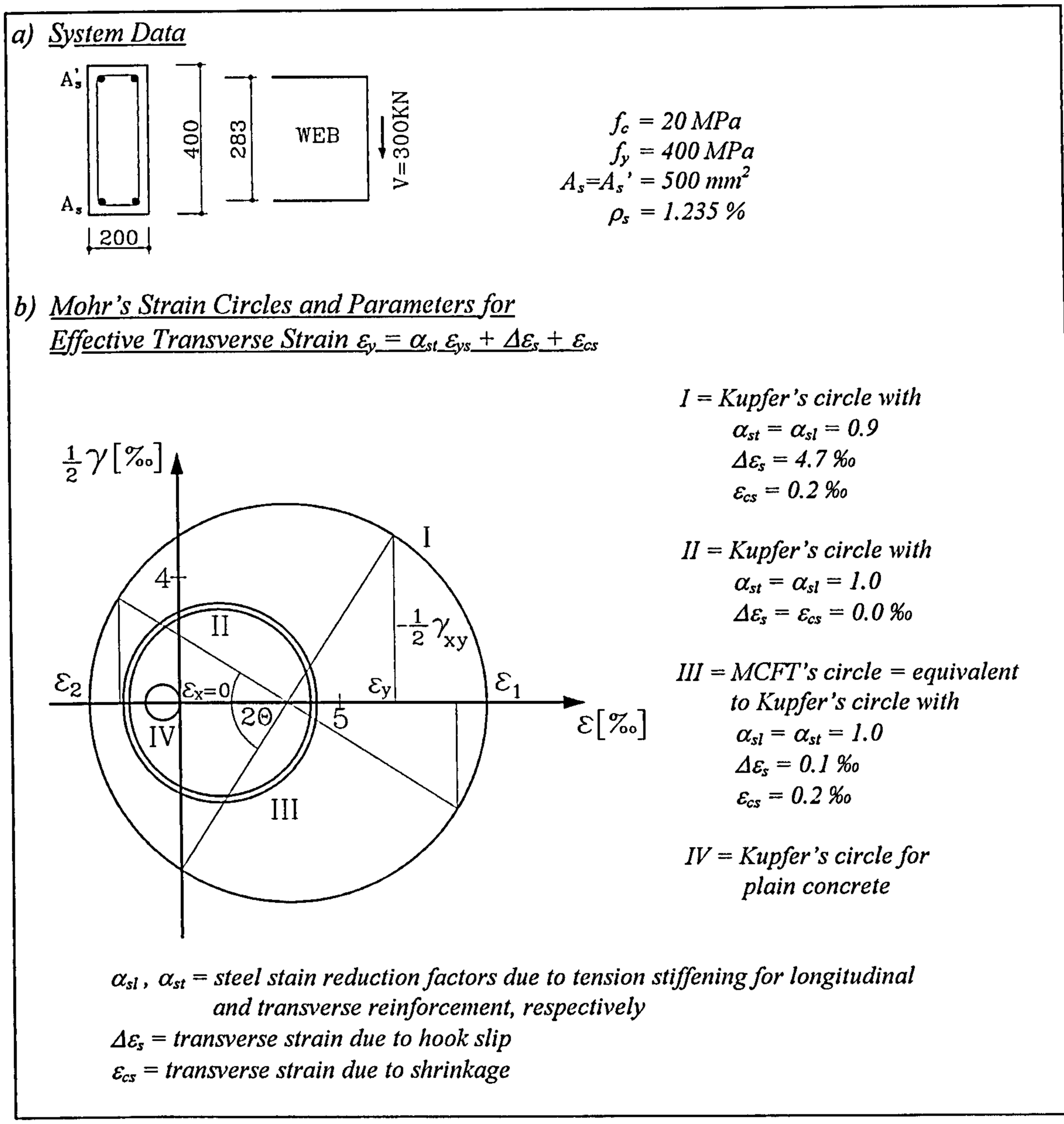

Fig.3.20 Comparison of MCFT's and Kupfer's Strain Circles

Fig.3.19.(b) describes the situation. In a rectangular beam the principal direction of the compression struts changes over the height of the member. At the bottom, compression struts have an inclination of nearly *90°* to the horizontal, while at the top fibre they are virtually horizontal. In between, compression struts undergo a smooth transition from *90°* to *0°*. This is visualised by the bending of shear cracks. The decrease of compression strut inclination coincides with a decline in stirrup stress, because a beam can be considered to consist of trusses arranged in horizontal layers of a certain height. Consequently, the stirrup stress drops towards the top fibre of a beam.

This decrease of stirrup stresses was measured by Leonhardt in many of his tests (see eg Leonhard/Walther, 1962, Page 34). It brings the crack propagation to a halt at a height which is usually far from the top fibre of a beam. This explains why in a rectangular beam the upper hooks do not yield any hook slip: The loss of bond provided by the crack, which is vital for any slip, does not occur in the vicinity of the hook.

In distinctly T or I shaped cross sections conditions are different. The inclination angle of the compression struts is nearly constant over the web height and drops to zero once the compression chord is reached. This means that the stirrup stress remains constantly high up to the bottom of the chord, as visualised by the crack pattern of these beams, where cracks propagate straight through the web up to the chord at an angle of about *45°*. Therefore, loss of stirrup bond occurs much nearer to the hook than in the case of a rectangular beam providing a substantial amount of hook slip.

The above considerations prove that in the sample of Fig.3.20 the upper hooks do not contribute to the hook slip at all, dropping the total value to far less than *50%* of the calculated one. It is obvious that the constitutive equation for hook slip used in Kupfer's theory is one reason for its restriction to distinctly T or I shaped cross sections. Kupfer's circle II is only slightly smaller than the MCFT's circle and by introducing a small amount of hook slip and a normal value of shrinkage, Kupfer's circle coincides exactly with the MCFT circle. This gives evidence that the MCFT yields reasonable results concerning the strain state of a web under shear action, although the angle of the principal stress direction θ_c according to both theories may differ to some extent. A check of the aggregate interlock stresses using the MCFT results and the data from the equivalent Kupfer run confirms the discrepancy in aggregate interlock modelling: The MCFT delivers zero values for the crack friction and the accompanying compression stress, while Kupfer's theory gives substantial amounts of crack stresses $\tau_{dr,II} = 1.8$ and $\sigma_{r,II} = -0.55$ *MPa* (see Fig.3.16).

The results of the investigations up to now depict that the compatibility equation used in the MCFT provides a certain amount of shear transfer through secondary shear carrying actions in an implicit way. Therefore, aggregate interlock is an intrinsic feature of the MCFT as are all other secondary actions, and there is no need for their treatment in any post-processing procedure.

3.7 Recalculation of Leonhardt's Shear Tests with LAYER

The most simple method to verify a theory is to confront it with test data which have not been used to establish the theory itself. In the early sixties Leonhardt/Walther (1964) started a series of tests which became famous as the Stuttgart shear tests. The reputation of the tests to this day is based on both the methodology, with which Leonhardt/Walther investigated the whole shear range and the comprehensive description and evaluation of all relevant test data. Therefore the shear tests of Leonhardt/Walther were chosen to scrutinise the reliability of the MCFT.

Beam			*ET1*	*ET2*	*ET3*	*ET4*	*T1*	*E4*	*E5-1*	*E5-2*
Test Data	l	*[m]*	*3.0*	*3.0*	*3.0*	*3.0*	*6.0*	*2.0*	*2.0*	*2.0*
	b_w	*[cm]*	*30*	*15*	*10*	*5*	*10*	*19*	*19*	*19*
	h	"	*35*	*35*	*35*	*35*	*90*	*32*	*32*	*32*
	d	"	*30*	*30*	*30*	*30*	*83*	*27*	*27*	*27*
	a/d		*3.5*	*3.5*	*3.5*	*3.5*	*3.0*	*2.8*	*2.8*	*2.0*
	f_c	*[MPa]*	*26.2*	*26.2*	*26.2*	*26.2*	*24.2*	*32.3*	*32.3*	*29.9*
	f_{ct}	"	*4.2*	*4.2*	*4.2*	*4.2*	*4.0*	*4.2*	*4.2*	*4.6*
	f_{yl}	"	*430*	*430*	*430*	*430*	*475*	*435*	*435*	*435*
	f_{yt}	"	*320*	*320*	*320*	*320*	*435*	*430*	*465*	*465*
	A_s	*[cm²]*	*12.6*	*12.6*	*12.6*	*12.6*	*85*	*12.7*	*12.7*	*12.7*
	ρ_{sy}	*[%]*	*0.17*	*0.35*	*0.52*	*1.04*	*2.83*	*0.64*	*0.71*	*0.71*
	$\sigma_{sy\,test}$*	*[MPa]*			*115*	*150*	*250*			
	$P_{u\,test}$	*[kN]*	*280*	*265*	*255*	*200*	*1600*	*375*	*380*	*530*
LAYER Calculation	*Concrete Layers*		*15*	*15*	*15*	*15*	*13*	*15*	*15*	*15*
	Steel Layers		*3*	*3*	*3*	*3*	*4*	*3*	*3*	*3*
	$\sigma_{sy\,cal}$*	*[MPa]*			*175*	*270*	*265*			
	$P_{u\,cal}$	*[kN]*	*290*	*260*	*250*	*195*	*1500*	*335*	*340*	*420*
	$P_{u\,test}/P_{u\,cal}$		*0.97*	*1.02*	*1.02*	*1.03*	*1.07*	*1.12*	*1.12*	*1.24*
	*Failure Mode***		*B*	*S1*	*S2*	*S3*	*S3*	*B*	*B*	*B/S2*

* ET3 and ET4 at serviceability level P=120 KN; T1 near ultimate limit P=1350 KN; ET1, ET2, E4, E5-1 and E5-2 no values
** B=Bending, S1=Shear (bending), S2=Shear (stirrup yielding), S3=Shear (diagonal compression)

Tab.3.3 Recalculation of Leonhardt's Beams with Transverse Reinforcement

Vecchio/Collins (1982) derived the constitutive laws of the MCFT from extensive testing of RC membrane panels. For the verification of their test data they used a concrete tensile strength of $f_{ct} = 0.33\sqrt{f_c}$. When recalculating Leonhardt's tests, as well as other shear tests described in the literature (eg in Kani, 1967), this was found to yield values too conservative for the section resistance of the scrutinised beams. Moreover, the tensile strength given in the descriptions of the various tests was in general much higher than the value taken by Vecchio/Collins. Therefore, for recalculations f_{ct} was either set to $0.75\sqrt{f_c}$, or taken from the test descriptions. In nearly all cases, both values proved to deliver good results.

In Tab.3.3 the recalculation of a selection of shear tests are depicted. The tests were deliberately chosen to reveal peculiarities of RC beams found to be worth mentioning. Some of the features are captured by the layered approach of the MCFT while others are not. The ET series was conducted at that time to investigate the influence of the web width on the capacity of reinforced concrete members. The series consisted of 4 specimens, the web width of which decreased in 4 steps from *30* to *5cm*, while all other quantities, such as concrete strength, longitudinal and transverse reinforcement and beam height, remained the same. The purpose of the tests was to prove that the capacity of RC beams is not proportional to the web width b_w when all other section properties are kept constant. The tests showed that the ultimate load dropped with b_w by only *30%* while the shear stresses in the web were nearly quadrupled. LAYER simulated this behaviour in a nearly perfect fashion, as can be seen from Tab.3.3.

For beams ET3 and ET4 computer runs were performed on the serviceability level of *120 kN* and stirrup stresses σ_{sy} were compared with those measured by Leonhardt. From Tab.3.3, it can be seen that the measured values are much smaller than the computed ones: For beam ET3 *35%*, and for beam ET4 even *45%*. The reason for this is the assumption of the MCFT that principal stress and strain directions for the concrete should coincide. It was seen earlier that a direct consequence of this assumption is the additional coincidence of principal stress and crack direction, so that $\theta' = \theta_c = \theta$ becomes valid. However, Kupfer showed that due to aggregate interlock crack angle, principal concrete stress direction and principal strain direction always deviate from each other to a certain extent. For normal section conditions (see Fig.3.21), which means that a positive moment and a negative shear force act on a positive cross section, the relationship $\theta' > \theta_c > \theta$ usually applies. This means that in reality the compression strut inclination is smaller than

given by the LAYER calculation. Consequently, the computed stirrup stresses are too high.

This shortcoming becomes only significant on the serviceability level of distinctly T shaped beams which fail in shear, therefore, it can be considered as being of minor importance. For instance, the run with beam T1 on a load level slightly below the ultimate limit yielded stirrup stresses only some *5%* higher than those measured during testing. In rectangular beams, in particular when failing in bending, the stirrup stresses are usually low and the differences vanish.

When the inclination angle of the compression struts is overestimated the stirrup stresses will go up. However, in this case the longitudinal reinforcement will be relieved thus keeping the total amount of reinforcing steel at the same level. From this point of view the MCFT cannot be regarded as yielding an uneconomic design.

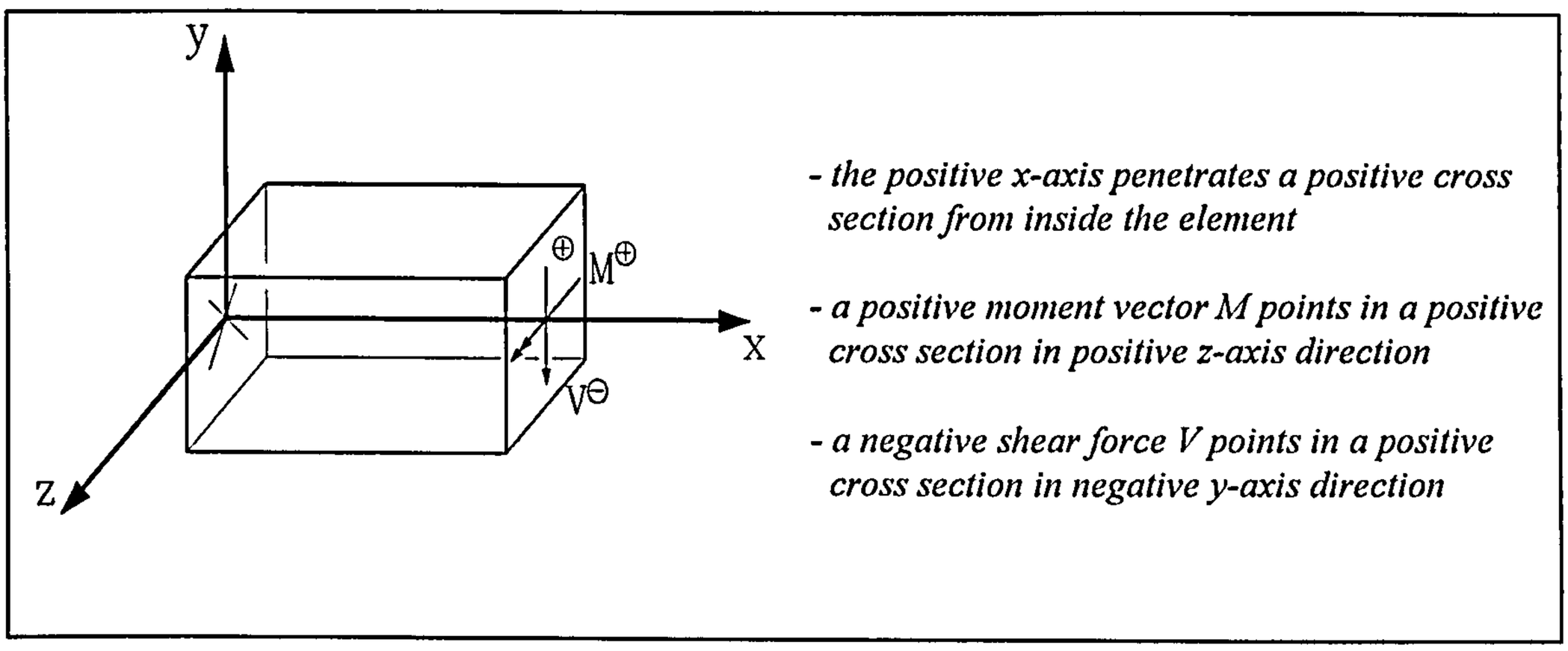

Fig.3.21 Sign Rules for Cross Sections and Section Forces

The beams of Leonhardt's E series which had a rectangular cross section all failed in bending and developed a flexural resistance which could not be verified with the material properties given in the test descriptions. The only possible explanation for this is that the yield strength of the reinforcing steel was higher than specified. It is surprising that Leonhardt did not comment on that issue. Despite the fact that the flexural resistance was *10* to *15%* higher than the yield strength of the steel could account for, it can be seen from test E5-2 that a substantial amount of shear must have been transferred by arch action. This is true because the recalculation gave an ultimate load of only *420 kN* by indicating a shear failure because of stirrup yielding.

From this result it becomes obvious that section analysis procedures are not suitable for calculations with RC elements having shear ratios in the range of *2.0*. Kani (1964) showed with his shear valley that arch action becomes substantial when the shear ratio drops below a value of *2.5*. This is the level where section analysis should no longer be employed.

In Tab.3.3 four different types of failure are specified. In fact, LAYER was able to identify all these failure types in a proper way. Bending failure was encountered when, after yielding of the longitudinal reinforcement, a given moment could not be reached. Shear failure *S1* happened when after stirrup yielding the compression strength of the concrete was attained, and shear failure of type *S2* occurred when after excessive stirrup yielding the longitudinal reinforcement approached the yield strain. Shear failure *S3* was identified when the concrete in the web was exhausted by reaching the admissible value without getting convergence any longer. Finally, shear failure of type *S4* occurred when, in runs without transverse reinforcement, the tension stress in the concrete of the web tried to exceed the admissible value and the run was terminated with convergence problems. Indeed, *S4* was the typical shear failure that was encountered in all recalculations of RC beams without stirrup reinforcement when the shear ratio was between *2.5* and *7*.

The introduction of the tensile strength of the concrete in the MCFT is equivalent to an additional tensile tie which acts perpendicular to the compression strut. This was explained in Sections 3.2 and 3.3 where it was shown that a crack does not interrupt the stress flow in this tensile tie as the aggregate interlocking forces ensure the ongoing transfer of tension stresses across a crack. If this is true then the MCFT truss is a stable mechanism even in the absence of those tensile ties which usually are supplied by the transverse reinforcement. In fact, when omitting the aggregate interlock check, LAYER can be used in exactly the same fashion as for beams with longitudinal and transverse reinforcement. As already mentioned, the results, obtained from LAYER when applying the original constitutive laws of the MCFT (see Vecchio/Collins, 1986), are useless as the relationship for the stresses σ_{cl} provides too much strength in its principal tensile direction. This is in particular true for beams with little or no transverse reinforcement.

Tab.3.4 contains a selection of tests carried out by Leonhardt/Walther (1964) on RC beams without transverse reinforcement. The selection includes the complete D-series performed to investigate the size effect, a curious structural behaviour encountered on

members without shear reinforcement. It can be seen that, when omitting the aggregate interlock check of the MCFT, LAYER is able to predict both ultimate load and failure mode in an appropriate way. Moreover, it can be seen from Tab.3.4 that the program even captures the size effect to a certain extend. This will be briefly explained hereafter.

Beam			*6*	*7-1*	*8-1*	*9-1*	*D1*	*D2*	*D3*	*D4*
Test Data	*l*	*[m]*	*2.35*	*3.1*	*3.6*	*5.8*	*0.52*	*1.04*	*1.56*	*2.08*
	b	*[cm]*	*19*	*19*	*19*	*19*	*5*	*10*	*15*	*20*
	h	*"*	*32*	*32*	*32*	*32*	*8*	*16*	*24*	*32*
	d	*"*	*27*	*27*	*27*	*27*	*7*	*14*	*21*	*28*
	a/d		*4*	*5*	*6*	*7*	*3*	*3*	*3*	*3*
	f_c	*[MPa]*	*30.2*	*30.2*	*30.2*	*30.2*	*38.0*	*38.0*	*39.4*	*36.1*
	f_{ct}	*"*	*3.6*	*3.6*	*3.6*	*3.6*	*4.6*	*4.6*	*4.7*	*4.3*
	f_{yl}	*"*	*420*	*420*	*420*	*420*	*460*	*435*	*420*	*450*
	A_s	*[cm²]*	*10.6*	*10.6*	*10.6*	*10.6*	*0.6*	*2.3*	*5.1*	*9.4*
	$P_{u\,test}$	*[kN]*	*128*	*118*	*119*	*105*	*15*	*45*	*90*	*145*
	$m_{us\,test}$	*[MPa]*					*6.4*	*4.8*	*4.3*	*4.0*
SMAL Calculation	*Concrete Layers*		*15*	*15*	*15*	*15*	*11*	*11*	*11*	*11*
	Steel Layers		*1*	*1*	*1*	*1*	*1*	*1*	*1*	*1*
	$P_{u\,cal}$	*[kN]*	*132*	*123*	*115*	*101`*	*13.5*	*45*	*94*	*145*
	$m_{us\,cal}$	*[MPa]*					*5.9*	*4.8*	*4.5*	*4.0*
	$P_{u\,test}/P_{u\,cal}$		*0.97*	*0.96*	*1.04*	*1.04*	*1.11*	*1.0*	*0.96*	*1.0*
	*Failure Mode**		*S4*	*S4*	*S4*	*B*	*S4*	*S4*	*S4*	*S4*

* B=Bending, S4=Shear (diagonal tension)

Tab.3.4 Recalculation of Leonhardt's Beams without Transverse Reinforcement (see Leonhardt/Walther, 1964)

It was recognised by many researchers (eg Leonhardt / Walther, 1964) that RC beams failing due to bending develop the same level of safety provided the mathematical conditions of similarity are met. This can be expressed by the equation: $m_u = M_u/(bd^2) = const$, where M_u is the section moment at the ultimate limit for an RC beam failing in bending. Leonhardt / Walther (1964) and Kani (1967) proved with their testing that the above equation does not apply for beams without stirrups failing in shear, which might be put simply by: $m_{us} = M_{us}/(bd^2) \neq const$. Here M_{us} denotes the section moment at the ultimate limit state for RC beams without stirrups failing in shear. This phenomenon was called size effect, and later in the 1980s could be explained by Reinhardt (1981) and Walraven/ Lehwalter (1990) by means of fracture mechanics.

For the sake of completeness it shall be mentioned that, in general, the size effect also applies to RC beams with web reinforcement failing in shear but the decrease in relative section strength is much smaller and, hence, the influence of h is usually neglected. However, as will be seen in the next section, when a structural wall with little transverse reinforcement but considerable length is analysed, the size effect might have a significant influence on the response of the wall. Tab.3.4 reveals the size effect with decreasing values m_{su} for the members of the D-series consisting of the geometrically similar specimens D1 through to D4.

3.8 The Calculation of Shear Deflections Using LAYER

In contrast to deflections due to bending, the evaluation of shear deflections in a cracked RC member has always been a difficult and controversial procedure. In 1966 Dilger calculated shear deflections in a cracked concrete beam based on the deformations of a truss, through which he modelled the loaded structure. His idea was that shear deflections must result from the deformations of those truss members which are linked to the transfer of shear. Consequently, he calculated shear deflections from the deformations of compression struts and tensile ties and assigned deflections due to bending to the chords. This means that for the calculation of shear deformations the chords are considered to be totally rigid while compression struts are shortened and tensile ties elongated. Fig.3.22 describes Dilger's method, through which he derived a cracked shear stiffness analogous to the elastic shear stiffness of isotropic material. Then he calculated the shear deflections of a cracked RC member in exactly the same way as for an uncracked beam. In his original work Dilger analysed a truss with inclined tensile ties. For the sake of simplicity and because this work concentrates on orthogonal grids of reinforcement, Dilger's original derivation was rewritten for vertical stirrups, as can be seen from Fig.3.22.

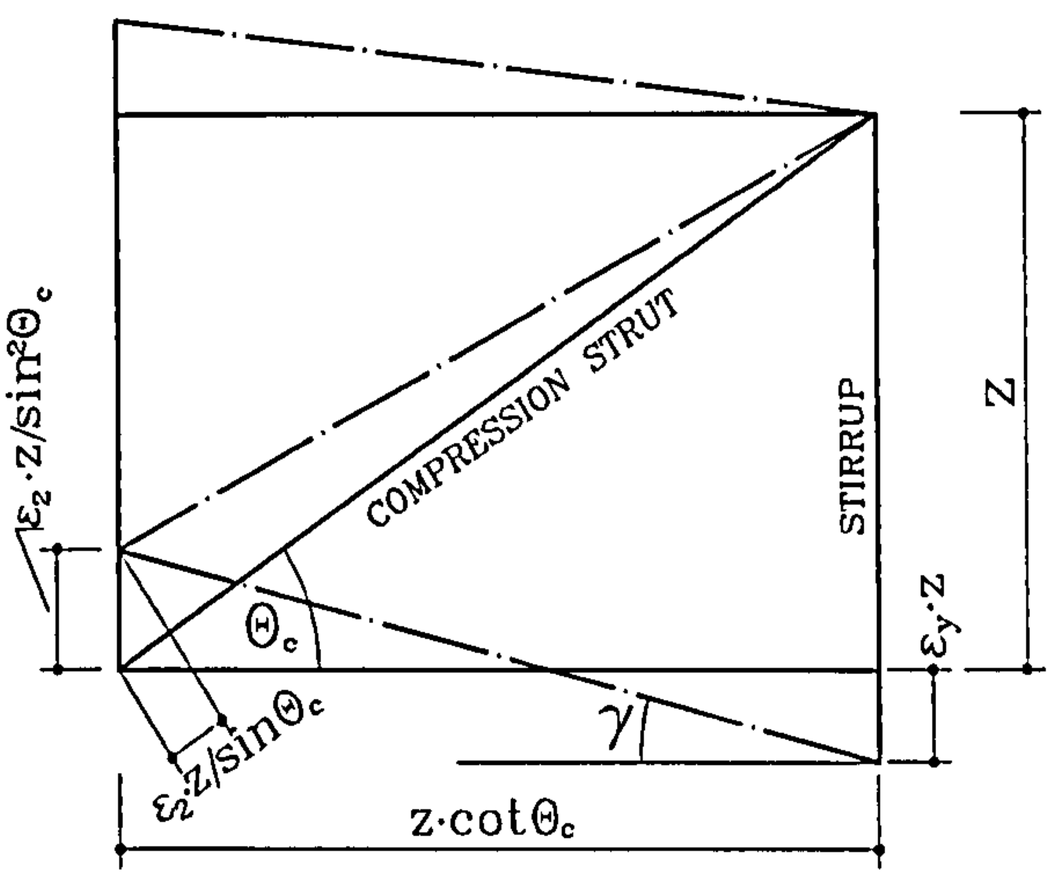

Fig.3.22 Dilger's Approach to Calculating Shear Deflections in a Cracked RC Beam

Dilger used only one truss for the entire beam height, as usual at the time. However, this assumption restricted his approach to distinctly T or I shaped cross sections, although he did not comment on this. It is, therefore, not surprising that he verified his method by recalculating Leonhardt's beam T1, the cross section of which is given in Fig.3.24. The method is certainly not to be used for rectangular beams where θ_c varies to a great extent over the web height.

If in Dilger's equation for K_{II}, ρ_{sy} is set to zero, then K_{II} will become zero as well. This means that Dilger's method yields no shear stiffness for beams without transverse reinforcement. As we know, this is in contrast to the physical reality. The shear stiffness of an element without stirrups is provided by the tensile strength of the concrete which Dilger did not account for. It is true, Dilger can simulate the tensile strength by varying the inclination angle of the compression struts, in the same way as Kupfer does with his model, but an appropriate treatment of shear should include the additional tension tie which is supplied by the tensile strength of the concrete.

a) System

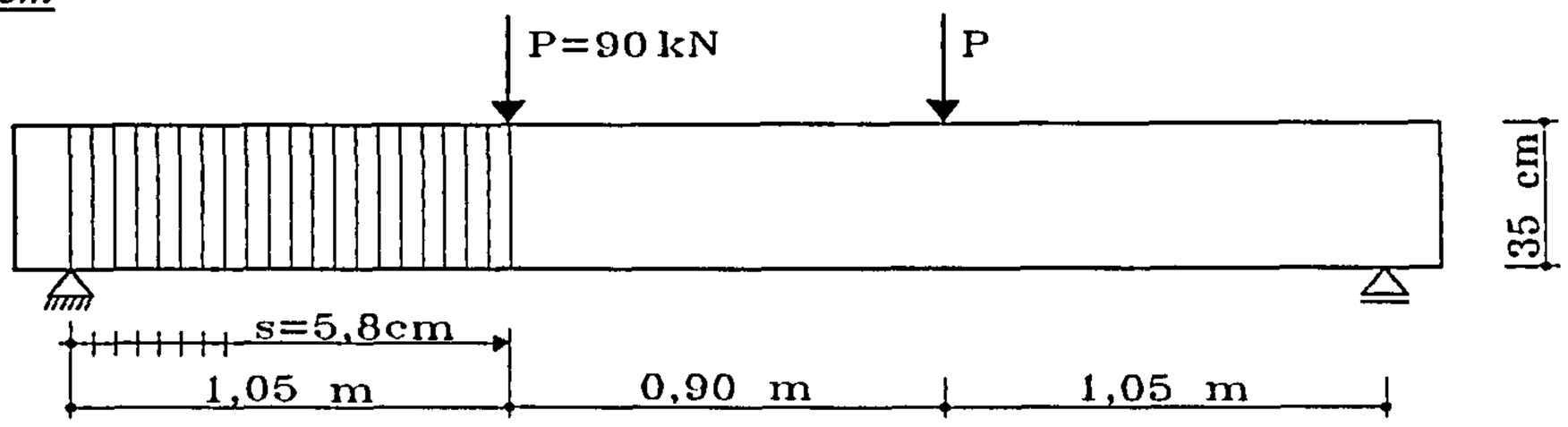

b) Moment Distribution

c) Curvature Distribution

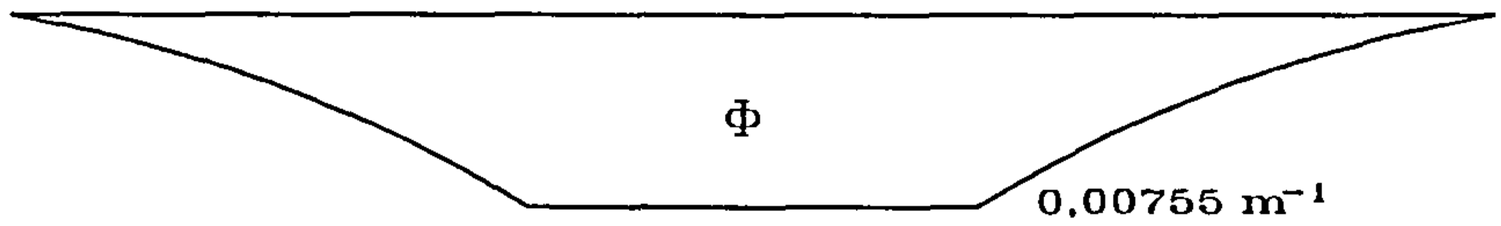

d) Moments due to Unity

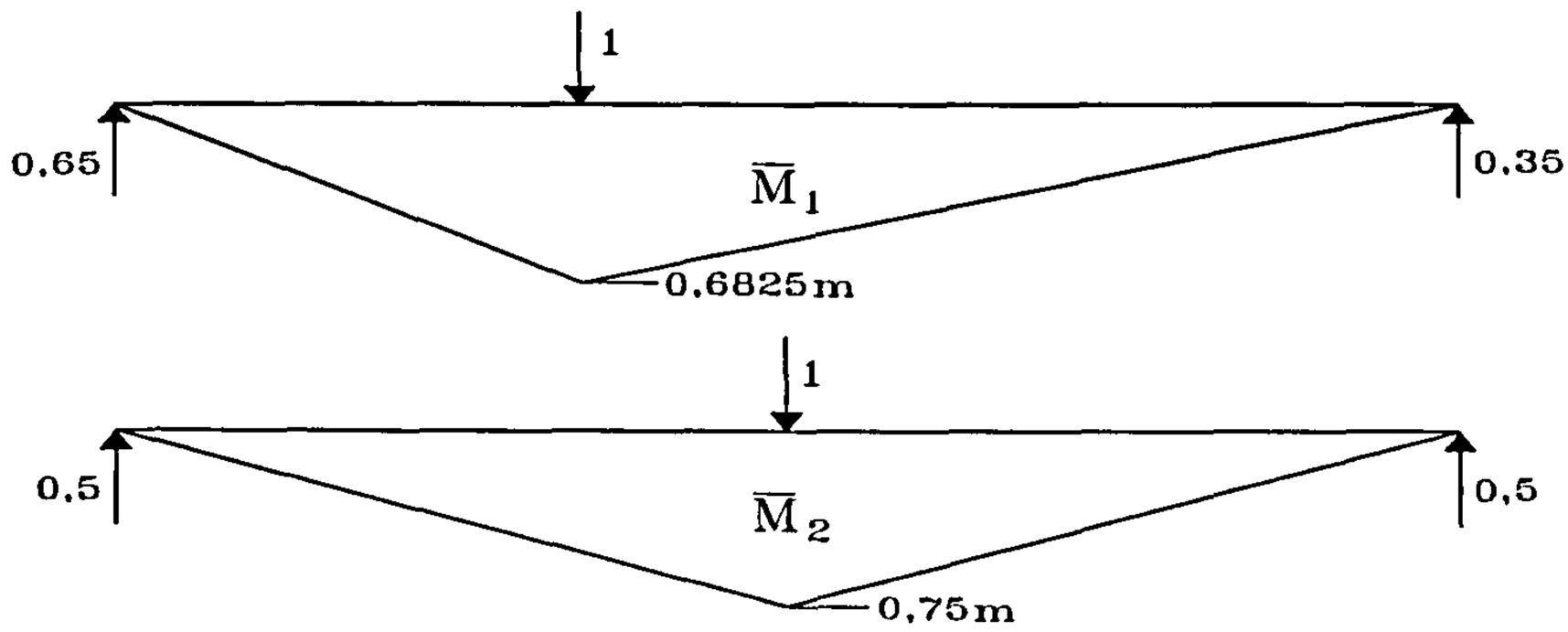

e) Calculation of Deflections

Deflections due to flexure:

$$\delta_{Mcal}^{load} = \int_l \overline{M}_1 \Phi dx = 6.34\ mm \qquad (3.13)$$

$$\delta_{Mcal}^{mid\text{-}span} = \int_l \overline{M}_2 \Phi dx = 7.11\ mm$$

Energy due to flexure:

$$E_M = \sum \sigma_x \varepsilon_x \Delta V = 1.13\ kNm$$

Total energy:

$$E_V = \sum \tau_{xy} \gamma_{xy} \Delta V = 0.34\ kNm$$

Energy due to shear:

$E_T = E_M + E_V = 1.47\ kNm$

Shear proportion:

$p_S = E_V/(E_M+E_V) = 23\%$

Work of the load:

$W_L = 0.00823 \cdot 180 = 1.48\ kNm$

Total deflection:

$\delta_{cal}^{load} = 6.34+6.34*0.23/(1-0.23) = 8.23\ mm$

Shear deflection:

$\delta_{V\,cal}^{load} = 6.34 \cdot 0.23/(1-0.23) = 1.89\ mm$

Check of shear proportion:

$p_s = \delta_{V\,cal}^{load} / \delta_{cal}^{load} = 1.89/8.23 = 0.23$

Fig.3.23 Calculation of the Shear Deflections of Leonhardt's Beam ET4 with the MCFT

In Dilger's equations two quantities remain obscure: The inclination angle θ_c and the Young's modulus E_c. If Dilger's method is used for T shaped beams under high shear, θ_c can be taken as approximately $45°$. However, E_c can vary in a wide range and its specification in a cracked beam is uncertain. It is the simple constitutive model and the lack of a compatibility relationship for θ_c which substantially restricts the method in its use for the calculation of shear deflections in a cracked reinforced concrete member. Nevertheless, Dilger successfully recalculated some of Leonhardt's test results, in particular the deflections of the T beams under high shear, but it is obvious that the method is by nature not suitable for implementation in an FE program.

It was explained in the first sections of Chapter 3 how the layered approach of the MCFT divides a structure in small portions, the stress and strain state of which can be considered to be uniform and is given by the constitutive laws of the theory. In this respect the MCFT is quite similar to the FE-Method which also models a structure with elements of finite size. However, it is clear that the layered approach is confined to structures with relatively simple shapes, such as beams or walls of constant cross sections and without any voids. The constitutive laws of the MCFT, derived from extensive testing, conceive a virtually new material which simulates the physical behaviour of cracked reinforced concrete. The new material is based on the σ/ε relationships of steel and concrete. It is completely described by its stress and strain states which can be visualised by Mohr's circles. The knowledge of the stress and strain state at each material point of the cracked reinforced concrete member enables the MCFT to calculate the deflections of the structure.

Fig.3.23 shows this calculation for Leonhardt's beam ET4 for a load stage of *180 kN* which is near the ultimate limit state. The procedure starts with the analysis of the various cross sections under consideration. The distance s between two adjacent cross sections should be in the range of $h/6$, where h is the beam height. In this case s was taken to be *5.8 cm* which means that in the shear span, *19* cross sections had to be analysed. The analysis delivers the stress and strain state in each layer necessary for both the equilibrium of the elements and that of the free beam bodies. From these data the curvature distribution given in Fig.3.23.(c) was extracted. The moment due to unity $\overline{M}_i$ was needed to calculate $\delta_{M\,cal}^{load}$ which is the deflection under the load due to flexure. $\delta_{M\,cal}^{load}$ is necessary to determine $\delta_{V\,cal}^{load}$ the deflection under the load due to shear, as the shear pro-

portion factor p_S refers to that point. The reason for this is the equivalence of the stress energy of the entire beam with the work of the load along its vertical displacement: $E_T=W_L$. The stress energy which is assigned to shear stresses and shear strains equals the work of the load along its vertical displacement due to shear and the energy assigned to normal stresses and normal strains consequently equals the work of the load along its vertical displacement due to flexure. Using this analogy the deflections generated by shear can be calculated, as the deflections due to flexure are known, as well as the energies due to flexure and shear, E_M and E_V, respectively.

Between the two applied loads P, no shear occurs and, hence, the shear energy is zero. This means that the deflection due to shear under the load is equal to the deflection due to shear in mid-span: $\delta_{V\,cal}^{load} = \delta_{V\,cal}^{mid\text{-}span}$. This yields the surprising result that the proportion of shear deflection to the total deflection is not constant, but increases from mid-span to the supports. This observation can be verified by the fact that the stress energy due to flexure decreases from mid-span to the supports to zero, whilst the shear energy decreases by a much smaller amount which is *50%* at the most in cases where shear deflections are higher than *15%* of the total deflections. The significant finding here is that the shear proportion factor p_S increases towards the supports.

For completeness it should be mentioned that the proportion of energy provided by the stresses and strains, σ_y and ε_y, respectively, is zero:

$$\sum \sigma_y \varepsilon_y \Delta V = \sum \sigma_{cy} \varepsilon_{cy} \Delta V + \sum \rho_{sy} \sigma_{sy} \varepsilon_{sy} \Delta V = 0\,.$$

The first term on the right side of the equation is the energy of the concrete stresses along the concrete strains and the second summation the energy of the steel stresses along the steel strains. The MCFT postulates that ε_{cy}, which is the strain in the plain concrete, is equal to ε_{sy}, which is the strain in the steel and both are equal to ε_y, which is the strain in the cracked reinforced concrete. As in y-direction no stresses are applied to the RC element, the stirrup stresses must counterbalance the concrete stresses which means that $\rho_{sy}\sigma_{sy} = -\sigma_{cy}$. With this, the above equation becomes zero.

A selection of Leonhardt's shear tests was taken to carry out calculations of deflections using the aforementioned method. Some of the specimens had a rectangular cross section without transverse reinforcement, while others were T or I shaped with varying amounts of stirrups. The results are depicted in Tab.3.5. It is obvious that in all cases the calcu-

lated deflections were smaller than the measured ones. This is typical for analyses based on the deformation method where structures tend to behave too stiffly. Therefore, quite the same observation can be made when evaluating deflection calculated with the finite element method. Sometimes the differences between the calculated and measured values are substantial and it is assumed that other reasons might also have contributed to that gap.

Beam:	*5*	*7-1*	*9-1*	*ET1*	*ET2*	*ET3*	*ET4*	*E4*	*E5-2*	*E6*	*T1*	*TA9*
Load:												
P [kN]	120	112	96	240	240	240	180	279	372	153	1400	600
Deflections:												
δ_{test} [mm]	2.57	9.48	50.7	13.2	15.4	17.8	11.9	5.93	7.00	2.76	19.2	14.16
$\delta_{pl\ test}$ "	0.32	1.79	12.3	3.64	5.28	7.25	3.83	0.95	-	0.49	-	-
δ_{cal} "	2.15	8.64	42.1	8.00	9.97	11.4	9.00	4.80	5.57	2.45	13.9	8.21
$\delta_{V\ cal\ (Shear)}$ "	0.17	0.50	0.8	0.24	0.71	1.44	1.89	0.43	0.44	0.19	6.0	1.72
$\delta_{M\ cal\ (Bend.)}$ "	1.98	8.14	41.3	7.76	9.26	9.96	7.11	4.37	5.13	2.26	7.9	6.49
$\delta_{cal} / \delta_{test}$	0.84	0.91	0.83	0.61	0.65	0.64	0.76	0.81	0.80	0.89	0.73	0.58
$\delta_{V\ cal} / \delta_{cal}$	0.08	0.06	0.02	0.03	0.07	0.13	0.21	0.09	0.08	0.08	0.43	0.21
Failure Mode:*	S4	S4	B	B	S1	S2	S3	B	B	S4	S3	B
Ult. Limit:												
$P_{u\ test}$ [kN]	137	122	111	280	263	255	198	375	528	186	1600	700
$P_{u\ cal}$ "	136	118	105	290	260	250	195	362	512	185	1500	682
Stirrups:												
ρ_s [%]	-	-	-	0.17	0.35	0.52	1.04	0.64	0.71	-	2.8	1.29
Shear Ratio:												
a/d	3.0	5.0	7.0	3.5	3.5	3.5	3.5	2.8	2.0	2.8	2.8	3.3

* B=Bending, S1=Shear (bending), S2=Shear (stirrup yielding), S3=Shear (diagonal compression), S4=Shear (diagonal tension)

Tab.3.5 Deflections Calculated from Leonhardt's Shear Tests Using LAYER

The applied load was always well above the serviceability level and in some cases near the ultimate limit. This means that plastic deformations might have occurred as well, although their amount cannot be high in beams mostly failing in shear. The method of calculating shear deflections explained above and shown in Fig.3.23 does not account for plastic deformations and, hence, a part of the difference in calculated and measured values might be attributed to that. In some of his tests Leonhardt gave the deflections that remained when the load was removed. Where available, these values were quoted in Tab.3.5 and in fact, the sum of calculated and plastic deflections matches the measured ones quite well.

Furthermore, Tab.3.5 reveals that in beams with a rectangular cross section no appreciable shear deflections occur and, hence, their proportion is usually less than *10%* of the total deflections, no matter whether the beam is stirrup reinforced or not. However, in transversely reinforced concrete beams which are distinctly T or I shaped, shear deflections are higher than *20%* and, under certain circumstances, for instance when very high shear stresses are generated, they can become as high as the deflections due to bending. In those beams occasionally a bending type of failure occurs, although high shear deflections are present and this gives rise to the assumption that a design which avoids shear failure does not necessarily avoid high shear deflections as well. In Chapter 5, where the influence of shear deflection on the ductility of RC structures is scrutinised, this finding will be dealt with in more detail.

In a building, quantities like deflection or ductility are global values and, as mentioned earlier, they can only be computed in a reasonable way by means of an FE method. Therefore, the results presented in this section can only give some indication of the direction which should be taken towards a general solution of the shear problem in FE procedures. Nevertheless, an investigation on displacement ductility will be presented here and the results will be used later to discuss calculations carried out with ABAQUS and given in Chapter 4 of this work.

Once again, one of Leonhardt's tests (1964) was chosen to investigate how the ratio of shear and total deformation develops in a beam under high shear when the load approaches the ultimate limit. Fig.3.24 shows the cross section of Leonhardt's beam T1 and the ω/δ-relationship, where ω is the ratio of shear and total deflection and δ the total deflection at a certain load stage. The load which generates the deflection δ is also given in the graph. Curve *1* represents the values given by Leonhardt where the deflections due to flexure were calculated from the relation $\delta_M = \int MM'/EI \, dx$. I is the inertia moment of the cracked cross section, while E is the Young's modulus of the concrete in compression. The proportion of δ which is attributed to shear was then obtained as $\delta_V = \delta - \delta_M$. Curve *2* was derived by calculating δ_V from the MCFT described in the above section and δ_M from the *moment-curvature* relationship of the given cross section. It can be seen from Fig.3.24 that the deflections due to shear are dependent on the applied load. Before cracking starts δ_V is between *0* and *20%* δ. However, at the end of the serviceability level, which is at a load of *1000 kN*, δ_V becomes as much as *50%* δ and at the ultimate

limit the percentage is only slightly higher. This proves that even at the serviceability level, shear deflections can be important for the evaluation of the displacement ductility.

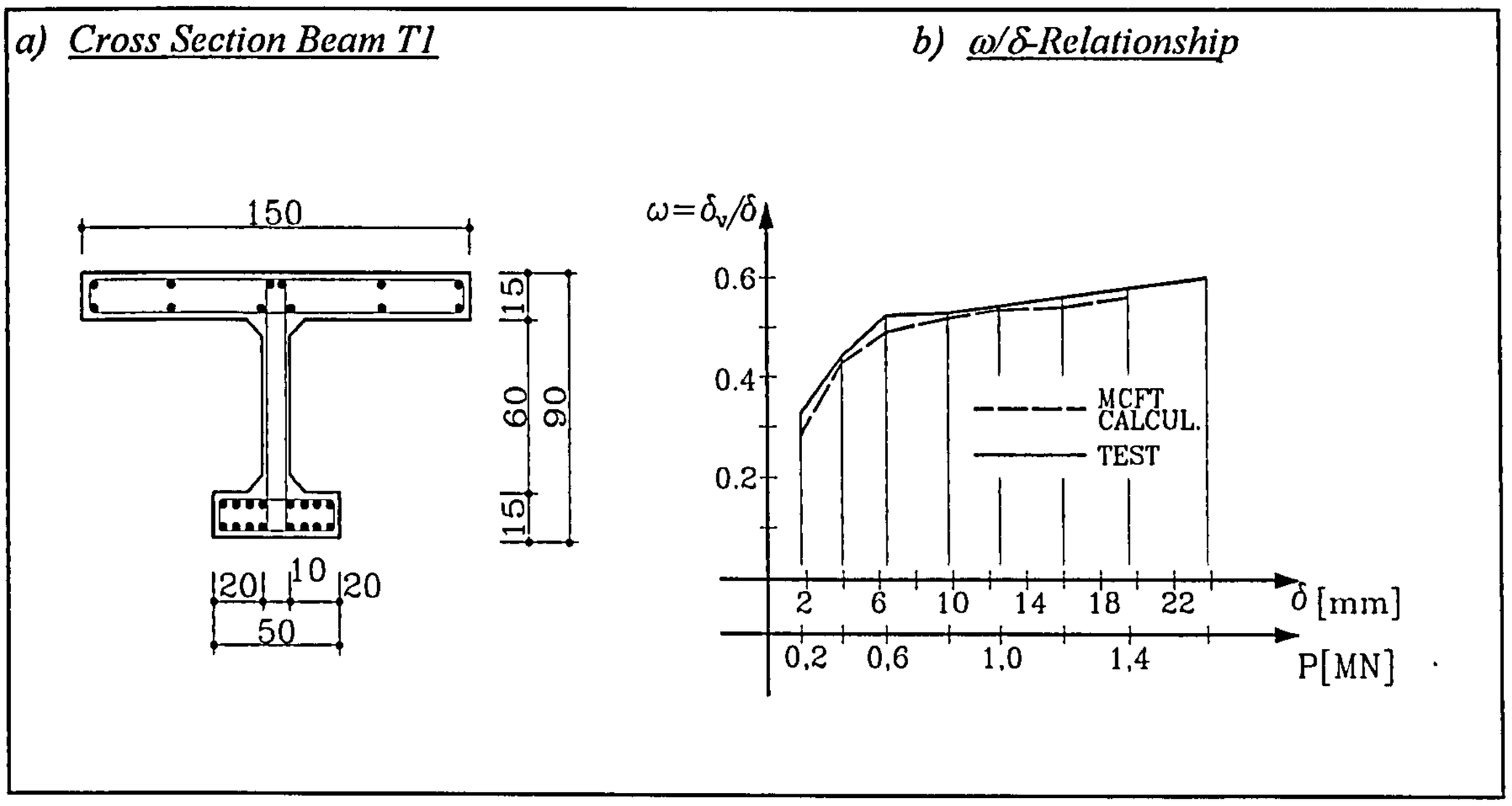

Fig.3.24 ω/δ-Relationship for Leonhardt's Beam T1 (Dim. of Cross Section in cm)

Finally, the influence of shear on the displacement ductility is checked using a wall investigated in earlier work (see Haas/Pilakoutas, 1994). This wall was then scrutinised by means of a non-linear time history calculation with a macro wall element, coded as a user defined Fortran subroutine and added to the FE program ABAQUS (1994). An EC8 compatible time acceleration history was employed and the top displacement of the four storey wall has been obtained to *6cm*. The recalculation with section analysis procedures confirmed this value; however, nearly *50%* of the now calculated top deflection was due to shear, although the wall was capacity designed and therefore, far from failing in shear.

The above mentioned maximum top displacement was only reached by the MCFT method when the tensile strength of the concrete was set to zero, which is equivalent to omitting aggregate interlock. When the tensile strength was added to the model, the stiffness of the wall was increased substantially by about *50%* and the wall remained nearly elastic under the same loading history, producing only a small top displacement of about *2 cm*. The investigations on the structural wall show again that shear deflections are not to be neglected, especially in deep elements, even though they may develop a flexural type of failure and that the response depends strongly on the evaluation of the tensile strength of the concrete.

The calculation of shear deflections using the provisions of the MCFT have shown that deformations due to shear can be substantial. However, the test specimens failing in shear developed only little displacement ductility as shear failure usually occurs shortly after the onset of yielding, and this is one of the main reasons why these members do not dissipate much energy. If an RC structure was designed for such a displacement ductility the equivalent lateral forces due to earthquake excitation could not be reduced much, and hence, a highly uneconomic structure would result. Fortunately, modern codes prevent engineers from designing in this manner. However, the above wall was capacity designed and therefore far from failing in shear. Nevertheless, a substantial proportion of the displacement ductility was due to shear deflections and therefore, should be included in ductility considerations. In Chapter 5 when global quantities are scrutinised the above statement will be investigated in greater detail.

3.9 Some Considerations on Arch Action

For the investigations made in this section a simply supported and symmetrically loaded reinforced concrete beam was assumed. The shear force acting on a cross section in the shear span of such a beam is always given by the change rate of the bending moment M: $V = dM/dx = d(Tz)/dx = z\,dT/dx + T dz/dx$. The physical interpretation of this purely formal derivation is that the shear force usually consists of two different parts, the first of which is caused by beam action while the second may be referred to as strut and tie action. It should be mentioned here that beam action is understood to consist of the previously described shear carrying actions like stirrups, aggregate interlock, dowel action or even tooth bending, while strut and tie action occurs when a load props itself directly up on the support. Fig.3.25.(a) and (b) gives an explanation for both shear force proportions: $V_1 = \tau_{xy} b_w z$ is the shear force as described by the technical bending theory and $V_2 = C \sin\theta$ is the vertical part of the inclined compression force C. The question is to what extent each term contributes to the total shear force in the cross section.

a) Shear Carried by Beam Action

$$V_1 = z\frac{dT}{dx} \qquad dT = \tau_{xy}\, b_w\, dx$$

$$V_1 = \tau_{xy}\, b_w\, z$$

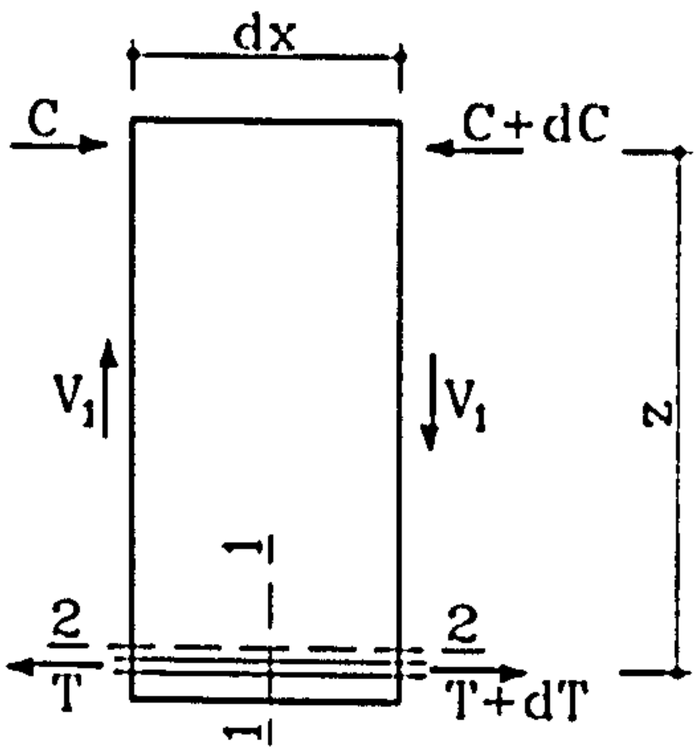

b) Shear Carried by a Strut and Tie Mechanism

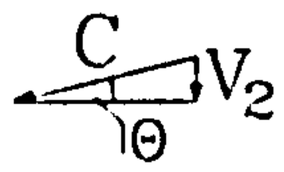

$$V_2 = T\frac{dz}{dx} \qquad V_2 = C\sin\theta$$

$$\tan\theta = \frac{dz}{dx} = \frac{V_2}{C\cos\theta} \rightarrow T = C\cos\theta$$

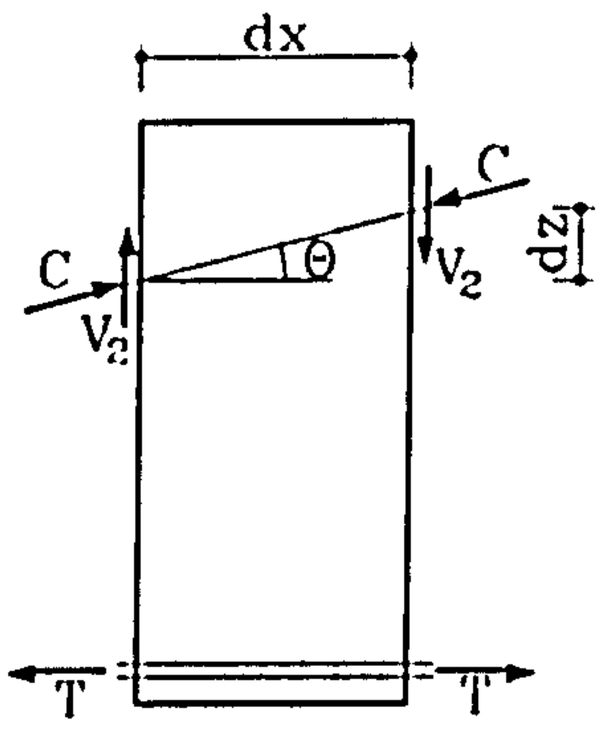

c) Beam Action

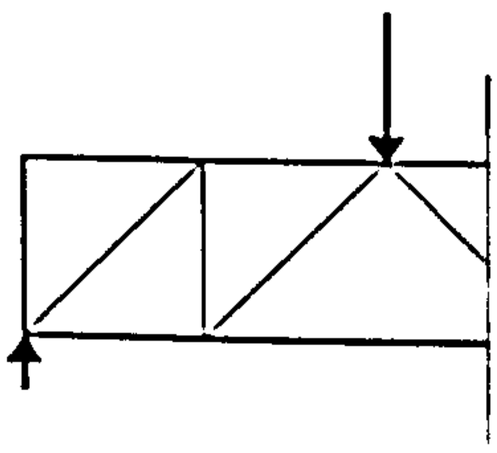

Deviation of compression forces by tensile ties and external loads

d) Strut and Tie Mechanism

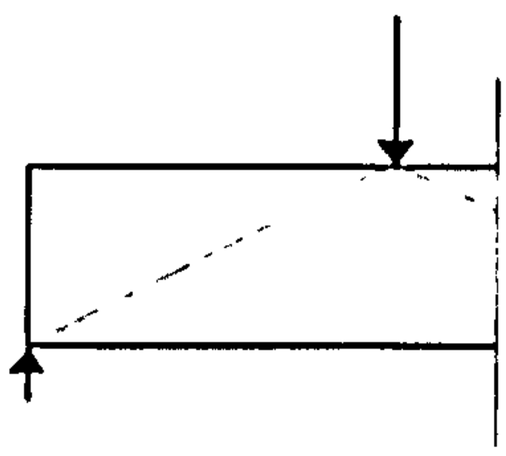

e) Arch Action

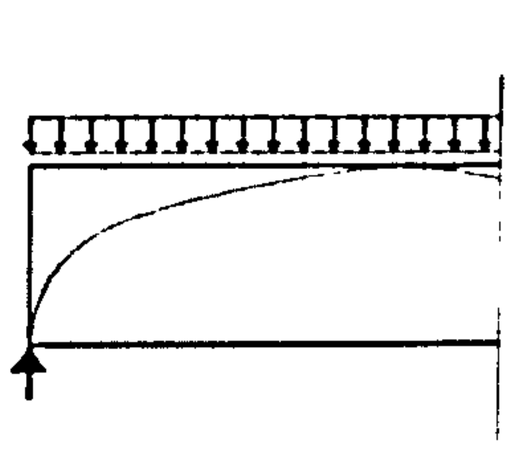

Deviation of compression forces by external loads only

Fig.3.25 Beam Action and Strut and Tie Mechanism in an RC Beam

It is obvious from Fig.3.25.(b) that V_2 can only develop when the tension force in the steel is constant over a certain beam length. Therefore, the proportion of T which remains at the supports may be responsible for shear transfer by strut and tie action while the rest must account for beam action. However, as will be described later in this section, only part of the tension in the steel bars which is still available at the supports can be attributed to strut and tie action, as the force in the tension chord of a truss does not drop to zero when approaching the supports. This fact is well-known and accounts for the importance of good anchorage of the longitudinal reinforcement in RC beams, even though no arch action may occur.

Fig.3.25.(c) - (e) tries to clarify what will be understood here by beam, strut and tie, or arch action. Most shear theories and in particular the MCFT explain beam action by a truss which carries external loads via its various bearing members to the supports. In this model the shear is attributed to the inclined compression struts or the tensile ties and the section moment to the chords. It is important to verify that, when pure beam action occurs, the deviation of the internal forces is accomplished by struts and ties and not by external loads. In contrast to this the strut and tie mechanism will always transfer an external load straight to the supports. In the case of arch action a distributed external load supplies the steady deviation of internal compression forces from mid-span to the supports. Both strut and tie mechanism and arch action have in common that no deviation forces propagate from the tension chord to the compression struts thus gradually reducing the tensile force in the longitudinal steel bars.

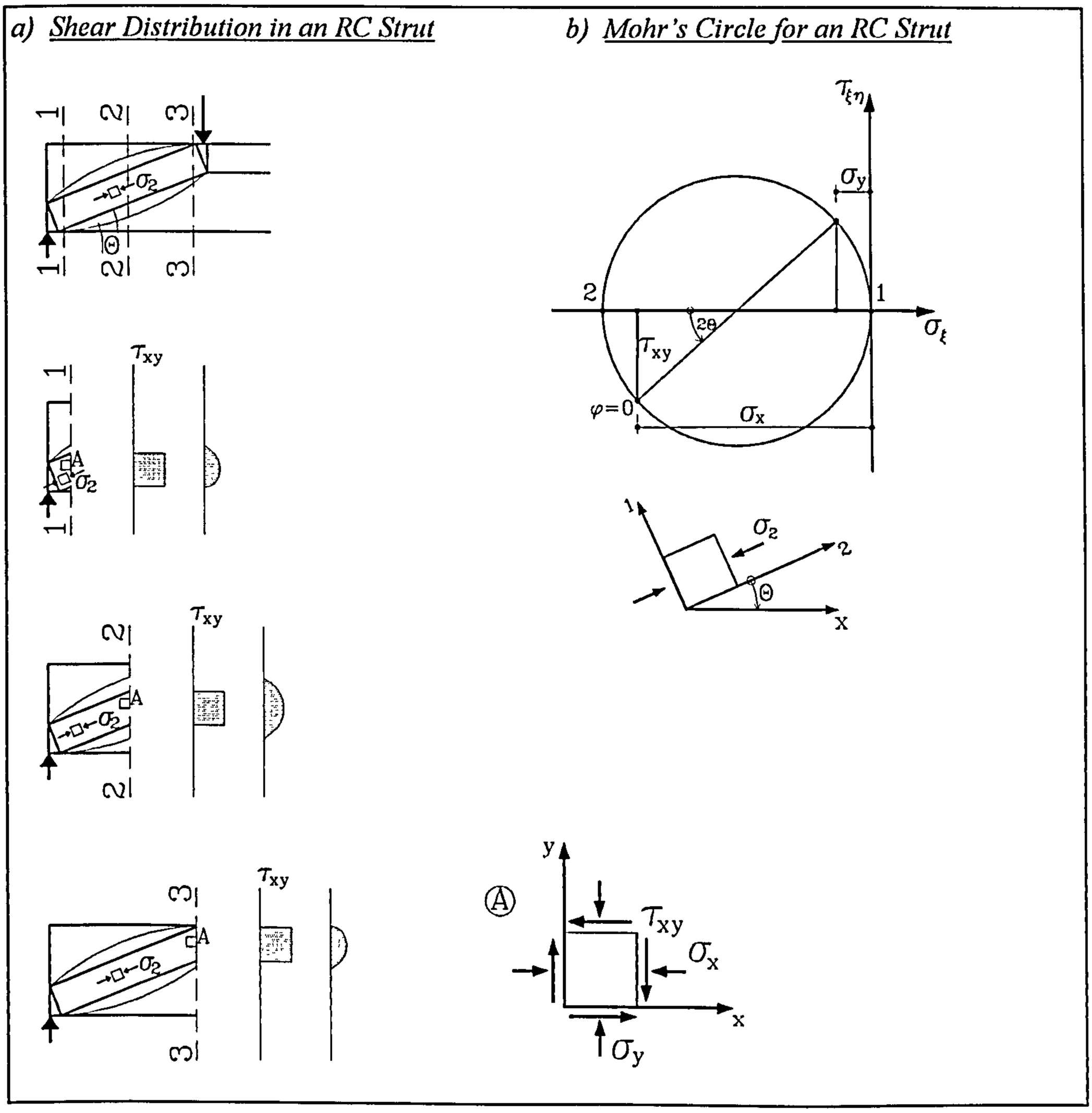

Fig.3.26 Shear Distribution in a Strut and Tie Mechanism

Fig.3.26 reveals the shear distribution in a cross section when the load is carried by a strut and tie mechanism. The shear stresses τ_{xy} are considered to be uniformly scattered along the vertical intersection line of the strut as a uniform principal compression stress state is assumed to apply. In reality the strut might bulge to a certain extent as the tensile strength of the concrete can also provide a certain amount of stress deviation in a compression strut as indicated in the figure. However, the curvature caused by f_{ct} is limited and this feature by nature cannot be referred to as arch action. In any case, the tensile strength causes a more parabolicly shaped shear distribution in the compression strut. When strut and tie or arch action occurs the shear is carried in the compression zone, but not necessarily at the upper edge of the beam, as is often claimed, because the compression zone can also be situated near the lower edge, depending on the cross section under consideration (see Fig.3.26).

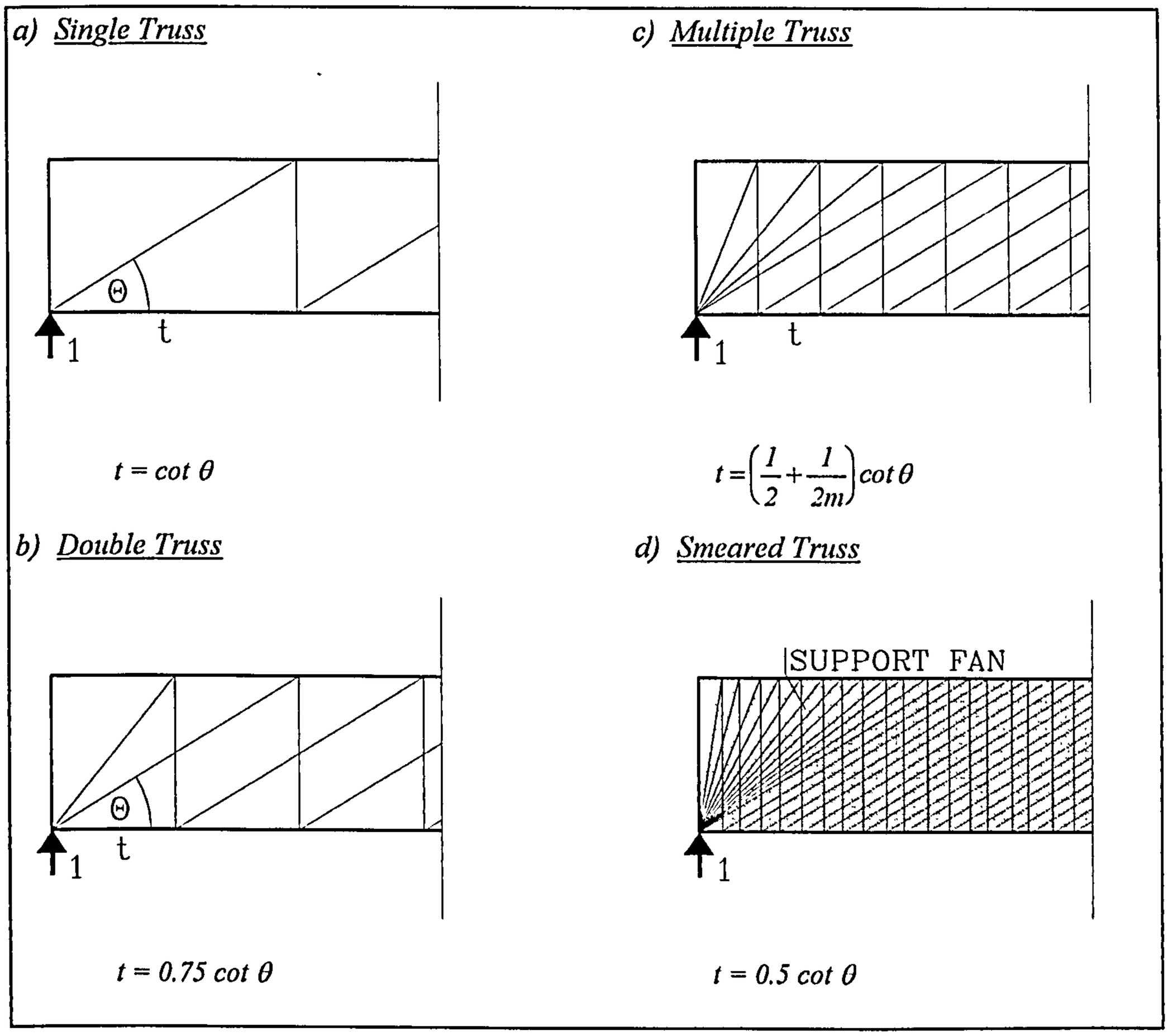

Fig.3.27 Force in Tensile Chord at the Support dependent on the Chosen Truss Model

It has already been mentioned that the force in the longitudinal reinforcement which remains at the supports is not always an indicator for a strut and tie mechanism. This is true because the stress in the tensile chord of a truss never drops to zero, not even in the vicinity of the supports. The stress conditions in the steel bars at the supports are depicted in Fig.3.27. When we assume a vertical unity force at the support of a truss, then the remaining force in the steel bars will be as high as $cot\theta$ for a single truss.

If the stirrups are considered to be perfectly distributed, then this value will drop to *0.5* $cot\theta$. In a real reinforced concrete member where the stirrups are well distributed the force might be between $cot\theta$ and *0.5* $cot\theta$ and can be calculated from the equation $t = cot\theta\,(1/2+1/2m)$ where m denotes the number of trusses. It is easy to recognise that for a single truss and for smeared stirrups the two given limit values arise. In their 1967 test, Rüsch and Mayer measured strains in the longitudinal reinforcement of RC beams with various stirrup spacing. The evaluation of the test data verifies the above at least in a qualitative fashion (see Rüsch/Mayer, 1967, Figure18, Page 19).

With the knowledge of the tension force at the supports it is possible to check from test data whether in a special case strut and tie action has occurred or not. Fig.3.28 shows the redrawing of test results of Leonhard's specimens TA11 and T1. From strain measurements carried out on longitudinal reinforcing bars in the span and near the supports steel stresses were calculated and plotted against the applied load. It can be seen that in mid-span of specimen TA11 the steel stresses followed almost exactly the dashed line given from a calculation according to the technical bending theory. The stresses near the supports at first followed the same dashed line up to a load of *20* tons but were in general slightly less, which means that at this load stage the concrete was only little cracked. At a service load of about *30* tons the values reached the dotted line calculated by applying a $45°$ truss. This means that at this load stage a truss mechanism had already formed and that the steel force was generated by this truss rather than by a strut and tie mechanism. At higher load stages up to the ultimate limit the tension stresses in the longitudinal reinforcement exceed the values from the $45°$ truss by about *15%*. However, not even this part of the tension could be attributed to strut and tie action as it is well-known that the concrete struts are substantially flatter than the crack inclination, thus producing higher values of tension stresses in the tensile chord near the support.

Beam TA11 was chosen because it provided the most unfavourable sample of Leonhard's TA series. In all other shear reinforced specimens the stresses of the longitudinal reinforcement exceeded the values of the *45°* truss to a much lesser extent. Unfortunately, the strain measurements in the steel bars were carried out at a relatively far distance to the supports. This was not only depicted in the test description but could be recalculated by the given σ_s line of the *45°* truss. The calculated distance was obtained to be *42cm* which is too far for a reliable proof calculation of the steel stresses at the support.

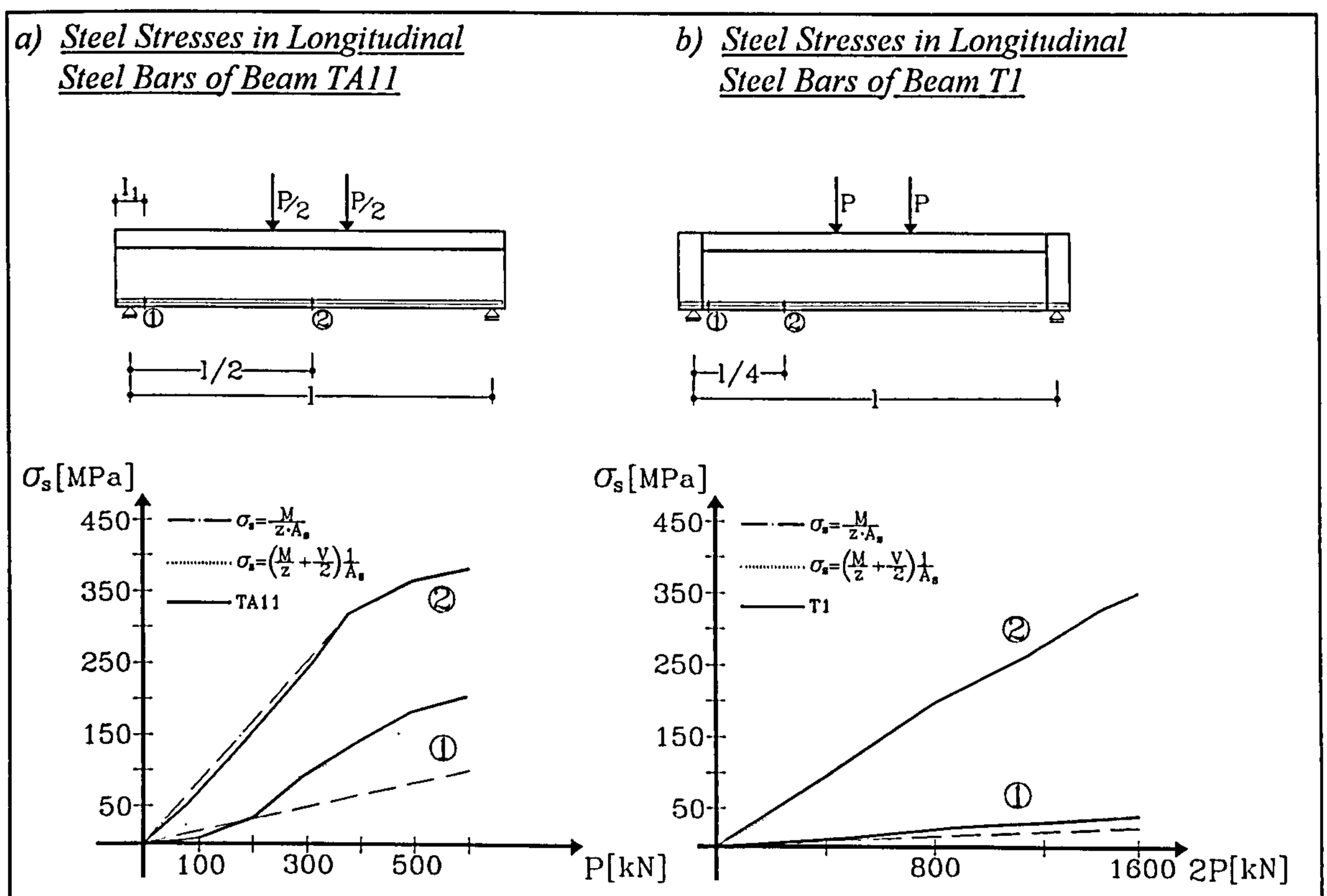

$$\sigma_s = \left(\frac{V_1 l_1}{z} + \frac{V}{2}\right)\frac{1}{A_s}$$

with: $\sigma_s = 200\ MPa$
$A_s = 26.4\ cm^2$
$V_1 = V = 300\ kN$
$z = 33.5\ cm$
follows: $l_1 = 42\ cm$

$T_{1\,cal} = V_1\ 0.5\ \cot\theta = 400\ kN$
with: $V_1 = 800\ kN$
$\theta = 45°$
$T_{1\,test} = \sigma_s A_s = 385\ kN$
with: $\sigma_s = 45\ MPa$
$A_s = 85\ cm^2$

T_1 = *tension force in longitudinal reinforcement at the support*

Fig.3.28 Steel Stresses in Longitudinal Reinforcement of RC Beams (see Leonhardt/Walther, 1964)

Fortunately, another Leonhardt test could be utilised to carry out this calculation as this time the strain measurements were taken right in the vicinity of the supports. Fig.3.28.(b) shows the stresses in the longitudinal reinforcement of beam T1 in approximately mid-shear-span and at the supports. While in mid-shear-span the steel stresses followed the truss line quite accurately, the steel stresses at the support could be verified as depicted in Fig.3.28.(b). From the measurements it can generally be concluded that at load stages far below the service load the elastic bending theory for isotropic material applies. When reaching the service load the full crack pattern develops and the tension force in the longitudinal reinforcement may be calculated using the truss analogy. At higher load stages up to the ultimate limit the tension stresses in the steel bars exceed the values from a *45°* truss but are still compatible with flatter concrete struts due to aggregate interlock. It is worth noting that the shear ratio of the tested beams was *3.3* and *2.8* for specimens TA11 and T1, respectively, and this gives evidence for the assumption that substantial strut and tie action occurs only at very low shear ratios of less than *2.5*.

The most impressive evidence for the occurrence of strut and tie, arch and beam action was given by Leonhardt by his comparative tests with RC members reinforced with either ribbed or plain steel bars. 8 specimens without transverse reinforcement were loaded to failure, 4 of which were fitted with ribbed bars while the others were reinforced with bright drawn engineering steel. Surprisingly, all specimens with smooth bars exhibited significantly higher failure loads than the corresponding beams with ribbed steel.

The MCFT and the truss analogy provide a simple explanation for this unexpected behaviour: The bond along the ribbed bars prevented the beams from the establishment of a strut and tie or arch mechanism by reducing the tension in the steel towards the supports. Consequently, a truss formed with compression struts and tensile ties to supply the longitudinal reinforcement with the deviation mechanism necessary for the decrease of the tension force. In the absence of stirrups only the concrete could provide the tensile ties and hence, came under substantial tension. With the increase in load, shear cracks started to form and once the failure crack propagated from the support to the load, a redistribution of forces towards a strut and tie or arch mechanism was no longer possible and a premature shear failure occurred. The described test series revealed impressively that even at a shear ratio of 2.8 no strut and tie or arching mechanism forms as long as ribbed bars are employed.

a) Compatibility Conditions in an RC Beam

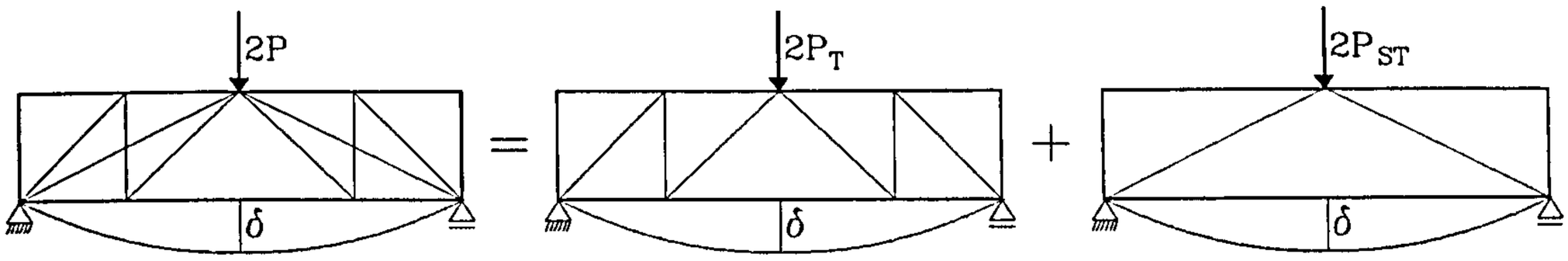

b) Deflections due to Truss and Strut and Tie Mechanisms

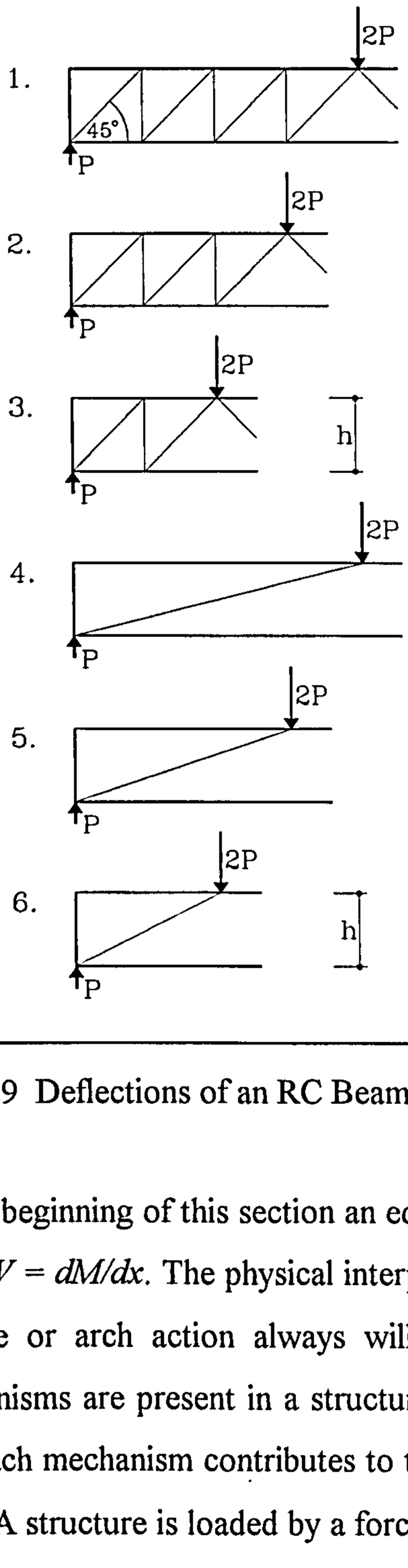

Longitudinal reinforcement:
$A_s = 1060\ mm^2$ $l = h$
$EA_s = 220\ MN$
Stirrups:
$A_s = 200\ mm^2$ $l = h$
$EA_s = 40\ MN$
Concrete chords and struts:
$A_c = 21000\ mm^2$ $l = h\ ;\ 1.4\ h$
$EA_c = (EA)_{max} = 630\ MN$
Normalised deflections under load:

$$\bar{\delta} = \delta \frac{(EA)_{max}}{2Ph} = \sum \left(\frac{N_i}{2P}\right)^2 \frac{l_i}{h} \Big/ \frac{(EA)_i}{(EA)_{max}}$$

1. $\bar{\delta} = 78$ 4. $\bar{\delta} = 126$
2. $\bar{\delta} = 42$ 5. $\bar{\delta} = 54$
3. $\bar{\delta} = 18$ 6. $\bar{\delta} = 17$

Fig.3.29 Deflections of an RC Beam

At the beginning of this section an equation was derived by merely differentiating the relation $V = dM/dx$. The physical interpretation was that in an RC member, beam and strut and tie or arch action always will occur simultaneously. Consequently, when both mechanisms are present in a structure, then compatibility conditions decide to what extent each mechanism contributes to the total shear force. Fig.3.29.(a) illustrates the principle: A structure is loaded by a force $2P$ which gives rise to the deflection δ. If two different load carrying mechanisms are present then each mechanism will carry that propor-

tion of $2P$ which causes the deflection δ in the same structure when consisting only of the respective transfer mechanism. This principle is the basis of each solution of an indeterminate static problem and it ensures that a weak mechanism carries little load while a strong one has to carry much.

It was the purpose of this section up to now to give evidence for the fact that in an RC beam, whether it is transverse reinforced or not, only little load can be transferred by a strut and tie or arch mechanism provided the shear ratio is higher than *2.0*. If this is true, then beam action must be a strong mechanism for $a/d > 2.0$, while the strut and tie or arch mechanism must be a weak one. This is shown in Fig.3.29.(b) by conducting a very simple calculation. A beam of various shear ratios was analysed by computing the deflection at mid-span for two different load transfer mechanisms. The first mechanism was conceived as a truss while the second consisted of a strut and tie. It is obvious from the results that the truss mechanism is much stronger as long as the shear ratio is higher than *2.0*. The investigations in this section strengthen the well-known fact that no appreciable strut and tie or arch action can occur for shear ratios more than *2.0*, no matter whether an RC member is transversely reinforced or not. This feature was the basis of all calculations in this part of the work as section analysis procedures which include shear considerations are usually not able to cope with arch or strut and tie action.

4 Investigations Using the Finite Element Method

4.1 Introductory Reflections

The proper calculation of the deflections of a complex structure is only possible by means of a finite element analysis. As already mentioned, section analysis procedures are confined to investigations on the local element level, where they are powerful tools to scrutinise quantities such as the ultimate capacity of a cross section or the stress and strain state in an RC element. Moreover, it has been seen that secondary shear carrying actions could be easily added to a shear theory. In contrast to this, global values, for instance the top displacement of a high rise building under lateral load, cannot be obtained from section analysis as far too many cross sections have to be analysed and the summing up of strains, which is necessary to determine deflections, is virtually impossible when dealing with a complex building.

Fortunately, this is the strength of finite elements and therefore, this method must be exclusively employed for the evaluation of global values such as deflections, inter-storey drifts or basement rotations. However, for the calculation of useful results in an FE analysis, the implementation of realistic material properties is of crucial importance. This fact is well-known since the early days of finite elements, and much work has been conducted on the development of material models which can accurately simulate the behaviour of cracked reinforced concrete. In this section, a brief summary of the work on RC modelling is given to show which direction the research in material laws has taken in the last few decades.

Reinforced concrete is a composite material consisting of concrete and steel bars. Therefore, its physical behaviour is best described by the material laws of both constituents and their interaction. Reinforcing steel is modelled as being linear elastic up to the yielding point and after the onset of yielding, as being either perfectly plastic or hardening. Kinematic hardening should be used when load cycles are applied to the structure to account for Bauschinger's effect. In contrast to reinforcing steel, the physical description of plain concrete is more elaborate and there exist various possibilities, the most common of which are both the elasticity and the plasticity theory.

The plasticity theory was first derived from investigations on metals but later adapted to the requirements of concrete under triaxial compression (see eg Chen, 1982). Various researchers have developed plasticity based models which take account of the fully three dimensional behaviour of concrete (for instance Kotsovos, 1980) and more details on plasticity modelling in FE analysis are provided in the state-of-the-art report of the American Society of Civil Engineers (ASCE, 1993). However, the implementation of a plasticity model is quite demanding and the efforts might not be justifiable in cases where the response of a structure is governed by the tensile behaviour of the concrete and the yielding of the reinforcement. In this case, the elasticity theory provides a much easier access to a reasonable constitutive law for concrete, as will be explained later, even for cyclic loading. Although the plasticity theory was recently successfully implemented in a number of FE codes for the analysis of cracked reinforced concrete (see for instance van Mier, 1987), it can be stated that the elasticity theory, together with a fracture criterion, is more convenient for modelling concrete in plane stress in cases where cracking rather than crushing is the dominant feature of the element. Therefore, only material models based on the elasticity theory are briefly described here.

Generally, there exist two different approaches to modelling plain and reinforced concrete: The discrete and the smeared concept.

4.1.1 Discrete Crack Concept

Ngo and Scordelis were the first to introduce this concept. In their 1967 publication they described linear elastic analyses of RC beams with fixed crack patterns. Fig.4.1 shows the finite element idealisation with the mesh they employed in their analysis. Also depicted in the figure is the analytical model and the linkage element with which they simu-

lated the bond slip of the reinforcement. This first attempt was followed by some other researchers (eg Nilson, 1968), but it soon appeared that the concept was rather unwieldy as it often required a redefinition of the mesh during the course of an analysis. This, together with the limited speed and space of the computers of those days, made the analysis time consuming and thus expensive. Moreover, the above features did not really match the nature of the finite element method and, therefore, it is not surprising that the concept was soon abandoned after these early attempts.

For the sake of completeness it should be mentioned that the concept of discrete modelling of displacement discontinuities is still widespread in use for the treatment of bond problems. However, in this case the location of the discontinuities is known from the beginning of the analysis and fixed throughout the calculation. Furthermore, due to the enormous increase in computational power, the concept was again picked up by some researchers (eg Wawrzynek and Ingraffea, 1987) introducing an approach by automatically generating discrete cracks.

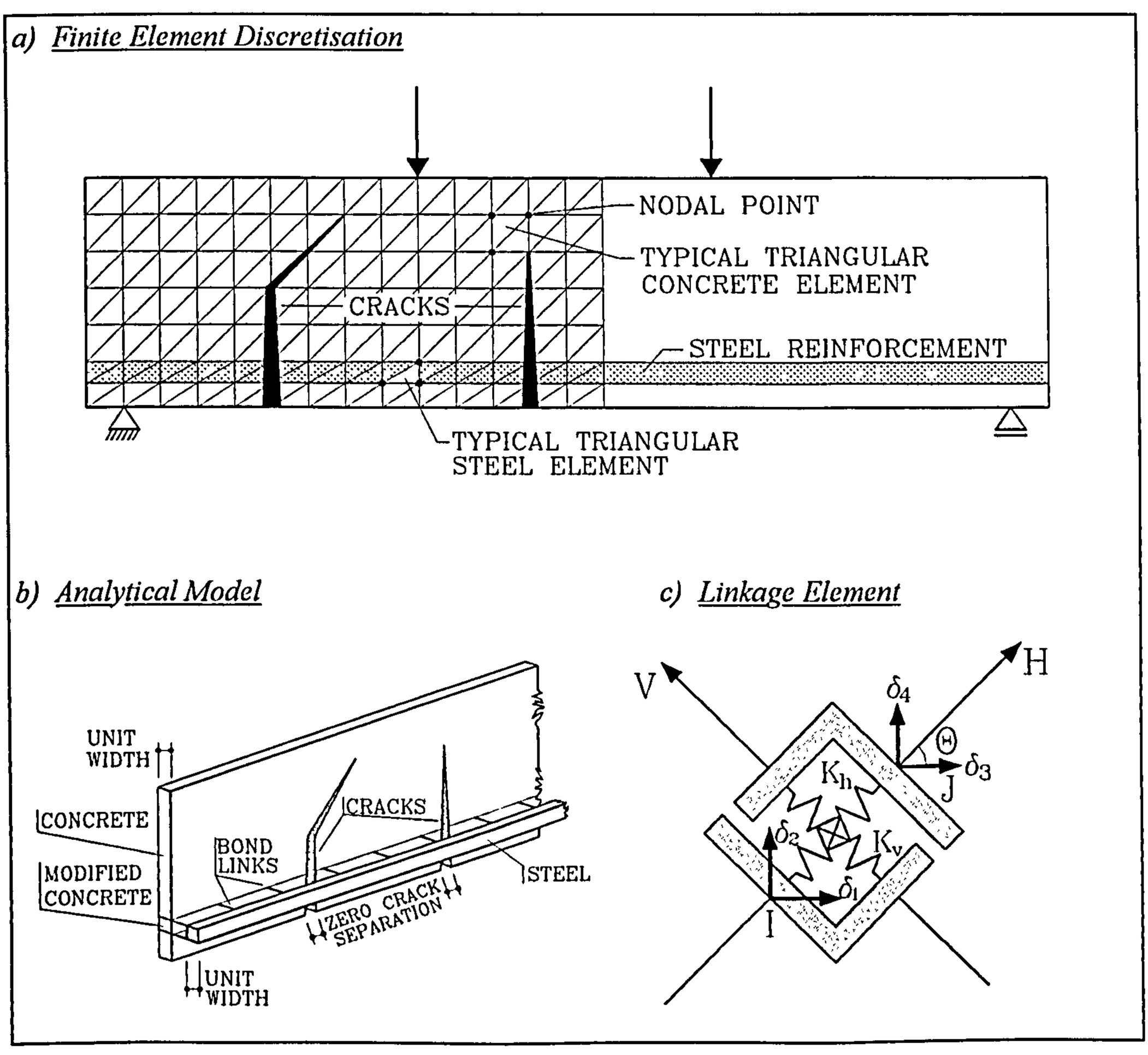

Fig.4.1 Discrete Crack Concept of Ngo and Scordelis (1967)

4.1.2 Smeared Crack Concept

Because of the above mentioned problems with the discrete crack approach, it was desirable to set up a constitutive model which imagines the concrete remaining a continuum even after cracks have started to form. This, of course, is only possible when the cracks are considered to be smeared out over the elements. Consequently, in 1968 this approach was introduced by Rashid, who replaced the initial isotropic *stress/strain* relationship after cracking by an orthotropic one.

Both equations the uncracked isotropic as well as the cracked orthotropic are given in Fig.4.2, together with the orientation of the principal directions and the transformation matrix $\boldsymbol{T}$ with which the orthotropic material matrix is rotated into the xy direction. The uncracked elastic isotropic material matrix must be independent of its orientation, which is easily verified by building the matrix product $\boldsymbol{T}^T\boldsymbol{E}\,\boldsymbol{T}$. The values τ_{12} and γ_{12} are both zero by definition and are only given here for formal reasons.

a) *Uncracked Elastic Isotropic Stress/Strain Relationship in Principal Direction*

$$\begin{bmatrix}\sigma_1\\ \sigma_2\\ \tau_{12}\end{bmatrix}=\frac{E_c}{1-\nu^2}\begin{bmatrix}1 & \nu & 0\\ \nu & 1 & 0\\ 0 & 0 & \frac{1-\nu}{2}\end{bmatrix}\begin{bmatrix}\varepsilon_1\\ \varepsilon_2\\ \gamma_{12}\end{bmatrix}$$

b) *Uncracked Elastic Isotropic Stress/Strain Relationship in xy Direction*

$$\begin{bmatrix}\sigma_x\\ \sigma_y\\ \tau_{xy}\end{bmatrix}=\frac{E_c}{1-\nu^2}\begin{bmatrix}1 & \nu & 0\\ \nu & 1 & 0\\ 0 & 0 & \frac{1-\nu}{2}\end{bmatrix}\begin{bmatrix}\varepsilon_x\\ \varepsilon_y\\ \gamma_{xy}\end{bmatrix}$$

c) *Cracked Orthotropic Stress/Strain Relationship in Principal Direction*

$$\begin{bmatrix}\sigma_1\\ \sigma_2\\ \tau_{12}\end{bmatrix}=\begin{bmatrix}0 & 0 & 0\\ 0 & E_c & 0\\ 0 & 0 & 0\end{bmatrix}\begin{bmatrix}\varepsilon_1\\ \varepsilon_2\\ \gamma_{12}\end{bmatrix}$$

d) *Cracked Orthotropic Stress/Strain Relationship in xy Direction*

$$\begin{bmatrix}\sigma_x\\ \sigma_y\\ \tau_{xy}\end{bmatrix}=[T]^T\begin{bmatrix}0 & 0 & 0\\ 0 & E_c & 0\\ 0 & 0 & 0\end{bmatrix}[T]\begin{bmatrix}\varepsilon_x\\ \varepsilon_y\\ \gamma_{xy}\end{bmatrix}$$

$$[T]=\begin{bmatrix}\cos^2\theta & \sin^2\theta & -\sin\theta\cos\theta\\ \sin^2\theta & \cos^2\theta & \sin\theta\cos\theta\\ 2\sin\theta\cos\theta & -2\sin\theta\cos\theta & \cos^2\theta-\sin^2\theta\end{bmatrix}$$

e) *Orientation of Principal Direction*

$$\theta=\frac{1}{2}\arctan\frac{\gamma_{xy}}{\varepsilon_x-\varepsilon_y}$$

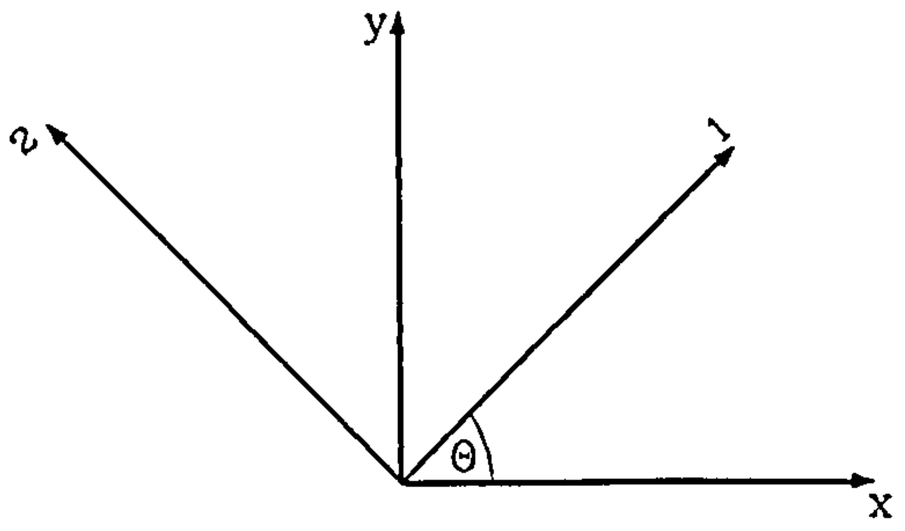

Fig.4.2 Rashid's Constitutive Model for Smeared Cracks

It is obvious that Rashid's attempt is equivalent to the setting to zero of both the normal stress perpendicular to the crack and the shear stress in the crack, which is in contrast to the physical reality. Consequently, the constitutive model was enhanced by adding the shear modulus G reduced by a factor β which was named the shear retention factor. In addition, Poisson's ratio ν together with the reduced Young's modulus μE_c was also re-inserted. βG was meant to account for aggregate interlock while μE_c should account for the transfer of the concrete stresses in principal tensile direction, also known as tension stiffening. Note that μ becomes negative in the case of softening.

Two popular versions of this constitutive model for concrete are shown in Fig.4.3: One including off-diagonal terms to account for Poisson's effect, and one without. As they are both widespread in use up to now (see for instance Leibengood et al, 1986 and Rots/ de Borst, 1987), some features of the models will be explained here in more detail.

a) *Orthotropic Material Stiffness Matrix in Principal Direction Including Tension Stiffening and Aggregate Interlock*

$$\begin{bmatrix} \mu E_c & 0 & 0 \\ 0 & E_c & 0 \\ 0 & 0 & \beta G \end{bmatrix}$$

with: $G = E_c/2$

b) *Orthotropic Material Stiffness Matrix in Principal Direction Including Tension Stiffening, Aggregate Interlock and Poisson's Effect*

$$\begin{bmatrix} \frac{\mu E_c}{1-\nu^2\mu} & \frac{\nu\mu E_c}{1-\nu^2\mu} & 0 \\ \frac{\nu\mu E_c}{1-\nu^2\mu} & \frac{E_c}{1-\nu^2\mu} & 0 \\ 0 & 0 & \beta G \end{bmatrix}$$

$$G = \frac{E_c}{2(1+\nu)}$$

ν = *Poisson's ratio*
μ = *reduction factor for Young's modulus due to tension stiffening*
β = *shear retention factor*

Fig.4.3 Fixed Crack Constitutive Models for Concrete in Principal Direction

The material models of Fig.4.3 are linearly elastic in both compression and tension as long as the tensile strength of the concrete is not reached. Once the cracking strain is exceeded in principal direction the tension stress does not drop immediately to zero but follows a descending slope until zero stress is reached at a particular strain, which for plain concrete can be calculated from the fracture energy G_f.

This feature is called tension or strain softening and it is responsible for the presence of tensile stresses in the concrete, even though the tensile strain might exceed by several times the cracking strain. However, tension softening is not the only cause for the presence of tensile stresses in the concrete of an element. There are two more features which generate tensile stresses upon cracking: Aggregate interlock and tension stiffening. As already mentioned, the reduced Young's modulus μE_c accounts for the tensile stress in the concrete and should include all the above features. However, the literature only reports strain softening and, in the case of reinforced concrete, also tension stiffening as causes for concrete tensile stresses upon cracking. In an unreinforced element no tension stiffening can occur as it is linked to the loss of bond along reinforcing bars.

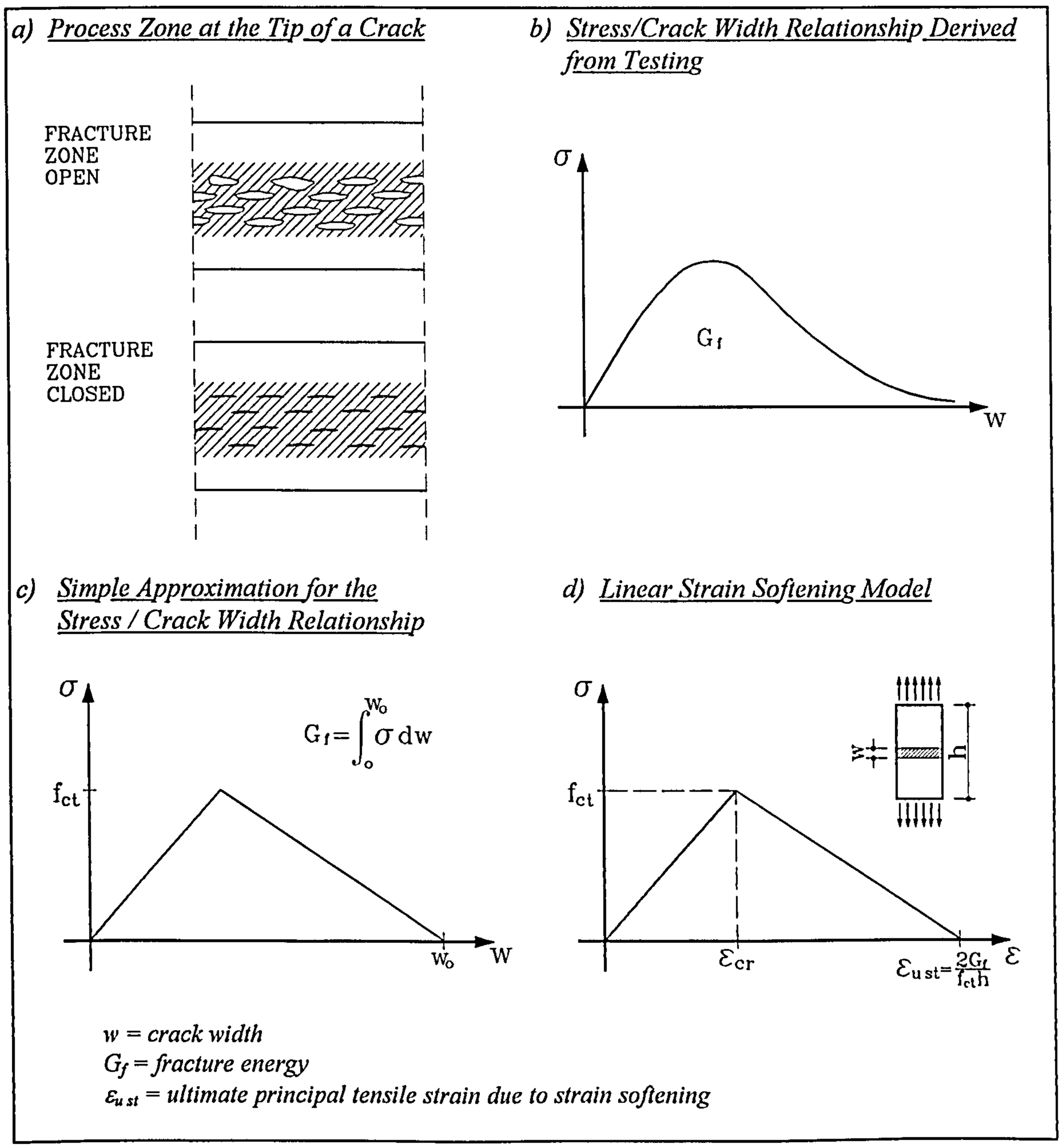

w = crack width
G_f = fracture energy
$\varepsilon_{u\,st}$ = ultimate principal tensile strain due to strain softening

Fig.4.4 Strain Softening Model for Concrete in Tension (see Reinhardt, 1984 and van Mier, 1987)

Strain softening is confined to the so-called process zone at the tip of the crack. Fig.4.4.(a) shows such a zone and it is assumed that, after microcracks have started to form, there is still enough material to bridge the crack faces which, at that stage of cracking, are not yet distinctly separated (see Reinhardt, 1984). The strain at zero tensile stress can be evaluated by means of the fracture energy which is necessary to separate the crack surfaces. The fracture energy is considered to be a material constant and can be calculated from the area below the *stress/crack width* relationship of plain concrete under tension.

In an element, cracking occurs at an integration point and separates the whole area associated with it. Therefore, the element size and hence, the area connected with an integration point must be fitted to the fracture energy. This imposes restrictions concerning the size of an element and accounts for a certain mesh sensitivity of the discretised model. Fig.4.4.(b) gives the *stress/crack width* relationship for concrete in tension derived from testing and Fig.4.4.(c) a simple approximation for the calculation of the fracture energy. Fig.4.4.(d) depicts the linear strain softening model commonly used in FE programming for plain concrete (see van Mier, 1987).

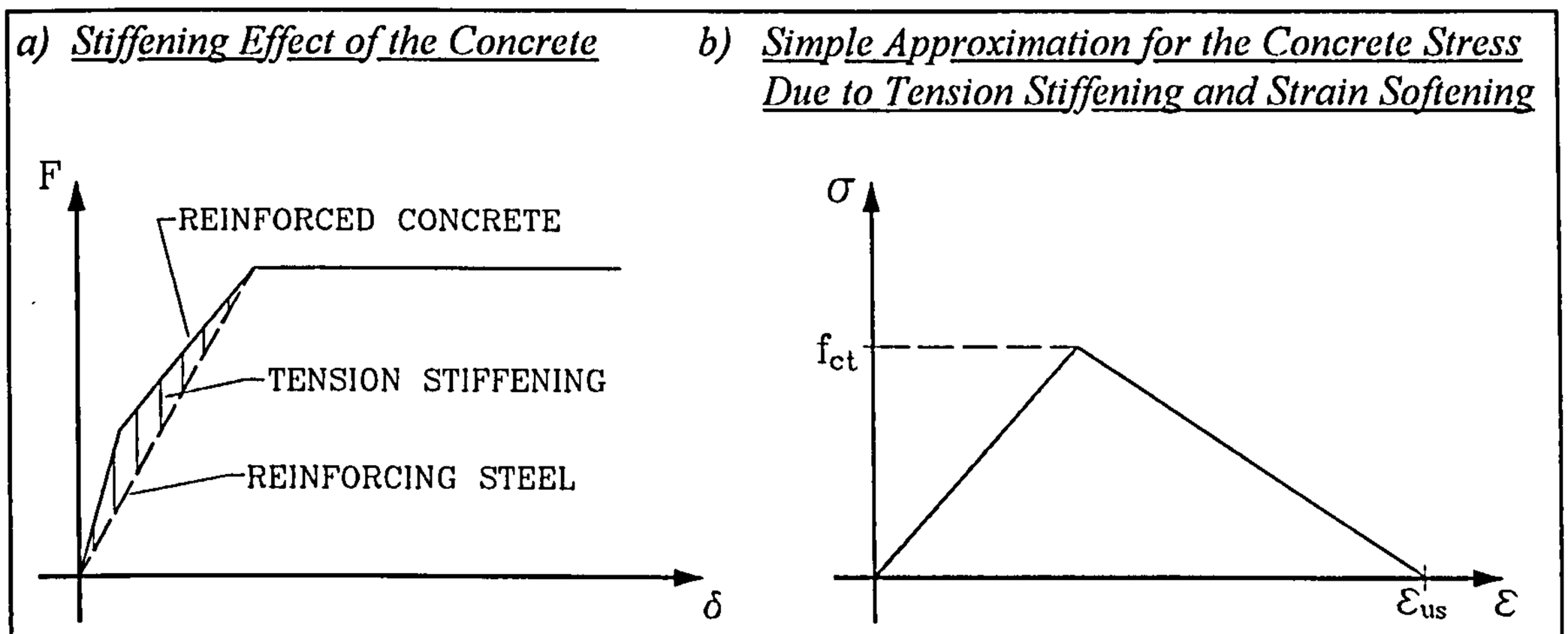

Fig.4.5 Tension Stiffening Concept

In cracked reinforced concrete the tensile stresses in the steel bars are not evenly distributed, but concentrated to some extent in the cracks. This means that, due to equilibrium, the concrete between the cracks still has to carry tensile stresses. This has a stiffening effect on the structural element and, hence, has been called tension stiffening. This mate-

rial property is usually captured by simply increasing the strain at zero stress of the linear strain softening model by a certain amount which can be estimated from the yield strain of the reinforcement. Fig.4.5 shows the tension stiffening concept and a *stress/strain* relationship which accounts for both strain softening and tension stiffening. It should be mentioned that the inclusion of tension stiffening in the constitutive model has a beneficial influence on the mesh sensitivity and usually enhances the performance of the FE material algorithm. In fact, as will be seen later in Section 4.3, the introduction of a high value ε_{us} for tension stiffening including strain softening is often necessary to ensure the convergence of an analysis, especially when little reinforcement is present in the structural model. The reason for this behaviour is the mesh sensitivity which can cause an FE analysis not to converge to a unique solution. However, the interaction of reinforcement and concrete which is simulated by tension stiffening has a mitigating effect on the mesh sensitivity (see eg ABAQUS User's Manual, Vol.1, Page 4.4.12-1, 1994 or Bažant /Oh, 1983).

The shear stiffness βG was reinserted in the cracked material stiffness matrix to account for secondary shear carrying actions such as aggregate interlock or dowel action. In contrast to aggregate interlock, dowel action can only occur in the vicinity of steel bars and hence, is confined to reinforced elements. Fig 4.6 shows an unreinforced element and the area associated with an integration point. Once the crack strain in principal tensile direction is exceeded, a crack will form which, at its nascent stage, has the direction of the principal compression stress. This means that no shear stresses can be generated along the crack surfaces. Only when the strain state changes, due to the crack displacements, can shear stresses develop which is connected with a rotation of the principal stress direction. This is depicted in Fig.4.6 by Mohr's stress circle. In the standard case of a web of an RC beam the slope of the compression stresses will flatten. The Mohr's circle also reveals that when substantial shear stresses are generated the accompanying stress in the direction perpendicular to the crack will change from tension to compression. As Walraven showed in his work on aggregate interlock, this feature is vital for the development of any higher shear stresses in a crack. Note that in the principal direction the stress, of course, remains tensile. However, this direction has then substantially changed in comparison with the crack direction. It was mentioned earlier in Chapter 3, that the assumption of a coincidence of principal stress and crack direction prevents the modified compression field theory from treating aggregate interlock in a physically correct way.

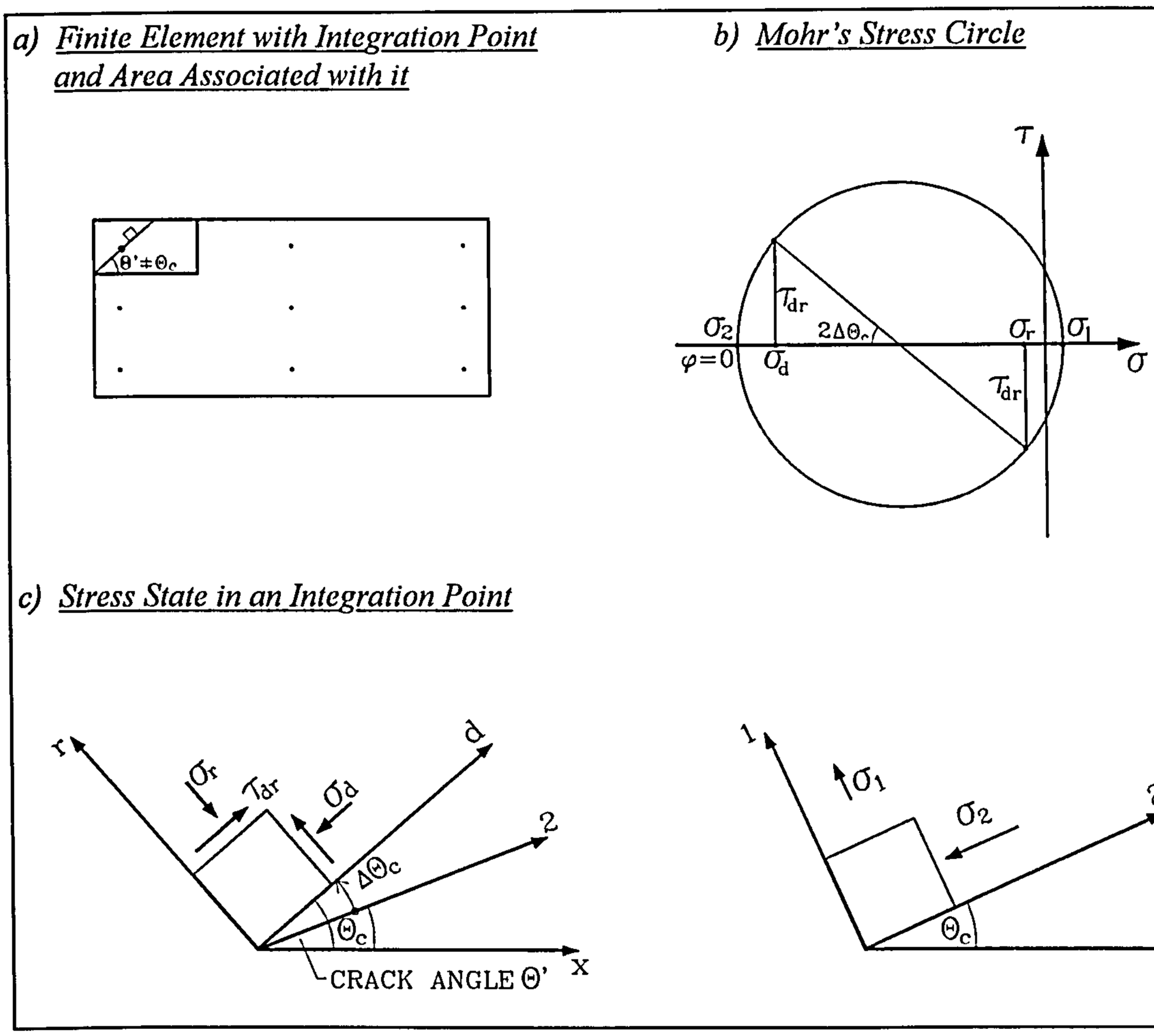

Fig.4.6 Aggregate Interlock in FE Modelling

The shear stress in a crack largely depends on its strain state and, hence, the shear retention factor β should be calibrated by a constitutive relation for aggregate interlock, for instance by that one suggested by Walraven. The constitutive models for cracked concrete which have briefly been described here, and the material stiffness matrices which are given in Fig.4.3 are, because of their simplicity, very popular for implementation in FE programs. However, there are severe restrictions as well. The shear retention factor β and the factor μ which accounts for tension stiffening are rather unknown quantities and no strict guidelines are available for their application. It is, therefore, not surprising that in the literature, for example for β, a wide range of values is reported, reaching from less than *1‰* up to more than *50%*. Finally, it should be mentioned that both models are not really suitable for cyclic loading as they are essentially based on linear elasticity together with fracture criteria. No plastic strain can be specified, especially for unloading in compression, and the same is valid for tension up to the tensile strength. Nevertheless, the material laws have recently been described for cyclic behaviour (Linde, 1993).

a) Incremental Orthotropic Stress Strain Relationship in Principal Direction

Non-symmetric form:

$$\begin{bmatrix} d\sigma_1 \\ d\sigma_2 \\ d\tau_{12} \end{bmatrix} = \frac{1}{1-\nu^2} \begin{bmatrix} E_1 & \nu E_1 & 0 \\ \nu E_2 & E_2 & 0 \\ 0 & 0 & (1-\nu^2)G \end{bmatrix} \begin{bmatrix} d\varepsilon_1 \\ d\varepsilon_2 \\ d\gamma_{12} \end{bmatrix}$$

$$d\sigma_1 = E_1 \frac{1}{1-\nu^2}(d\varepsilon_1 + \nu d\varepsilon_2)$$

$$d\sigma_2 = E_2 \frac{1}{1-\nu^2}(\nu d\varepsilon_1 + d\varepsilon_2)$$

$$d\tau_{12} = G\, d\gamma_{12}$$

Symmetric form:

$$\begin{bmatrix} d\sigma_1 \\ d\sigma_2 \\ d\tau_{12} \end{bmatrix} = \frac{1}{1-\nu^2} \begin{bmatrix} E_1 & \nu\sqrt{E_1 E_2} & 0 \\ \nu\sqrt{E_1 E_2} & E_2 & 0 \\ 0 & 0 & (1-\nu^2)G \end{bmatrix} \begin{bmatrix} d\varepsilon_1 \\ d\varepsilon_2 \\ d\gamma_{12} \end{bmatrix}$$

b) Incremental Orthotropic Stress Strain Relationship in Principal Direction Using Uniaxial Strains

$$\begin{bmatrix} d\sigma_1 \\ d\sigma_2 \\ d\tau_{12} \end{bmatrix} = \begin{bmatrix} E_1 & 0 & 0 \\ 0 & E_2 & 0 \\ 0 & 0 & G \end{bmatrix} \begin{bmatrix} d\varepsilon_{1u} \\ d\varepsilon_{2u} \\ d\gamma_{12} \end{bmatrix}$$

c) Equivalent Incremental Uniaxial Strains

with: $d\varepsilon_{1u} = d\sigma_1 / E_1$ *and*
$d\varepsilon_{2u} = d\sigma_2 / E_2$ *follows:*

$$d\varepsilon_{1u} = \frac{1}{1-\nu^2}(d\varepsilon_1 + \nu d\varepsilon_2)$$

$$d\varepsilon_{2u} = \frac{1}{1-\nu^2}(\nu d\varepsilon_1 + d\varepsilon_2)$$

d) Shear Modulus G

$$G = \frac{1}{4(1-\nu^2)}\left(E_1 + E_2 - 2\nu\sqrt{E_1 E_2}\right)$$

E_1 , E_2 = incremental tangent material stiffness moduli

$d\varepsilon_{1u}$, $d\varepsilon_{2u}$ = incremental equivalent uniaxial strains

Fig.4.7 Non-linear Elastic Orthotropic Material Law for Concrete

A more elaborate model for cracked concrete can be provided by using non-linear elasticity together with fracture criteria. The non-linearity is due to a non-linear response of concrete in compression. The general form of the incremental orthotropic *stress/strain* relationship is given in Fig.4.7.(a), where E_1 and E_2 are incremental tangent material stiffness moduli, the values of which are unknown and have to be determined from a suitable concrete model. The incremental material law is given in principal direction and can be rotated in the usual fashion to the *xy* direction by means of the rotation matrix $\boldsymbol{T}$ (see Fig.4.2). The determination of E_1, E_2 and G will be briefly described, using the equivalent uniaxial strain approach of Darwin/Pecknold (1976) which is, up to now, still commonly in use (see for instance Stempniewski, 1990). The shear modulus is derived from the assumption that its value is invariant to the orientation of the coordinate system. Hence, G can be obtained by equilibrating the shear terms of the material matrices in both principal and *xy* direction, yielding the expression given in Fig.4.7.(d).

a) Uniaxial Concrete Law of Saenz

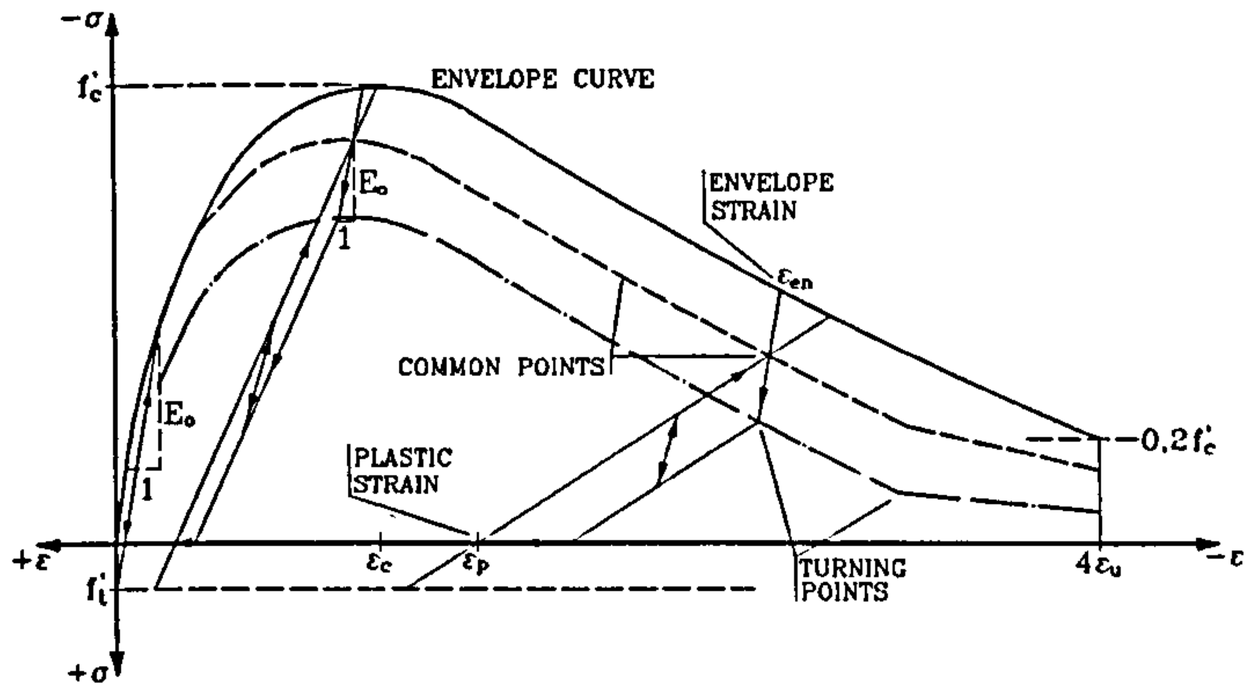

σ_c = *max. compressive stress*
ε_c = *uniaxial strain corresponding to* σ_c
ε_{en} = *envelope strain*
ε_p = *plastic strain corresponding to the envelope strain*
E_c = *initial tangent Young's modulus*
E_s = *secant modulus* σ_c/ε_c

$$\sigma = \frac{E_c \varepsilon}{1 + \left[\left(E_c/E_s\right) - 2\right]\left(\varepsilon/\varepsilon_c\right) + \left(\varepsilon/\varepsilon_c\right)^2}$$

$$\frac{\varepsilon_p}{\varepsilon_c} = 0.145\left(\frac{\varepsilon_{en}}{\varepsilon_c}\right)^2 + 0.13\frac{\varepsilon_{en}}{\varepsilon_c}$$

b) Principal Stresses from the Saenz Curve Using Equivalent Strains

$$\sigma_1 = \frac{E_c \varepsilon_{1u}}{1 + \left[\left(E_c/E_{1s}\right) - 2\right]\left(\varepsilon_{1u}/\varepsilon_{1c}\right) + \left(\varepsilon_{1u}/\varepsilon_{1c}\right)^2}$$

$$\sigma_2 = \frac{E_c \varepsilon_{2u}}{1 + \left[\left(E_c/E_{2s}\right) - 2\right]\left(\varepsilon_{2u}/\varepsilon_{2c}\right) + \left(\varepsilon_{2u}/\varepsilon_{2c}\right)^2}$$

Fig.4.8 Principle of Equivalent Uniaxial Strain according to Darwin/Pecknold (1976)

For the final determination of E_1 and E_2 the concrete law from which the uniaxial stresses should be taken has now to be specified. Darwin/Pecknold, who derived this method of treating a biaxial stress state by switching to equivalent uniaxial stress states, used the uniaxial concrete law of Saenz (1964) which is given in Fig.4.8. The ascending branch of the curve is non-linear, while the softening of the concrete occurs along a linear slope. The crucial point of the method is that, for a stress state given in principal direction, the values can be taken from the Saenz curve provided the corresponding strains are taken as the equivalent values of Fig.4.7.(c). E_1 and E_2 are then calculated with the linear expressions also given in Fig.4.7.(c). It is obvious that this approach needs neither to specify the shear retention factor β nor the value μ for tension stiffening, as the model is calibrated by a material law which in the present case is the Saenz curve. It can be seen from Fig.4.8.(a) that the concrete law of Saenz was extended by Darwin/Pecknold to cyclic loading by introducing a remaining plastic strain ε_p upon unloading. This plastic strain value is calculated from an empirically derived equation given in Fig.4.8.(a).

4.2 A User Defined Material for Cracked Reinforced Concrete

It was stated in the introductory reflections to Chapter 4 that the method of Darwin/ Pecknold is based on non-linear elasticity together with a uniaxial concrete material law which was taken from the work of Saenz (1964). In a similar way, the material law for cracked reinforced concrete, derived from testing on shear panels by Vecchio/Collins (1986), can be prepared for its use in finite element analysis and fitted in a material routine for calculations together with the commercial FE package ABAQUS (1994). ABAQUS is a general purpose finite element program which allows for connecting a user-defined constitutive model to its source code. The connection is achieved via an interface which supplies all necessary information and takes care of the proper transfer of data calculated in the user material (UMAT) and required from the main program.

In modern FE programming, the role of the material routine is exactly defined. Once material non-linearities are present in a constitutive model, the task of the routine can be described as calculating at each integration point for a given strain state both the stress state and the tangent material stiffness matrix which from now on will also be referred to as the Jacobian. In addition, when cyclic loading is accounted for, the plastic proportion of the strain has to be specified in the material routine. ABAQUS needs the tangent material stiffness matrix to be supplied by the UMAT rather than the secant version, regardless of whether in an analysis the load can be applied in one increment or not. This is because ABAQUS uses for non-linear material problems a Newton/Raphson algorithm in its solver which requires the tangent values for convergence. For more details on non-linear solution techniques see Zienkiewicz/Taylor, 1991, or Bathe, 1982.

In the Darwin/Pecknold method, both the stress state and the Jacobian were quickly obtained by means of the equivalent uniaxial strain concept. Because of the complexity of the constitutive model of Vecchio/Collins, known as the modified compression field theory (MCFT), it is more convenient to apply a different approach, although the use of the Darwin/Pecknold method would generally be possible as well. Therefore, the structure of the UMAT, and the way it works, will hereafter be described in detail. Cyclic and path dependent effects are deliberately not included as the work focuses mainly on more general issues connected with the shear behaviour of cracked reinforced concrete structures.

a) General Form of an Elastic Orthotropic Stress/Strain Relationship in xy Direction

$$\begin{bmatrix}\sigma_{cx}\\ \sigma_{cy}\\ \tau_{xy}\end{bmatrix}=\begin{bmatrix}E^c_{xx} & E^c_{xy} & E^c_{x\gamma}\\ E^c_{xy} & E^c_{yy} & E^c_{y\gamma}\\ E^c_{\tau x} & E^c_{\tau y} & E^c_{\tau\gamma}\end{bmatrix}\begin{bmatrix}\varepsilon_x\\ \varepsilon_y\\ \gamma_{xy}\end{bmatrix} \quad\rightarrow\quad \begin{aligned}\sigma_{cx}&=E^c_{xx}\varepsilon_x+E^c_{xy}\varepsilon_y+E^c_{x\gamma}\gamma_{xy}\\ \sigma_{cy}&=E^c_{yx}\varepsilon_x+E^c_{yy}\varepsilon_y+E^c_{y\gamma}\gamma_{xy}\\ \tau_{xy}&=E^c_{\tau x}\varepsilon_x+E^c_{\tau y}\varepsilon_y+E^c_{\tau\gamma}\gamma_{xy}\end{aligned}$$

b) Total Differential of Stress/Strain Relationship

$$\begin{aligned}d\sigma_{cx}&=\frac{\partial\sigma_{cx}}{\partial\varepsilon_x}d\varepsilon_x+\frac{\partial\sigma_{cx}}{\partial\varepsilon_y}d\varepsilon_y+\frac{\partial\sigma_{cx}}{\partial\gamma_{xy}}d\gamma_{xy}\\ d\sigma_{cy}&=\frac{\partial\sigma_{cy}}{\partial\varepsilon_x}d\varepsilon_x+\frac{\partial\sigma_{cy}}{\partial\varepsilon_y}d\varepsilon_y+\frac{\partial\sigma_{cy}}{\partial\gamma_{xy}}d\gamma_{xy}\\ d\tau_{xy}&=\frac{\partial\tau_{xy}}{\partial\varepsilon_x}d\varepsilon_x+\frac{\partial\tau_{xy}}{\partial\varepsilon_y}d\varepsilon_y+\frac{\partial\tau_{xy}}{\partial\gamma_{xy}}d\gamma_{xy}\end{aligned} \quad\rightarrow\quad \begin{bmatrix}d\sigma_{cx}\\ d\sigma_{cy}\\ d\tau_{xy}\end{bmatrix}=\begin{bmatrix}\frac{\partial\sigma_{cx}}{\partial\varepsilon_x} & \frac{\partial\sigma_{cx}}{\partial\varepsilon_y} & \frac{\partial\sigma_{cx}}{\partial\gamma_{xy}}\\ \frac{\partial\sigma_{cy}}{\partial\varepsilon_x} & \frac{\partial\sigma_{cy}}{\partial\varepsilon_y} & \frac{\partial\sigma_{cy}}{\partial\gamma_{xy}}\\ \frac{\partial\tau_{xy}}{\partial\varepsilon_x} & \frac{\partial\tau_{xy}}{\partial\varepsilon_y} & \frac{\partial\tau_{xy}}{\partial\gamma_{xy}}\end{bmatrix}\begin{bmatrix}d\varepsilon_x\\ d\varepsilon_y\\ d\gamma_{xy}\end{bmatrix}$$

c) Tangent Material Stiffness Matrix

$$\begin{bmatrix}E'^c_{xx} & E'^c_{xy} & E'^c_{x\gamma}\\ E'^c_{yx} & E'^c_{yy} & E'^c_{y\gamma}\\ E'^c_{\tau x} & E'^c_{\tau y} & E'^c_{\tau\gamma}\end{bmatrix}=\begin{bmatrix}\frac{\partial\sigma_{cx}}{\partial\varepsilon_x} & \frac{\partial\sigma_{cx}}{\partial\varepsilon_y} & \frac{\partial\sigma_{cx}}{\partial\gamma_{xy}}\\ \frac{\partial\sigma_{cy}}{\partial\varepsilon_x} & \frac{\partial\sigma_{cy}}{\partial\varepsilon_y} & \frac{\partial\sigma_{cy}}{\partial\gamma_{xy}}\\ \frac{\partial\tau_{xy}}{\partial\varepsilon_x} & \frac{\partial\tau_{xy}}{\partial\varepsilon_y} & \frac{\partial\tau_{xy}}{\partial\gamma_{xy}}\end{bmatrix} \quad\rightarrow\quad \begin{aligned}E'^c_{xx}&=\frac{\partial\sigma_{cx}}{\partial\varepsilon_x};\quad E'^c_{xy}=\frac{\partial\sigma_{cx}}{\partial\varepsilon_y};\quad E'^c_{x\gamma}=\frac{\partial\sigma_{cx}}{\partial\gamma_{xy}}\\ E'^c_{yx}&=\frac{\partial\sigma_{cy}}{\partial\varepsilon_x};\quad E'^c_{yy}=\frac{\partial\sigma_{cy}}{\partial\varepsilon_y};\quad E'^c_{y\gamma}=\frac{\partial\sigma_{cy}}{\partial\gamma_{xy}}\\ E'^c_{\tau x}&=\frac{\partial\tau_{xy}}{\partial\varepsilon_x};\quad E'^c_{\tau y}=\frac{\partial\tau_{xy}}{\partial\varepsilon_y};\quad E'^c_{\tau\gamma}=\frac{\partial\tau_{xy}}{\partial\gamma_{xy}}\end{aligned}$$

Fig.4.9 Derivation of the Tangent Material Stiffness Matrix of Plain Concrete

For instance, deflections at the onset of yielding, necessary for any proper evaluation of the displacement ductility, are best obtained by an analysis which does not take cyclic effects into account. Note that a complete Fortran code is provided in Appendix A and, in addition, an input file for the analysis of a 4-storey wall is given in Appendix B.

4.2.1 Tangent Material Stiffness Matrix for Plain Concrete

The crucial part of any non-linear material programming is the derivation of the tangent material stiffness matrix for the concrete. When a smeared crack concept, together with a non-linear elastic fracture model, is adopted, the starting point is the elastic orthotropic *stress/strain* relationship, a general form of which is given in Fig.4.9.(a). A brief explanation is given here for the indices in Fig.4.9. As the stress state is considered to be that of the plain concrete, the normal stresses have been given the index *c*. For the shear stress, *c* was omitted as the shear inevitably has to be carried by the concrete. The strain state of the plain concrete is the same as the strain state of the reinforced concrete element and hence, no material index has been specified for strains at all.

a) Concrete in Compression

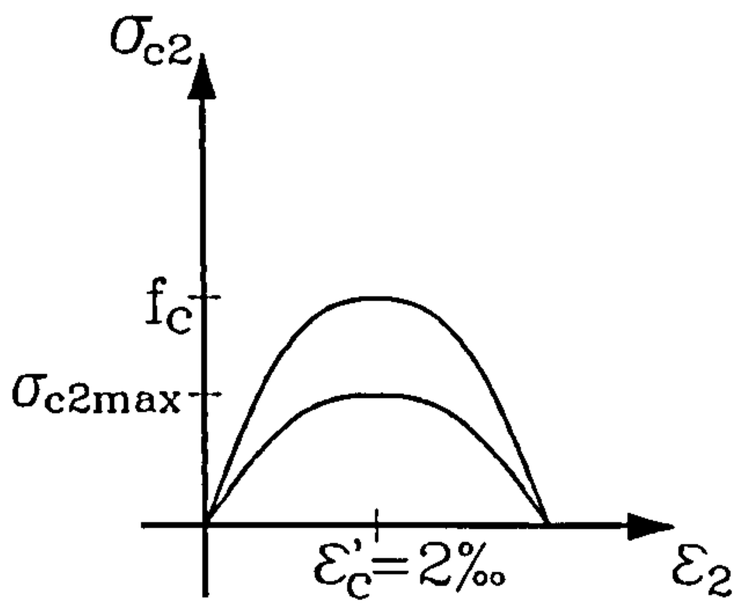

$$\sigma_{c2} = \sigma_{c2max}\left[2\frac{\varepsilon_2}{\varepsilon_c'} - \left(\frac{\varepsilon_2}{\varepsilon_c'}\right)^2\right]$$

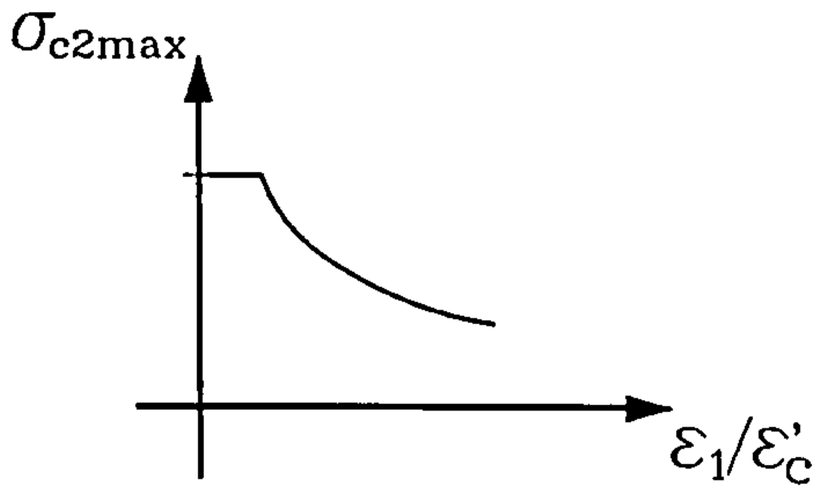

$$\sigma_{c2max} = \frac{f_c}{0.8 - 0.34\varepsilon_1 / \varepsilon_c'}$$

b) Concrete in Tension

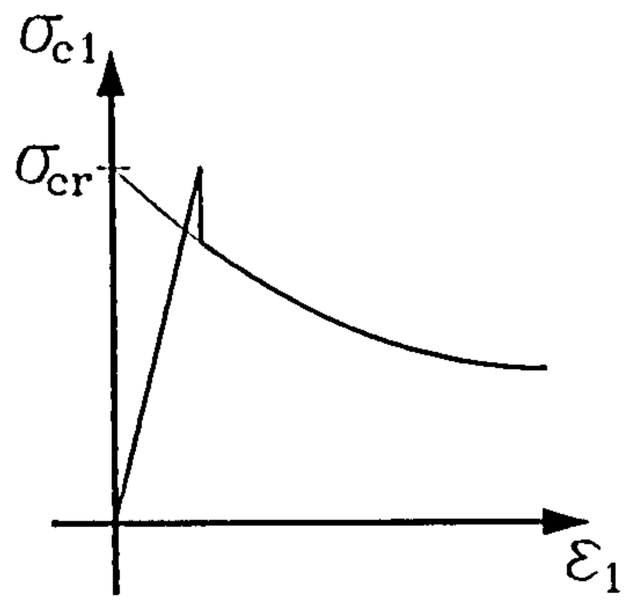

$$\sigma_{cr} = f_{ct}$$

$$\sigma_{c1} = \frac{f_{ct}}{1 + \sqrt{200\varepsilon_1}} \qquad (4.1)$$

for $\varepsilon_1 \geq \varepsilon_{ct}$ *with* $f_{ct} = \alpha\sqrt{f_c}$

$\alpha = 0.33 \div 0.75$

$$\sigma_{c1} = E_c \varepsilon_1$$

for $\varepsilon_1 < \varepsilon_{ct}$ *with* $E_c = 2f_c / \varepsilon_c'$

Fig.4.10 Constitutive Model of the MCFT (see Vecchio/Collins, 1982)

The first step towards developing the Jacobian is to establish the incremental form of this material law. The transition from a function to its incremental form is achieved by differentiating. When the function has only one dependent variable this is a trivial procedure. However, when more dependent variables are involved, as in the present case, the total differential has to be built. As each stress component is a function of the strain state, the total differential takes the form given in Fig.4.9.(b) and can also be written in terms of a matrix equation.

It is obvious from comparison that the matrix containing the partial differentials must be the tangent material stiffness matrix sought after. The next step involves the calculation of the various components of the Jacobian. This is only possible by evaluating the constitutive model under consideration. Therefore, the material laws of the MCFT are depicted in Fig.4.10.

a) Mutual Stress/Strain Dependencies

$$\sigma_{cx} = \sigma_{c1}\cos^2\theta_c + \sigma_{c2}\sin^2\theta_c \qquad \sigma_{cx} = f(\sigma_{c1}, \sigma_{c2}, \theta_c)$$
$$\sigma_{cy} = \sigma_{c1}\sin^2\theta_c + \sigma_{c2}\cos^2\theta_c \quad \rightarrow \quad \sigma_{cy} = f(\sigma_{c1}, \sigma_{c2}, \theta_c)$$
$$\tau_{xy} = 0.5\,(\sigma_{c1} - \sigma_{c2})\sin 2\theta_c \qquad \tau_{xy} = f(\sigma_{c1}, \sigma_{c2}, \theta_c)$$

$$\text{Constitutive laws} \quad \rightarrow \quad \sigma_{c1} = f(\varepsilon_1, \varepsilon_2)$$
$$\sigma_{c2} = f(\varepsilon_1, \varepsilon_2)$$

$$\varepsilon_1 = \varepsilon_x\cos^2\theta_c + \varepsilon_y\sin^2\theta_c + \gamma_{xy}\sin\theta_c\cos\theta_c \quad \rightarrow \quad \varepsilon_1 = f(\varepsilon_x, \varepsilon_y, \gamma_{xy}, \theta_c)$$
$$\varepsilon_2 = \varepsilon_x\sin^2\theta_c + \varepsilon_y\cos^2\theta_c - \gamma_{xy}\sin\theta_c\cos\theta_c \qquad \varepsilon_2 = f(\varepsilon_x, \varepsilon_y, \gamma_{xy}, \theta_c)$$

b) Components of the Tangent Material Stiffness Matrix

$$E^{tc}_{xx} = \frac{\partial\sigma_{cx}}{\partial\varepsilon_x} = \frac{\partial\sigma_{cx}}{\partial\sigma_{c1}}\frac{\partial\sigma_{c1}}{\partial\varepsilon_x} + \frac{\partial\sigma_{cx}}{\partial\sigma_{c2}}\frac{\partial\sigma_{c2}}{\partial\varepsilon_x} + \frac{\partial\sigma_{cx}}{\partial\theta_c}\frac{\partial\theta_c}{\partial\varepsilon_x}$$

$$E^{tc}_{xy} = \frac{\partial\sigma_{cx}}{\partial\varepsilon_y} = \frac{\partial\sigma_{cx}}{\partial\sigma_{c1}}\frac{\partial\sigma_{c1}}{\partial\varepsilon_y} + \frac{\partial\sigma_{cx}}{\partial\sigma_{c2}}\frac{\partial\sigma_{c2}}{\partial\varepsilon_y} + \frac{\partial\sigma_{cx}}{\partial\theta_c}\frac{\partial\theta_c}{\partial\varepsilon_y}$$

$$E^{tc}_{x\gamma} = \frac{\partial\sigma_{cx}}{\partial\gamma_{xy}} = \frac{\partial\sigma_{cx}}{\partial\sigma_{c1}}\frac{\partial\sigma_{c1}}{\partial\gamma_{xy}} + \frac{\partial\sigma_{cx}}{\partial\sigma_{c2}}\frac{\partial\sigma_{c2}}{\partial\gamma_{xy}} + \frac{\partial\sigma_{cx}}{\partial\theta_c}\frac{\partial\theta_c}{\partial\gamma_{xy}}$$

$$E^{tc}_{yx} = \frac{\partial\sigma_{cy}}{\partial\varepsilon_x} = \frac{\partial\sigma_{cy}}{\partial\sigma_{c1}}\frac{\partial\sigma_{c1}}{\partial\varepsilon_x} + \frac{\partial\sigma_{cy}}{\partial\sigma_{c2}}\frac{\partial\sigma_{c2}}{\partial\varepsilon_x} + \frac{\partial\sigma_{cy}}{\partial\theta_c}\frac{\partial\theta_c}{\partial\varepsilon_x}$$

$$E^{tc}_{yy} = \frac{\partial\sigma_{cy}}{\partial\varepsilon_y} = \frac{\partial\sigma_{cy}}{\partial\sigma_{c1}}\frac{\partial\sigma_{c1}}{\partial\varepsilon_y} + \frac{\partial\sigma_{cy}}{\partial\sigma_{c2}}\frac{\partial\sigma_{c2}}{\partial\varepsilon_y} + \frac{\partial\sigma_{cy}}{\partial\theta_c}\frac{\partial\theta_c}{\partial\varepsilon_y}$$

$$E^{tc}_{y\gamma} = \frac{\partial\sigma_{cy}}{\partial\gamma_{xy}} = \frac{\partial\sigma_{cy}}{\partial\sigma_{c1}}\frac{\partial\sigma_{c1}}{\partial\gamma_{xy}} + \frac{\partial\sigma_{cy}}{\partial\sigma_{c2}}\frac{\partial\sigma_{c2}}{\partial\gamma_{xy}} + \frac{\partial\sigma_{cy}}{\partial\theta_c}\frac{\partial\theta_c}{\partial\gamma_{xy}}$$

$$E^{tc}_{\tau x} = \frac{\partial\tau_{xy}}{\partial\varepsilon_x} = \frac{\partial\tau_{xy}}{\partial\sigma_{c1}}\frac{\partial\sigma_{c1}}{\partial\varepsilon_x} + \frac{\partial\tau_{xy}}{\partial\sigma_{c2}}\frac{\partial\sigma_{c2}}{\partial\varepsilon_x} + \frac{\partial\tau_{xy}}{\partial\theta_c}\frac{\partial\theta_c}{\partial\varepsilon_x}$$

$$E^{tc}_{\tau y} = \frac{\partial\tau_{xy}}{\partial\varepsilon_y} = \frac{\partial\tau_{xy}}{\partial\sigma_{c1}}\frac{\partial\sigma_{c1}}{\partial\varepsilon_y} + \frac{\partial\tau_{xy}}{\partial\sigma_{c2}}\frac{\partial\sigma_{c2}}{\partial\varepsilon_y} + \frac{\partial\tau_{xy}}{\partial\theta_c}\frac{\partial\theta_c}{\partial\varepsilon_y}$$

$$E^{tc}_{\tau\gamma} = \frac{\partial\tau_{xy}}{\partial\gamma_{xy}} = \frac{\partial\tau_{xy}}{\partial\sigma_{c1}}\frac{\partial\sigma_{c1}}{\partial\gamma_{xy}} + \frac{\partial\tau_{xy}}{\partial\sigma_{c2}}\frac{\partial\sigma_{c2}}{\partial\gamma_{xy}} + \frac{\partial\tau_{xy}}{\partial\theta_c}\frac{\partial\theta_c}{\partial\gamma_{xy}}$$

with:

$$\frac{\partial\sigma_{c1}}{\partial\varepsilon_x} = \frac{\partial\sigma_{c1}}{\partial\varepsilon_1}\frac{\partial\varepsilon_1}{\partial\varepsilon_x} + \frac{\partial\sigma_{c1}}{\partial\varepsilon_2}\frac{\partial\varepsilon_2}{\partial\varepsilon_x} \quad ; \quad \frac{\partial\sigma_{c2}}{\partial\varepsilon_x} = \frac{\partial\sigma_{c2}}{\partial\varepsilon_1}\frac{\partial\varepsilon_1}{\partial\varepsilon_x} + \frac{\partial\sigma_{c2}}{\partial\varepsilon_2}\frac{\partial\varepsilon_2}{\partial\varepsilon_x}$$

$$\frac{\partial\sigma_{c1}}{\partial\varepsilon_y} = \frac{\partial\sigma_{c1}}{\partial\varepsilon_1}\frac{\partial\varepsilon_1}{\partial\varepsilon_y} + \frac{\partial\sigma_{c1}}{\partial\varepsilon_2}\frac{\partial\varepsilon_2}{\partial\varepsilon_y} \quad ; \quad \frac{\partial\sigma_{c2}}{\partial\varepsilon_y} = \frac{\partial\sigma_{c2}}{\partial\varepsilon_1}\frac{\partial\varepsilon_1}{\partial\varepsilon_y} + \frac{\partial\sigma_{c2}}{\partial\varepsilon_2}\frac{\partial\varepsilon_2}{\partial\varepsilon_y}$$

$$\frac{\partial\sigma_{c1}}{\partial\gamma_{xy}} = \frac{\partial\sigma_{c1}}{\partial\varepsilon_1}\frac{\partial\varepsilon_1}{\partial\gamma_{xy}} + \frac{\partial\sigma_{c1}}{\partial\varepsilon_2}\frac{\partial\varepsilon_2}{\partial\gamma_{xy}} \quad ; \quad \frac{\partial\sigma_{c2}}{\partial\gamma_{xy}} = \frac{\partial\sigma_{c2}}{\partial\varepsilon_1}\frac{\partial\varepsilon_1}{\partial\gamma_{xy}} + \frac{\partial\sigma_{c2}}{\partial\varepsilon_2}\frac{\partial\varepsilon_2}{\partial\gamma_{xy}}$$

Fig.4.11 Tangent Material Stiffness Matrix (Jacobian) for Plain Concrete in *xy* Direction

Fig.4.10 reveals that the material laws are noted in terms of principal directions. However, the components of the Jacobian are noted in *xy* direction and have, therefore, to be transformed in a suitable fashion. In Fig.4.11.(a), the relations between a stress state in *xy* and principal direction are given. It is obvious that each component of the stress state in *xy* direction is a function of both the stress state in principal direction and the angle θ_c. Furthermore, the constitutive laws reveal that each component of the stress state in principal direction is a function of the strain state in principal direction. Finally, the relations between a strain state in principal and *xy* direction are depicted. The equations show that each strain component in principal direction is a function of both the strain state in *xy* direction and the angle θ_c. With these dependencies the components of the tangent material stiffness matrix can be expressed as shown in Fig.4.11.(b).

$$E_{xx}^{'c} = \frac{\partial \sigma_{cx}}{\partial \sigma_{c1}}\left(\frac{\partial \sigma_{c1}}{\partial \varepsilon_1}\frac{\partial \varepsilon_1}{\partial \varepsilon_x} + \frac{\partial \sigma_{c1}}{\partial \varepsilon_2}\frac{\partial \varepsilon_2}{\partial \varepsilon_x}\right) + \frac{\partial \sigma_{cx}}{\partial \sigma_{c2}}\left(\frac{\partial \sigma_{c2}}{\partial \varepsilon_1}\frac{\partial \varepsilon_1}{\partial \varepsilon_x} + \frac{\partial \sigma_{c2}}{\partial \varepsilon_2}\frac{\partial \varepsilon_2}{\partial \varepsilon_x}\right) + \frac{\partial \sigma_{cx}}{\partial \theta_c}\frac{\partial \theta_c}{\partial \varepsilon_x}$$

$$\frac{\partial \sigma_{c1}}{\partial \varepsilon_1} = E_{11}^{'c} \quad ; \quad \frac{\partial \sigma_{c1}}{\partial \varepsilon_2} = E_{12}^{'c} \quad ; \quad \frac{\partial \sigma_{c2}}{\partial \varepsilon_1} = E_{21}^{'c} \quad ; \quad \frac{\partial \sigma_{c2}}{\partial \varepsilon_2} = E_{22}^{'c}$$

$$\frac{\partial \sigma_{cx}}{\partial \sigma_{c1}} = \cos^2\theta_c \quad ; \quad \frac{\partial \sigma_{cx}}{\partial \sigma_{c2}} = \sin^2\theta_c \quad ; \quad \frac{\partial \varepsilon_1}{\partial \varepsilon_x} = \cos^2\theta_c \quad ; \quad \frac{\partial \varepsilon_2}{\partial \varepsilon_x} = \sin^2\theta_c$$

$$\frac{\partial \sigma_{cx}}{\partial \theta_c} = -2\sin\theta_c\cos\theta_c\left(\sigma_{c1} - \sigma_{c2}\right)$$

$$\frac{\partial \theta_c}{\partial \varepsilon_x} = -\frac{\sin\theta_c\cos\theta_c}{\varepsilon_1 - \varepsilon_2} \qquad \textit{with:} \qquad \gamma_{xy} = \left(\varepsilon_x - \varepsilon_y\right)\tan 2\theta_c$$

$$E_{xx}^{'c} = E_{11}^{'c}\cos^4\theta_c + \left(E_{12}^{'c} + E_{21}^{'c}\right)\sin^2\theta_c\cos^2\theta_c + E_{22}^{'c}\sin^4\theta_c + 2\frac{\sigma_{c1} - \sigma_{c2}}{\varepsilon_1 - \varepsilon_2}\sin^2\theta_c\cos^2\theta_c$$

Fig.4.12 Evaluation of $E_{xx}^{'c}$ in Terms of Principal Direction

The expression given for $E_{xx}^{'c}$ in Fig.11.(b) is evaluated in Fig.4.12 and, for completeness, the results of the evaluation of each component of the Jacobian are depicted in Fig.4.13. For each component of the tangent material stiffness matrix in *xy* direction, the mathematical procedure up to now has yielded the corresponding expression in terms of principal direction. The various elements of the Jacobian can now be calculated from the material laws given in the constitutive model.

$$E_{xx}^{ic} = E_{11}^{ic}\cos^4\theta_c + \left(E_{12}^{ic} + E_{21}^{ic}\right)\sin^2\theta_c\cos^2\theta_c + E_{22}^{ic}\sin^4\theta_c + 2\frac{\sigma_{c1}-\sigma_{c2}}{\varepsilon_1-\varepsilon_2}\sin^2\theta_c\cos^2\theta_c$$

$$E_{xy}^{ic} = E_{12}^{ic}\cos^4\theta_c + \left(E_{11}^{ic} + E_{22}^{ic}\right)\sin^2\theta_c\cos^2\theta_c + E_{21}^{ic}\sin^4\theta_c - 2\frac{\sigma_{c1}-\sigma_{c2}}{\varepsilon_1-\varepsilon_2}\sin^2\theta_c\cos^2\theta_c$$

$$E_{x\gamma}^{ic} = \left(E_{11}^{ic} - E_{12}^{ic}\right)\sin\theta_c\cos^3\theta_c + \left(E_{21}^{ic} - E_{22}^{ic}\right)\sin^3\theta_c\cos\theta_c - \frac{\sigma_{c1}-\sigma_{c2}}{\varepsilon_1-\varepsilon_2}\sin\theta_c\cos\theta_c\left(\cos^2\theta_c - \sin^2\theta_c\right)$$

$$E_{yx}^{ic} = E_{21}^{ic}\cos^4\theta_c + \left(E_{11}^{ic} + E_{22}^{ic}\right)\sin^2\theta_c\cos^2\theta_c + E_{12}^{ic}\sin^4\theta_c - 2\frac{\sigma_{c1}-\sigma_{c2}}{\varepsilon_1-\varepsilon_2}\sin^2\theta_c\cos^2\theta_c$$

$$E_{yy}^{ic} = E_{22}^{ic}\cos^4\theta_c + \left(E_{12}^{ic} + E_{21}^{ic}\right)\sin^2\theta_c\cos^2\theta_c + E_{11}^{ic}\sin^4\theta_c + 2\frac{\sigma_{c1}-\sigma_{c2}}{\varepsilon_1-\varepsilon_2}\sin^2\theta_c\cos^2\theta_c$$

$$E_{y\gamma}^{ic} = \left(E_{11}^{ic} - E_{12}^{ic}\right)\sin^3\theta_c\cos\theta_c + \left(E_{21}^{ic} - E_{22}^{ic}\right)\sin\theta_c\cos^3\theta_c + \frac{\sigma_{c1}-\sigma_{c2}}{\varepsilon_1-\varepsilon_2}\sin\theta_c\cos\theta_c\left(\cos^2\theta_c - \sin^2\theta_c\right)$$

$$E_{\gamma x}^{ic} = \left(E_{11}^{ic} - E_{21}^{ic}\right)\sin\theta_c\cos^3\theta_c + \left(E_{12}^{ic} - E_{22}^{ic}\right)\sin^3\theta_c\cos\theta_c - \frac{\sigma_{c1}-\sigma_{c2}}{\varepsilon_1-\varepsilon_2}\sin\theta_c\cos\theta_c\left(\cos^2\theta_c - \sin^2\theta_c\right)$$

$$E_{\gamma y}^{ic} = \left(E_{11}^{ic} - E_{21}^{ic}\right)\sin^3\theta_c\cos\theta_c + \left(E_{12}^{ic} - E_{22}^{ic}\right)\sin\theta_c\cos^3\theta_c + \frac{\sigma_{c1}-\sigma_{c2}}{\varepsilon_1-\varepsilon_2}\sin\theta_c\cos\theta_c\left(\cos^2\theta_c - \sin^2\theta_c\right)$$

$$E_{\gamma\gamma}^{ic} = \left(E_{11}^{ic} - E_{12}^{ic} - E_{21}^{ic} + E_{22}^{ic}\right)\sin^2\theta_c\cos^2\theta_c + \frac{1}{2}\frac{\sigma_{c1}-\sigma_{c2}}{\varepsilon_1-\varepsilon_2}\left(\cos^2\theta_c - \sin^2\theta_c\right)^2$$

Fig.4.13 Complete Tangent Material Stiffness Matrix for Plain Concrete in *xy* Direction

For computational efficiency, it is more convenient to establish the Jacobian in principal direction and to rotate it in the UMAT to the *xy* direction, rather than to code the complicated expressions of the components of the tangent material stiffness matrix as they are given in Fig.4.13. The easiest way to obtain the Jacobian in the principal direction is to use the transformation matrix $\boldsymbol{T}$ in the well-known fashion. Fig.4.14 once again shows the procedure. From this it is clear that the Jacobian in principal direction represents a far simpler mathematical expression than the tangent material stiffness matrix given in Fig.4.13. However, the effort to perform the transformation is considerable.

It is worth noting that the Jacobian does not contain any factors for adjusting tension stiffening or secondary shear carrying actions such as aggregate interlock. This is typical for tangent material stiffness matrices which are calibrated by empirically derived constitutive laws. For instance, the Jacobian derived from the Darwin/Pecknold concept and calibrated with the concrete law of Saenz, showed the same feature. In addition, the

shear stiffness component $E'^{c}_{33}=0.5(\sigma_{c1}-\sigma_{c2})/(\varepsilon_1-\varepsilon_2)$ reveals that the applied method can be attributed to the rotating crack approach which is a direct consequence of the assumption that the principal stress direction of the plain concrete coincides with the principal strain direction of the reinforced element (Crisfield/Wills, 1989). In Chapter3 this assumption was expressed by $\theta_c=\theta=\theta'$ and this means that when both stress and strain direction coincide, then the crack angle θ' coincides with each of the other angles as well. Consequently, a crack angle will change together with the stress state in the concrete. This is to some extent against the physical reality and hence, this assumption was criticised by Bažant and Oh (1983). It was shown earlier that Kupfer abandoned this assumption, which led to three different values for θ_c, θ and θ' but made the theory rather complex.

$$\left[E'^{c}\right]_{12}=[T]^{T}\left[E'^{c}\right]_{xy}[T]=\begin{bmatrix} E'^{c}_{11} & E'^{c}_{12} & 0 \\ E'^{c}_{21} & E'^{c}_{22} & 0 \\ 0 & 0 & \dfrac{\sigma_{c1}-\sigma_{c2}}{2(\varepsilon_1-\varepsilon_2)} \end{bmatrix}$$

$\left[E'^{c}\right]_{12}$ = *Jacobian for plain concrete in principal direction*

$\left[E'^{c}\right]_{xy}$ = *Jacobian for plain concrete in xy direction (see Fig.4.13)*

$[T]$ = *transformation matrix (see Fig.4.2)*

Fig.4.14 Tangent Material Stiffness Matrix for Plain Concrete in Principal Direction

In the linear elastic case, which is, for instance, given in the MCFT when both principal components of a stress state consist of tension stresses below the tensile strength (see Case 4 in Fig.4.15), the Jacobian in principal direction yields the isotropic material stiffness matrix for $\nu=0$. This feature is equivalent to the fact that the above mentioned assumption for the coincidence of principal stress and strain directions suppresses the Poisson's effect. Note that an isotropic material matrix is invariant of directions and therefore, the Jacobian in xy direction must yield the same result which can easily be verified by the tangent material stiffness matrix of Fig.4.13.

4.2.2 Assembling of the Jacobian in the UMAT

In the derivations up to now the material laws have not been involved. They are now necessary to specify the values for the stiffness moduli $E_{11}^{lc}, E_{12}^{lc}, E_{21}^{lc}$ and E_{22}^{lc}. These values depend on the stress and strain state given in an integration point at a certain stage of a calculation. Prior to the assembling of the Jacobian in the UMAT, the stress state in an integration point is calculated from the strain state by means of the material laws. Usually the strain state is supplied by the main program in *xy* direction. Therefore, the first step in the UMAT is its rotation to the principal direction. The next step is to determine the concrete and steel stresses from the material laws and to rotate them back to the *xy* direction. Finally, concrete and steel stresses are added together to yield the stress state of the reinforced concrete element which has to be transferred to the main program in order to advance the analysis.

Once the stress states of both the plain concrete and the steel are known the assembling of the Jacobian can too be performed. While the stiffness supplied by the steel to the material moduli is most easily calculated from the steel law, the proportion given by the plain concrete needs appropriate consideration. Generally, there are six different possibilities to distinguish. Fig.4.15 shows the entire spectrum of sets of stiffness values for plain concrete.

Fig.4.15 reveals that in the occurrence of Case 3 the tangent material stiffness matrix becomes unsymmetric. As this case represents a standard situation for concrete under high shear this unsymmetry will not be a rare event when analysing RC beams or shear walls. The unsymmetry of the Jacobian is caused by the material law for concrete in compression which considers the compressive stress in principal direction as being a function of the strain in the principal tensile direction, provided the cracking strain is exceeded.

Case 1: $\varepsilon_1<0$ $\varepsilon_2<0$

$$E_{11}^{'c}=\frac{2f_c}{\varepsilon_{cu}}-\frac{2f_c}{\varepsilon_{cu}^2}\varepsilon_1 \qquad E_{12}^{'c}=E_{21}^{'c}=0 \qquad E_{22}^{'c}=\frac{2f_c}{\varepsilon_{cu}}-\frac{2f_c}{\varepsilon_{cu}^2}\varepsilon_2$$

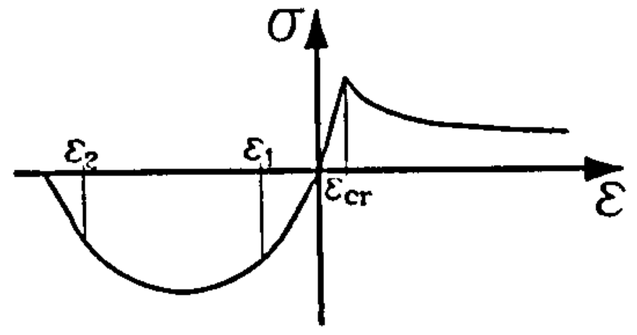

Case 2a: $0<\varepsilon_1<\varepsilon_{cr}$ $\varepsilon_2<0$

$$E_{11}^{'c}=\frac{2f_c}{\varepsilon_{cu}} \qquad E_{12}^{'c}=E_{21}^{'c}=0 \qquad E_{22}^{'c}=\frac{2f_c}{\varepsilon_{cu}}-\frac{2f_c}{\varepsilon_{cu}^2}\varepsilon_2$$

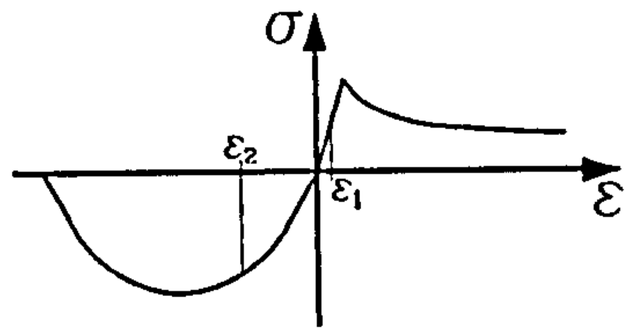

Case 2b: $\varepsilon_1<0$ $0<\varepsilon_2<\varepsilon_{cr}$

$$E_{11}^{'c}=\frac{2f_c}{\varepsilon_{cu}}-\frac{2f_c}{\varepsilon_{cu}^2}\varepsilon_1 \qquad E_{12}^{'c}=E_{21}^{'c}=0 \qquad E_{22}^{'c}=\frac{2f_c}{\varepsilon_{cu}}$$

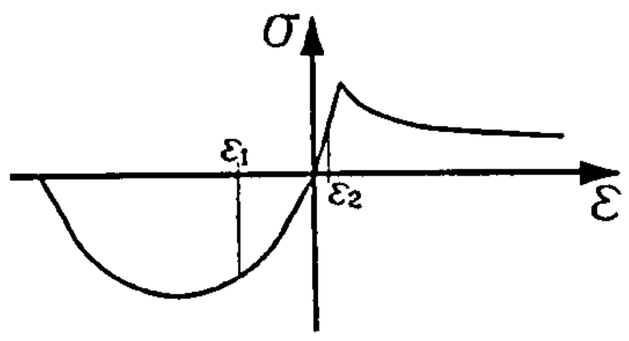

Case 3a: $\varepsilon_1>\varepsilon_{cr}$ $\varepsilon_2<0$

$$E_{11}^{'c}=\frac{-10f_{ct}}{\sqrt{2\varepsilon_1}\left(1+\sqrt{200\varepsilon_1}\right)^2} \qquad E_{12}^{'c}=0$$

$$E_{21}^{'c}=\frac{0.34f_c}{\left(0.8\varepsilon_{cu}-0.34\varepsilon_1\right)^2}\left(2\varepsilon_2-\frac{\varepsilon_2^2}{\varepsilon_{cu}}\right) \qquad E_{22}^{'c}=\frac{2f_c}{0.8\varepsilon_{cu}-0.34\varepsilon_1}\left(1-\frac{\varepsilon_2}{\varepsilon_{cu}}\right)$$

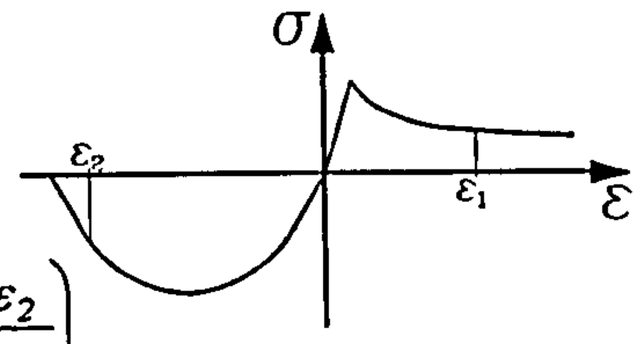

Case 3b: $\varepsilon_1<0$ $\varepsilon_2>\varepsilon_{cr}$

$$E_{11}^{'c}=\frac{2f_c}{0.8\varepsilon_{cu}-0.34\varepsilon_2}\left(1-\frac{\varepsilon_1}{\varepsilon_{cu}}\right) \qquad E_{21}^{'c}=0$$

$$E_{12}^{'c}=\frac{0.34f_c}{\left(0.8\varepsilon_{cu}-0.34\varepsilon_2\right)^2}\left(2\varepsilon_1-\frac{\varepsilon_1^2}{\varepsilon_{cu}}\right) \qquad E_{22}^{'c}=\frac{-10f_{ct}}{\sqrt{2\varepsilon_2}\left(1+\sqrt{200\varepsilon_2}\right)^2}$$

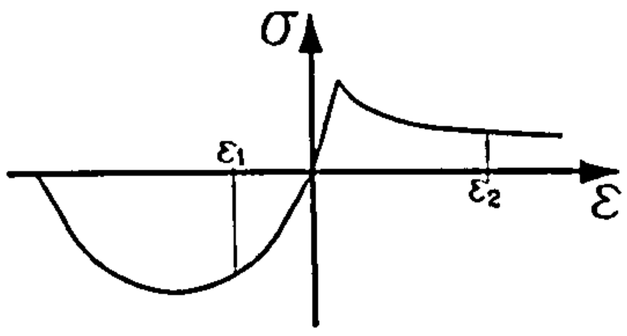

Case 4: $0<\varepsilon_1<\varepsilon_{cr}$ $0<\varepsilon_2<\varepsilon_{cr}$

$$E_{11}^{'c}=\frac{2f_c}{\varepsilon_{cu}} \qquad E_{12}^{'c}=E_{21}^{'c}=0 \qquad E_{22}^{'c}=\frac{2f_c}{\varepsilon_{cu}}$$

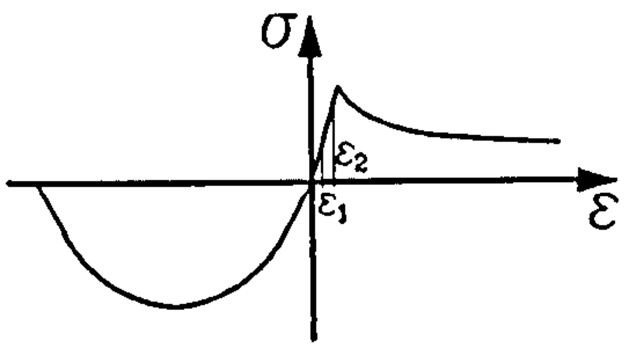

Case 5a: $\varepsilon_1>\varepsilon_{cr}$ $0<\varepsilon_2<\varepsilon_{cr}$

$$E_{11}^{'c}=\frac{-10f_{ct}}{\sqrt{2\varepsilon_1}\left(1+\sqrt{200\varepsilon_1}\right)^2} \qquad E_{12}^{'c}=E_{21}^{'c}=0 \qquad E_{22}^{'c}=\frac{2f_c}{\varepsilon_{cu}}$$

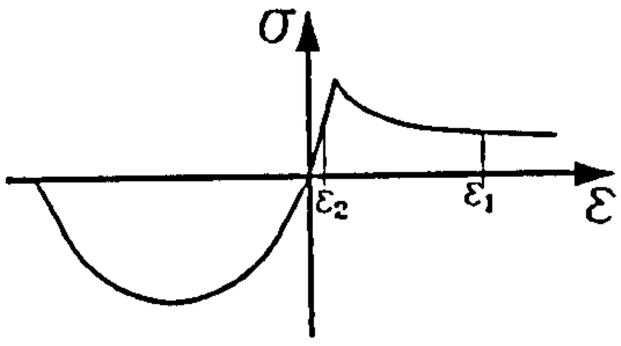

Case 5b: $0<\varepsilon_1<\varepsilon_{cr}$ $\varepsilon_2>\varepsilon_{cr}$

$$E_{11}^{'c}=\frac{2f_c}{\varepsilon_{cu}} \qquad E_{12}^{'c}=E_{21}^{'c}=0 \qquad E_{22}^{'c}=\frac{-10f_{ct}}{\sqrt{2\varepsilon_2}\left(1+\sqrt{200\varepsilon_2}\right)^2}$$

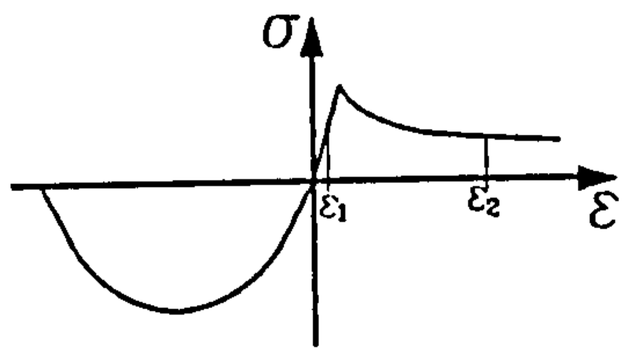

Case 6: $\varepsilon_1>\varepsilon_{cr}$ $\varepsilon_2>\varepsilon_{cr}$

$$E_{11}^{'c}=\frac{-10f_{ct}}{\sqrt{2\varepsilon_1}\left(1+\sqrt{200\varepsilon_1}\right)^2} \qquad E_{22}^{'c}=\frac{-10f_{ct}}{\sqrt{2\varepsilon_2}\left(1+\sqrt{200\varepsilon_2}\right)^2}$$

$$E_{12}^{'c}=E_{21}^{'c}=0$$

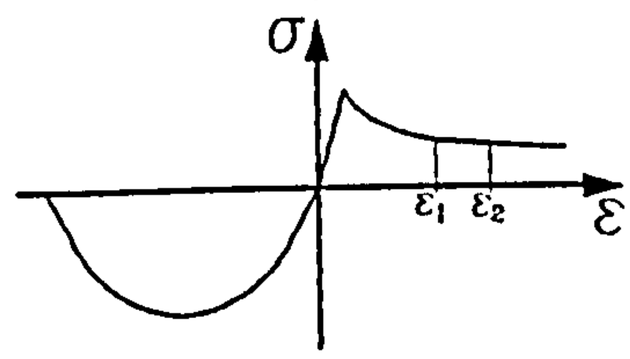

Fig.4.15 Tangent Material Stiffness Moduli for Plain Concrete in Principal Direction

Because of the unsymmetric Jacobian, the solver of the main program has to invert the complete system stiffness matrix unless the initial stress method is used. This is time-consuming and expensive and is therefore a certain disadvantage of the material law of the MCFT. ABAQUS provides a solver for unsymmetric system stiffness matrices by specifying this feature on the input deck. However, many FE codes do not cater for that facility and, hence, a constitutive law causing unsymmetry in the Jacobian would be not suitable for implementation in such programs.

a) Jacobian for Plain Concrete in xy Direction

$$\left[E'^{c}\right]_{xy} = \left[T^{-1}\right]^{T}\left[E'^{c}\right]_{12}\left[T^{-1}\right] = \begin{bmatrix} E'^{c}_{xx} & E'^{c}_{xy} & E'^{c}_{x\gamma} \\ E'^{c}_{yx} & E'^{c}_{yy} & E'^{c}_{y\gamma} \\ E'^{c}_{\tau x} & E'^{c}_{\tau y} & E'^{c}_{\tau\gamma} \end{bmatrix}$$

with:

$$\left[T^{-1}\right] = \begin{bmatrix} \cos^2\theta_c & \sin^2\theta_c & \sin\theta_c\cos\theta_c \\ \sin^2\theta_c & \cos^2\theta_c & -\sin\theta_c\cos\theta_c \\ -2\sin\theta_c\cos\theta_c & 2\sin\theta_c\cos\theta_c & \cos^2\theta_c - \sin^2\theta_c \end{bmatrix}$$

$\left[T^{-1}\right]$ = *inverse of* $\left[T\right]$ *(see Fig.4.2)*

b) Jacobian for Steel in xy Direction

$$\left[E'^{s}\right]_{xy} = \left[R\right]^{T}\left[E'^{s}\right]_{\xi\eta}\left[R\right] = \begin{bmatrix} E'^{s}_{xx} & E'^{s}_{xy} & E'^{s}_{x\gamma} \\ E'^{s}_{yx} & E'^{s}_{yy} & E'^{s}_{y\gamma} \\ E'^{s}_{\tau x} & E'^{s}_{\tau y} & E'^{s}_{\tau\gamma} \end{bmatrix}$$

with:

$$\left[E'^{s}\right]_{\xi\eta} = \begin{bmatrix} \rho_\xi E_s & 0 & 0 \\ 0 & \rho_\eta E_s & 0 \\ 0 & 0 & 0 \end{bmatrix}$$

and:

$$\left[R\right] = \begin{bmatrix} \cos^2\alpha & \sin^2\alpha & \sin\alpha\cos\alpha \\ \sin^2\alpha & \cos^2\alpha & -\sin\alpha\cos\alpha \\ -2\sin\alpha\cos\alpha & 2\sin\alpha\cos\alpha & \cos^2\alpha - \sin^2\alpha \end{bmatrix}$$

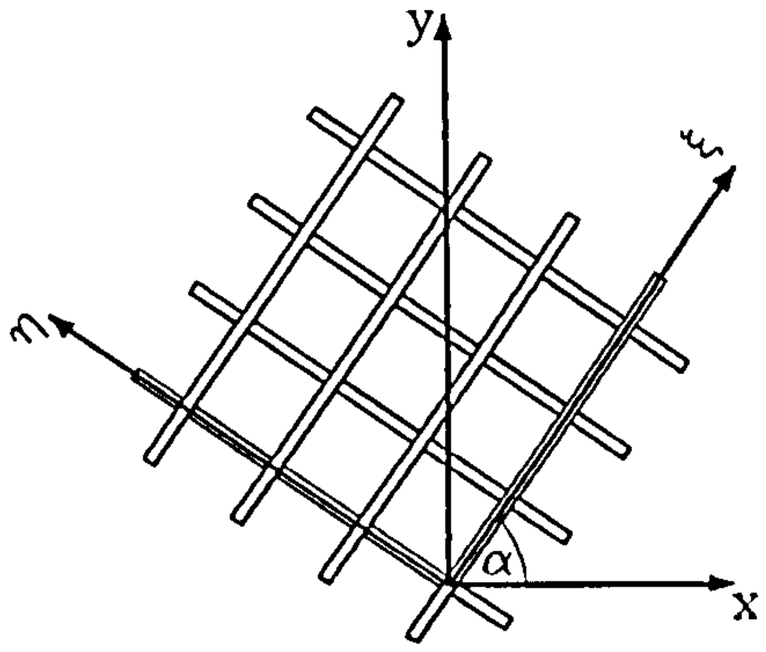

E_s = *Young's modulus of steel*
ρ_ξ, ρ_η = *steel ratio in* ξ *and* η *direction, respectively*

c) Jacobian for Reinforced Concrete in xy Direction

$$\left[E'\right]_{xy} = \left[E'^{c}\right]_{xy} + \left[E'^{s}\right]_{xy} = \begin{bmatrix} E'^{c}_{xx}+E'^{s}_{xx} & E'^{c}_{xy}+E'^{s}_{xy} & E'^{c}_{x\gamma}+E'^{s}_{x\gamma} \\ E'^{c}_{yx}+E'^{s}_{yx} & E'^{c}_{yy}+E'^{s}_{yy} & E'^{c}_{y\gamma}+E'^{s}_{y\gamma} \\ E'^{c}_{\tau x}+E'^{s}_{\tau x} & E'^{c}_{\tau y}+E'^{s}_{\tau y} & E'^{c}_{\tau\gamma}+E'^{s}_{\tau\gamma} \end{bmatrix} = \begin{bmatrix} E'_{xx} & E'_{xy} & E'_{x\gamma} \\ E'_{yx} & E'_{yy} & E'_{y\gamma} \\ E'_{\tau x} & E'_{\tau y} & E'_{\tau\gamma} \end{bmatrix}$$

Fig.4.16 Tangent Material Stiffness Matrix of Reinforced Concrete Element

Fig.4.16.(b) shows the tangent material stiffness matrix of the reinforcing steel when an orthogonal grid of steel bars is assumed. In addition, the transformation of both the Jacobian for concrete and steel to the *xy* direction is depicted and their assembling to the tangent material stiffness matrix of the reinforced concrete element.

It is worth noting that the transformation matrix $\boldsymbol{T}^{-1}$ of Fig.4.16.(a) must be the inverse of the transformation matrix $\boldsymbol{T}$ of Fig.4.2. In Fig.4.2 the rotation from the *xy* direction to the principal direction is performed by applying $\boldsymbol{T}$ in the usual way and hence, the rotation back to the *xy* direction must be performed with the inverse of $\boldsymbol{T}$. Therefore, the inverse $\boldsymbol{T}^{-1}$ is most easily obtained by replacing θ_c by $-\theta_c$ in the transformation matrix $\boldsymbol{T}$. The accuracy of the procedure can be verified by the matrix multiplication $\boldsymbol{T}^{-1} * \boldsymbol{T}$ which yields the unity matrix $\boldsymbol{I}$.

4.2.3 A Modification of the MCFT

The material routine coded according to the rules described on the previous pages was extensively tested on a great variety of structural elements. It turned out that the performance of the UMAT was good in all cases where shear dominated the response of the analysed structure. However, when tension or compression rather than shear prevailed, the capacity could not be predicted in a satisfactory fashion. The investigation of this behaviour revealed a shortcoming of the constitutive model of the MCFT which necessitated an adaptation of its laws. This improved the performance of the UMAT considerably and will be explained here in detail.

Two features of the material laws of the MCFT are noticeable at first sight: The high values for both the compressive strength degradation and the tension stiffening. Fig.4.17.(a) and (b) shows an RC panel loaded in pure shear which is equivalent to a uniform state of tension and compression. The compression strength of the concrete must be reduced according to the constitutive laws. However, the degradation is to some extent neutralised by the high value of tension stiffening which is introduced in the perpendicular direction. The compressive strength degradation is dependent on the principal tensile strain which itself is a function of the principal tensile stresses. Due to the tension stiffening model of the MCFT the tensile stresses are considered to be relatively high, although the accompanying tensile strains might be high as well, in which case the principal compression strength will be considerably reduced. The same result could have been

achieved with a constitutive model providing a smaller amount of strength degradation in conjunction with lower tension stiffening.

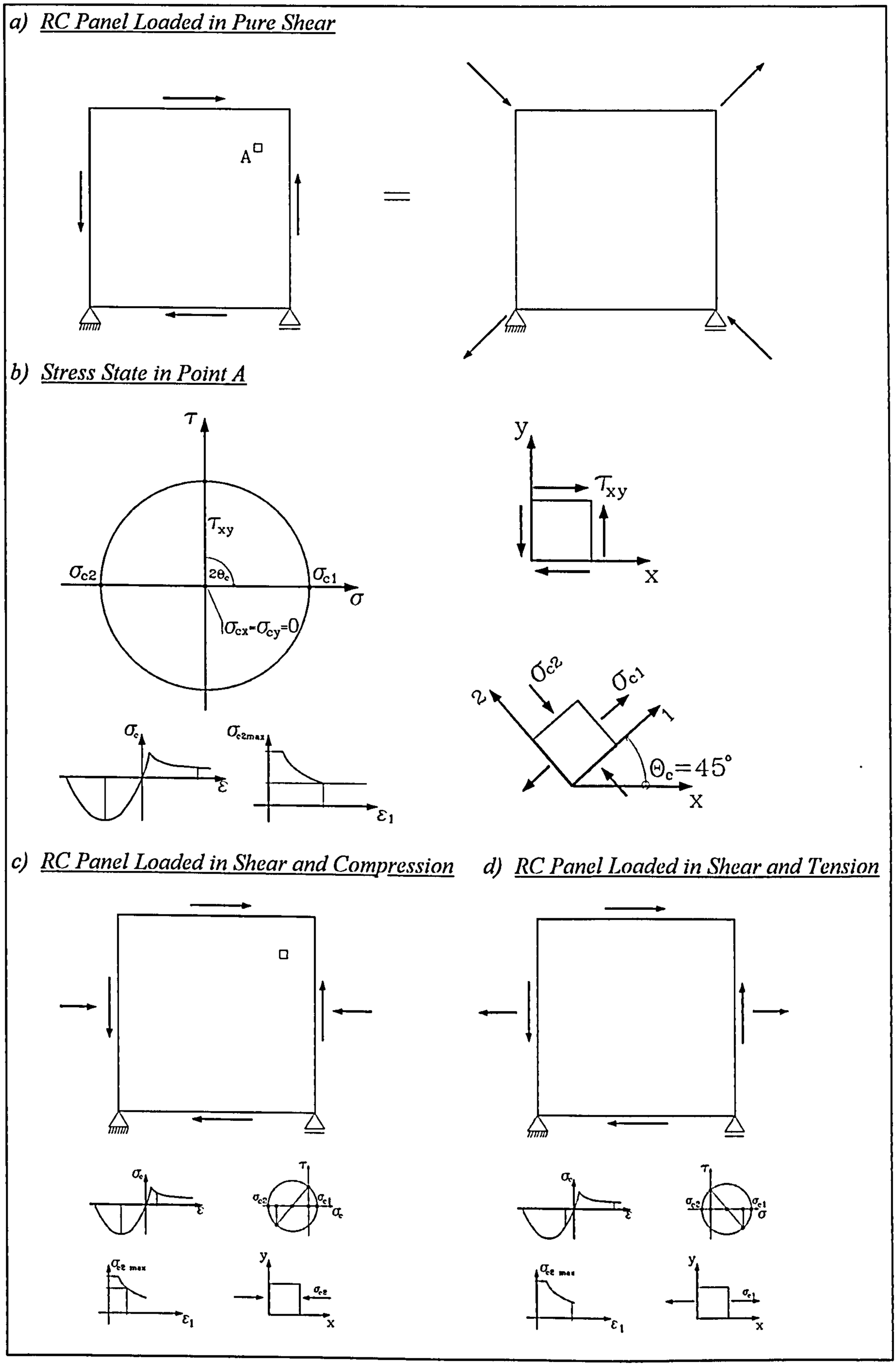

Fig.4.17 RC Panels under Various Loading Conditions

However, this is only true for prevalent shear loading. Once panels are loaded in shear and compression as depicted in Fig.4.17.(c), their response is mainly dependent on the compressive part of the constitutive law. This means that appreciable strength degradation might occur although the straining in perpendicular direction is relatively low. Moreover, panels loaded in shear and tension as shown in Fig.4.17.(d) are governed by the tension part of the constitutive law. This means that high tensile stresses are assigned to the concrete which is against the physical reality. A similar case is given when the specimens are only slightly reinforced or mild steel is used. Then tension stiffening contributes considerably to the response which results in an overestimation of the tensile strength. It is therefore necessary to check whether the proposed constitutive rules of the MCFT represent tension stiffening and compression strength degradation as realistic material properties for cracked reinforced concrete.

A simple consideration on tension stiffening confirms that the MCFT overestimates the principal tensile stresses in the cracked concrete. The stresses due to strain softening can be considered to vanish once the principal tensile strains approach a value of approximately *10* times the cracking strain. For normal concrete this occurs in the region of *1‰*. Tension stiffening stresses have dropped to zero by the time the tensile strain in *xy* direction is in the range of the yield strain of the reinforcing steel, which normally happens at *2‰*. Therefore, it can be assumed that at a strain of $\varepsilon_1 = 4‰$, no appreciable tension stresses are present in the concrete. However, it is easy to verify that the constitutive laws of the MCFT assume tensile stresses of more than *50%* the tensile strength of the concrete at the above mentioned strain of *4‰*. This is definitely a value which is far too high, even though aggregate interlock action might also generate some tensile stresses across cracks.

In 1990, Kollegger/Mehlhorn reported tests on RC specimens biaxially loaded in compression and tension. The results clearly showed that the degradation of the compressive strength of the concrete is usually less than *40%* the initial value. However, the constitutive laws of Vecchio/Collins assume a degradation of up to *80%* the uniaxial strength. In fact, this shows that, as earlier suspected, the overestimation of tension stiffening supersedes the underrating of the remaining compressive strength to yield good results in all cases where shear is predominant.

Panel	*Load Ratio* $\tau_{xy}/\sigma_x/\sigma_y$	*Longitud. Steel* ρ_x [%]	f_y [MPa]	*Transverse Steel* ρ_y [%]	f_y [MPa]	τ_u [MPa] *Test*	*UMAT*	*Ratio* $\tau_{u\,test}/\tau_{u\,cal}$
Overestimation Due to Low Steel Reinforcement:								
PV2	*1:0:0*	*0.18*	*428*	*0.18*	*428*	*1.16*	*1.57*	*0.74*
PV3	*1:0:0*	*0.48*	*662*	*0.48*	*662*	*3.07*	*3.94*	*0.78*
Overestimation Due to Mild Steel:								
PV4	*1:0:0*	*1.06*	*242*	*1.06*	*242*	*2.89*	*3.51*	*0.83*
PV6	*1:0:0*	*1.79*	*266*	*1.79*	*266*	*4.55*	*5.69*	*0.80*
Overestimation Due to Predominant Tension:								
PB8	*1:2.98:0*	*1.09*	*425*	*0.0*	-	*0.79*	*1.10*	*0.72*
PB10	*1:5.94:0*	*1.09*	*433*	*0.0*	-	*0.56*	*0.79*	*0.71*
Realistic Prediction for Pure Shear:								
PV22	*1:0:0*	*1.79*	*458*	*1.52*	*420*	*6.07*	*6.21*	*0.98*
PV26	*1:0:0*	*1.79*	*456*	*1.01*	*463*	*5.41*	*5.77*	*0.94*
PV27	*1:0:0*	*1.79*	*442*	*1.79*	*442*	*6.35*	*6.47*	*0.98*
Underestimation Due to Predominant Compression:								
PV23	*1:-0.39:-0.39*	*1.79*	*518*	*1.79*	*518*	*8.87*	*7.35*	*1.20*
PV25	*1:-0.69:-0.69*	*1.79*	*466*	*1.79*	*466*	*9.12*	*7.95*	*1.15*

Tab.4.1 Results with UMAT Based on Original Constitutive Model of MCFT

Tab.4.1 shows results of calculations with a UMAT coded according to the original constitutive laws of the MCFT (see Fig.4.10). The table contains five sorts of panels of the Toronto PV and PB series. It is obvious that the panels under pure shear were recalculated in a proper fashion, provided they were reasonably reinforced with high strength steel. The panels additionally loaded in compression were distinctly underestimated, while the panels under tension developed a strength which was not reached by the tests.

Because of the above mentioned features of the MCFT it was intended to modify the constitutive laws in a fashion which weakens the tensile response and improves the compressive behaviour according to the explanations of tension stiffening and strength degradation given before. The best way to achieve this aim would be to conduct a comprehensive parametric study to calibrate the MCFT on a representative selection of test data. However, such a task would be beyond the scope of this work. Therefore, various modifications of the concrete laws of the MCFT were incorporated in the UMAT and tested against the experimental data of Leonhardt and Vecchio/Collins. This optimisation procedure led to three minor adaptations of the model which are briefly explained hereafter.

The principal tensile stress in the concrete is assumed to have dropped to zero once a strain of approximately *4‰* is reached. In addition, the strength degradation has been adjusted in such a way that it will decrease to a maximum of *50%* the initial value at a tensile strain of *10‰*. These measures, depicted in Fig.4.18, proved to enhance the performance of the UMAT considerably, as will be seen in Section 4.3 dealing with the verification of the UMAT.

A third small change to the constitutive law for concrete in tension was performed by replacing Eq.(4.1) from Fig.4.10 by Eq.(4.2) from Fig.4.18. Comparison of Fig.4.10.(b) with Fig.4.18.(b) clarifies the modification which ensures a smooth transition of the concrete tensile stresses in the strain range beyond ε_{cr} . It should be mentioned that the discontinuities in the tensile law did not lead to any apparent convergence problems. A straight line which was used as softening curve beyond the cracking strain did not reveal a significantly enhanced performance of the UMAT.

a) *Concrete in Compression*

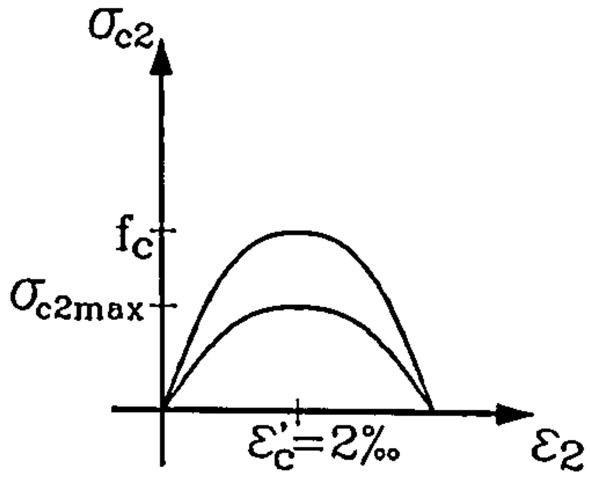

$$\sigma_{c2} = \sigma_{c2max}\left[2\frac{\varepsilon_2}{\varepsilon_c'} - \left(\frac{\varepsilon_2}{\varepsilon_c'}\right)^2\right]$$

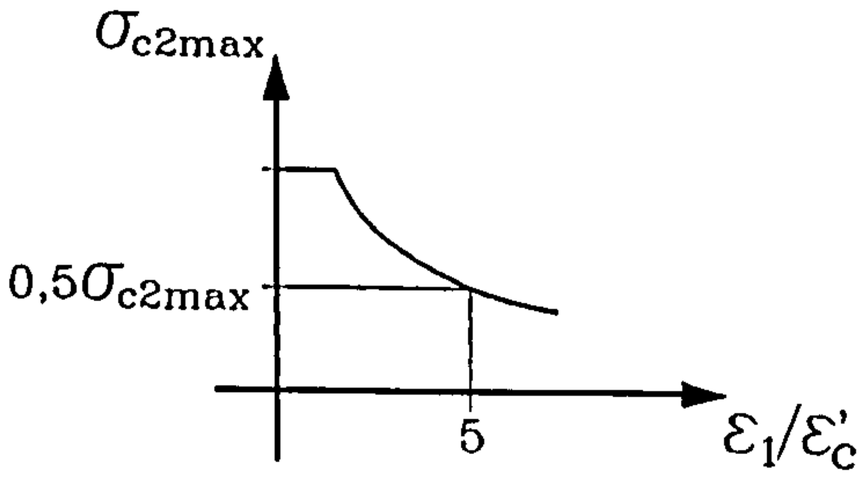

$$\sigma_{c2max} = \frac{f_c}{0.8 - 0.24\varepsilon_1 / \varepsilon_c'}$$

b) *Concrete in Tension*

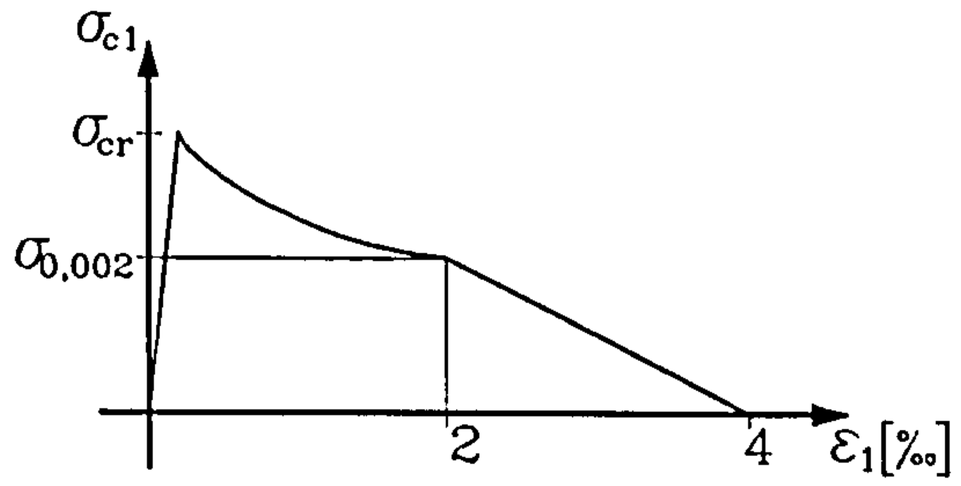

$$\sigma_{cr} = f_{ct}$$

for $\varepsilon_1 < \varepsilon_{cr}$

$$\sigma_{c1} = E_c \varepsilon_1 \quad with \quad E_c = 2f_c / \varepsilon_c'$$

for $\varepsilon_{cr} < \varepsilon_1 < 0.002$

$$\sigma_{c1} = \frac{f_{ct}}{1 + \sqrt{200\left(\varepsilon_1 - \varepsilon_{cr}\right)}} \qquad (4.2)$$

with $f_{ct} = \alpha\sqrt{f_c}$

$\alpha = 0.33 \div 0.75$

for $0.002 < \varepsilon_1 < 0.004$

$$\sigma_{c1} = \sigma_{0.002}\left(2 - \frac{\varepsilon_1}{0.002}\right)$$

for $0.004 < \varepsilon_1$ $\sigma_{c1} = 0$

Fig.4.18 Proposed Constitutive Model of the MCFT

4.3 Verification of User Material Subroutine

4.3.1. The Toronto PV Series

The modified compression field theory was derived by Vecchio/Collins from extensive testing on RC shear panels. It was intended to establish a material model for reinforced concrete elements which are mainly subjected to in-plane loading. Such structural elements typically occur, for instance, in shear walls of high-rise buildings, in webs of box-girder bridges or in caissons of off-shore platforms.

It is obvious that the tests which served for the calibration of the MCFT are best suited to check the proper implementation of the constitutive model in the user subroutine. Therefore, the Toronto tests of series PV were recalculated with the UMAT and the results are presented in this section of Chapter 4. Fig 4.19.(a) shows the test set-up with the specimen, the shear keys and the loading jacks with which a well-defined load could be applied on the RC panels. Fig.4.19.(b) depicts the analysed model with its element mesh and the 2D-Solid CPS4 which was chosen for calculations.

Generally, all two-dimensional plane stress solid elements from the ABAQUS element library are suitable for employing together with the UMAT. In contrast, not every 2D Solid for plane stress problems can be used together with the standard material concrete options for the analysis of reinforced concrete structures. The reason for this is that the *REBAR option of ABAQUS Standard, which is necessary for the reinforcing of elements, is not available for some of the 2D Solids, such as the 3-node linear element CPS3 or the 6-node quadratic element CPS6. This reveals that the UMAT offers a greater versatility in analysing reinforced concrete structures than the standard ABAQUS concrete options. Tab.4.2 gives a brief overview of the usage of the most common plane stress elements together with ABAQUS Standard or UMAT.

In the Toronto PV series, conducted between March 1979 and August 1981, 30 RC shear panels were tested. Each specimen was 89 cm square and 7 cm thick. The test observations reveal that some of the samples sustained a premature failure, especially in corner regions, which in most cases occurred because the shear keys pulled out of the concrete. Another reason for premature failures were voids in the concrete caused by poor casting. Although it is obvious that test results reported on specimens with a premature failure are not reliable, some of the tests have nevertheless been recalculated.

Panel PV29 was loaded under changing conditions which are not further specified in the test descriptions and therefore, the recalculation of this panel was omitted. This means that a total of 19 tests were recalculated using the UMAT described above.

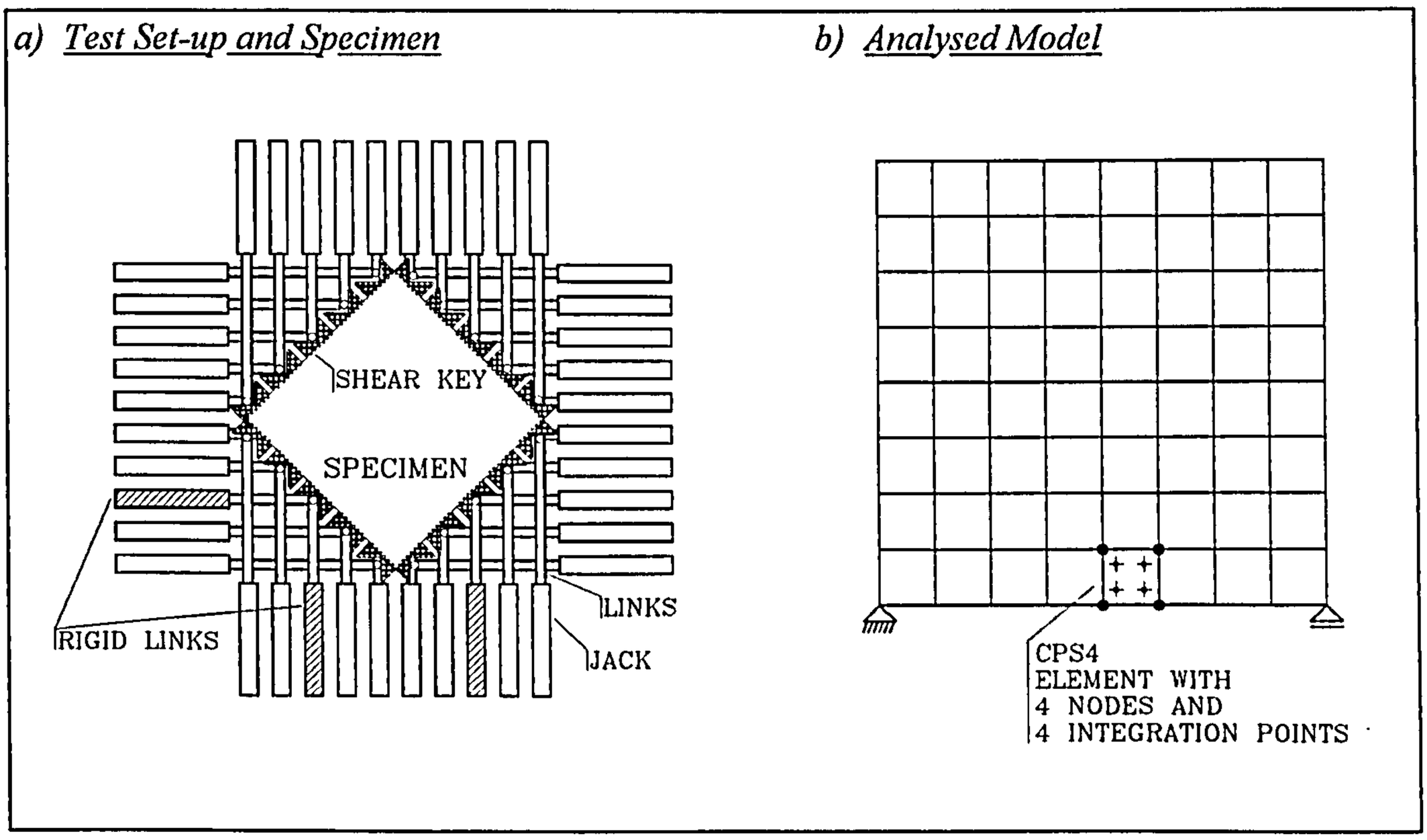

Fig.4.19 Test Set-up for Toronto PV and PB Series and Analysed Model

Tab.4.3 shows all relevant data of the analysed specimens and Tab.4.4 gives both the measured and the calculated ultimate shear stress of each sample. In addition, in Tab.4.4 the results of a nearly comprehensive recalculation of the PV series by Stevens/Uzumeri/ Collins/Will (1991) is depicted. Researchers who also analysed part of the tests were, among others, Crisfield / Wills (1989), Hu / Schnobrich (1990) and Feenstra / de Borst (1993). Comments on the results of their investigations will be given later in this chapter.

Element	*Standard Material Options*		*UMAT*
	Plain Concrete	*Reinf. Concrete*	*Plain + Reinf. Concrete*
CPS3 = 3-node linear	*yes*	*no*	*yes*
CPS4 = 4-node bilinear	*yes*	*yes*	*yes*
CPS4I = 4-node bilinear, incompatible modes	*yes*	*yes*	*yes*
CPS4R = 4-node bilinear, reduced integration	*yes*	*yes*	*yes*
CPS6 = 6-node quadratic	*yes*	*no*	*yes*
CPS8 = 8-node biquadratic	*yes*	*yes*	*yes*
CPS8R = 8-node biquadratic, reduced integration	*yes*	*yes*	*yes*

Tab.4.2 ABAQUS Element Library for Plane Stress 2D Solids

The concrete laws of the MCFT do not explicitly specify the tensile strength of the concrete. However, Vecchio/Collins (1986) and Stevens et al (1991) fixed f_{ct} at a level of $0.33\sqrt{f_c}$ which is in accordance with the provisions of the ACI. To avoid any adjusting of calculated values on test results this value was retained and kept constant throughout all calculations. This might be responsible for part of the differences in the predicted and measured ultimate capacity, as occasionally the cracking stress given in the test description deviates appreciably from the tensile strength calculated from the above ACI equation.

Panel	*Loading Ratio* $\tau_{xy}/\sigma_x/\sigma_y$	*Longitudinal Steel* ρ_x [%]	f_y [MPa]	*Transverse Steel* ρ_y [%]	f_y [MPa]	*Concrete* ε'_c [‰]	f_c [MPa]	$f_{ct}=0.33\sqrt{f_c}$ [MPa]
PV2	*1:0:0*	*0.18*	*428*	*0.18*	*428*	*2.3*	*23.5*	*1.60*
PV3	*1:0:0*	*0.48*	*662*	*0.48*	*662*	*2.3*	*26.6*	*1.70*
PV4	*1:0:0*	*1.06*	*242*	*1.06*	*242*	*2.5*	*26.6*	*1.70*
PV6	*1:0:0*	*1.79*	*266*	*1.79*	*266*	*2.5*	*29.8*	*1.80*
PV9	*1:0:0*	*1.79*	*455*	*1.79*	*455*	*2.8*	*11.6*	*1.12*
PV10	*1:0:0*	*1.79*	*276*	*1.00*	*276*	*2.7*	*14.5*	*1.26*
PV11	*1:0:0*	*1.79*	*235*	*1.31*	*235*	*2.6*	*15.6*	*1.30*
PV12	*1:0:0*	*1.79*	*469*	*0.45*	*269*	*2.5*	*16.0*	*1.32*
PV16	*1:0:0*	*0.74*	*255*	*0.74*	*255*	*2.0*	*21.7*	*1.54*
PV18	*1:0:0*	*1.79*	*431*	*0.32*	*412*	*2.2*	*19.5*	*1.46*
PV19	*1:0:0*	*1.79*	*458*	*0.71*	*299*	*2.2*	*19.0*	*1.44*
PV20	*1:0:0*	*1.79*	*460*	*0.89*	*297*	*1.8*	*19.6*	*1.46*
PV21	*1:0:0*	*1.79*	*458*	*1.30*	*302*	*1.8*	*19.5*	*1.46*
PV22	*1:0:0*	*1.79*	*458*	*1.52*	*420*	*2.0*	*19.6*	*1.46*
PV23	*1:-0.39:-0.39*	*1.79*	*518*	*1.79*	*518*	*2.0*	*20.5*	*1.49*
PV25	*1:-0.69:-0.69*	*1.79*	*466*	*1.79*	*466*	*1.8*	*19.2*	*1.45*
PV26	*1:0:0*	*1.79*	*456*	*1.01*	*463*	*1.9*	*21.3*	*1.52*
PV27	*1:0:0*	*1.79*	*442*	*1.79*	*442*	*1.9*	*20.5*	*1.49*
PV28	*1:0.32:0.32*	*1.79*	*483*	*1.79*	*483*	*1.9*	*19.0*	*1.44*

Tab.4.3 Material Properties of Toronto Test Series PV

Stevens et al (1991) developed a complete finite element program and implemented the MCFT in the material routine. They omitted the check of the reinforcement stresses in the cracks but extended the constitutive laws to include both confinement of concrete under compression and a more complicated relationship for strain softening of concrete

under tension. In addition, a factor was introduced to account for loss of bond and the *stress/strain* relation of the reinforcing steel was fitted with a work hardening rule.

In contrast, the material laws of the UMAT remained nearly the same as those initially derived by Vecchio/Collins from the Toronto PV tests. A check of steel stresses in the cracks was also omitted as it was earlier argued that the increase of steel stresses in cracks is due to debonding rather than aggregate interlock. Hence, only the inclusion of a proper bond slip model would enable the program to carry out such a steel check. Moreover, it is the advantage of the MCFT that secondary shear carrying actions such as aggregate interlock and dowel action are an intrinsic feature of the theory. This is because of the shear stiffness term $E'^{c}_{33}=0.5(\sigma_{c1}-\sigma_{c2})/(\varepsilon_1-\varepsilon_2)$ which delivers in an integration point, for each stress and strain state, a certain amount of shear stiffness, even if the element is cracked. Therefore, no aggregate interlock, dowel action or bond slip has to be modelled explicitly.

Panel	*Ultimate Shear Stress* τ_u *[MPa]*				*Ratio* $\tau_{u\,test} / \tau_{u\,cal}$		
	Test	*ABAQUS*		*Stevens et al*	*ABAQUS*		*Stevens et al*
		UMAT	*Standard*		*UMAT*	*Standard*	
PV2	*1.16*	*1.33*	*2.24*	-	*0.88*	*0.52*	-
PV3	*3.07*	*3.17*	*2.57*	*3.38*	*0.97*	*1.19*	*0.91*
PV4	*2.89*	*2.98*	*2.59*	*3.12*	*0.97*	*1.12*	*0.93*
PV6	*4.55*	*4.75*	*3.13*	*5.30*	*0.96*	*1.45*	*0.86*
PV9	*3.74*	*4.47*	*5.16*	*4.47*	*0.84*	*0.72*	*0.84*
PV10	*3.97*	*3.69*	*2.46*	*3.97*	*1.08*	*1.61*	*1.00*
PV11	*3.56*	*3.60*	*2.36*	*3.96*	*0.99*	*1.51*	*0.90*
PV12	*3.13*	*2.50*	*2.98*	*2.79*	*1.25*	*1.05*	*1.12*
PV16	*2.14*	*2.35*	*2.46*	*2.27*	*0.91*	*0.87*	*0.94*
PV18	*3.04*	*2.77*	*2.88*	*3.07*	*1.10*	*1.06*	*0.99*
PV19	*3.95*	*3.67*	*3.29*	*3.87*	*1.08*	*1.20*	*1.02*
PV20	*4.26*	*4.00*	*3.49*	*4.25*	*1.06*	*1.22*	*1.00*
PV21	*5.03*	*5.06*	*3.90*	*5.16*	*0.99*	*1.29*	*0.97*
PV22	*6.07*	*6.57*	*4.67*	*6.16*	*0.92*	*1.30*	*0.99*
PV23	*8.87*	*7.55*	*9.71*	*7.37*	*1.17*	*0.91*	*1.20*
PV25	*9.12*	*8.27*	*9.61*	*7.98*	*1.10*	*0.95*	*1.14*
PV26	*5.41*	*5.80*	*4.14*	*5.37*	*0.93*	*1.31*	*1.01*
PV27	*6.35*	*6.55*	*5.09*	*6.43*	*0.97*	*1.25*	*0.99*
PV28	*5.8*	*5.91*	*4.17*	*5.59*	*0.98*	*1.39*	*1.04*

Tab.4.4 Results of Recalculation of Toronto Test Series PV

For the recalculation of the Toronto shear tests neither confinement of concrete nor strain hardening of reinforcing steel was added to the material laws as it was obvious from the test concept that both features would not have affected the results of the recalculation of the RC panels at all. Hence, the constitutive model of the MCFT was used in the form specified in Fig.4.18. However, it is worth mentioning that for investigations on ductility, concrete confinement plays a major role and, therefore, its beneficial effect on the rotational capacity of plastic hinges is accounted for in all calculations reported in Chapter 5.

The results of the calculations of the panel tests show that in terms of ultimate shear stress acceptable agreement with the test results could be achieved. Some values of Stevens et al (1991) are slightly better while most others are worse or virtually the same. Where distinct differences in calculated and measured values are encountered, both programs either over or underestimated the measured values simultaneously. This demonstrates that the differences between analysis and testing are due to the assumptions of the MCFT. Both programs tend to overrate the shear resistance of panels reinforced with little or mild steel, while the shear resistance of panels loaded in shear and compression is noticeably underestimated. An explanation for this behaviour was given in Section 4.2, where a minor modification of the constitutive model was justified.

Figs.4.20 through to 4.22 show the shear response of all recalculated panels. In some of the graphs the response calculated by other researchers is also depicted. In addition, where the reinforcement ratio in x direction differs from that in y direction, the θ_c/τ_{xy} relationship is given in a graph as well. It can be seen that the calculated response of the various panels captures the post-peak behaviour quite well. Stevens et al (1991) give the mean value of the ratio $\tau_{u\,test}/\tau_{u\,cal}$ and the coefficient of variation in their table. However, the mean value which is close to *1* is a rather meaningless quantity since the reason for the major deviations is known. As already mentioned, programs which are based on the MCFT, such as the UMAT or the FE code of Stevens et al (1991), obviously tend to overestimate the shear resistance in cases where panels are slightly reinforced, while underpredicting the shear resistance where high compression forces are applied together with shear. If the test series consisted exclusively of underreinforced panels subjected to pure shear, then the mean value would be far below *1*, and a mean value much higher than *1* would be obtained if the test series only consisted of panels under combined compression and shear. Here, therefore, the specification of a mean value was omitted.

Panel PV2

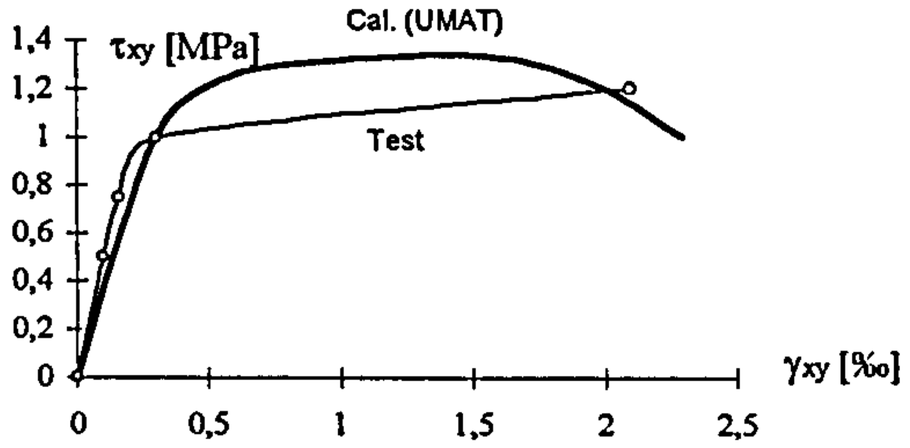

Panel PV3

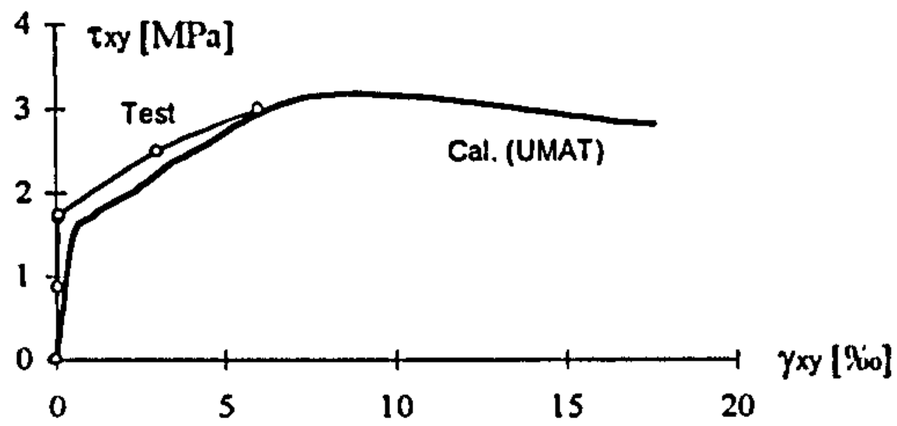

Panel PV4

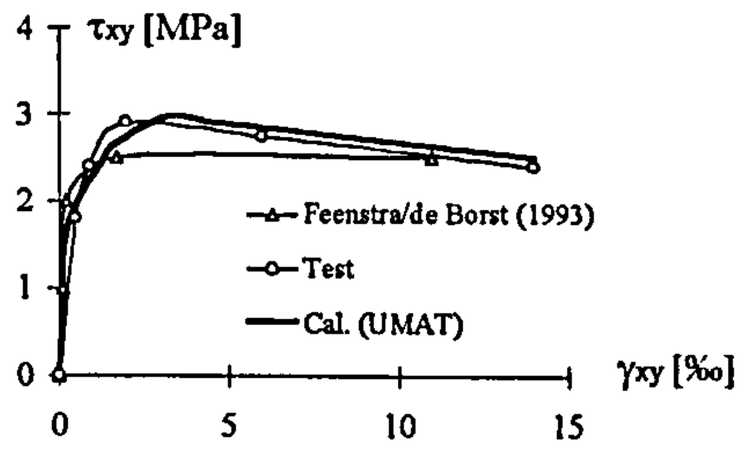

Panel PV6

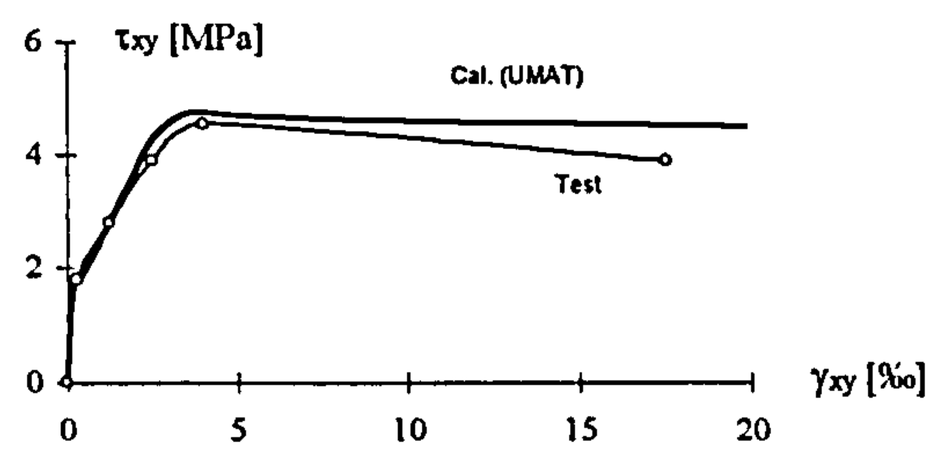

Panel PV9

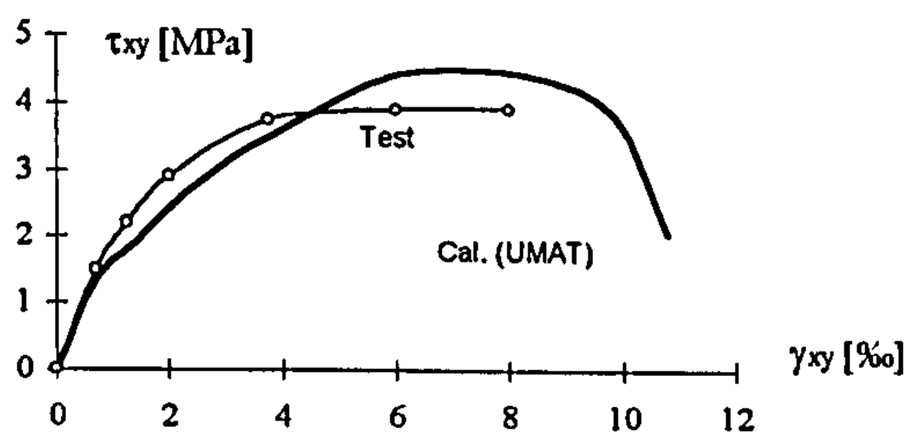

Panel PV16

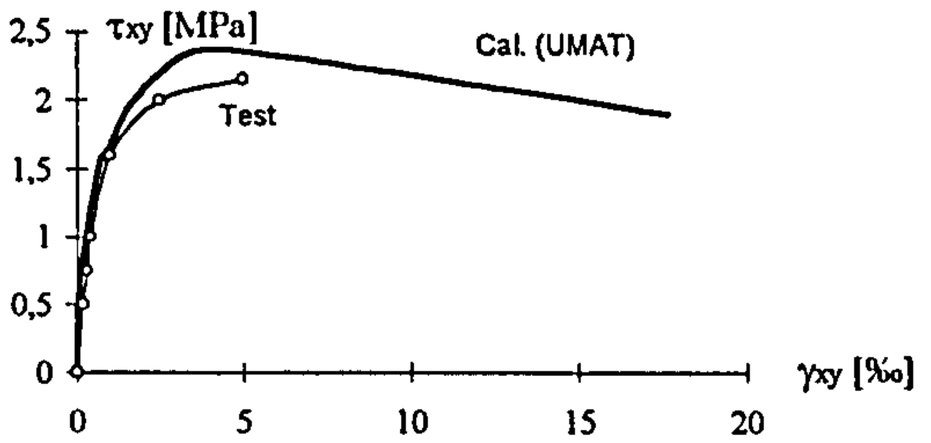

Panel PV10

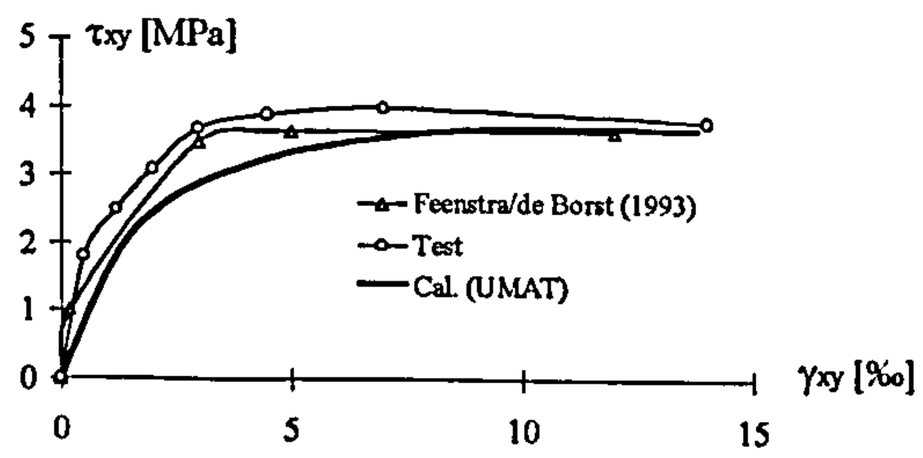

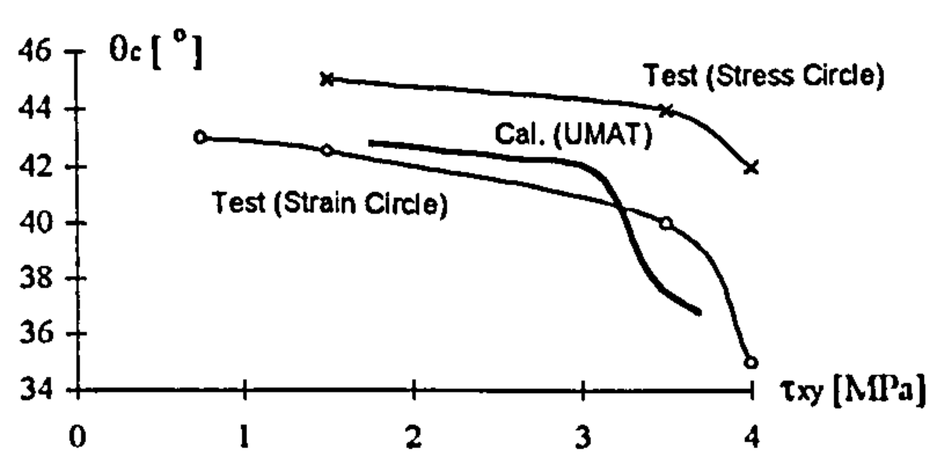

Panel PV11

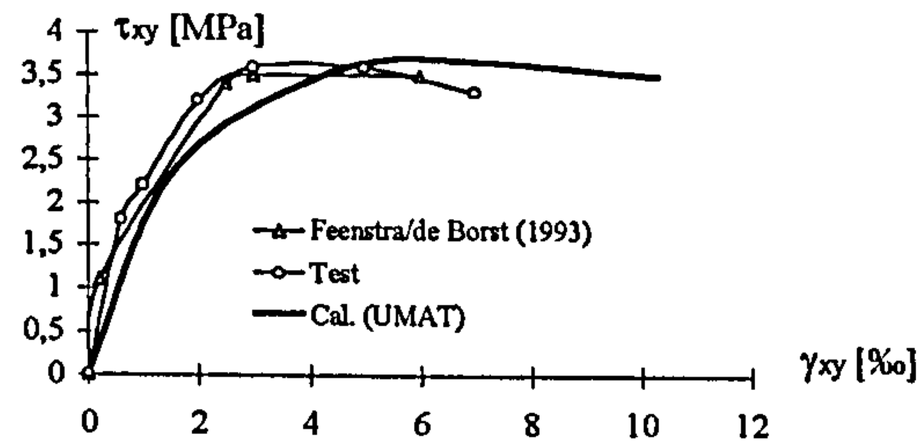

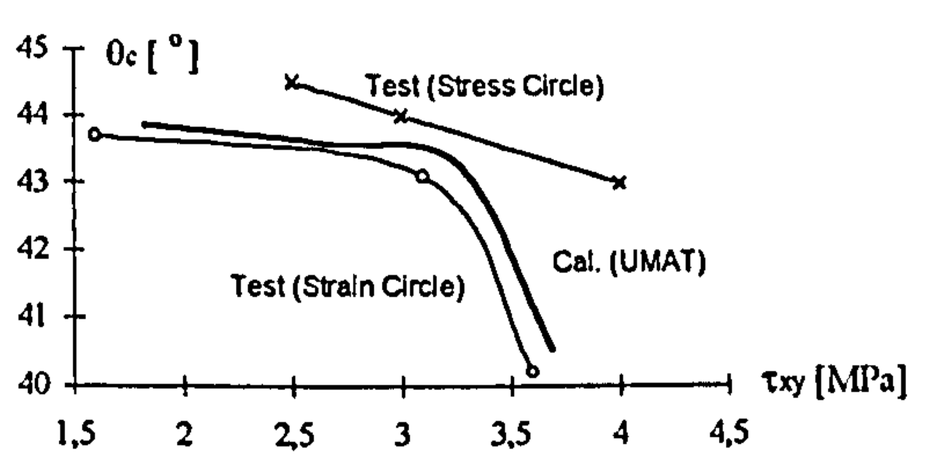

Fig.4.20 τ_{xy} / γ_{xy} Relationship for Panels PV2 ÷ PV4, PV6, PV9 and PV16
τ_{xy} / γ_{xy} and θ_c / τ_{xy} Relationship for Panels PV10 and PV11

Panel PV12

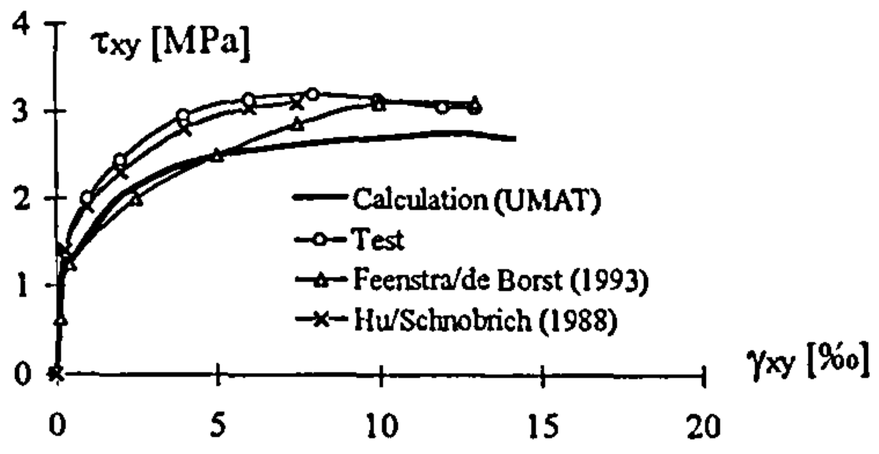

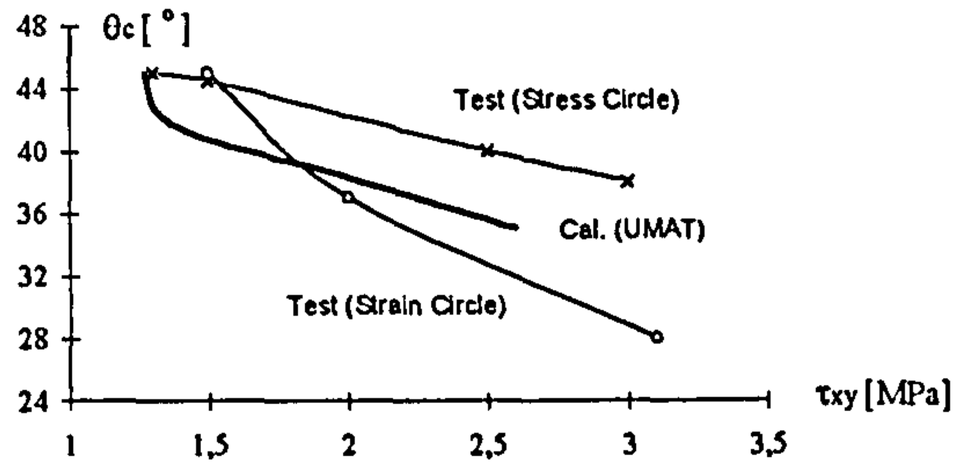

Panel PV18

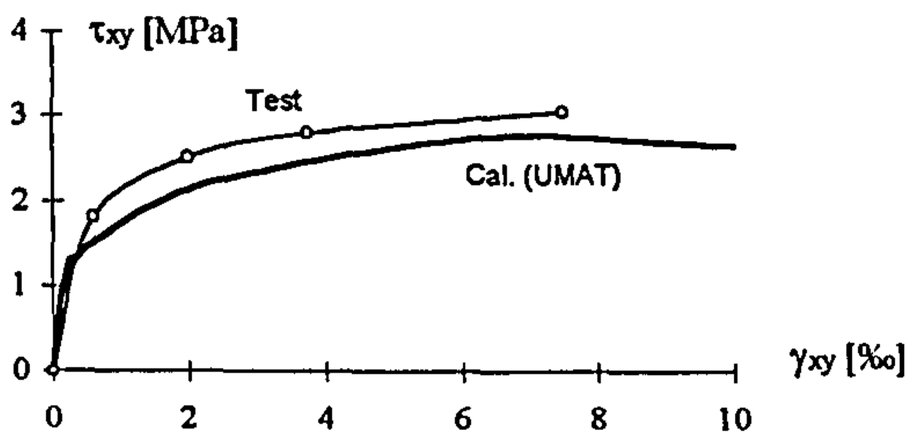

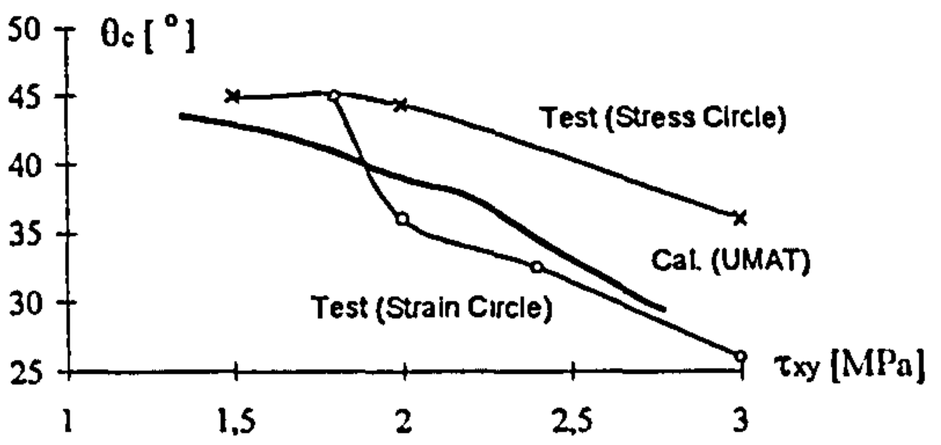

Panel PV19

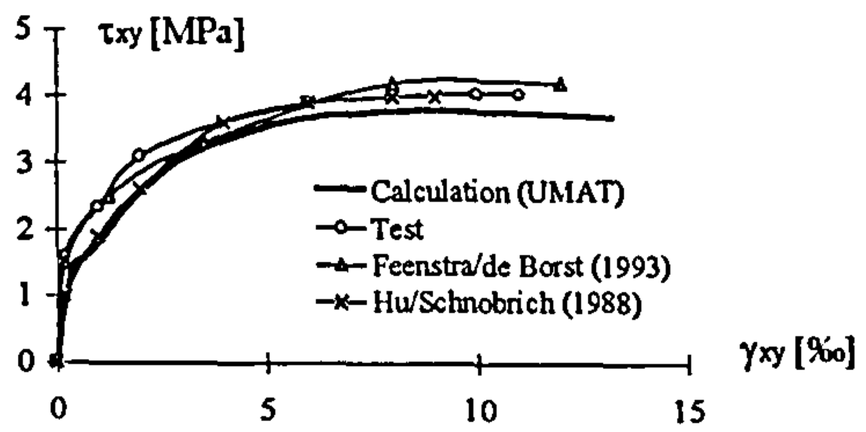

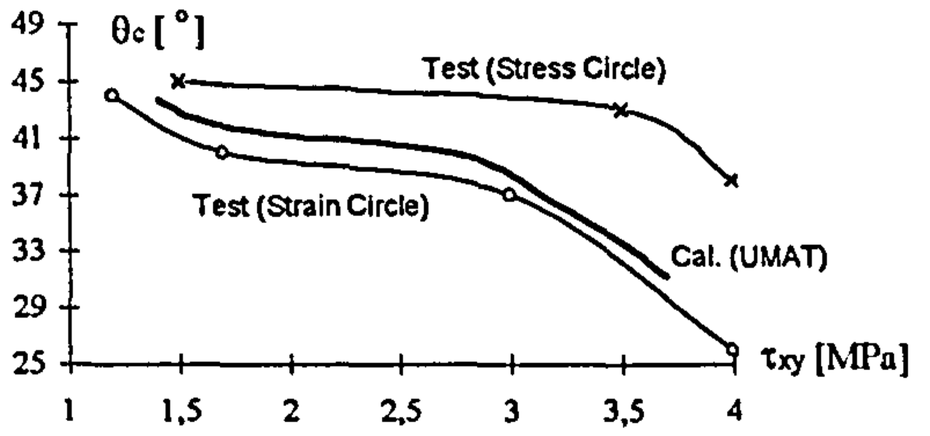

Panel PV20

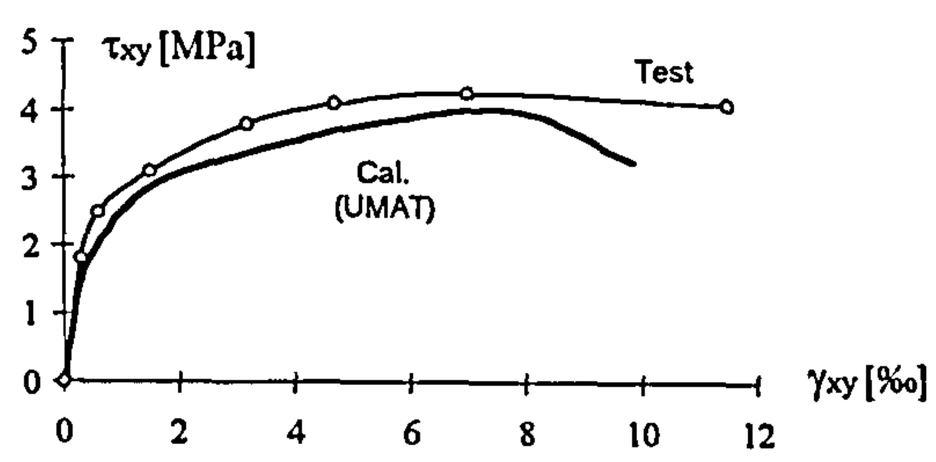

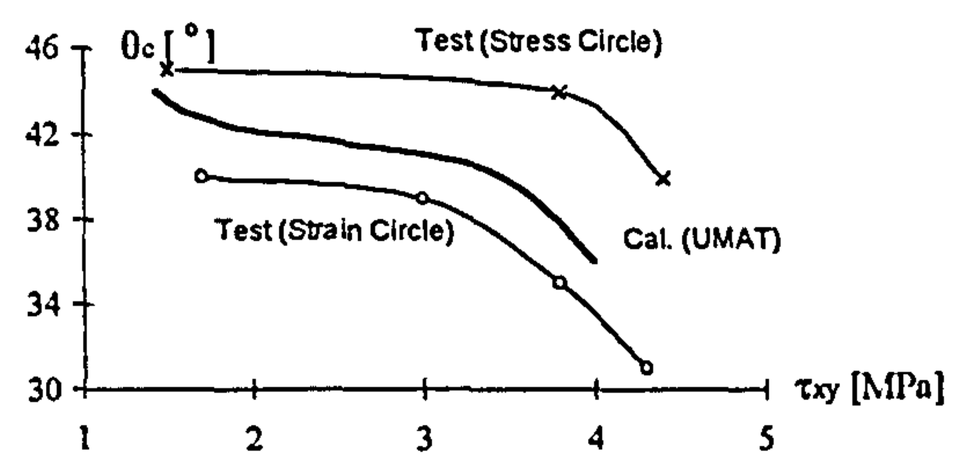

Panel PV21

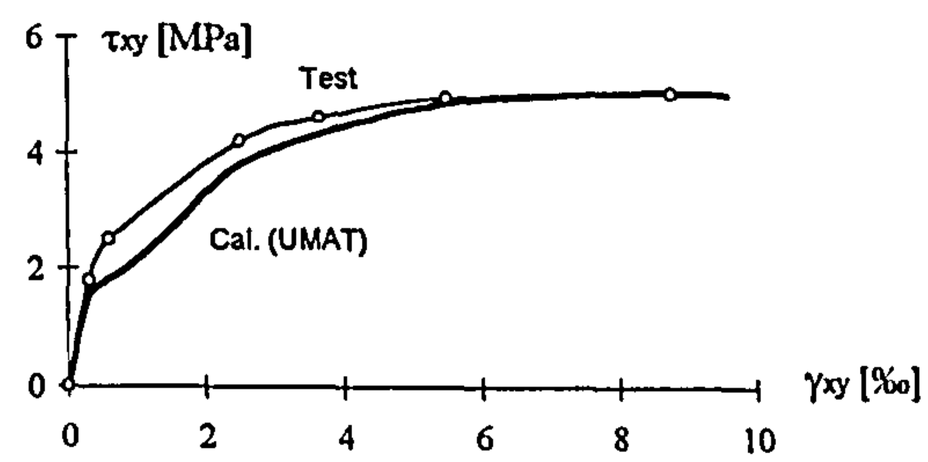

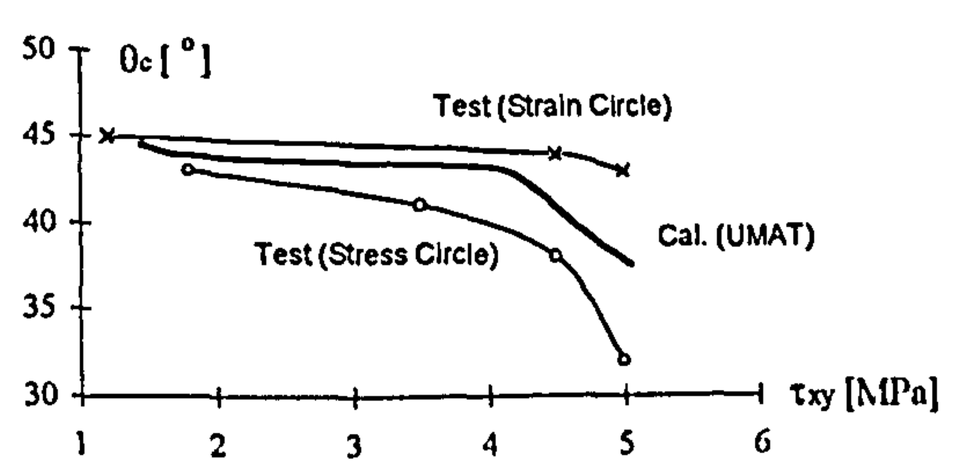

Fig.4.21 τ_{xy} / γ_{xy} and θ_c / τ_{xy} Relationship for Panels PV12 and PV18 ÷ PV21

Panel PV22

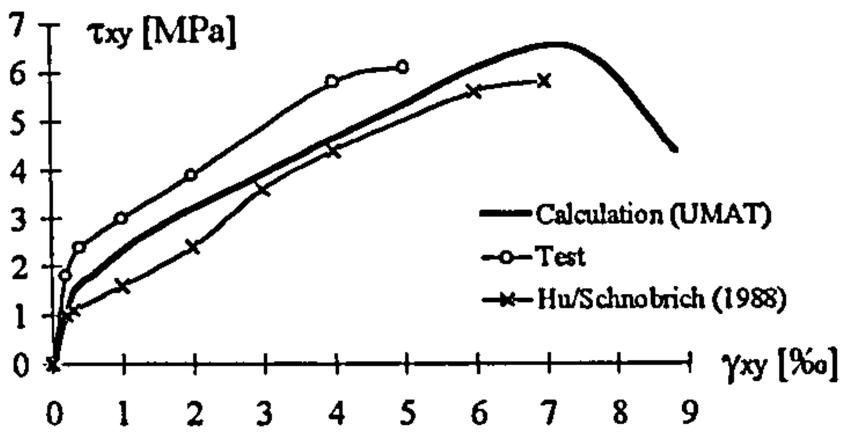

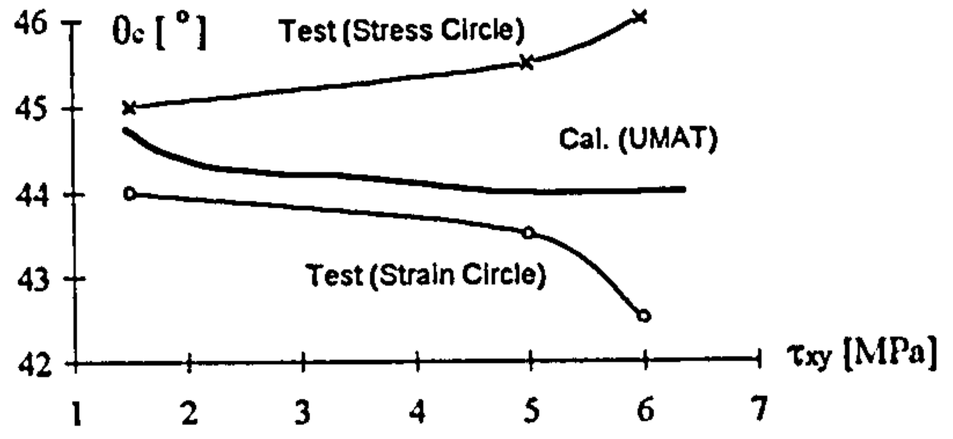

Panel PV26

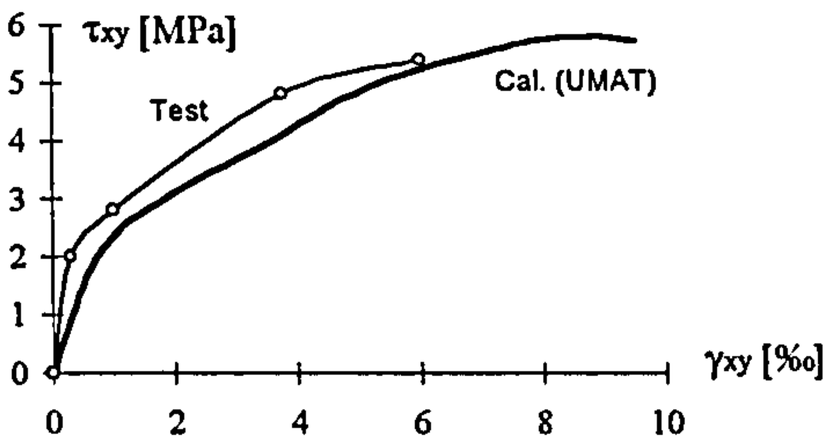

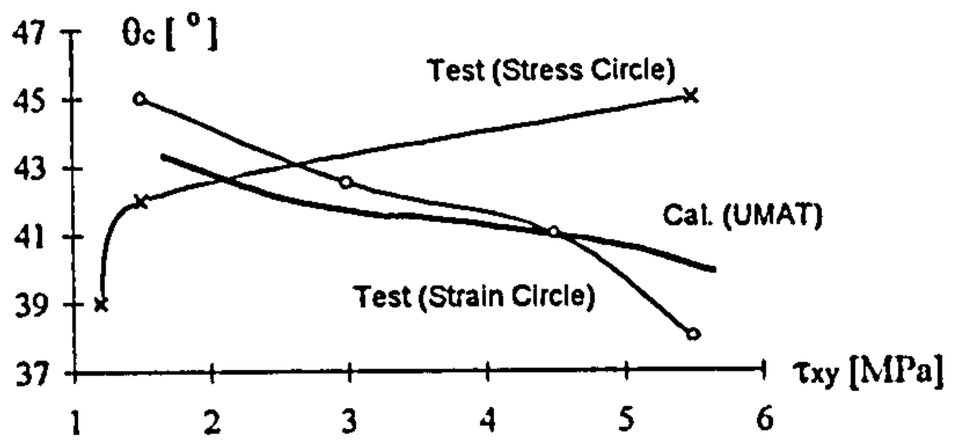

Panel PV23

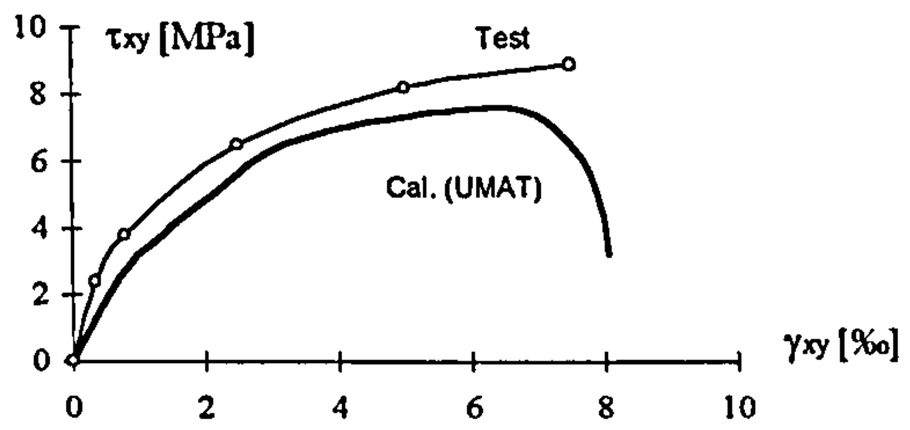

Panel PV25

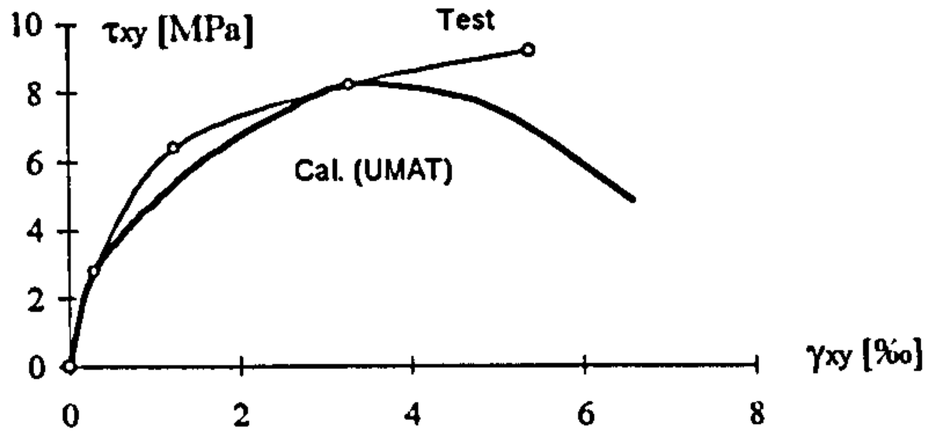

Panel PV27

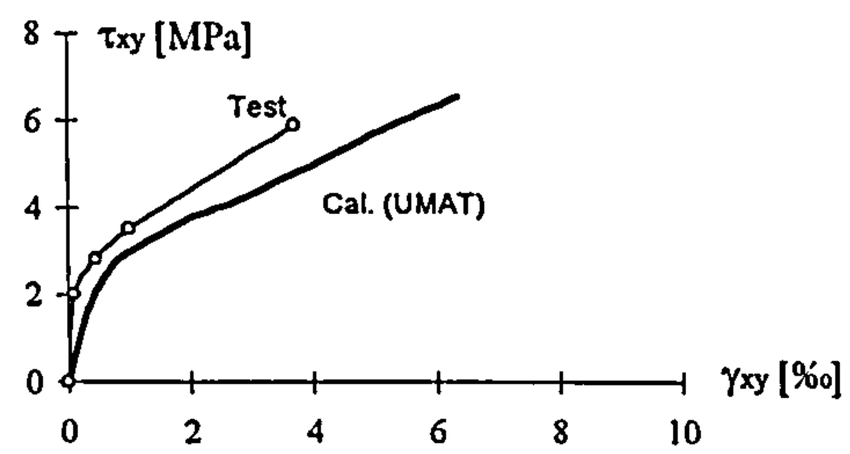

Panel PV28

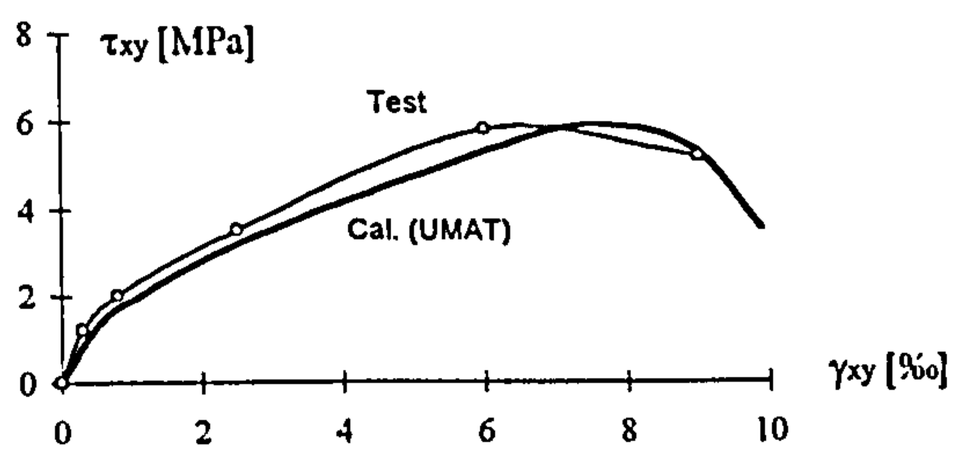

Fig.4.22 τ_{xy} / γ_{xy} Relationship for Panels PV23, PV25, PV27 and PV28
τ_{xy} / γ_{xy} and θ_c / τ_{xy} Relationship for Panels PV22 and PV26

4.3.2 The Toronto PB Series

In addition to the PV series of Vecchio/Collins (1982), a second test series was conducted by Bhide / Collins (1987). The specimens were longitudinally reinforced and loaded in combined uniaxial tension and shear. The test set-up and FE model were the same as for the PV series and are depicted in Fig.4.19. Stevens et al (1991) recalculated a selection of the PB tests and, hence, these panels were also analysed using ABAQUS together with the UMAT. Tab.4.5 shows load conditions, material properties and the calculated shear capacity in comparison with the test results and the predictions of Stevens et al (1991).

Panel	*Load Ratio* $\tau_{xy}/\sigma_x/\sigma_y$	*Longit. Steel* ρ_x [%]	f_y [MPa]	*Concrete* ε'_c [‰]	f_c [MPa]	f_{ct} [MPa]	*Ultimate Shear Stress* τ_u [MPa] Test	UMAT	Stev.	*Ratio* $\tau_{u\,test}/\tau_{u\,cal}$ UMAT	Stev.
PB4	*1:0.96:0*	*1.085*	*423*	*1.9*	*16.4*	*1.33*	*1.16*	*1.07*	*0.88*	*1.08*	*1.32*
PB5	*1:0.97:-1.03*	*1.085*	*415*	*1.8*	*23.5*	*1.60*	*2.64*	*2.93*	*2.43*	*0.90*	*1.09*
PB6	*1:1:0*	*1.085*	*425*	*1.9*	*17.6*	*1.38*	*1.15*	*1.09*	*0.90*	*1.05*	*1.29*
PB7	*1:1.89:0*	*1.085*	*425*	*2.2*	*20.2*	*1.48*	*0.86*	*1.01*	*0.72*	*0.85*	*1.19*
PB8	*1:2.98:0*	*1.085*	*425*	*2.0*	*20.4*	*1.48*	*0.79*	*0.89*	*0.59*	*0.89*	*1.35*
PB10	*1:5.94:0*	*1.085*	*433*	*1.9*	*24.0*	*1.62*	*0.56*	*0.73*	*0.55*	*0.77*	*1.02*
PB12	*1:0:0*	*1.085*	*433*	*1.5*	*23.1*	*1.59*	*1.53*	*1.53*	*1.59*	*1.00*	*0.97*
PB14	*1:3.01:0*	*1.085*	*489*	*2.8*	*41.1*	*2.12*	*1.54*	*1.40*	*1.43*	*1.10*	*1.08*
PB15	*1:0:0*	*2.023*	*485*	*3.2*	*38.4*	*2.04*	*1.96*	*2.00*	*2.05*	*0.98*	*0.98*
PB16	*1:1.96:0*	*2.023*	*502*	*3.2*	*41.7*	*2.13*	*1.42*	*1.55*	*1.44*	*0.91*	*0.99*
PB17	*1:5.93:0*	*2.023*	*502*	*3.1*	*41.6*	*2.13*	*1.22*	*1.11*	*1.21*	*1.10*	*1.01*
PB18	*1:0:0*	*2.195*	*402*	*2.2*	*25.3*	*1.66*	*1.72*	*1.72*	*1.72*	*1.00*	*1.00*
PB19	*1:1.01:0*	*2.195*	*402*	*1.9*	*20.0*	*1.48*	*1.28*	*1.36*	*1.27*	*0.94*	*1.01*
PB20	*1:2.04:0*	*2.195*	*424*	*1.9*	*21.7*	*1.54*	*1.42*	*1.26*	*1.14*	*1.12*	*1.25*
PB21	*1:3.08:0*	*2.195*	*402*	*1.8*	*21.8*	*1.54*	*1.42*	*1.15*	*1.08*	*1.24*	*1.32*
PB22	*1:6.09:0*	*2.195*	*433*	*2.0*	*17.6*	*1.38*	*1.03*	*0.88*	*0.98*	*1.18*	*1.05*
PB28	*1:1.98:0*	*2.195*	*426*	*2.0*	*22.7*	*1.57*	*1.53*	*1.29*	*1.17*	*1.19*	*1.32*
PB29	*1:2.02:0*	*2.023*	*496*	*2.6*	*41.6*	*2.13*	*1.49*	*1.55*	*1.44*	*0.96*	*1.04*
PB30	*1:2.96:0*	*2.023*	*496*	*2.6*	*40.4*	*2.10*	*1.48*	*1.39*	*1.42*	*1.07*	*1.04*
PB31	*1:5.78:0*	*2.023*	*496*	*3.0*	*43.4*	*2.17*	*1.15*	*1.14*	*1.36*	*1.01*	*0.84*

Tab.4.5 Recalculation of Toronto Test Series PB (see Bhide/Collins 1987)

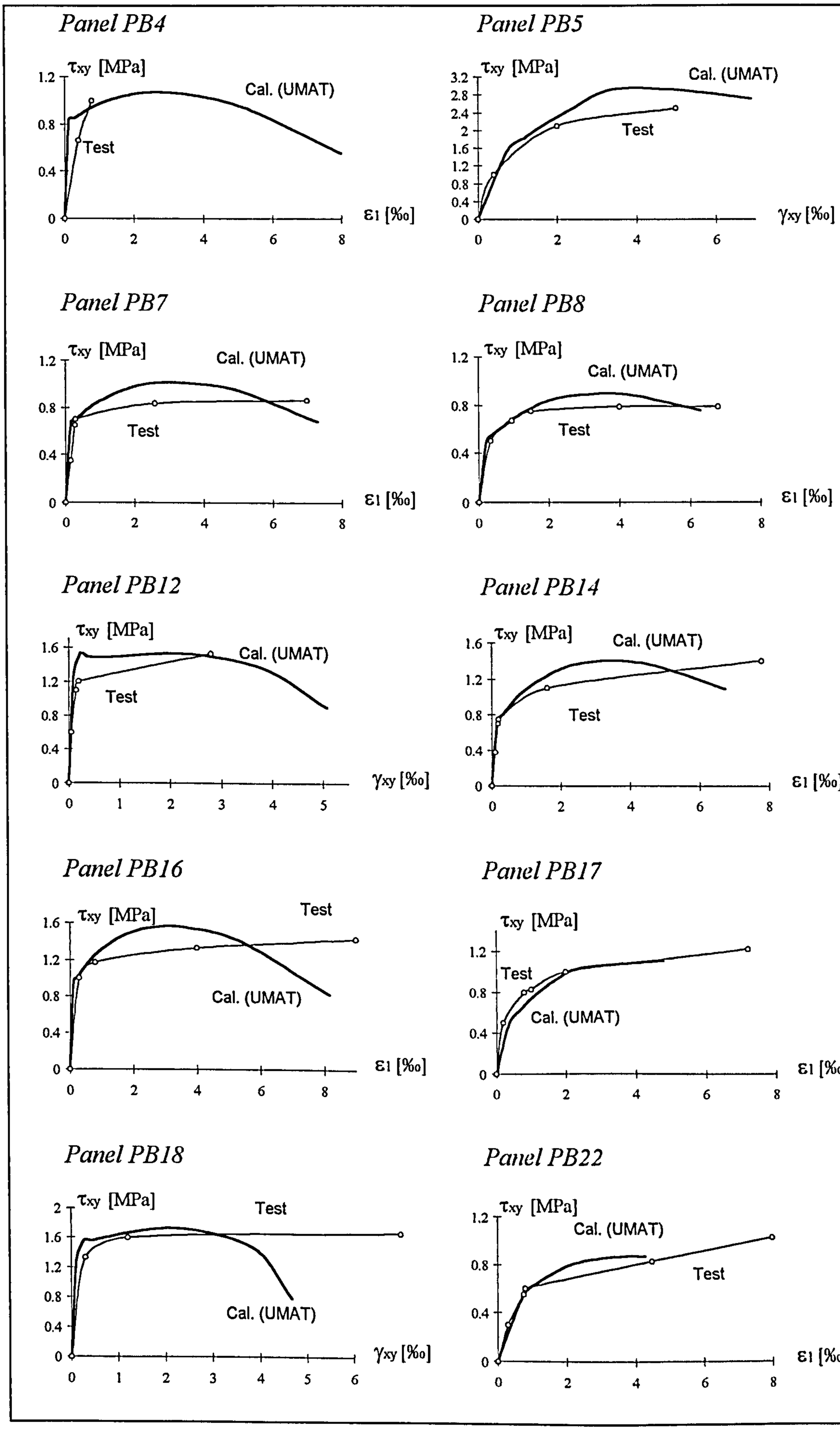

Fig.4.23 τ_{xy} / γ_{xy} Relationship for Panels PB5, PB12 and PB18
$\tau_{xy} / \varepsilon_1$ Relationship for Panels PB4, PB7, PB8, PB14, PB16, PB17 and PB22

It should be mentioned that the Toronto PB series of Bhide/Collins was not performed to calibrate the material laws of the MCFT as was the case with the PV series of Vecchio/ Collins. It is, therefore, not surprising that the results occasionally revealed differences from the test results, although the mean deviation for calculations with the UMAT was less than *2%*. This shows that the UMAT delivered distinctly better predictions than the FE analyses of Stevens et al (1991). The ABAQUS Standard concrete options could not recalculate the tests in a satisfactory fashion and, hence, no results were given in Tab.4.5. For some of the panels the *shear stress / normal strain* response is given in Fig.4.23. The comparison with the test values shows an acceptable agreement in all cases. As the literature does not report much on FE analyses conducted with the PB panels, no results from other researchers were added.

4.3.3 Comparison with ABAQUS Standard Options

For the purpose of comparison, the complete Toronto PV series has been recalculated with the ABAQUS Standard concrete options. ABAQUS provides a rather complicated model for cracked reinforced concrete which is essentially based on concrete plasticity. It was stated earlier in Section 4.1 that these material models are best suited for 3D solids as the plasticity theory is well established for triaxial stress conditions. On the tensile side of the concrete the material laws are described by the well-known orthotropic material matrix including the shear retention factor β to account for secondary shear carrying actions and a sectionally linear strain softening rule. Additionally, for concrete under biaxial stress conditions the failure curve of Kupfer/Gerstle (1973) was implemented.

ABAQUS allows for wide-ranging adjustment of the constitutive laws, but gives some reasonable recommendations as well. If nothing is specified on the input deck in the *SHEAR RETENTION option, then the default value for β is one which means that a full shear retention applies. If the *FAILURE RATIO option is omitted, then the default set up accounts for an increase in biaxial compression up to $1.16\, f_c$ and the cracking stress of concrete under tension is given by $0.09\, f_c$. The recommendation for tension stiffening is that the tensile stresses should drop to zero after a strain of ten times the cracking strain has occurred.

a) General Form of Material Laws

Concrete under Uniaxial Stress Conditions:

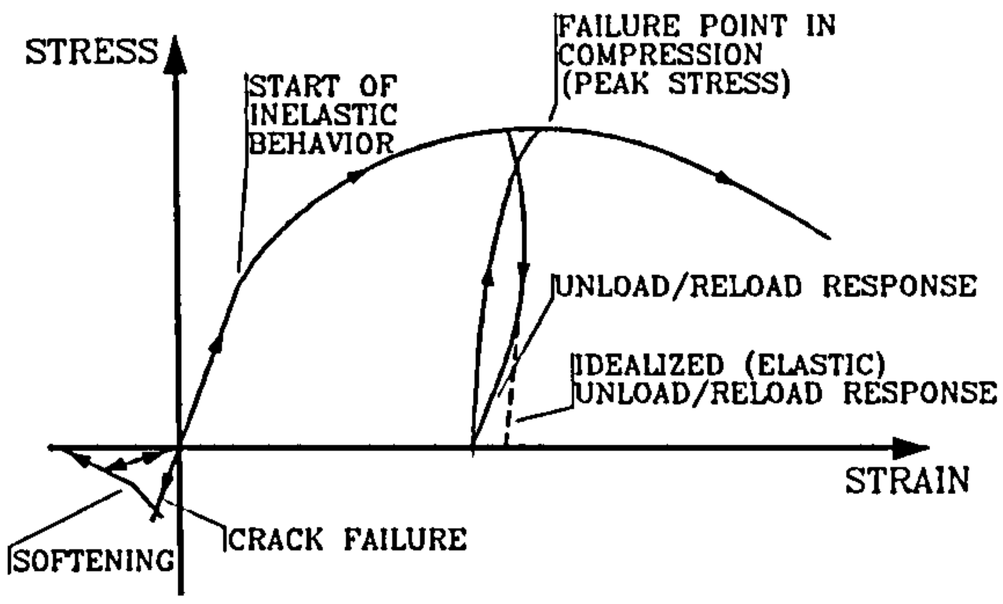

Concrete under Biaxial Stress Conditions:

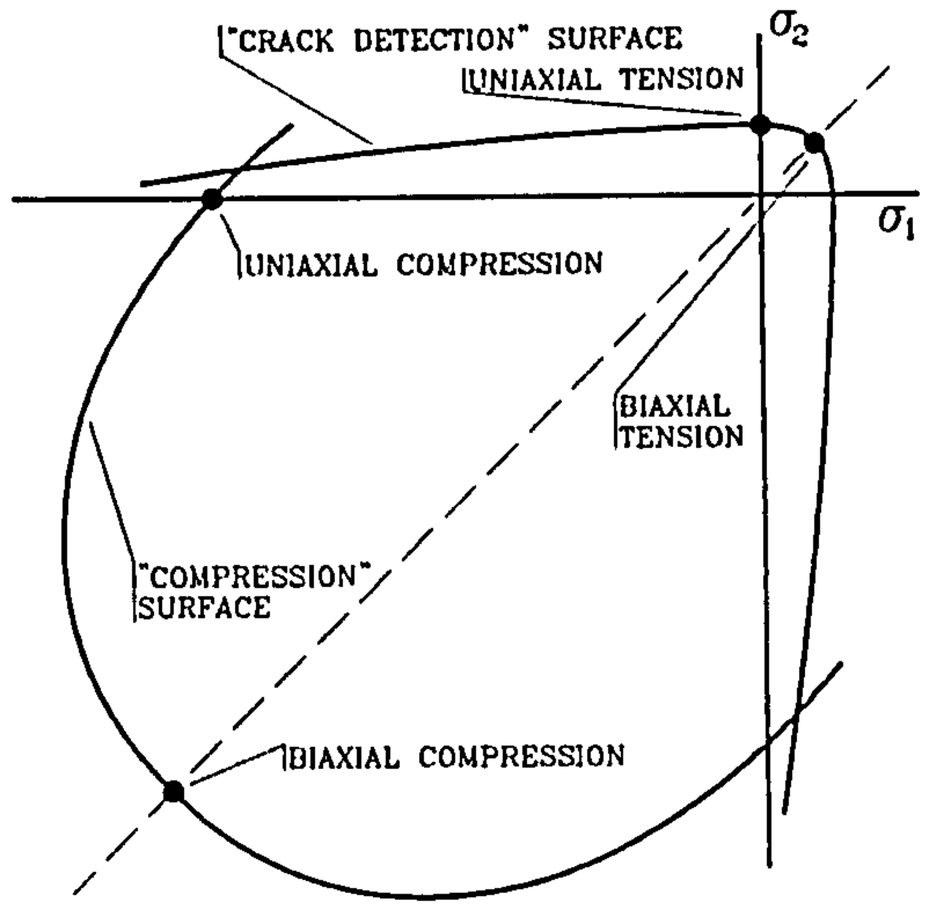

b) Adopted Material Model

Concrete in Uniaxial Compression:

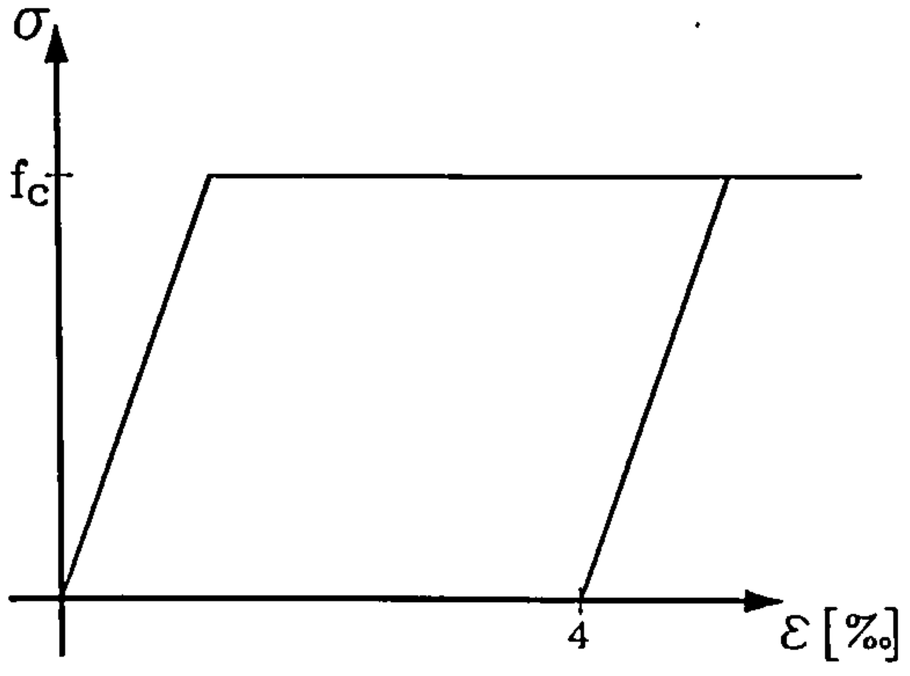

Tension Stiffening:

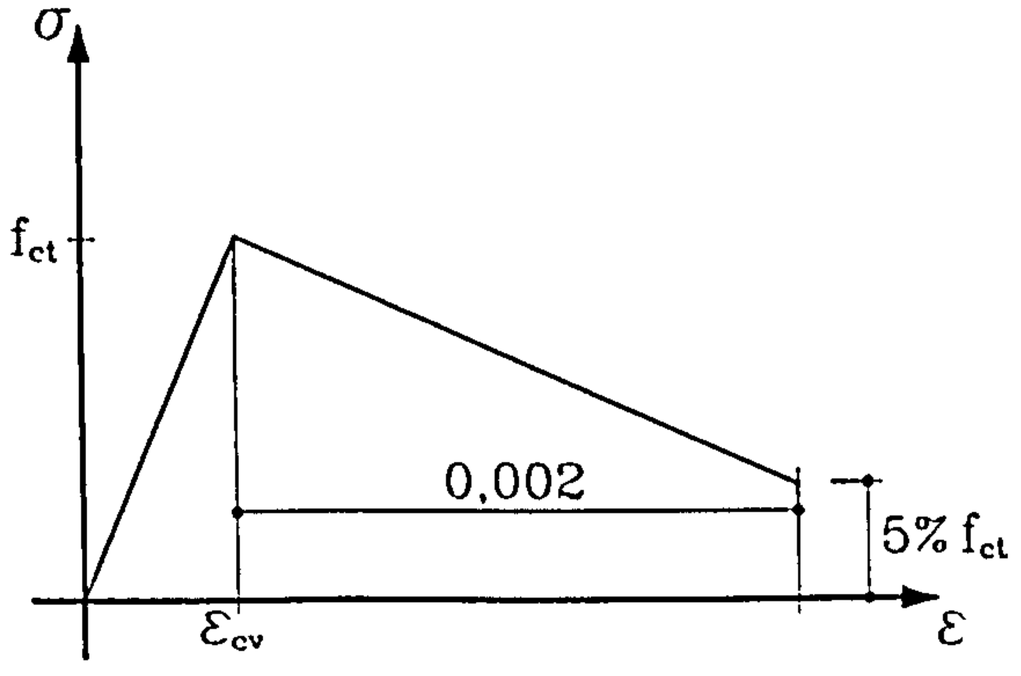

Fig.4.24 Material Set-up of the ABAQUS Standard Options for the PV Series

The default values for the shear retention factor, the failure ratios and the recommendations for tension stiffening have been retained for all calculations on the PV panels. In addition, a simple *stress/strain* relationship for concrete in compression was adopted. The material laws for concrete in uniaxial compression and for tension stiffening are depicted in Fig.4.24.(b). It should be mentioned that the results obtained from the default values are on the safe side. A shear retention factor $\beta = 1$ means that in terms of shear no cracking is assumed. A tensile strength of *9%* of the compressive strength is a value which is in all cases higher than the $0.33\sqrt{f_c}$ taken for the calculations with the UMAT. In addition, the amount of strain softening can be considered appreciable.

The *stress/strain* relationship of concrete in compression is conservative against the parabola of the MCFT and a softening in compression is not specified in the constitutive model. With these material properties it should be expected that the calculated response reveals the real behaviour of the specimens. However, it can be seen from the results in Tab.4.4 that the ultimate resistance was seldom predicted in a satisfying fashion. The less sophisticated model of the UMAT reveals a much better performance in analysing the panel tests.

4.4 Recalculation of Leonhardt's Shear Tests with UMAT

The MCFT was conceived by Vecchio/Collins as a shear theory which assumes a uniform stress and strain state in a particular area of a structural member. The panels of the PV test series were deliberately loaded in a way which ensured such uniform conditions. Hence, the theory could be directly applied on the recalculation of the specimens (see Vecchio/Collins, 1982). However, when stress and strain conditions change from point to point, as it is the case in an RC beam subjected to flexure with shear, then a structure must be modelled of small elements where the stress and strain state can be considered to be more or less uniform. On the edges of these elements conditions of equilibrium and compatibility must be satisfied. The layered model of Vecchio/Collins (1988) was based on this principle and fitted for the analysis of reinforced concrete beams. It is obvious that the most natural way to cope with such an approach to structural analysis is the finite element method and from that point of view it seems to be quite normal to use the MCFT in an FE package not only for the calculation of shear elements but also for investigations on RC beams.

In the past various types of finite elements have been developed according to the particular purpose they should serve. For flexural members, in particular, one dimensional elements are commonly in use which are, in general, more conveniently applied than 2 or 3-D solids. The reason for this is that they are much easier to handle with far less time needed on discretisation and data input. Usually, these structural elements provide generalised section properties such as moments, shear forces or curvatures which are more simply dealt with than stresses and strains. However, the disadvantage of these elements is the poor performance concerning their shear behaviour. As a goal of this work is to clarify the effect of shear deflections on the ductility of RC members under bending and shear it is evident that a solid element based on a proper shear theory is more suitable for these investigations than the above mentioned beam elements. It should be noted that it is not intended to replace structural beam elements by plane stress solids which are comparatively difficult to handle. For everyday design work, structural beam elements are more convenient than solids. Therefore, the UMAT should mainly serve as a tool for research on shear and is here only applied on beams to carry out investigations on the shear performance of RC members.

Beam	*ET1*	*ET2*	*ET3*	*ET4*	*T1*	*E4*	*E5-1*	*E6*	*5*	*7-1*
$P_{u\,test}$ [kN]	*280*	*263*	*255*	*198*	*1600*	*375*	*378*	*186*	*137*	*118*
$P_{u\,cal}$ [kN]	*288*	*245*	*248*	*188*	*1566*	*345*	*345*	*190*	*138*	*103*
$P_{u\,test}/P_{u\,cal}$	*0.97*	*1.07*	*1.03*	*1.05*	*1.02*	*1.08*	*1.09*	*0.98*	*0.99*	*1.14*
*Failure Mode**	*B*	*S1*	*S2*	*S3*	*S3*	*B*	*B*	*S4*	*S4*	*S4*

* B=Bending, S1=Shear (bending), S2=Shear (stirrup yielding), S3=Shear (diagonal compression), S4=Shear(diagonal tension)

Tab.4.6 Recalculation of Leonhardt's Beams with UMAT

In Section 3.7 a selection of Leonhardt's shear tests was recalculated with program LAYER and the constitutive model of the MCFT was applied in the slightly adjusted form of Fig.4.18. It was stated there and confirmed in the previous section that programs based on the MCFT tend to overestimate the resistance of structural members with little or no reinforcement. Therefore, the changes in the material laws specified in Section 4.2 are applied here as well.

Tab.4.6 gives results of analyses carried out on some of the shear tests of Leonhardt/ Walther (1964). Most of the arbitrarily chosen samples have also been recalculated with program LAYER (see Tabs.3.3 and 3.4) and the material properties are given there. It can be seen from the results that the UMAT predicts the section resistance in a satisfactory fashion.

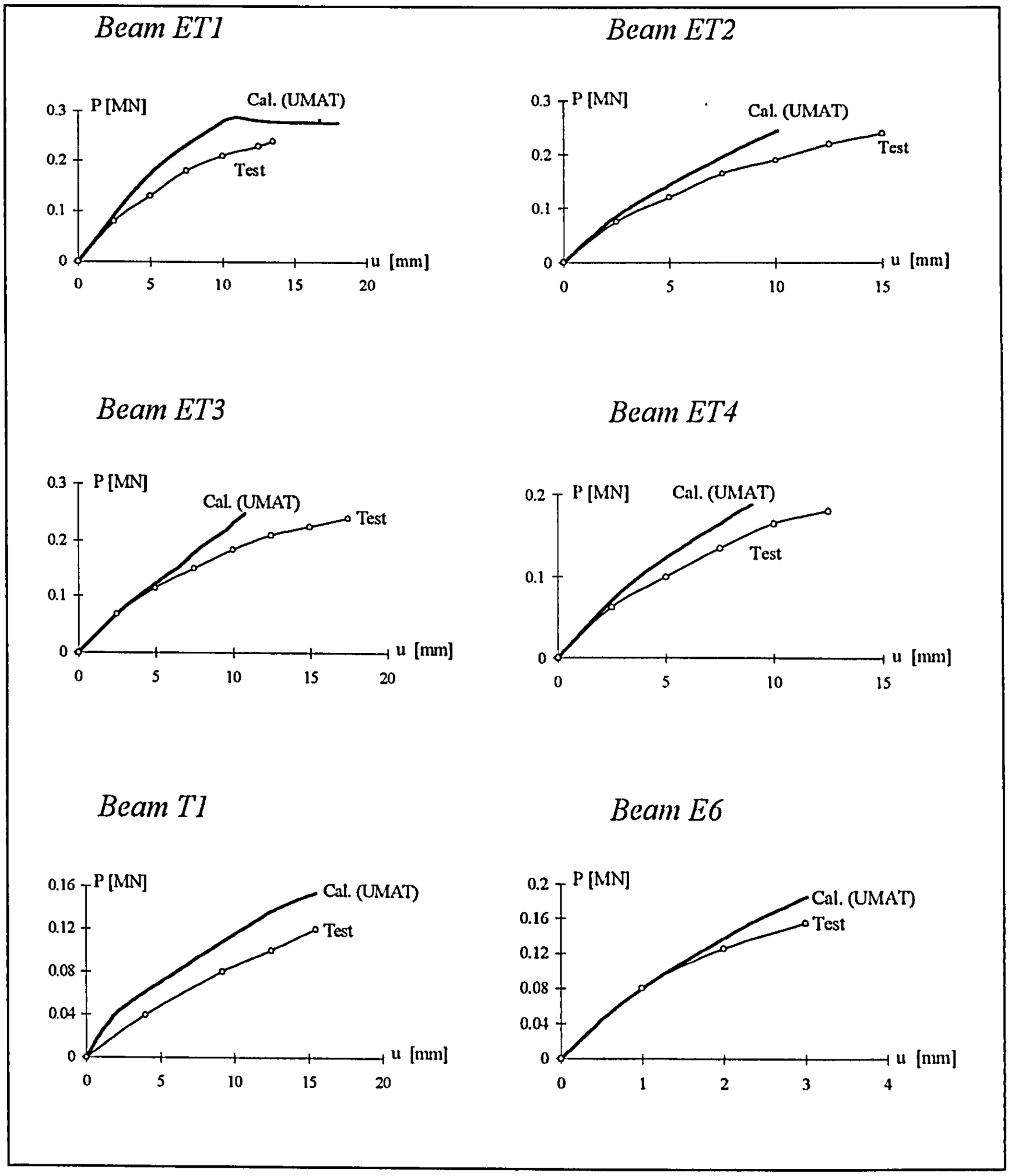

Fig.4.25 Load / Deflection Relationship for Beams ET1-4, T1, E6 (see Leonhardt/ Walther, 1964)

Fig.4.25 shows the *load/deflection* response of the recalculated specimens. The curves reveal that the model always behaves somewhat too stiff. This is visualised in the graphs by the fact that the calculated deflections are in general smaller than the measured ones. Tab.4.6 includes the recalculation of three beams without shear reinforcement. These beams failed in diagonal tension after the development of a distinct shear crack which propagated from the support towards the load. It is obvious that this local failure cannot be properly simulated with a theory which treats cracked reinforced concrete as a continuous material in which the notion of stresses and strains applies. One should, therefore, not expect too much of an analysis of a transversely unreinforced RC beam using an FE program the material subroutine of which is based on the MCFT.

A finite element code for calculations with partly unreinforced RC members should at least incorporate features like aggregate interlock, dowel action and bond slip in an explicit manner. However, the really correct approach would be a discrete concept for modelling structures with such distinct failures. With the recalculation of the specimens without stirrups, it was only intended to show that the introduction of f_{ct} provides enough strength, virtually as a new smeared truss member (see Fig.3.3), to maintain a stable force carrying mechanism in an RC beam, even in the absence of transverse reinforcement.

Fig.3.10 (see Page 52) depicts stress and strain distributions of various beams under failure conditions. The cross sections to which the graphs apply are those situated exactly under the load. As no attention was paid to the phenomenon known as the St.Venant disturbances in the vicinity of concentrated loads (see Fig.2.3, Page 8), the given stress distributions are only correct provided the load is applied in a way which is equivalent to the τ_{xy} distribution shown in the graphs of Fig.3.10. However, the load and its reaction forces at the supports were applied in a concentrated fashion. This reveals that the layered approach of the MCFT cannot cope with St.Venant's disturbances and hence, the method will only yield correct stress and strain distributions at a distance from concentrated loads which is, in beams, approximately equal to the beam height. Moreover, the straight ε_x distribution in Fig.3.10 is input, since for program LAYER the plane section hypothesis of Bernoulli applies. It is clear that for cross sections under concentrated loads this assumption is not valid at all.

In contrast to program LAYER, the finite element method does not reveal such shortcomings as it is a more general approach to structural analysis which is not restricted by a plane section assumption. Therefore, under concentrated loads more realistic stress and strain distributions are obtained. Fig.4.26 shows the σ_{cx}, τ_{xy} and ε_x distribution of beam T1 at the ultimate limit in three different cross sections. It is obvious that the stress and strain distribution of cross section *2 - 2* corresponds with the shape of the graphs of Fig.3.10.(d), while conditions at the support and under the load are different.

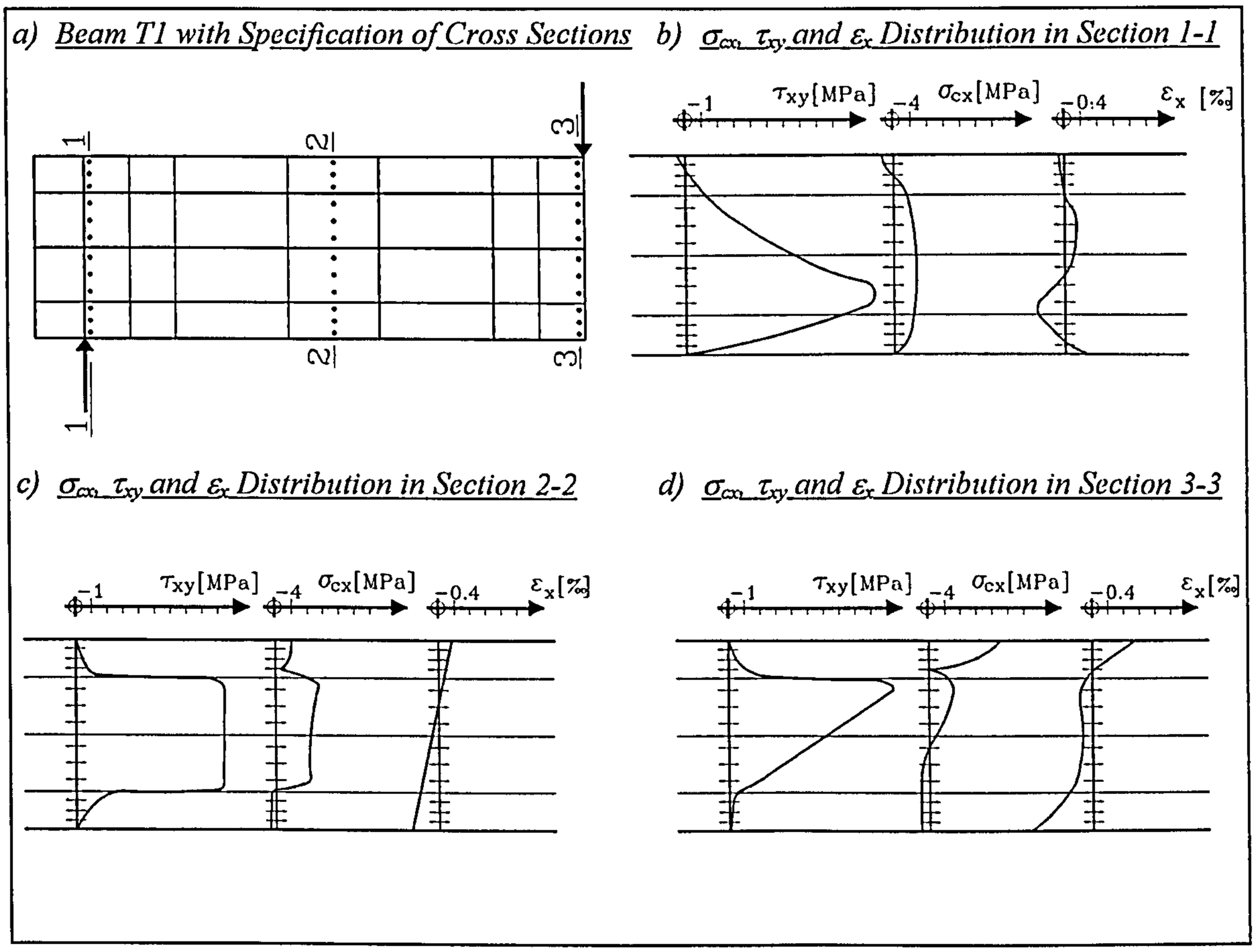

Fig.4.26 Stress and Strain Distribution in Various Cross Sections of Beam T1

An important observation is that under concentrated loads the shear distribution is shifted towards the point of application *A*. This is a feature necessary for the occurrence of strut and tie action. Fig.4.27 shows a half of Leonhardt's beam 3 in scale. This beam had a shear ratio of *2* and it is expected that an appreciable amount of load was carried by a strut and tie mechanism. Furthermore, it can be seen that the shear stresses τ_{xy} are concentrated in the vicinity of the loads, while in the shear span the stresses are high in mid-height. This coincides exactly with explanations on strut and tie action given in Section 3.9 and depicted in Fig.3.26.

For the occurrence of strut and tie action it is necessary that the centres of the shear stress distributions form a straight line from support to load. Once this line has a horizontal part as shown in Fig.4.27.(b), then no strut and tie action will occur and stirrups are necessary for the deviation of the compression struts at the top and bottom of the beam.

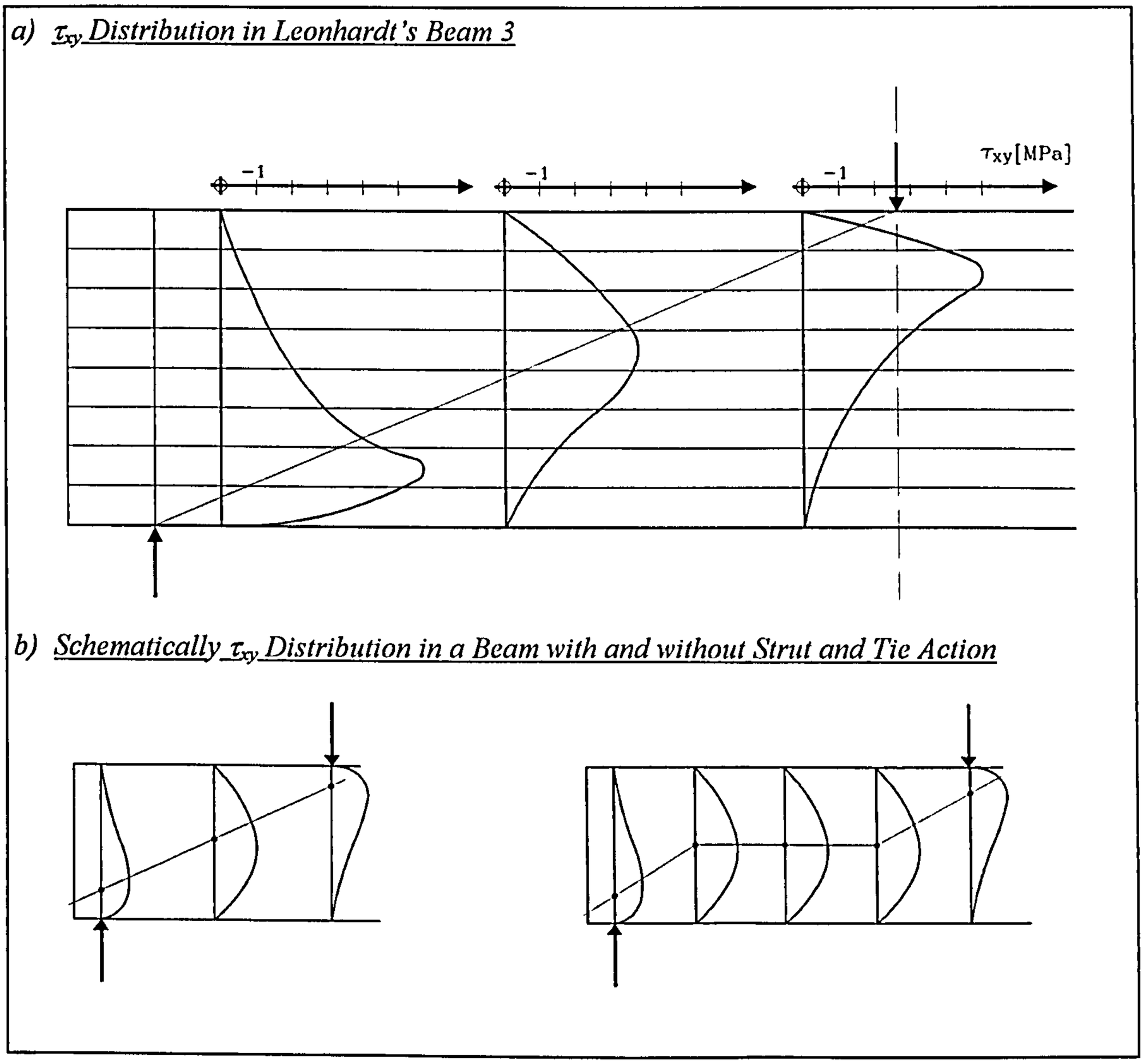

Fig.4.27 τ_{xy} Distribution in a Beam with Strut and Tie Action

4.5 The Calculation of Shear Deflections Using the UMAT

In Section 3.8 a method was presented how to calculate shear deflections in an RC beam using program LAYER. The method was essentially based on energy considerations with the main idea that deflections due to shear must be proportional to the shear energy while deflections due to bending can be assigned to the flexural energy present in a structure. In addition, the sum of both energies has to match the work of the applied load.

This method will now be utilised to calculate the deflections of the beams of Tab.3.5 (see Page 79) which were first analysed with LAYER. Fig.4.28.(a) shows a plane stress element with 8 nodes and 9 integration points. The volume ΔV_i, associated with an integration point can be determined using the Gauß integration method. Flexural and shear energy of an element are given in Fig.4.28.(a) as well as the total energy of a structure which is simply the sum of the element energies.

Beam:	*5*	*7-1*	*9-1*	*ET1*	*ET2*	*ET3*	*ET4*	*E4*	*E5-2*	*E6*	*T1*	*TA9*
Load:												
P *[kN]*	*120*	*103*	*96*	*240*	*240*	*240*	*180*	*279*	*372*	*153*	*1400*	*600*
Deflections:												
δ_{test} *[mm]*	*2.57*	*9.48*	*50.7*	*13.2*	*15.4*	*17.8*	*11.9*	*5.93*	*7.00*	*2.76*	*19.2*	*14.16*
$\delta_{pl\ test}$ "	*0.32*	*1.79*	*12.3*	*3.64*	*5.28*	*7.25*	*3.83*	*0.95*	-	*0.49*	-	-
δ_{cal} "	*2.05*	*7.51*	*39.6*	*7.89*	*9.83*	*10.3*	*8.84*	*4.23*	*4.28*	*2.22*	*12.80*	*8.06*
$\delta_{V\ cal\ (Shear)}$ "	*0.10*	*0.30*	*0.79*	*0.47*	*0.98*	*1.34*	*1.68*	*0.34*	*0.30*	*0.22*	*5.89*	*1.93*
$\delta_{M\ cal\ (Bend.)}$ "	*1.95*	*7.21*	*38.8*	*7.42*	*8.85*	*8.96*	*7.16*	*3.89*	*3.98*	*2.00*	*6.91*	*6.13*
$\delta_{cal} / \delta_{test}$	*0.80*	*0.79*	*0.78*	*0.60*	*0.64*	*0.58*	*0.74*	*0.71*	*0.61*	*0.80*	*0.67*	*0.57*
$\delta_{V\ cal} / \delta_{cal}$	*0.05*	*0.04*	*0.02*	*0.06*	*0.10*	*0.13*	*0.19*	*0.08*	*0.07*	*0.10*	*0.46*	*0.24*
Failure Mode:*	*S4*	*S4*	*B*	*B*	*S1*	*S2*	*S3*	*B*	*B*	*S4*	*S3*	*B*
Ult. Limit:												
$P_{u\ test}$ *[kN]*	*137*	*118*	*111*	*280*	*263*	*255*	*198*	*375*	*528*	*186*	*1600*	*700*
$P_{u\ cal}$ "	*138*	*103*	*103*	*288*	*245*	*248*	*188*	*345*	*507*	*190*	*1566*	*667*
Stirrups:												
ρ_s *[%]*	-	-	-	*0.17*	*0.35*	*0.52*	*1.04*	*0.64*	*0.71*	-	*2.8*	*1.29*
Shear Ratio:												
a/d	*3.0*	*5.0*	*7.0*	*3.5*	*3.5*	*3.5*	*3.5*	*2.8*	*2.0*	*2.8*	*2.8*	*3.3*

* B=Bending, S1=Shear (bending), S2=Shear (stirrup yielding), S3=Shear (diagonal compression), S4=Shear (diagonal tension)

Tab.4.7 Deflections Calculated from Leonhardt's Shear Tests Using UMAT

a) Finite Element with Integration Points and Element Energy

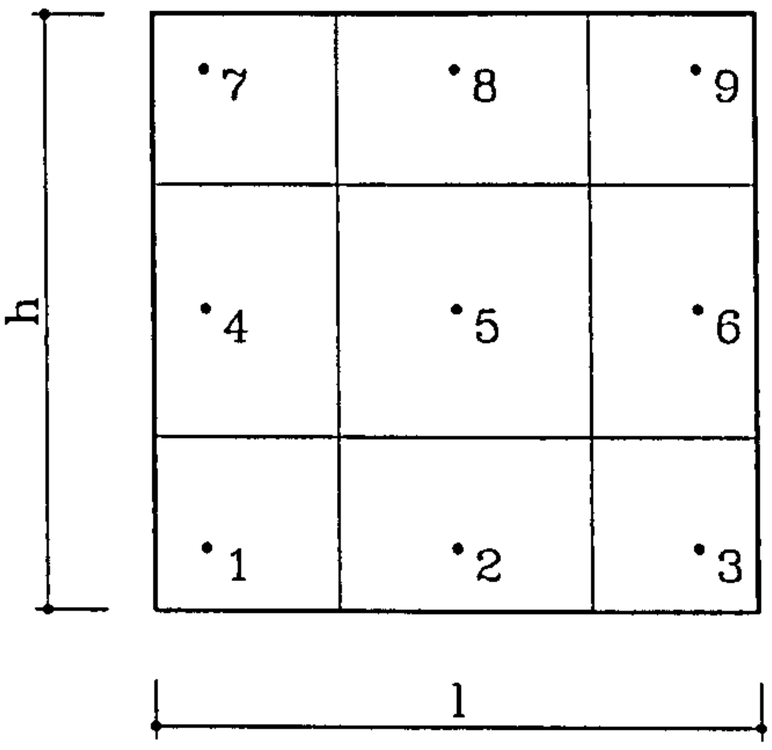

$$E_M^e = \sum_{i=1}^{9} \sigma_{xi} \varepsilon_{xi} \Delta V_i + \sum_{i=1}^{9} \sigma_{yi} \varepsilon_{yi} \Delta V_i$$

$$E_V^e = \sum_{i=1}^{9} \tau_{xyi} \gamma_{xyi} \Delta V_i$$

$$\Delta V_{1,3,7,9} = \frac{25}{81} l\, h\, b$$

$$\Delta V_{2,4,6,8} = \frac{40}{81} l\, h\, b$$

$$\Delta V_5 = \frac{64}{81} l\, h\, b$$

$$E_T^e = E_M^e + E_V^e$$

$$E_T = \sum_e E_T^e = \sum_e E_M^e + \sum_e E_V^e$$

b) Energies and Shear Deflections of Beam ET4

Energy compression zone:

$E_M^C = 0.00041$ MNm
$E_V^C = 0.0$ "

$E_T^C = 0.00041$ MNm

web:

$E_M^W = -0.00002$ MNm
$E_V^W = 0.00024$ "

$E_T^W = 0.00022$ MNm

tension zone:

$E_M^T = 0.00076$ MNm
$E_V^T = 0.00004$ "

$E_T^T = 0.0008$ MNm

Total energy: $E_T = E_T^C + E_T^W + E_T^T = 0.00143$ MNm

Deflection under load: $\delta_{cal}^{load} = 0.008$ m

Deflection in mid-span: $\delta_{cal}^{mid\text{-}span} = 0.0089$ m

Work of the load: $W_L = 0.008 * 0.18 = 0.00144$ MNm

Shear proportion: $p_s = \frac{0.00028}{0.00143} = 19.6\%$

Fig.4.28 Calculation of Shear Deflections of Leonhardt's Beam ET4 with the UMAT

For Leonhardt's beam ET4 the calculation of the shear deflections with program LAYER was given in Fig.3.23 (see Page 76). For the purpose of comparison the same specimen was chosen to investigate the shear deflections with the UMAT. The results of these calculations are depicted in Fig.4.28.(b). The energy contents of compression zone, web and tension zone are listed separately which reveals that more than half of the energy is situated in the tension zone while the web carries nearly all the shear energy. In the compression zone no shear energy is present which confirms that in a distinctly T shaped RC beam the forces in the compression zone are flowing virtually horizontally without generating any appreciable shear.

The specimens of Tab.3.5 (see Page 79) were recalculated with the method described in Fig.4.28 and the results are depicted in Tab.4.7. It can be seen that the calculated deflections were generally slightly smaller than those of Tab.3.5. The calculated values were in a range of *60 - 80%* the measured ones which is due to the well-known fact that FE codes based on the displacement method usually behave too stiff. This is visualised by an underestimation of calculated deflections.

In Section 3.8 the deflections due to bending were obtained from Eq.(3.13) (see Fig.3.23) by integrating the product of curvature and moment due to unity. This was possible as the plane section hypothesis of Bernoulli was retained in the layered approach, resulting in a constant curvature distribution along the cross section of an RC beam. Usually, an FE algorithm is not restricted by a plane section assumption and therefore, the above method should not be applied to check the flexural part of the calculated deflections. In simple cases, especially when symmetric load conditions apply to a single-span beam, bending deflections can be extracted from the rotations of cross sections which remain plane during the loading process. The procedure will be explained hereafter.

Fig.4.29.(a) shows half of a simply supported RC beam which is subjected to two symmetrically arranged concentrated loads. Fig.4.29.(b) gives the deformed shape in a qualitative fashion. The movements which the various particles of the beam undergo during the loading process can be considered to consist of both deformations due to strains ε_x , ε_y and γ_{xy} and rigid body displacements. However, the cross section along the axis of symmetry remains plane and perpendicular to the beam axis even after applying the load.

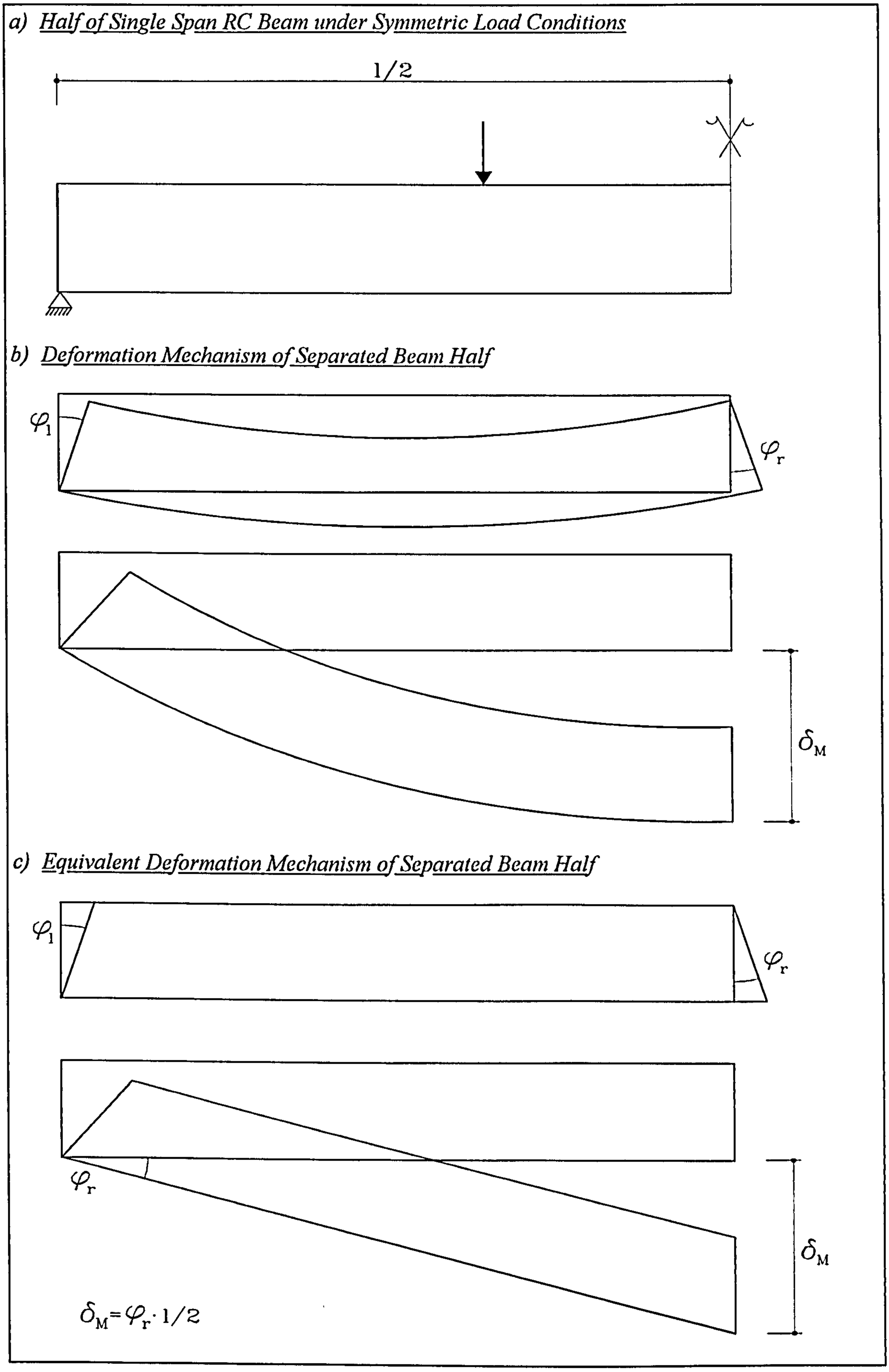

Fig.4.29 Bending Mechanism in a Symmetrically Loaded Single Span Beam

The deflection in mid-span seems to result out of a rigid body rotation alone, which is not influenced by the deformation of the beam itself. If the beam is imagined to consist of two separate parts, the deflection in mid-span can be considered to develop in two steps: At first, the separate parts will individually bend as indicated in Fig.4.29.(b). Then the deformed parts will be moved to their end position by a rigid body rotation.

In RC beams the strains ε_y are negligibly small and, as the determination of deformations due to bending are the objective of the here described method, the shear strains γ_{xy} together with the transverse strains ε_y should be excluded from the current considerations. In this case, the mid-span deflection δ_M , as indicated in Fig.4.29.(b), is composed of the normal strains ε_x alone. This means that δ_M could have developed as depicted in Figure 4.29.(c): The bottom and top strains ε_x elongate and shorten their respective fibre separately causing the same end rotation as those of Fig.4.29.(b). This is true, as we are still dealing with a linearised theory in which deformations and displacements are small in relation to the total dimension of the structure. The deflection δ_M is then generated in the same fashion as before by a rigid body rotation around the support of the beam half.

The described method was applied to Leonhardt's beam ET4 to corroborate the ratio of shear to total mid-span deflection, which was derived with the energy method of Fig.4.28 as $p_s = 19.6\%$. Fig.4.30.(a) shows one half of Leonhardt's beam ET4 and the discretisation with which the beam was analysed using the UMAT together with ABAQUS. In the elements along the lower and upper edge of the beam the integration points next to bottom and top are indicated in Fig.4.30.(a). The normal strains ε_x in these integration points are applied in the graph of Fig.4.30.(b) along the beam length and the values are approximated by straight lines to represent the ε_x distribution in the top and bottom fibre of beam ET4 in a sufficiently exact manner. From the explanations to Fig.4.29 it becomes clear that only the section rotation φ_r contributes to the deflection due to flexure δ_M. Therefore, both rotations of the end sections have to be determined. Fig.4.30.(c) shows the procedure. First, the centre of movement has to be fixed which is accomplished by taking the centre of the area between the two ε_x curves for the location of the zero point of the x-axis. Now the integration of the normal strains along the straight lines of bottom and top fibre starts from this point to the cross sections at the end of this half beam.

a) Half of Leonhardt's Beam ET4 with Discretisation

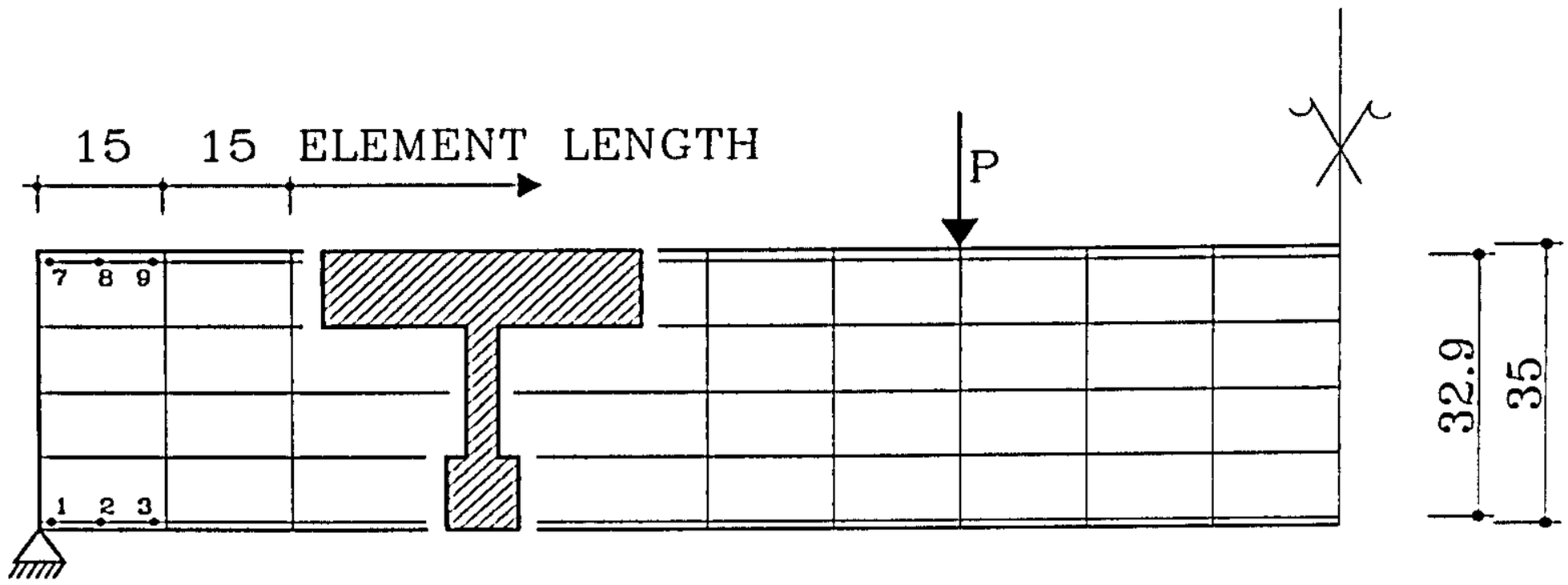

b) Normal Strain Distribution of Top and Bottom Fibre

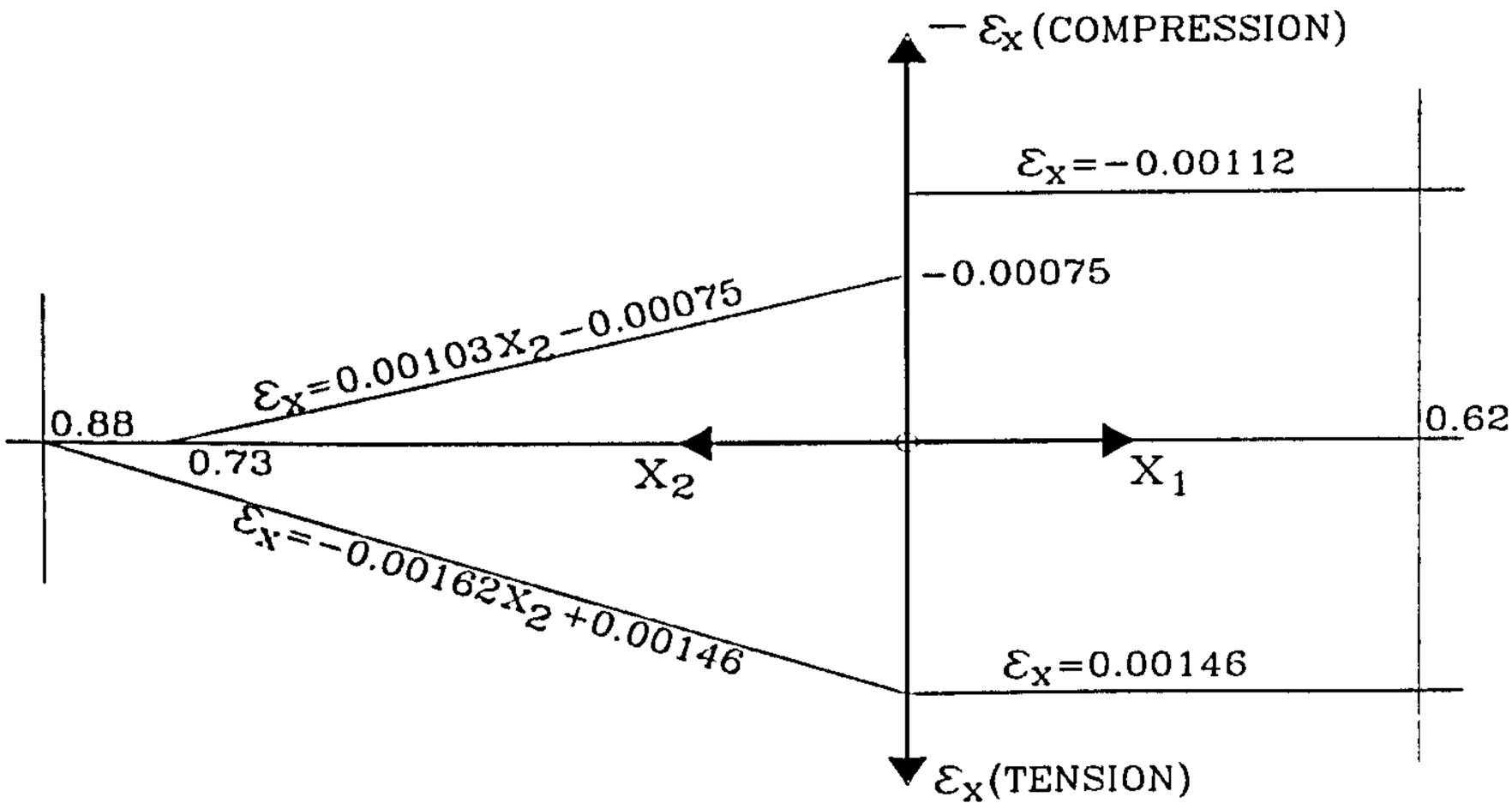

c) Calculation of Deflection out of Section Rotations

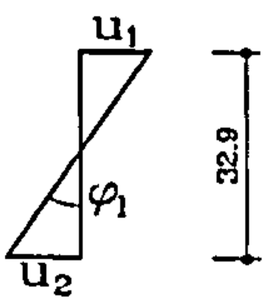

$$u_1 = \int_0^{0.73} \left(0.00103\, x_2 - 0.00075\right) dx_2 = -0.000273 \quad m$$

$$u_2 = \int_0^{0.88} \left(-0.00162\, x_2 + 0.00146\right) dx_2 = 0.000658 \quad m$$

$$\varphi_1 = \frac{0.000658 + 0.000273}{0.329} = 0.00283$$

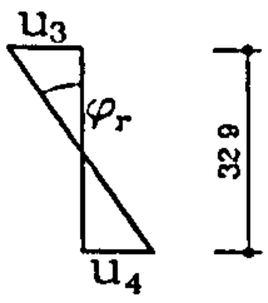

$$u_3 = -0.00112 \cdot 0.62 = -0.000694 \quad m$$

$$u_4 = 0.00146 \cdot 0.62 = 0.000905 \quad m$$

$$\varphi_r = \frac{0.000694 + 0.000905}{0.329} = 0.00486$$

$$\delta_M = 0.00486 \cdot 1.5 = 0.0073 \quad m \qquad \delta_T = \frac{0.0073}{0.804} = 0.0091 \ m \text{ with } \rho_s = 19.6\,\%$$

Fig.4.30 Calculation of Deflections of Leonhardt's Beam ET4

This procedure yields the four values for u_1 - u_4 which define both angles φ_r and φ_l of the end sections in the way given in Fig.4.30.(c). The deflection due to flexure δ_M is then easily obtained by multiplying φ_r with half of the beam length $l/2$. It can be seen from Fig.4.30 that this method delivers a rather exact value for the deflection δ_M and, hence, for δ_V as the total deflection δ is provided by the FE calculation itself.

5 The Ductility of Reinforced Concrete Walls

It was stated in the introduction to this work that the forthcoming release of the EC8 will introduce capacity design procedures in the European design practice. The method is essentially based on the displacement ductility of a structure which is the ratio of top deflection at the ultimate limit to that at the onset of yielding. The main idea is that the lateral design load specified in the code should be dependent on the ability of a structure to sustain large deformations far into the post-elastic range. Hence, the proper evaluation of deflections is crucial for the correct application of this method.

It was an objective of this work to develop a tool which, in connection with a powerful FE program, enables the designer to properly calculate deflections and ductilities of an RC structure and to assess the necessary equivalent seismic load which is needed for a safe and economic earthquake design.

In Chapter 4 the MCFT was incorporated in a material subroutine for ABAQUS. Numerous test runs proved the suitability of the implementation which together with ABAQUS provides an engineering tool for the reliable calculation of cracked reinforced concrete structures.

In the last chapter of this work it is shown how this tool can be utilised for investigations on the ductility of RC walls, a structural element often used in buildings to resist lateral load especially due to earthquake excitation.

5.1 Seismic Design of an 8-Storey Wall

A wall described and investigated in earlier work (see Haas, 1993 and Haas/Pilakoutas, 1994) will be used for calculations with the UMAT. The wall may be part of a building consisting of a multi-storey structure above ground level with an open layout as it is typically found in office or administration buildings. Fig.5.1 shows the sketch of the building. The lateral forces are resisted by one structural wall in each face of the building while the gravity loads are mainly carried by RC columns arranged in a regular grid. Fig.5.2 depicts the derivation of the dynamic values and Fig.5.3 the design of the wall in some detail. The provisions of the EC8 (1993) are met as well as the rules of the capacity design method.

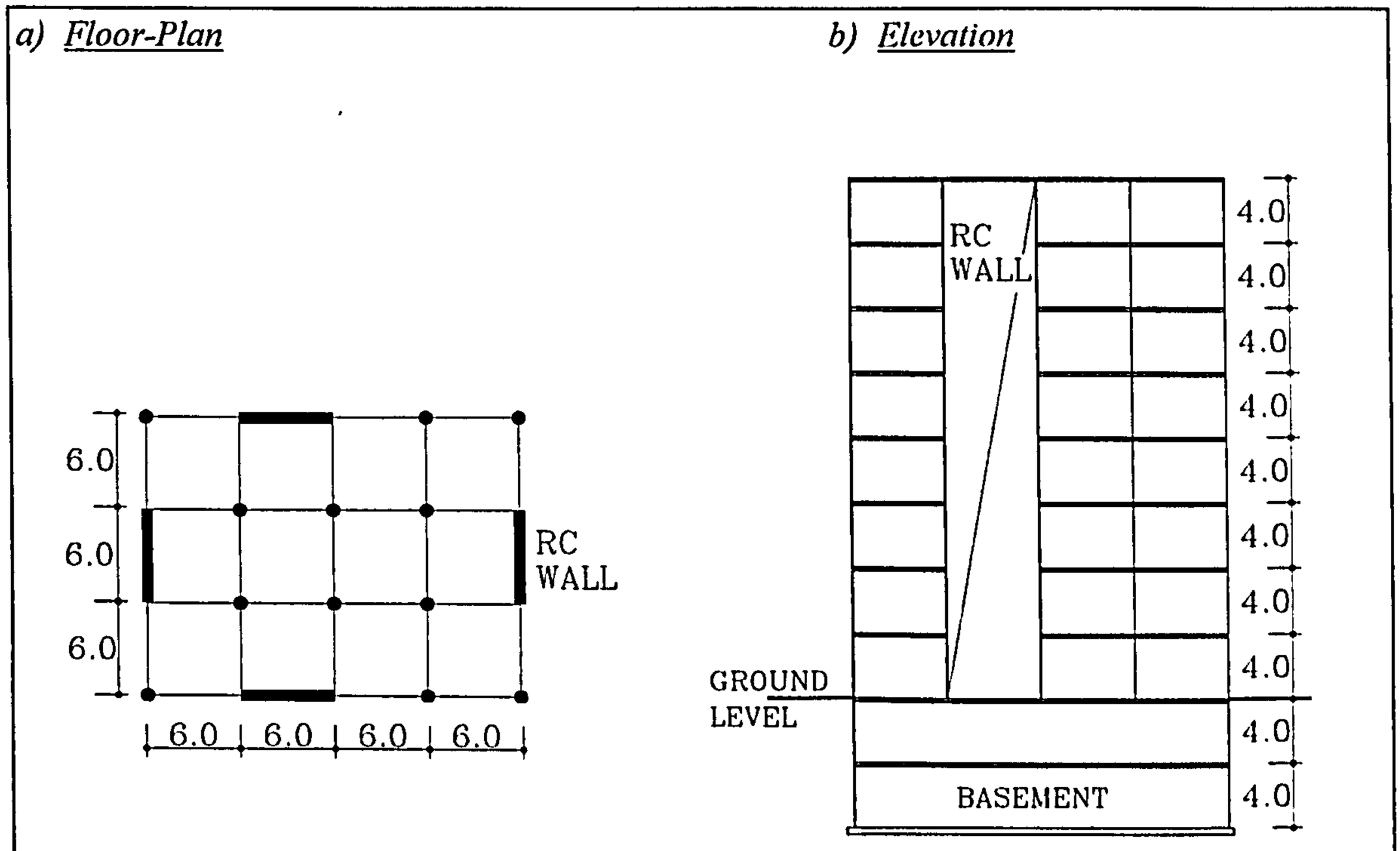

Fig.5.1 Floor-Plan and Elevation of an 8-Storey Building (Dimensions in Meters)

Fig.5.1 reveals that the wall fulfils all criteria for regularity in plan and elevation. Therefore, it is allowable to design the wall by means of the equivalent lateral force approach. The EC8 attributes particular emphasis to this possibility of a simplified design method, especially if the flow of forces is transparent. In this case the code provides simple equations for calculating the base shear force and the distribution of the seismic action along the height of the wall.

a) First Eigenmode

Dynamic model:

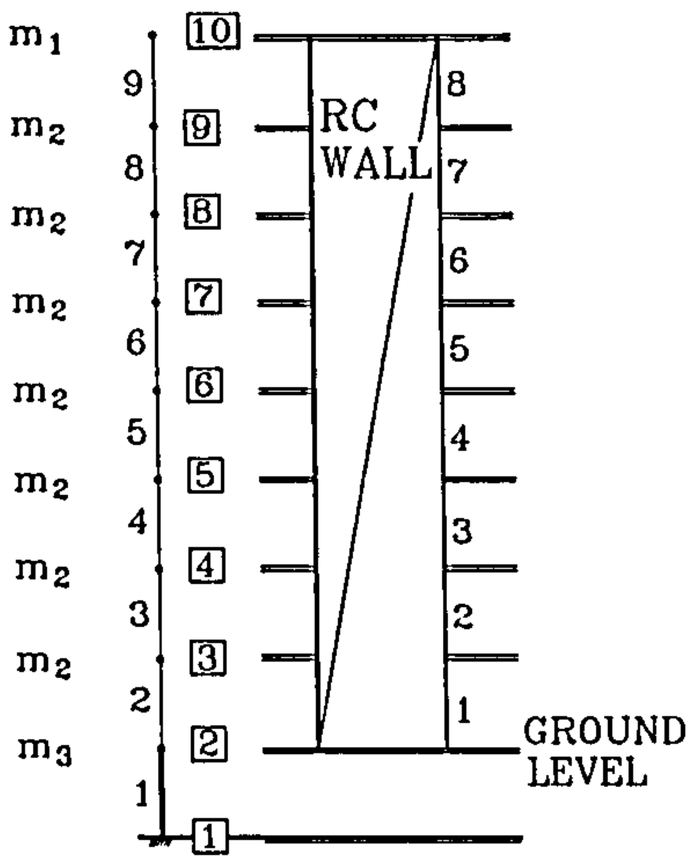

Masses:

$m_1 = 0.226\ MNs^2/m$ *(see Haas, 1993)*
$m_2 = 0.261$ „
$m_3 = 0.296$ „

Uncracked wall stiffness:

$I = 6^3\ 0.3 / 12 = 5.4\ m^4$

Active wall stiffness:

element 1	→	*rigid*
elements 2,3	→	*60 % uncracked*
elements 4-9	→	*100 % uncracked*

First eigenfrequency:

$f_1 = 0.55\ Hz$ → $T = 1.82\ s$

b) Equivalent Lateral Forces

Lateral force distribution:

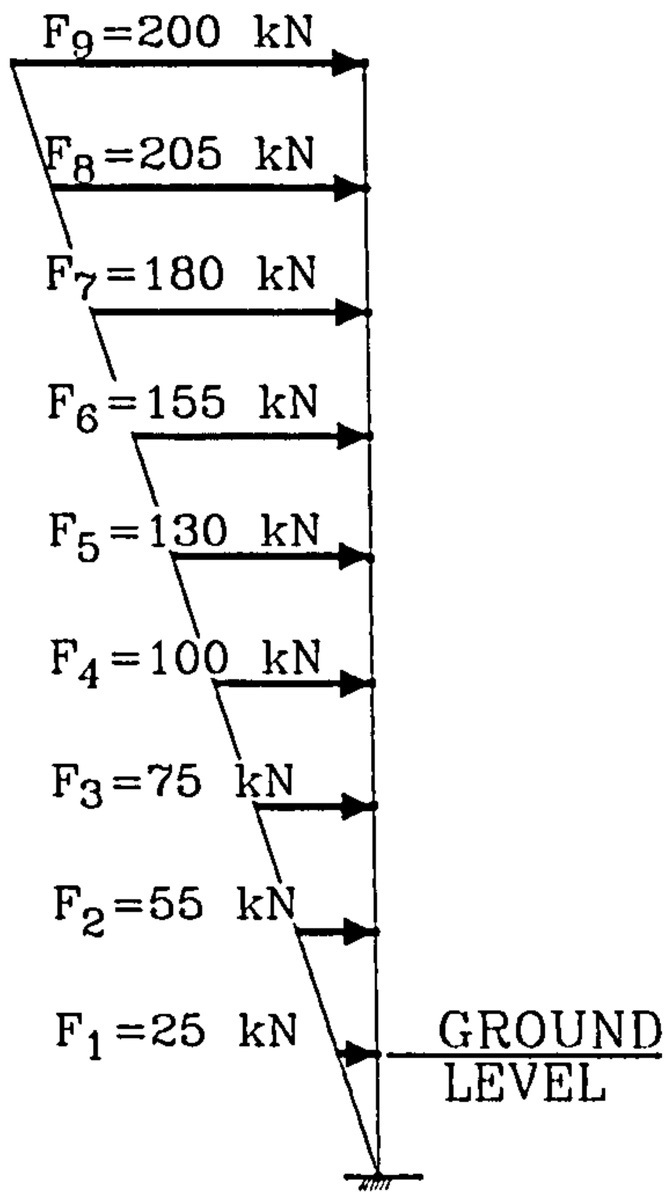

Design ground acceleration:

$a_g = 1.6\ m/s^2$ *(see Haas, 1993)*

Subsoil class: *B* *(see Haas/Pilakoutas, 1994)*

Parameters: *(see EC8, Part 1-1, Tabs. 4.1 and 4.2)*

$S = 1$	$T_B = 0.15\ s$
$\beta_0 = 2.5$	$T_C = 0.6\ s$
$K_1 = 1$	$K_{d1} = 0.667$
$K_2 = 2$	$K_{d2} = 1.667$

Response spectrum: (see EC8, Part 1-1, Section 4.2.2)

$$S_e(T_C) = 1.6 \cdot 2.5 = 4.0 \quad m/s^2$$

$$S_e(T) = 1.6 \cdot 2.5 \frac{0.6}{1.82} = 1.32 \quad m/s^2$$

Design spectrum: *(see EC8, Part 1-1, Section 4.2.4)*

$$S_d(T) = 0.16 \frac{2.5}{4} \left(\frac{0.6}{1.82} \right)^{0.667} = 0.0478$$

Behaviour factors: *(see EC8, Part 1-3, Sect. 2.3.2)*

$q_0 = 4$	*(uncoupled walls)*
$K_D = 1$	*(ductility class 'high')*
$K_R = 1$	*(regular elevation)*
$K_W = 1$	*(wall system)*

Base shear force: *(see EC8, Part 1-2, Sect. 3.3.2.2)*

$$F_b = S_d(T)\ w = 0.0478\ (2260+7 \cdot 2610+2960)$$
$$= 1125\ kN$$

Fig.5.2 Dynamic Values of an 8-Storey Wall according to the EC8 (1993)

For the determination of the equivalent lateral forces the evaluation of the current wall stiffness is of crucial importance, provided the important first eigenfrequency is below a value of *1.7 Hz*. The reason for this is the rapidly descending branch of the design spectrum for a ground period of more than *0.6 s*. An overestimation of the wall stiffness usually results in too high lateral forces and, hence, in an uneconomic although conservative design.

When assigning ductility class *H*, factor k_w , reflecting the prevailing failure mode in structural systems with walls, becomes equal to *1* and the highest possible value of the behaviour factor *q*, permitted by the EC8, is determined to be *4* for the wall system considered. This value is also assumed to be the design displacement ductility μ_Δ. The equivalent lateral forces due to this ductility level, and their distribution along the height of the wall are shown in Fig.5.2.(b). When calculating these forces, the design response spectrum for subsoil class *B* and a ground acceleration of $a_g = 0.16\ g$ were used, where *g* denotes the acceleration due to gravity.

From Fig.5.2.(b) it can be seen that a lateral force is applied at the base of the wall, because the built-in level was lowered one storey for the purpose of calculating the equivalent lateral forces. The EC8 does not require this measure. However, it was considered to be reasonable to introduce it here to provide conservative values for the moment envelope and the shear force distribution due to a certain amount of rotation at the wall base. It is worth mentioning that the Swiss code SIA 160 comments on this issue and incorporated this design rule in its earthquake provisions. When computing the equivalent lateral forces and their distribution according to the EC8 (see Part 1-2, Equation 3.3), the weight of the sub-foundation storey should not be regarded as part of the building, otherwise excessively high values for the lateral forces might be obtained.

The lowering of the built-in level of the structural wall is a conservative measure for the determination of section moments and shear forces, but leads to unconservative estimates of the frequency of the first vibration mode of the building. Structures like the one being considered, invariably have their first eigenfrequency in the range of *0.5* to *2 Hz*. However, the lowering of the built-in level, decreases the frequency and, hence, the spectral forces unjustifiably. To avoid this unfavourable behaviour it is necessary to stiffen up the bottom storey for the purpose of calculating the first eigenmode.

a) Distribution of Section Forces

Normal force: *Design envelope for moment:* *and shear force:*

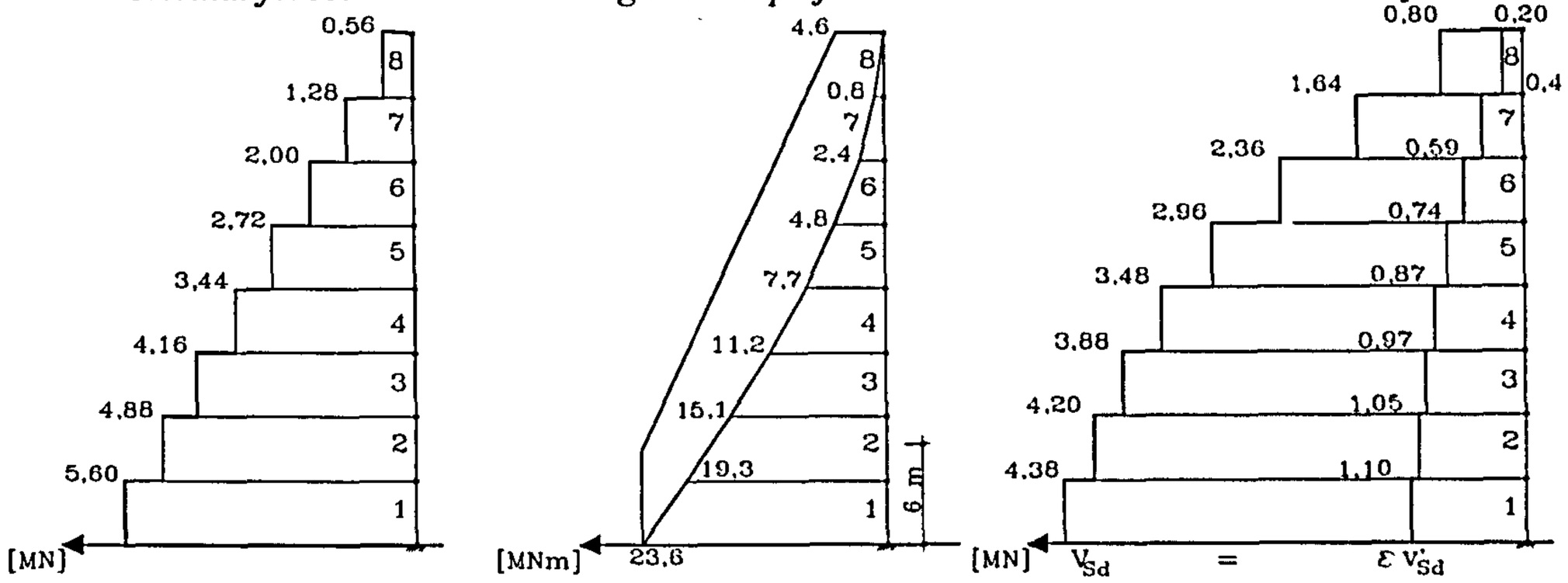

b) Design for Flexure with Normal Forces

Built-in level:

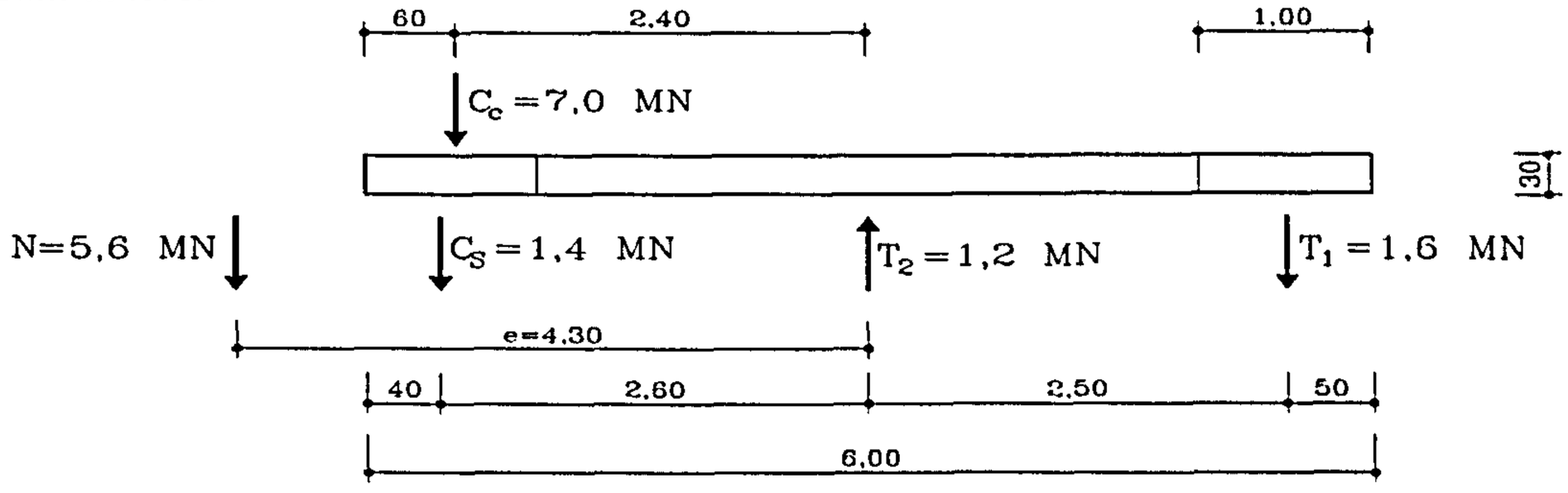

Section resistance: $M = 7.0 \cdot 2.4 + 1.6 \cdot 2.5 + 1.4 \cdot 2.6 = 24.4\ MNm$ $N = 5.6\ MN$

Section strains:

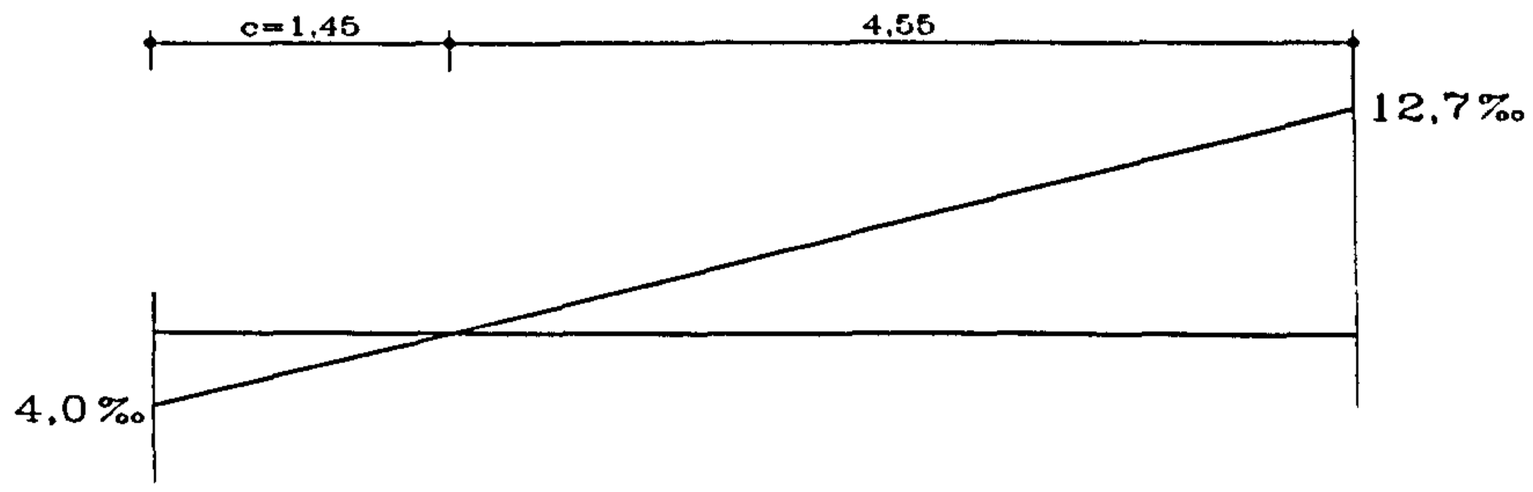

c) Design for Shear (see EC8, 1993, Part 1-3, Section 2.11.2)

Magnification factor: $$\varepsilon \le 4\sqrt{\left(\frac{1.25}{4}1.05\right)^2 + 0.1\left(\frac{4}{1.32}\right)^2} = 4.05 \ge q \rightarrow \varepsilon = 4$$

Design shear force: $V_{Sd} = \varepsilon V'_{Sd} = 4 \cdot 1095 = 4380kN = 4.38MN$

Diagonal compression: $V_{Sd} \le V_{Rd2}$ $V_{Rd2} = 0.4\left(0.7 - {}^{30}/_{200}\right) 20 \cdot 0.3 \cdot 0.8 \cdot 6 = 6.34\ MN$

Diagonal tension: $V_{Sd} \le V_{Rd3} = V_{Cd} + V_{Wd}$ $a_s = \frac{23.6}{4.4 \cdot 6} = 0.89$

$A_{sl} = 0.003 + 0.0032 = 0.0062m^2$ $\rho_l = \frac{0.0062}{0.3 \cdot 0.8 \cdot 6} = 0.0043$

$V_{Cd} = 0.34\left(1.2 + 4 \cdot 0.0043\right) 0.3 \cdot 0.8 \cdot 6 = 0.7\ MN$

Shear reinforcement: stirrups Φ10/9.5cm $\rightarrow$ $\rho_h = 0.0054$

$V_{Wd} = 0.0054 \cdot 480 \cdot 6 \cdot 0.8 \cdot 0.3 = 3.7\ MN$

$V_{Rd3} = V_{Cd} + V_{Wd} = 3.7 + 0.7 = 4.4\ MN \ge V_{Sd}$

Fig.5.3 Design for Flexure and Shear of an 8-Storey Wall

Fig.5.3 shows the design for flexure and shear of the 8-storey wall (for more details see Haas, 1993). The moment and shear envelopes were obtained by means of the EC8 provisions which are based on capacity design procedures. The flexural resistance of the wall section at the built-in level was calculated with simple section analysis (see Haas, 1993). The seismic shear force at the base of the wall was computed with the magnification factor ε to $V_{Sd} = \varepsilon \cdot V'_{Sd}$, where V'_{Sd} is the sum of the equivalent lateral forces resisted by the structural wall.

a) Design for Confinement

$$eff\ N_{Sd} = 0.6\left(\frac{N_{Sd}}{2} + \frac{M_{Sd}}{z}\right) = 0.6\left(\frac{5.6}{2} + \frac{23.6}{5}\right) = 4.5\ MN$$

$A_c = 1.0 \cdot 0.3 = 0.3\ m^2$ $\quad k_0 = 0.9$ $\quad \sum b_i^2 = 10 \cdot 0.2^2 = 0.4$

$A_0 = 0.9 \cdot 0.2 = 0.18\ m^2$ $\quad l_c \geq 0.15\ l_w = 0.9\ m$ $\quad s = 0.095\ m$ $\quad b_0 = 0.2\ m$

$$a_n = 1 - \frac{\sum b_i^2}{6A_0} = 1 - \frac{0.4}{6 \cdot 0.18} = 0.63 \qquad a_s = \left(1 - \frac{s}{2b_0}\right)^2 = \left(1 - \frac{0.11}{2 \cdot 0.2}\right)^2 = 0.53$$

$$\alpha = \alpha_n\, \alpha_s = 0.63 \cdot 0.53 = 0.33 \qquad \nu_d = \frac{eff\ N_{Sd}}{A_c\, f_{cd}} = \frac{4.5}{0.3 \cdot 20} = 0.75 \rightarrow \qquad \nu_{d,max} = 0.55$$

Required ratio of confining hoops:

$$\omega_{Wd} = \frac{k_0}{a}(0.9\nu_d + 0.1)\left(0.35\frac{A_c}{A_0} + 0.15\right) = \frac{0.9}{0.33}(0.9 \cdot 0.55 + 0.1)\left(0.35\frac{0.3}{0.18} + 0.15\right) = 1.2$$

By shear reinforcement provided ratio of confining hoops:

$$\omega_{Wd} = \frac{4 \cdot 0.2 \cdot 0.000154}{0.2^2 \cdot 0.18}\frac{480}{20} = 0.4$$

b) Reinforcement Details

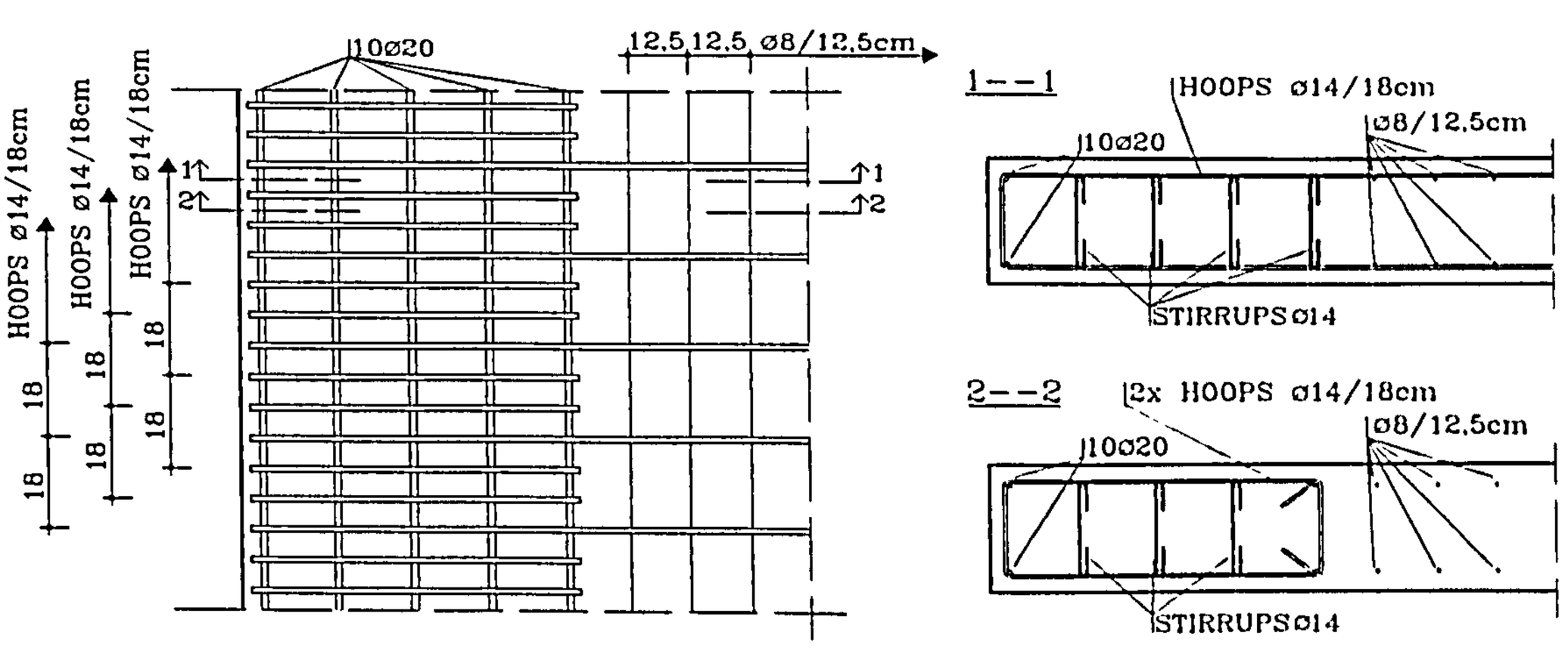

Fig.5.4 Design for Confinement and Reinforcement Details of an 8-Storey Wall

Fig.5.4 depicts the design for confinement according to the Eurocode (see EC8, 1993 and Frangou / Pilakoutas, 1994) as well as material properties and some reinforcing details. Finally, Fig 5.5 gives the FE discretisation together with the reinforcement ratios of the provided steel. The ratios have been obtained taking consideration of the design envelopes for moment and shear. It can be seen from Fig.5.4 that the EC8 provisions for the confinement of the compression zone requires a substantial amount of reinforcing steel, which in the present case is as much as three times the lateral reinforcement necessary to resist the seismic shear forces.

a) FE Discretisation

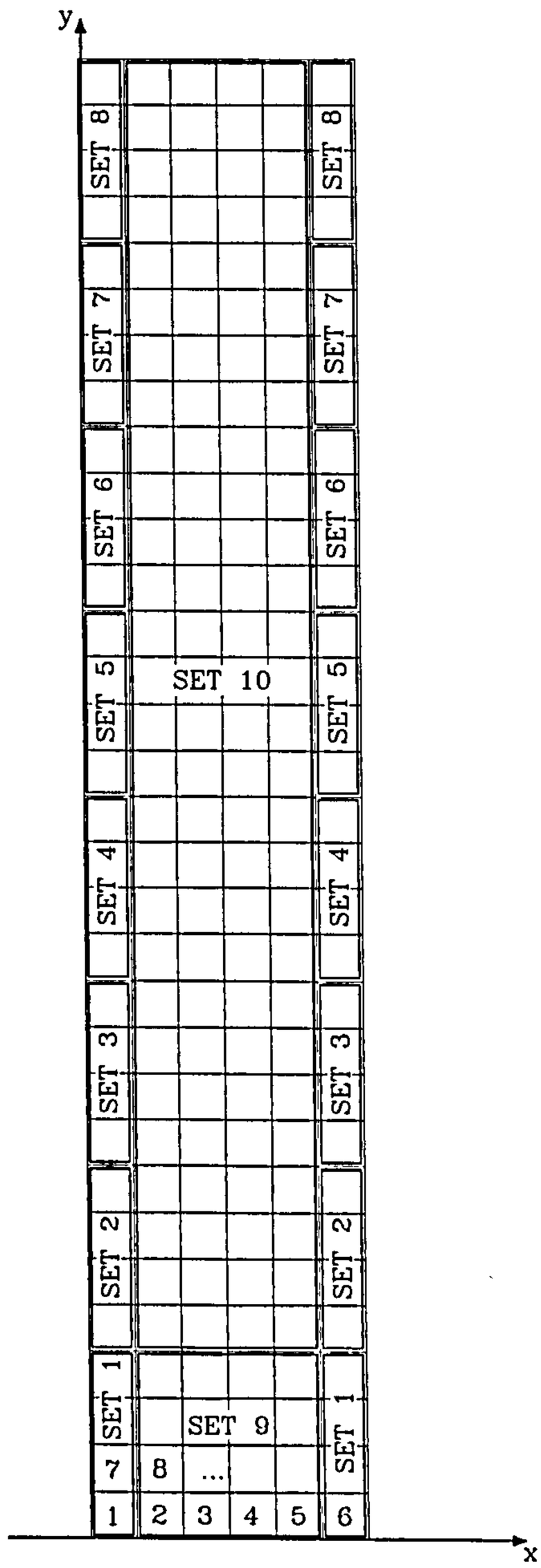

b) Reinforcement Ratios

ρ_x → *shear reinforcement*
ρ_y → *longit. reinforcement*

SET 1:	$\rho_x = 0.0171$
	$\rho_y = 0.01$
SET 2	$\rho_x = 0.0057$
	$\rho_y = 0.01$
SET 3	$\rho_x = 0.0022$
	$\rho_y = 0.009$
SET 4	$\rho_x = 0.0022$
	$\rho_y = 0.08$
SET 5	$\rho_x = 0.0022$
	$\rho_y = 0.0065$
SET 6	$\rho_x = 0.0022$
	$\rho_y = 0.0055$
SET 7	$\rho_x = 0.0022$
	$\rho_y = 0.004$
SET 8	$\rho_x = 0.0022$
	$\rho_y = 0.003$
SET 9	$\rho_x = 0.0057$
	$\rho_y = 0.0027$
SET 10	$\rho_x = 0.0027$
	$\rho_y = 0.0027$

Fig.5.5 FE Discretisation and Reinforcement Ratios of an 8-Storey Wall

5.2 Investigations on Ductility

5.2.1 An 8-Storey Wall

The 8-storey wall designed and detailed in the previous section was investigated with ABAQUS and the UMAT. Fig.5.6 shows the *load stage / deflection* response of the structural wall. The normal forces were kept constant while the horizontal forces due to earthquake action were simultaneously increased until failure occurred. At a load stage of $H = 0.75\ H_{ult}$ the outer steel bars of the reinforcement started yielding at the wall base. This happened at a top displacement of *16.3 cm* while the ultimate limit was reached at a top displacement of *63.6 cm*. From these results a displacement ductility of $\mu_\Delta = 63.6 / 16.3 = 3.9$ can be calculated, which coincides quite well with the nominal displacement ductility obtained from the EC8 provisions. For the purpose of comparison the *load stage/deflection* response of the same wall, however, without any confinement reinforcement, is also depicted. It is obvious that the confinement of the concrete in compression is crucial for the displacement ductility but does not significantly influence the flexural capacity of the structural member: The displacement ductility of the wall without confinement reinforcement is as little as *2.0* while the section resistance is only increased by approximately *10%*.

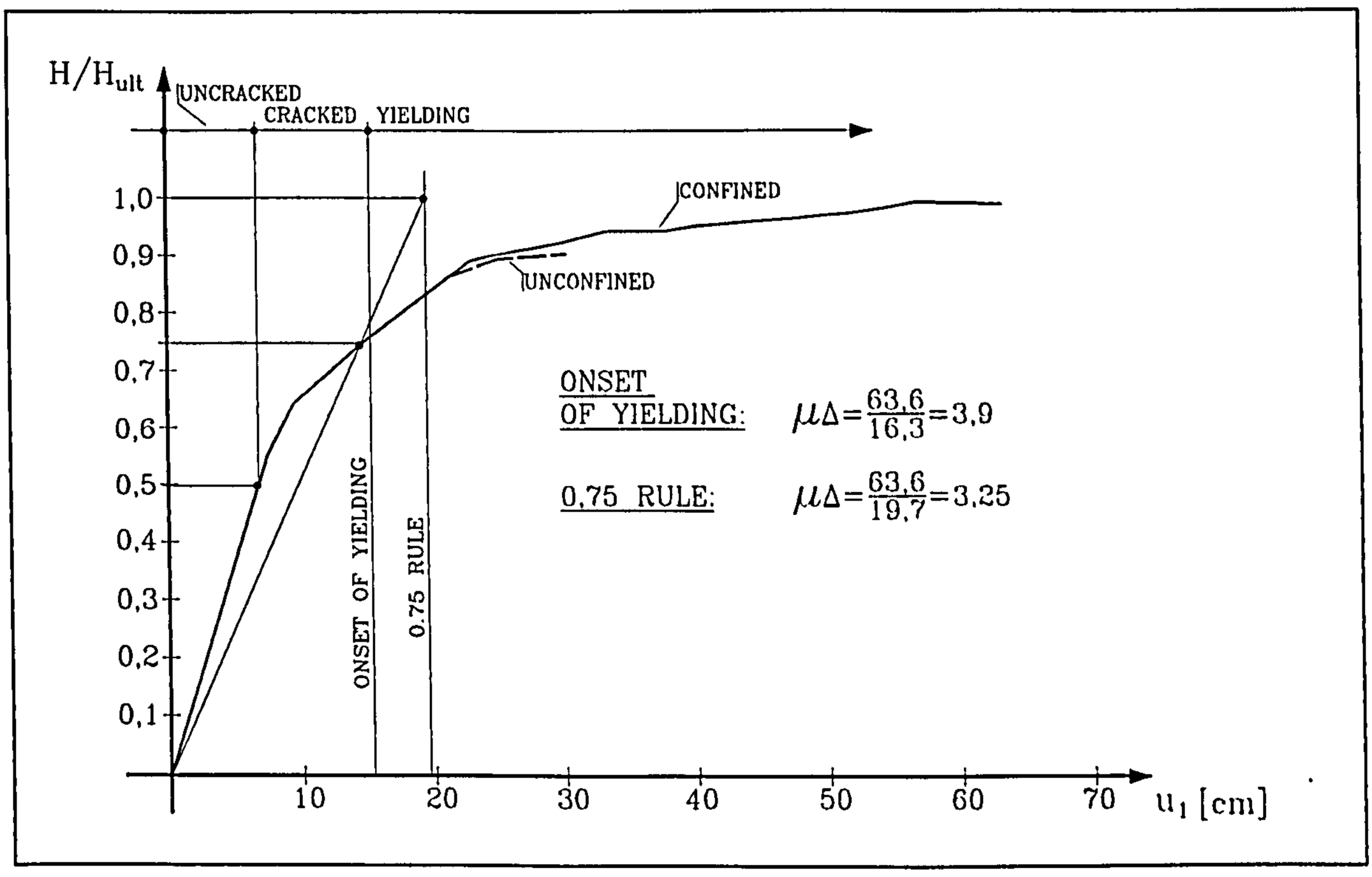

Fig.5.6 Confined and Unconfined Load Stage/Deflection Response of an 8-Storey Wall

Another important observation is that without confinement the wall fails early after the onset of yielding, while the ultimate limit of the confined wall is reached during heavy yielding of the flexural reinforcement. This is a structural behaviour widely appreciated in earthquake resistant design. The graph of Fig.5.6 also reveals that cracks start forming at a load level of approximately *50%* of the ultimate limit.

In Paulay / Priestley (1992) a rule is derived for the evaluation of the displacement ductility of a structure. This rule claims that the non-linear *load/deflection* response of a structure might be approximated by an elastic/perfectly plastic relationship which can be composed by taking the displacement at *75%* of the ultimate load as part of the approximated curve. Fig.5.6 shows the details, and the value for the displacement ductility according to the *75%* rule becomes *3.2*.

Curvature Ductility according to

EC8 provisions (see Part 1-3, Equation 2.62): $\mu_{1/r} = 1.2\, q^2 = 19.2$

Results of UMAT analysis:

ultimate limit

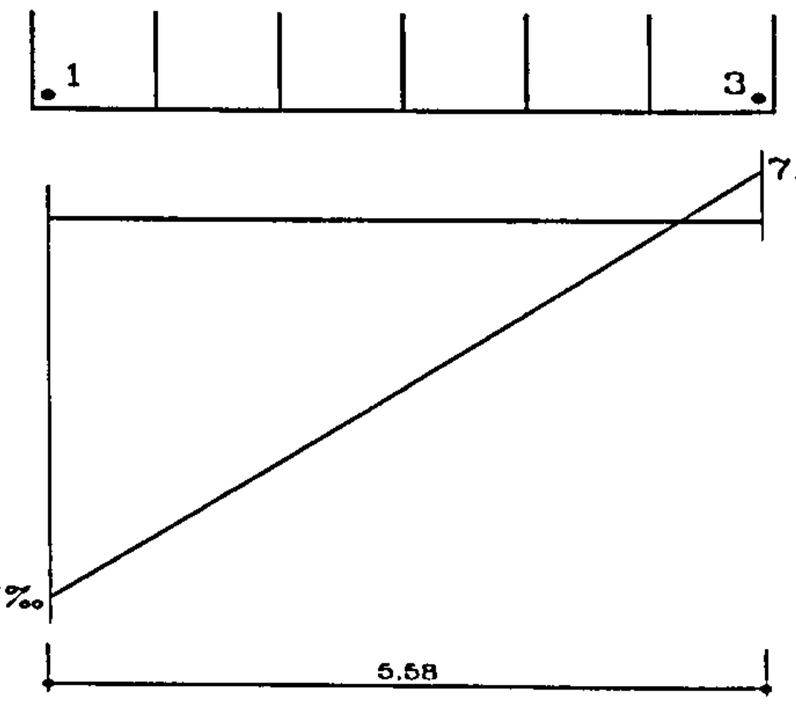

$\Phi_{ult} = \frac{57.7 + 7.3}{5.58} 10^{-3} = 11.7 \cdot 10^{-3} \quad m^{-1}$

onset of yielding

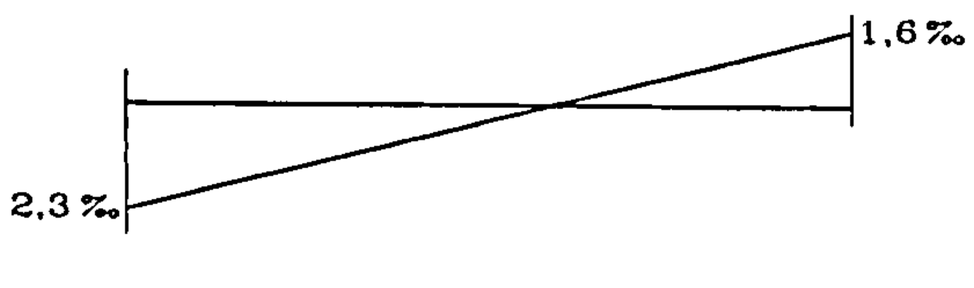

$\Phi_{el,onset} = \frac{2.3 + 1.6}{5.58} 10^{-3} = 0.69 \cdot 10^{-3} \quad m^{-1}$

$\mu_\Phi = \frac{\Phi_{ult}}{\Phi_{el,onset}} = \frac{11.7}{0.69} = 17$

75% rule (Paulay/Priestley, 1992)

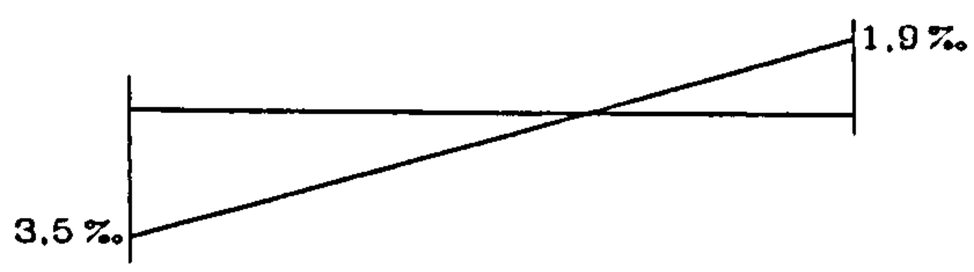

$\Phi_{el,75\%} = \frac{3.5 + 1.9}{5.58} 10^{-3} = 0.97 \cdot 10^{-3} \quad m^{-1}$

$\mu_\Phi = \frac{\Phi_{ult}}{\Phi_{el,75\%}} = \frac{11.7}{0.97} = 12$

Tassios (1989): $\mu_\Phi = 1 + 3.5\left(\mu_\Delta - 1\right) = 11.1$

Pilakoutas (1992): $\mu_\Phi = 1 + 6.8\left(\mu_\Delta - 1\right) = 20.7$

Fig.5.7 Curvature Ductility of an 8-Storey Wall

The design for confinement according to the EC8 (1993) should ensure a curvature ductility of $\mu_{1/r} = 1.2q^2$ for an isolated wall. With a behaviour factor of $q = 4$ for the wall under consideration this yields a conventional curvature ductility factor (CCDF) of $\mu_{1/r} = 19.2$. Fig.5.7 shows the procedure how the curvature ductility μ_Φ, which is equivalent to the conventional curvature ductility factor $\mu_{1/r}$ of the EC8, can be obtained from the results of the UMAT analysis. The calculation gives a value of *17* for the curvature ductility μ_Φ. For the purpose of comparison the curvature ductility was also determined from the *75%* rule of Paulay/Priestley and from two expressions derived by Tassios (1989) and Pilakoutas/Elnashai (1991), respectively. It is obvious that the curvature ductility from the equation of Pilakoutas best matches both the value obtained from the provisions of the EC8 and that computed from the UMAT results.

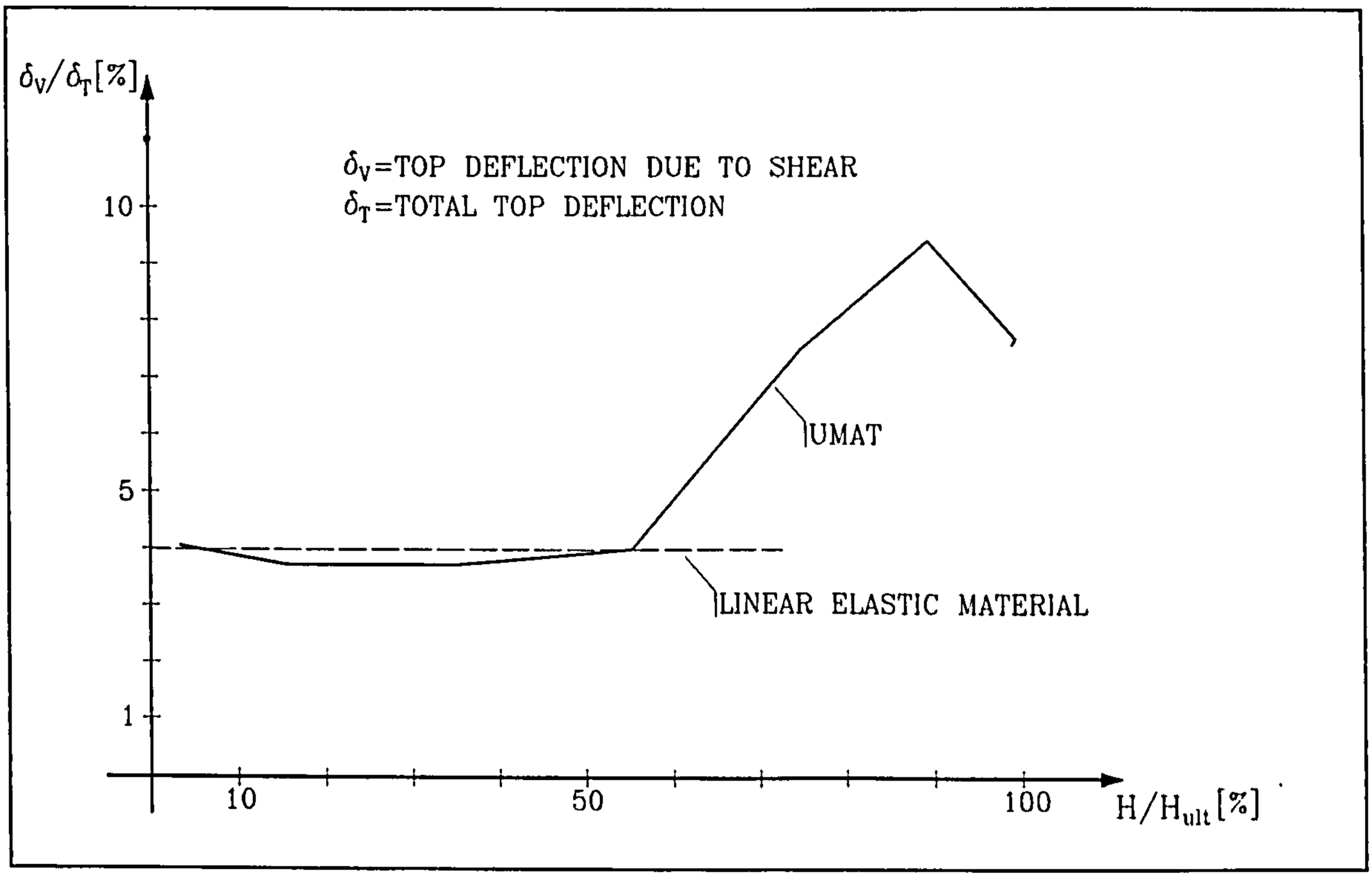

Fig.5.8 Relationship of Shear Deflections and Load Stage of an 8-Storey Wall

An important issue in seismic design is to answer the question whether the deflections due to shear influence the ductility of an RC structure, which in the current case might be the 8-storey wall under consideration. It was, therefore, necessary to establish a relationship which provides, at every load stage, that proportion of the deflections which can be attributed to shear action. Fig.5.8 depicts a graph in which the percentage of the top deflection due to shear is plotted against the load stage. The shear deflections were calculated by means of the energy method described in Sections 3.8 and 4.5 in detail. From the

relationship of Fig.5.8 it can be seen that the portion of shear deflections is between *4* and approximately *10%* of the total deflections depending on the applied load.

It is interesting to recognise that before failure this proportion drops to a certain amount. The reason for this is the fact that at the ultimate limit the longitudinal reinforcement is heavily yielding which is accompanied by a substantial increase in flexural energy, thus noticeably dropping the shear proportion of the total energy. Another observation is that the shear proportion remains nearly constant at a low level until cracks have started forming. If a linear elastic material was applied then this percentage would be constant for the complete load history.

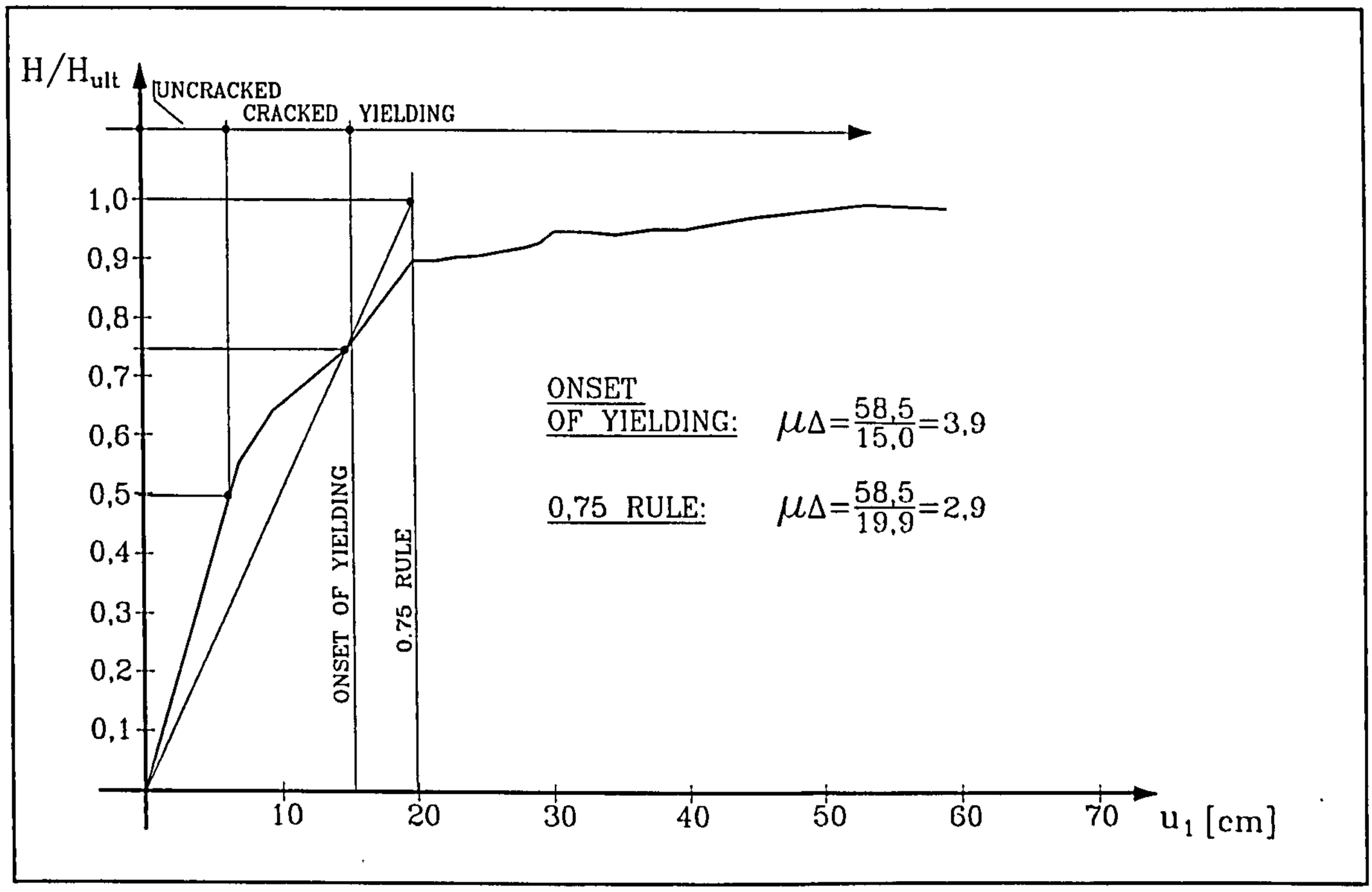

Fig.5.9 Load Stage/Flexural Deflection Response of an 8-Storey Wall

With the graph of Fig.5.8 it was possible to remove the deflections due to shear from the *load stage/deflection* relationship of Fig.5.6, thus giving the curve shown in Fig.5.9. The displacement ductility was now obtained to be 3.9 which is the same value extracted from the graph in Fig.5.6.

a) 4-Storey Wall

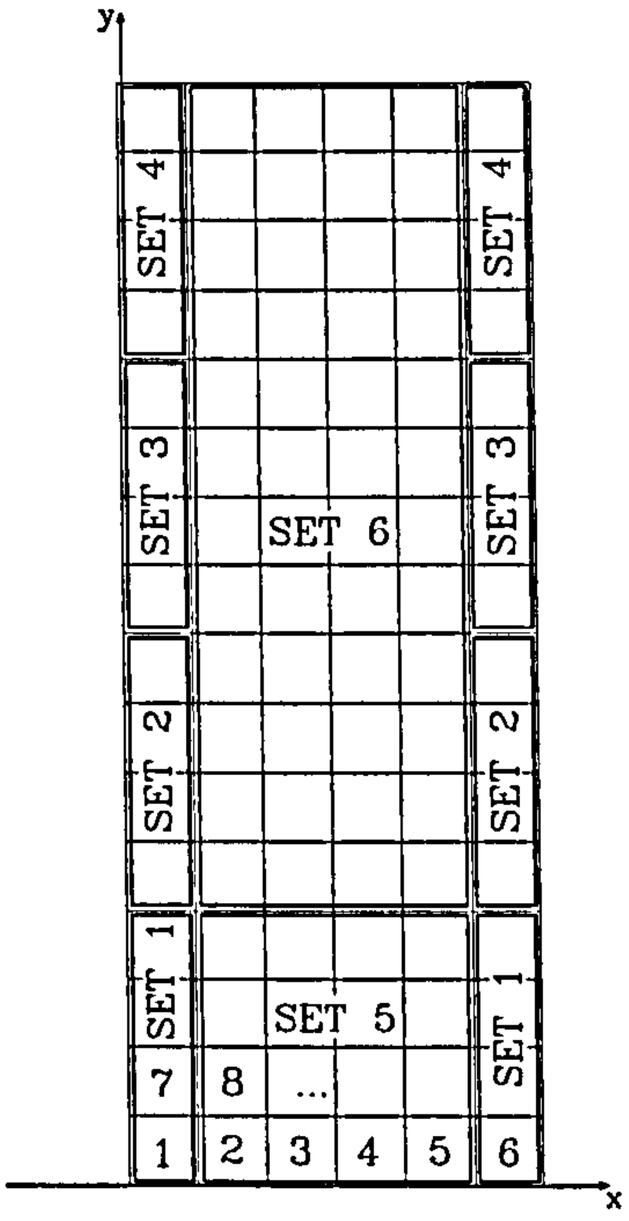

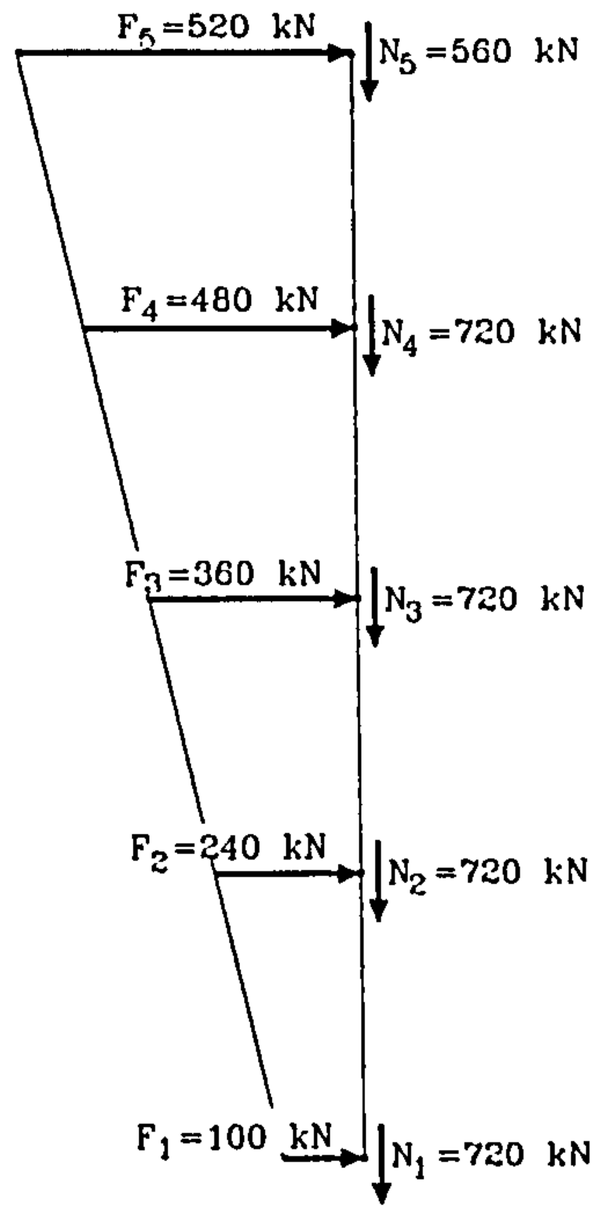

ρ_x → *shear reinforcem.*
ρ_y → *longit. reinforcem.*

SET 1: $\rho_x = 0.0104$, $\rho_y = 0.0067$

SET 2 $\rho_x = 0.0052$, $\rho_y = 0.0067$

SET 3 $\rho_x = 0.0022$, $\rho_y = 0.0052$

SET 4 $\rho_x = 0.0022$, $\rho_y = 0.0028$

SET 5 $\rho_x = 0.0026$, $\rho_y = 0.0027$

SET 6 $\rho_x = 0.0022$, $\rho_y = 0.0028$

b) 6-Storey Wall

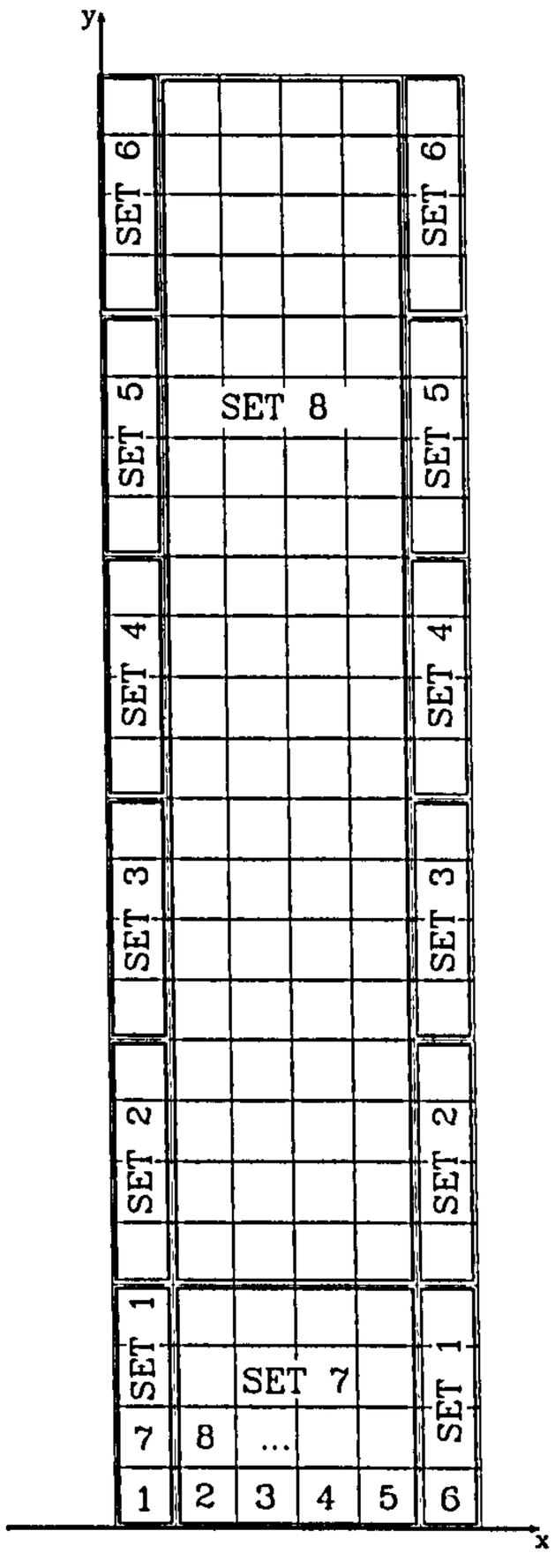

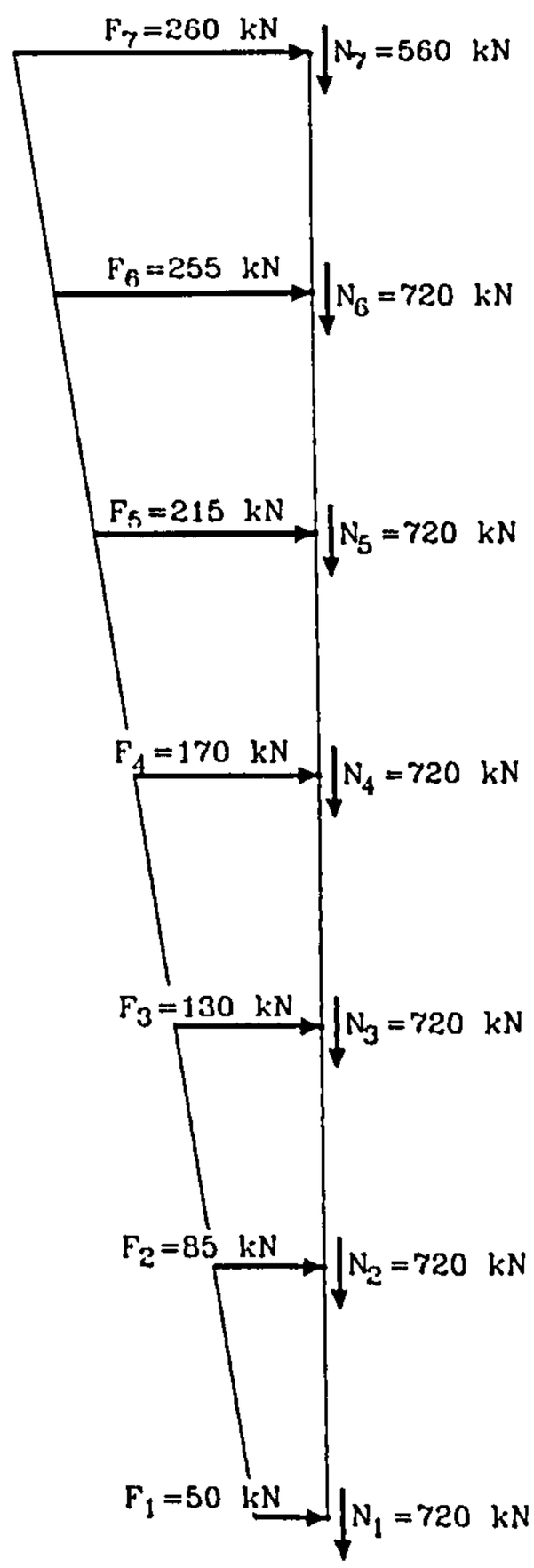

SET 1: $\rho_x = 0.0123$, $\rho_y = 0.0057$

SET 2 $\rho_x = 0.0062$, $\rho_y = 0.0057$

SET 3 $\rho_x = 0.0022$, $\rho_y = 0.0051$

SET 4 $\rho_x = 0.0022$, $\rho_y = 0.0044$

SET 5 $\rho_x = 0.0022$, $\rho_y = 0.0041$

SET 6 $\rho_x = 0.0022$, $\rho_y = 0.0035$

SET 7 $\rho_x = 0.0031$, $\rho_y = 0.0027$

SET 8 $\rho_x = 0.0022$, $\rho_y = 0.0027$

Fig.5.10 Discretisation with Load Conditions and Steel Ratios of a 4 and 6-Storey Wall

Similar results were calculated from two other capacity designed walls which, additionally, were detailed according to the provisions of the EC8. The results of the investigation of these walls are presented in Section 5.2.2. It can, therefore, be stated that in structural walls, which are capacity designed and detailed according to the provisions of the EC8, the deflections due to shear do not affect the displacement ductility in a significant fashion. However, it will be seen later that this is not the case with squat walls which usually develop an appreciable amount of shear deflections.

5.2.2 Analysis of a 4 and 6-Storey Wall

In Section 5.1 an 8-storey wall was designed and detailed according to the provisions of the EC8 and in Section 5.2.1 this wall was analysed using ABAQUS together with the UMAT. In the same way two rather similar walls were designed and investigated and the results are summarised here. The walls under scrutiny could be part of a building equal to that of Fig.5.1 but with only 4 and 6 stories above ground level.

Fig 5.10 depicts the discretisation of the walls and the reinforcement ratios obtained from the EC8 design as well as the loading conditions. Additionally, Tab 5.1 gives some dynamic values necessary for the analysis of the walls.

			4-Storey Wall	*6-Storey Wall*
1. Eigenfrequency	f	*[Hz]*	*2.0*	*0.85*
Design Ground Acceleration	a_g	$[m/s^2]$	*1.6*	*1.6*
Elastic Response Spectral Value	$S_e(T)$	$[m/s^2]$	*4.0*	*4.0*
Behaviour Factor	q	*[-]*	*3.4*	*4.0*
Normal Force at Wall Base	N_b	*[MN]*	*2.7*	*4.2*
Seismic Base Shear Force	F_b	*[MN]*	*1.57*	*1.17*
Required Section Resistance	M_R	*[MNm]*	*16.1*	*18.2*
at Wall Base	V_R	*[MN]*	*2.5*	*3.1*
Mechanical Volum. Steel Ratio	ω_{wd}	*[-]*	*0.7*	*1.2*

Tab.5.1 Seismic Design Values for a 4 and 6-Storey Wall

From Tab.5.1 it can be seen that the seismic base shear force for the 6-storey wall is less than that for the 4-storey wall. This is due to the much smaller first eigenfrequency of the taller wall and the reduction of the equivalent lateral forces connected with this feature. Nevertheless, the required shear resistance at the wall base is higher for the 6-storey wall because of the increased behaviour factor.

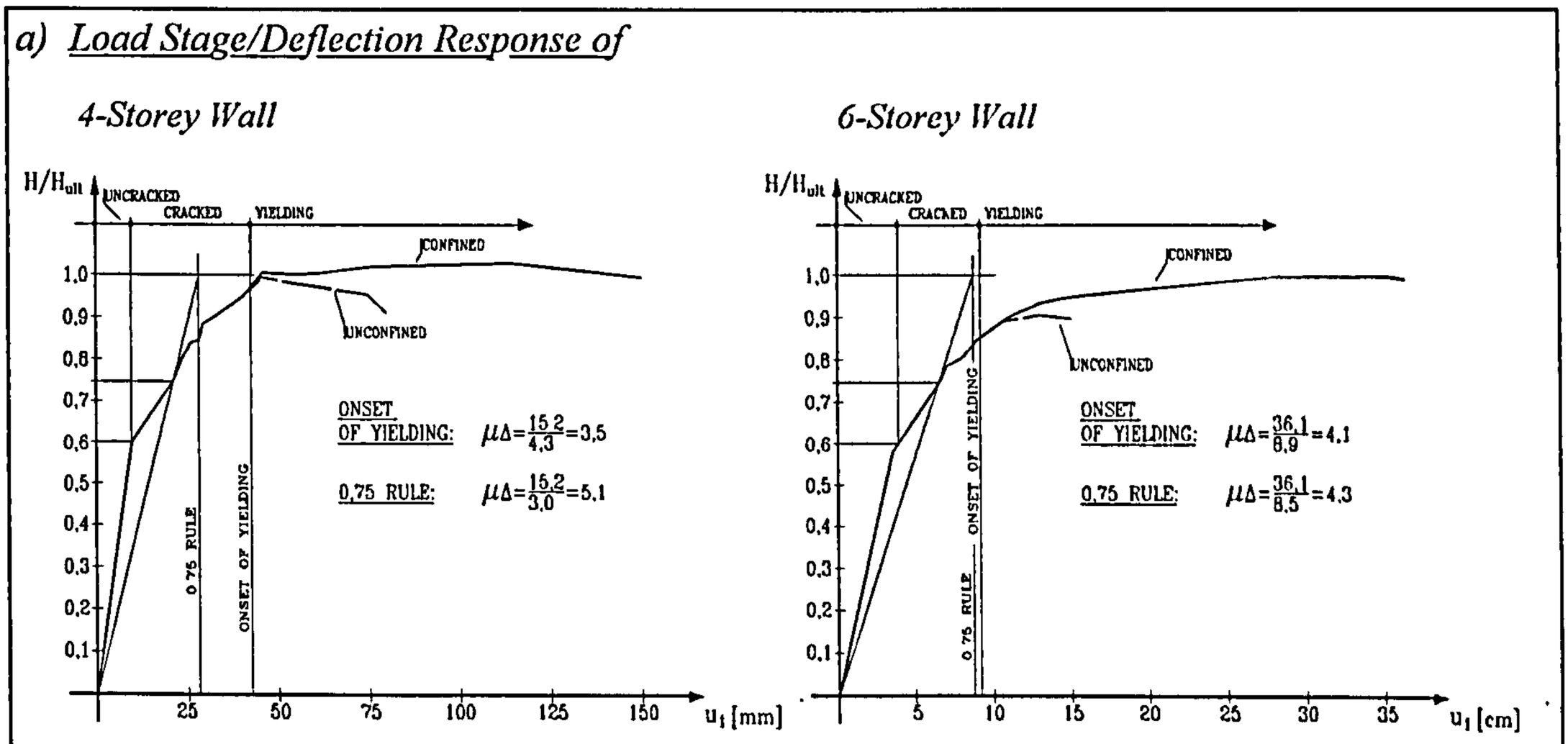

Fig.5.11 Load Stage/Deflection Response and δ_V/δ_T depending on Load Stage

Fig.5.11 shows the *load stage/deflection* response of both walls. Once again the results of the calculations concerning the unconfined walls are included in the figure to demonstrate the importance of the confinement of the concrete under compression. In addition, Fig.5.11 depicts the relationship of δ_V/δ_T and *load stage*. Finally, Tab.5.2 summarises the investigations on displacement and curvature ductility. The analyses with the UMAT reveal quite a good coincidence of calculated values and EC8 provisions.

	4-Storey Wall	6-Storey Wall
Behaviour Factor q (EC8)	3.4	4.0
Displacement Ductility μ_Δ		
UMAT, Onset of Yielding (Confined):	3.5	4.1
(Unconfined):	1.9	2.4
75% Rule (Confined):	4.9	4.3
Conv. Curv. Ductility Factor $\mu_{1/r}$ (CCDF, EC8):	13.9	19.2
Curvature Ductility μ_Φ		
UMAT, Onset of Yielding (Confined):	12.5	16.8
75% Rule (Confined):	16.9	19.0
Tassios (1989):	9.4	11.5
Pilakoutas (1992):	17.3	21.4

Tab.5.2 Displacement and Curvature Ductility for 4 and 6-Storey Wall

In Fig.5.12 the displacement ductility for each wall was calculated with the help of the respective *load stage/deflection* response, derived by using the graphs in Fig.5.11.(b). It can be seen that the obtained ductilities are slightly higher than those computed from the *load stage/ deflection* relationships which include the shear deflections (see Fig.5.11). An explanation for this behaviour will be given in the next section where the influence of the shear deflection on the displacement ductility is investigated with a squat wall which produces a substantial amount of shear deflections.

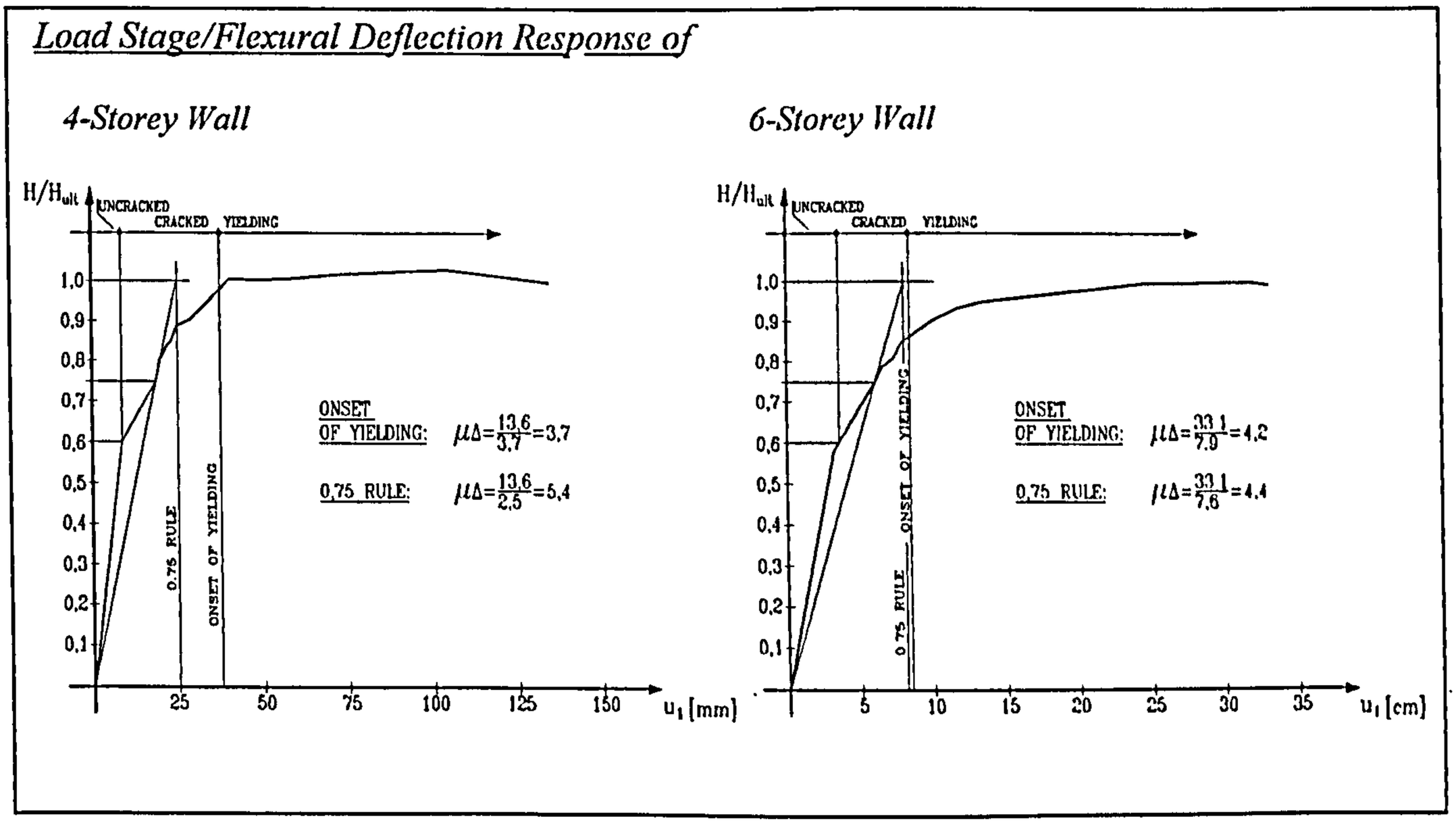

Fig.5.12 Load Stage/Flexural Deflection Response of a 4 and 6-Storey Wall

5.2.3 Analysis of a Squat 1-Storey Wall

a) Wall SW9 with Reinforcement Grid

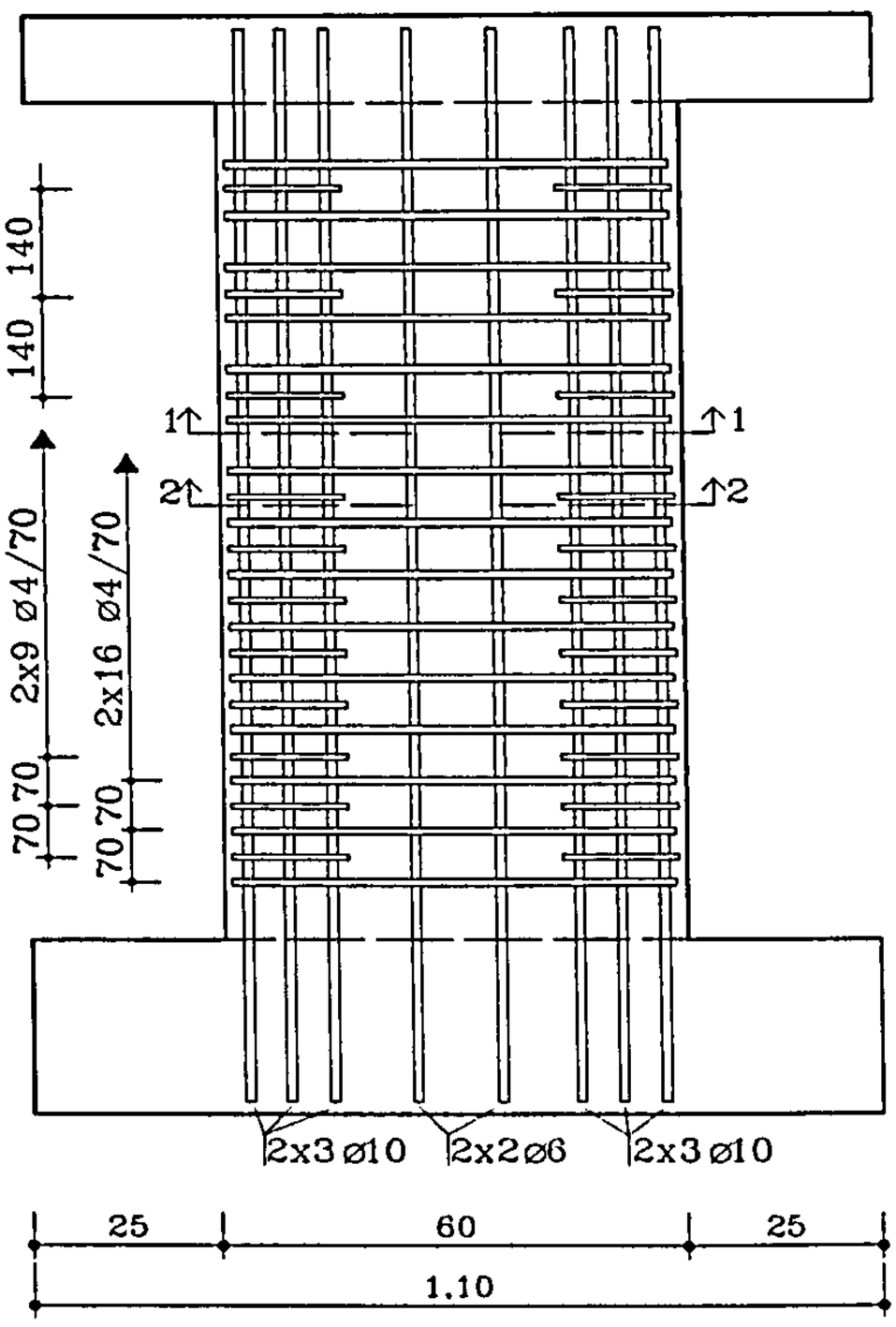

1--1

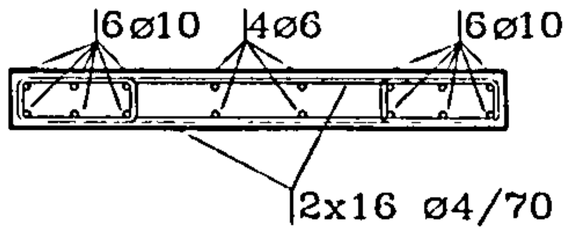

2--2

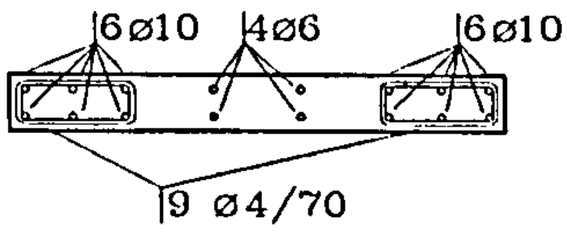

b) Discretisation and Steel Ratios

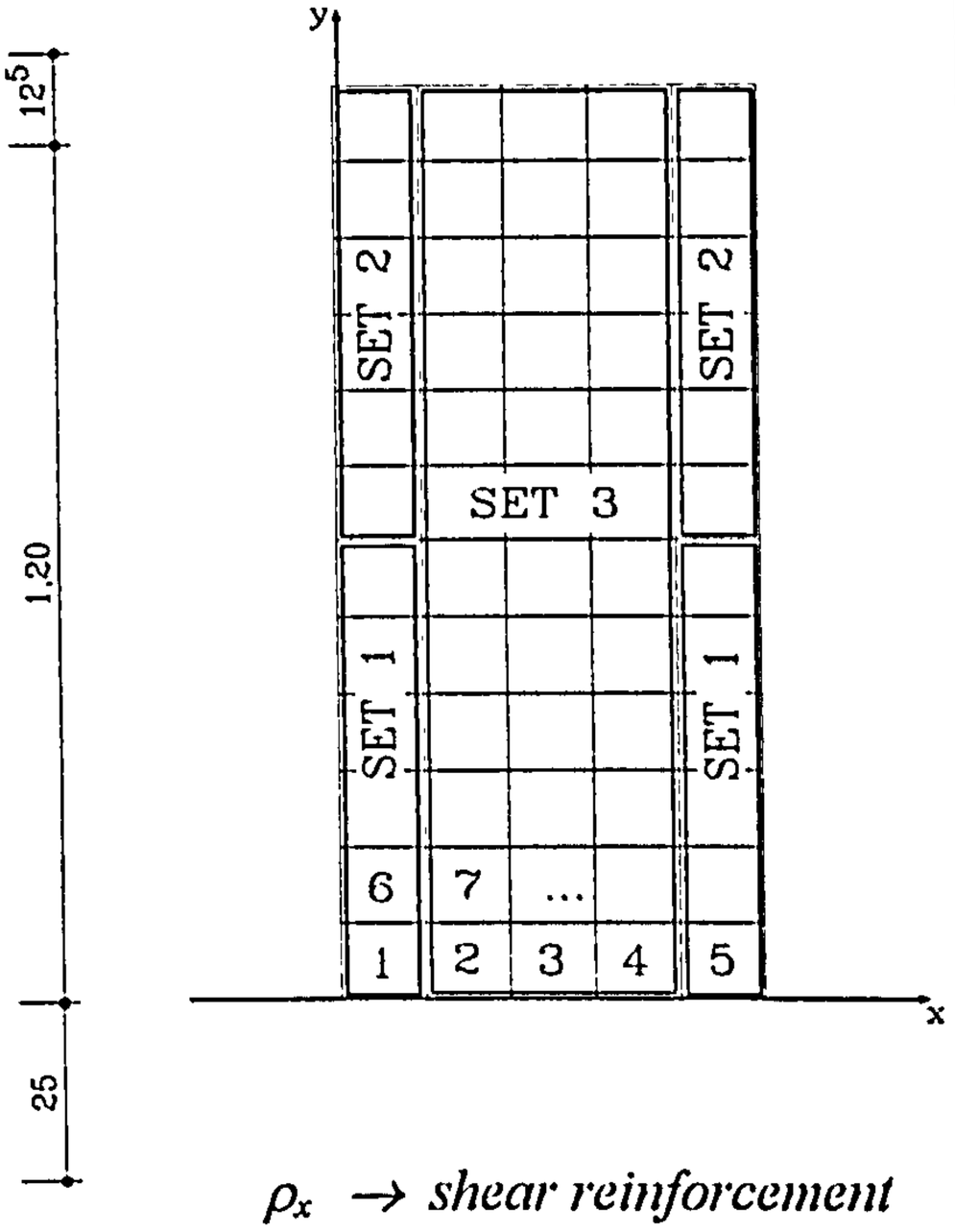

ρ_x → *shear reinforcement*
ρ_y → *longit. reinforcement*

SET 1: $\rho_x = 0.018$
$\rho_y = 0.079$

SET 2 $\rho_x = 0.009$
$\rho_y = 0.079$

SET 3 $\rho_x = 0.006$
$\rho_y = 0.0019$

c) Material Properties

Concrete strength (unconfined)	f_c	= 38.9	*MPa*
(confined)	f_{cc}	= 49	"
Concrete peak strain (unconf.)	ε_{co}	= 2.4	‰
(confined)	ε_{cc}	= 5.5	"
Steel yield strength Φ4	f_{sy}	= 400	*MPa*
Φ6	f_{sy}	= 545	"
Φ10	f_{sy}	= 430	"
Steel Young's modulus	E_s	= 200000	*MPa*
Global effectiveness of confinement	α	= 0.2	
Mechanical reinforcement ratio	ω_{wd}	= 0.35	

d) Test Results

Ultimate load H_{ult} = 97.4 *kN*
Top displacement δ_h = 22 *mm*

e) Results of Analysis

Ultimate load H_{ult} = 102.4 *kN*
Top displacement δ_h = 19 *mm*

Φ = *bar diameter of reinforcement*

Fig.5.13 Wall SW9 (Pilakoutas, 1990) with FE Discretisation and Material Properties

In 1990 a series of squat walls with aspect ratio *2* was tested by Pilakoutas at the Imperial College in London. Wall SW9 from the test series was recalculated with the UMAT and the results are presented in this section of the work.

a) Load Stage/Deflection Response

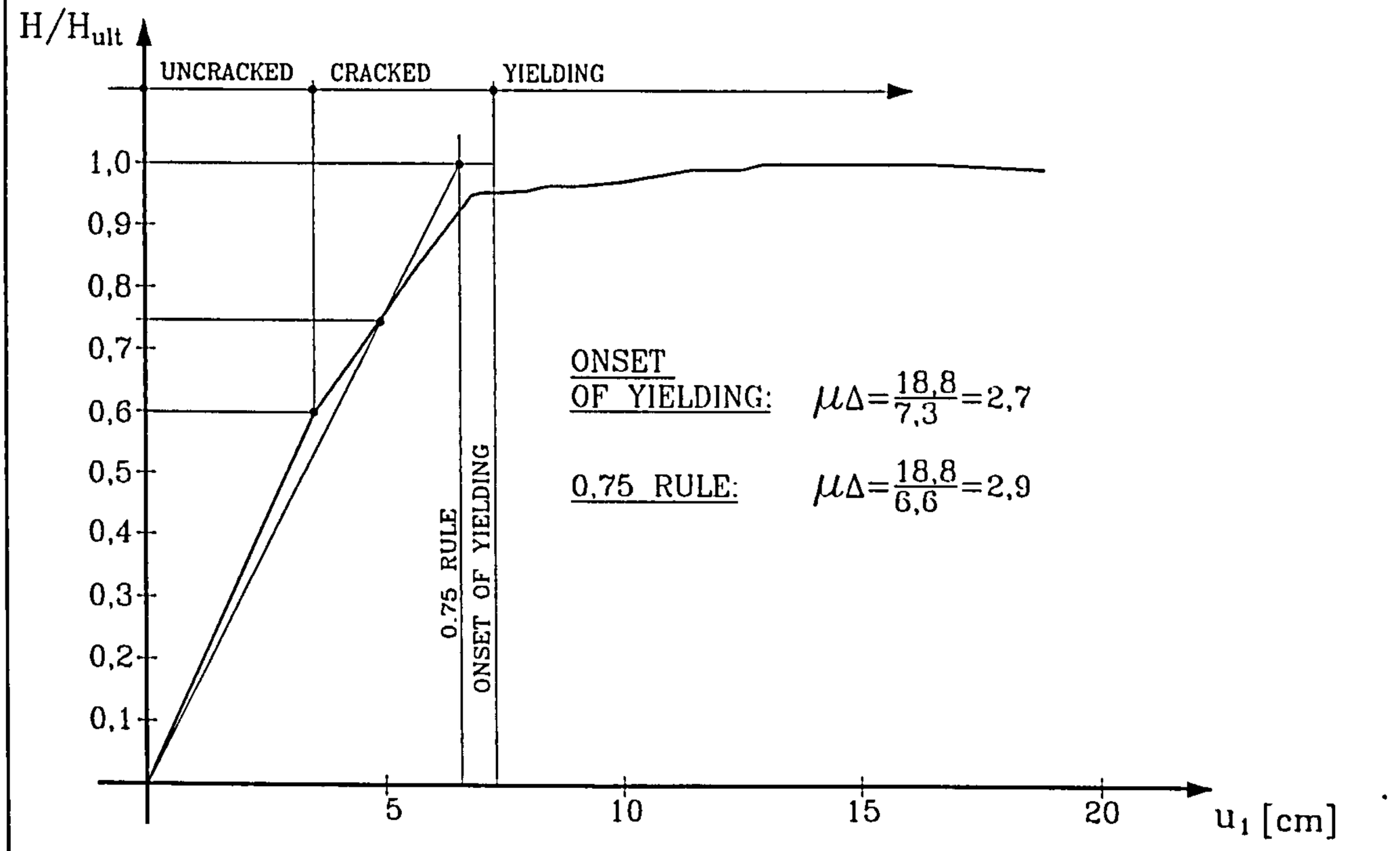

b) Normal Strain/Load Stage Response

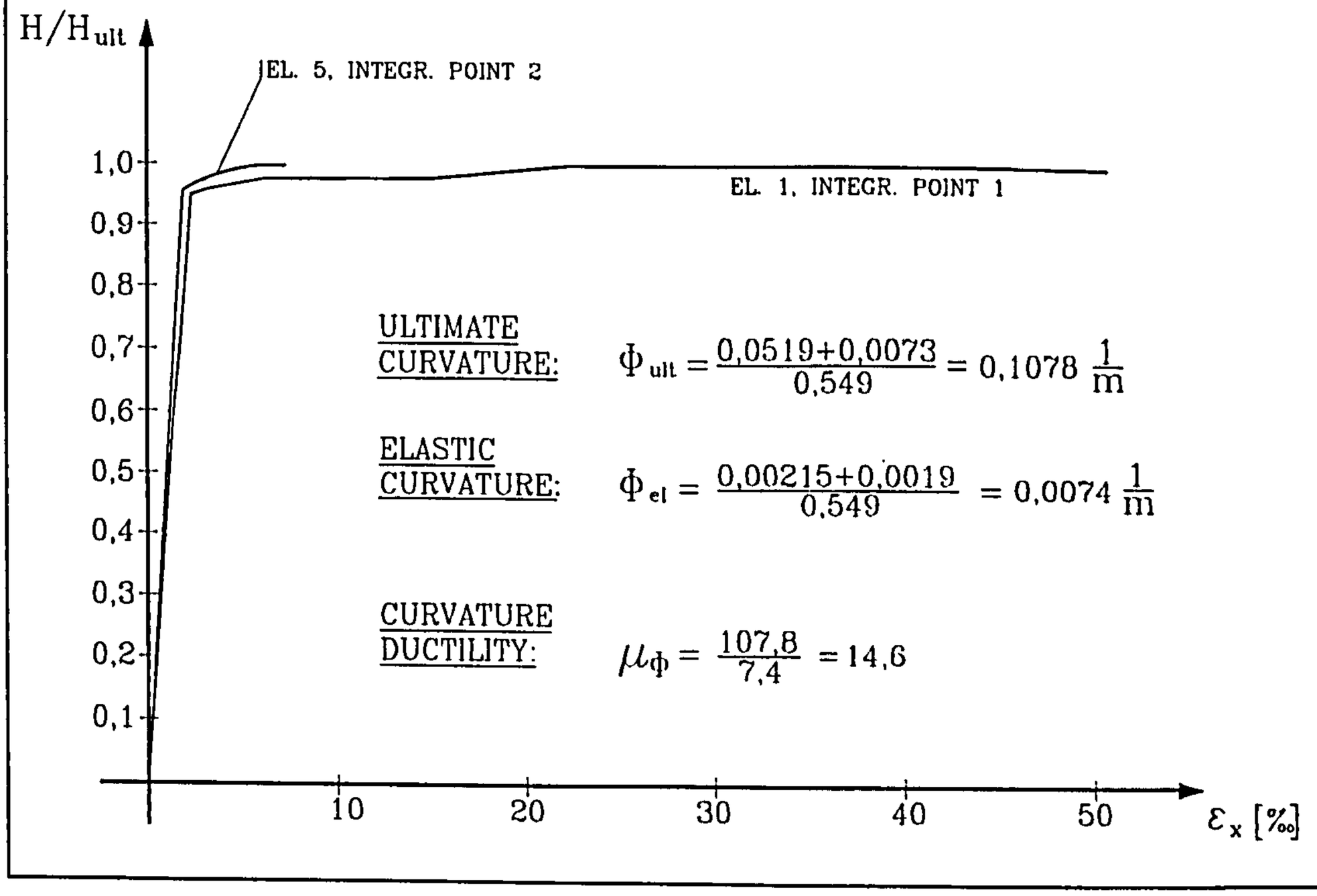

Fig.5.14 Load Stage/Deflection and Load Stage/Normal Strain Response of Wall SW9

Fig.5.13.(a) shows a redrawing of the wall with its reinforcing cage and Fig.5.13.(b) the discretisation with the steel ratios. The material properties are specified in Fig.5.13.(c) and Fig.5.13.(d) and (e) contains the ultimate load and top displacement, according to testing and ABAQUS analysis, respectively. Fig.5.14.(a) depicts the *load stage/deflection* relationship of the wall and Fig.5.14.(b) the *load stage/normal strain* response at the integration points *1* of element *1* and *2* of element *5*.

From the results of the analysis both the displacement and curvature ductility were derived as shown in Fig.5.14.(a). It can be seen that the behaviour factor q calculated from the EC8 provisions coincides with the displacement ductility μ_Δ obtained from the *load stage/deflection* response. However, the conventional curvature ductility factor (CCDF) $\mu_{\mathit{l/r}}$, calculated according to the EC8, yields too low a value compared with the UMAT results. This gives rise to the assumption that the EC8 expression for the conventional curvature ductility factor (CCDF) $\mu_{\mathit{l/r}} = 1.2\ q^2$ delivers too high values for high behaviour factors and too low values for $\mu_{\mathit{l/r}}$ once q drops significantly. Tab.5.3 reveals that the estimation of Pilakoutas confirms the results of the UMAT analysis.

	Wall SW9
Behaviour Factor q (EC8)	*2.7*
Displacement Ductility μ_Δ	
UMAT, Onset of Yielding:	*2.7*
75% Rule:	*2.9*
Convent. Curvature Ductility Factor $\mu_{\mathit{l/r}}$ *(CCDF, EC8):*	*8.8*
Curvature Ductility μ_Φ	
UMAT, Onset of Yielding:	*14.6*
Tassios (1989):	*7.0*
Pilakoutas (1992):	*12.6*

Tab.5.3 Displacement and Curvature Ductility for Wall SW9 (Pilakoutas, 1990)

Fig.5.15 depicts the relationship between the ratio of shear deflections to total deflections and the load stage. In the elastic range before cracks have started to occur δ_V/δ_T remains nearly constant at a level of approximately *15%*. After the onset of cracking at a load stage of *40%* of the ultimate limit the shear proportion of the total deflections increases and its maximum value is reached at more than *50%*, when the longitudinal reinforcement begins to yield. This happens just before the ultimate limit is reached at a load stage of *96%*. Subsequently, excessive yielding of the longitudinal steel bars increases the element energy substantially, which is connected with a perceptible drop of the shear portion of the total element energy. Fig.5.15 reveals that at the ultimate limit δ_V/δ_T decreases to approximately *30%* and the post peak yielding leads to a further drop of δ_V/δ_T.

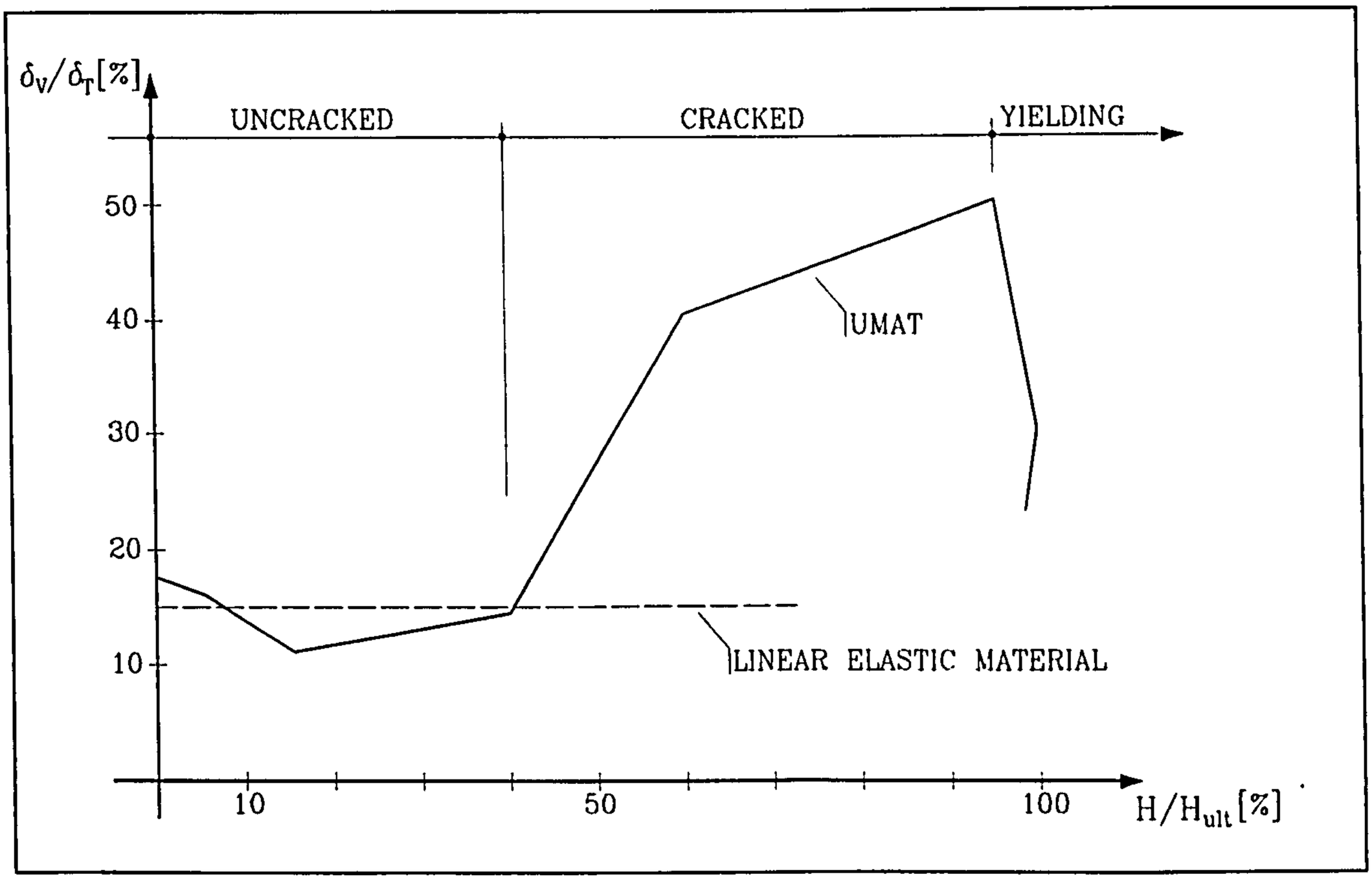

Fig.5.15 Ratio of Shear and Total Deflection versus Load Stage of Wall SW9

Finally, Fig.5.16 shows the *load stage/flexural deflection* response of wall SW9 and the displacement ductility calculated with the help of Fig.5.15. Surprisingly, μ_Δ becomes as much as *4* which is *50%* higher than the value calculated from the *load stage/deflection* response including shear deflections. The reason for this behaviour is the substantial drop of the proportion of shear to total energy triggered off by the post peak yielding of the longitudinal reinforcement. This gives evidence that in squat walls, where appreciable shear develops, a reliable investigation of the shear deformations must be included in ductility considerations, otherwise too high displacement ductilities might result from the evaluation of an analysis.

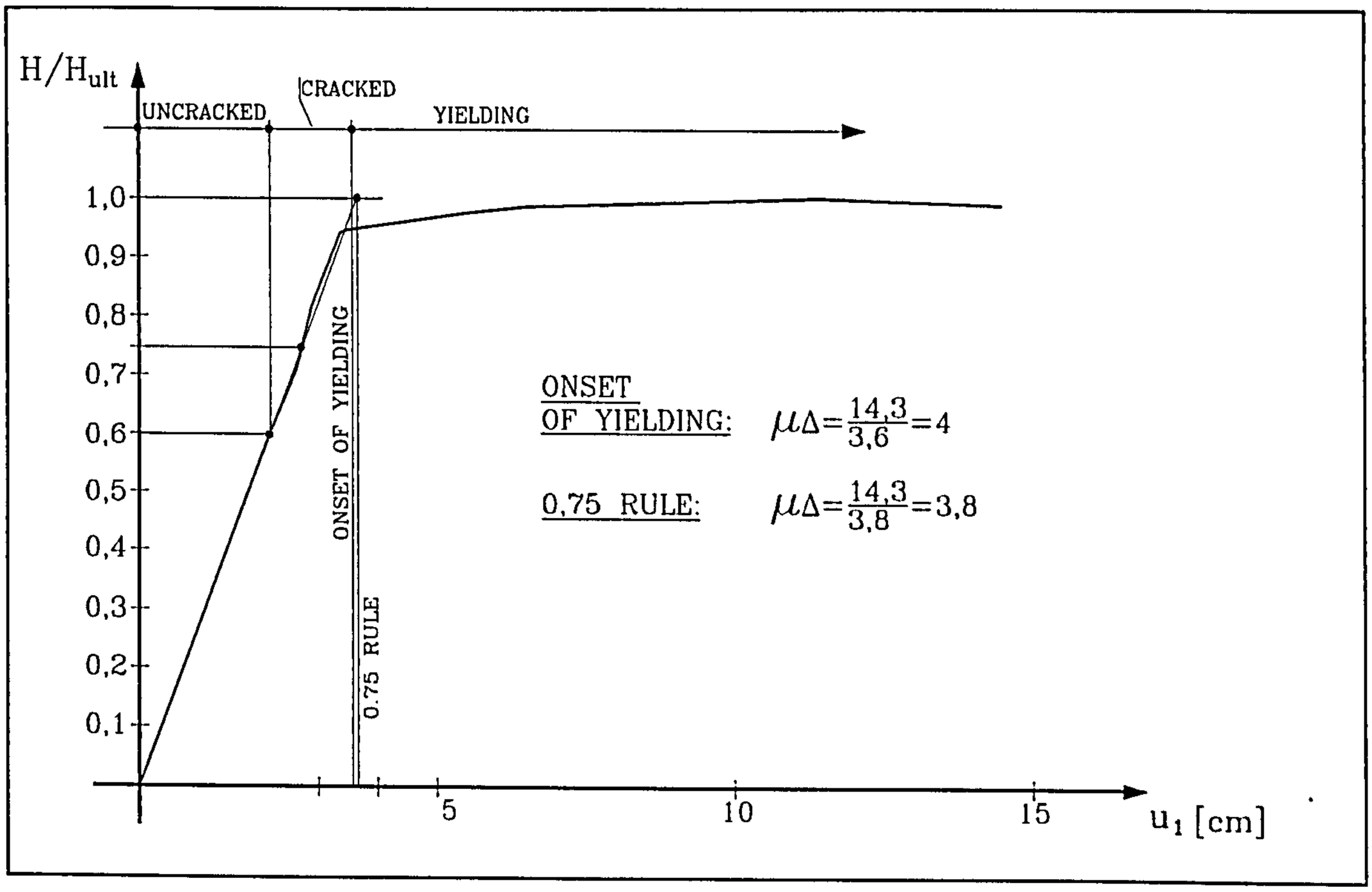

Fig.5.16 Load Stage/Flexural Deflection Response of Wall SW9 (Pilakoutas, 1990)

6 Conclusions and Further Research Work

The finite element analysis of cracked reinforced concrete structures is, up to now, essentially based on procedures which treat shear in a more general way by introducing parameters like the shear retention factor, to account for shear mechanisms such as aggregate interlock or dowel action. A rather unsatisfactory feature of this method is that nearly no guidelines are available for the application of these parameters. It is, therefore, not surprising that the literature reports values for the shear retention factor in the range of about 5‰ and more than *50%*.

It was the objective of this work to contribute to the idea of founding FE modelling of shear in RC members on a more elaborate method which complies better with the physical reality of shear behaviour identified and described, on a section analysis level, by various shear theories in the last few decades. This goal was achieved in several steps, the first of which was the review of the most important shear theories for cracked reinforced concrete. This review, summarised in the state-of-the-art report in Chapter 2, revealed merits and shortcomings and led to the modified compression field theory as a suitable shear model worth being implemented in an FE program. It was shown that the MCFT incorporates secondary shear carrying actions in an intrinsic fashion by applying a simple compatibility condition on which the MCFT is based. In addition, the assumption of a locally constant stress and strain state predestined the MCFT for its use in FE analysis.

In Chapter 3 the MCFT was extensively checked to yield satisfactory results in comparison to tests reported in the literature. To conduct these checks the section analysis program LAYER was coded which is based on a layered approach of analysing RC structures. LAYER showed a much better performance than the program SMAL provided by the authors of the MCFT. However, a modification of the material laws had to be introduced to account for the gradual loss of shear transfer in element regions mainly subjected to flexure.

In contrast to SMAL which needs the specification of reinforcement in each element, LAYER can cope with unreinforced elements, thus enhancing the versatility of the section analysis program substantially: LAYER is able to analyse RC beams without shear reinforcement.

Chapter 4 reports the development of a material subroutine which is based on the MCFT including the aforementioned modification on the tensile side of the material laws. The UMAT was tested in great detail by recalculating many tests described in the literature. It revealed in all cases a much better performance than the ABAQUS Standard options for cracked reinforced concrete, the shear behaviour of which is essentially based on the well-known parameters like the shear retention factor.

In Chapter 5 the UMAT was utilised for investigations on ductility. The surprising result is that ductility calculations essentially based on flexural deflections deliver μ_Δ values, which are higher than those derived from calculations including shear deflections. In capacity designed structural walls, detailed according to the provisions of the EC8 and having an aspect ratio well above *2.5* with a flexural type of failure, this difference is less than *10%* and might be negligible. However, squat walls with aspect ratios of less than *2.5* can develop shear deflections of more than *50%* of the total value. In this case, the displacement ductility of the structure is strongly influenced by the shear deflections which must be evaluated in a reliable fashion.

With the newly developed UMAT an analysis tool for the reliable calculation of cracked reinforced concrete structures is now available to be used together with the highly recognised commercial FE program ABAQUS.

The material laws of the MCFT were derived from extensive testing on shear panels. It is obvious that this restricts to some extent their performance concerning structures with distinct flexural behaviour. Therefore, a modification on the tensile side of the material model was introduced which greatly improved the performance of the UMAT. However, it is desirable to calibrate the material laws on a more comprehensive selection of available test data. It is expected that this measure, together with an extension to dynamic cyclic, path dependent loading, would further improve the capabilities of finite element analyses of cracked reinforced concrete with UMAT and ABAQUS.

References

ABAQUS, 1994, 'User's Manual', Version 5.4, Hibbitt, Karlsson and Sorensen, Pawtucket, USA

ASCE, 1993, 'Finite Element Analysis of Reinforced Concrete Structures II', Isenberg

Bathe, K.-J., 1982, 'Finite Element Procedures in Engineering Analysis', Prentice Hall, Englewood Cliffs/NJ, USA

Baumann, T. and Rüsch, H., 1970, 'Versuche zum Studium der Verdübelungswirkung der Biegezugbewehrung eines Stahlbetonbalkens (Tests and Investigations on Dowel Action of Flexural Reinforcement in RC Beams)', Deutscher Ausschuß für Stahlbeton, Heft 210, Berlin

Bažant , Z.P. and Oh, B.H., 1983, 'Crack Band Theory for Fracture of Concrete', Materials and Structures/Research and Testing (RILEM, Paris), Vol.16, No.93, pp. 155-177

Bhide, S.B. and Collins, M.P., 1987, 'Reinforced Concrete Elements in Shear and Torsion', University of Toronto, Department of Civil Engineering, Publication No. 87-02

Chen, W.F., 1982, 'Plasticity in Reinforced Concrete', McGraw-Hill, USA

Collins, M.P., 1978, 'Towards a Rational Theory for RC Members in Shear', Journal of the Struct. Division, ASCE, Vol. 104, pp. 649-666

Collins, M.P. and Michell, D., 1980, 'Shear and Torsion of Prestressed and Non-Prestressed Concrete Beams', PCI Journal, pp. 32-100

Crisfield, M.A. and Wills, J., 1989, 'Analysis of RC Panels Using Different Concrete Models', Journal of Eng. Mechanics, ASCE , Vol. 115, pp. 578-597

Darwin, D. and Pecknold, D.A., 1976, 'Analysis of RC Shear Panels under Cyclic Loading', Journal of the Struct. Division, ASCE, Vol. 102, pp. 355-369

Dilger, W., 1966, 'Veränderlichkeit der Biege- und Schubsteifigkeit bei Stahlbetontragwerken und ihr Einfluß auf Schnittkraftverteilung und Traglast bei statisch unbestimmter Lagerung (Variation of Flexural and Shear Stiffness in RC Members and their Influence on Section Forces and Ultimate Resistance)', Deutscher Ausschuß für Stahlbeton, Heft 179, Berlin

Eurocode No.8, 1993, 'Earthquake Resistant Design of Structures', Part 1, General Rules, 2nd Draft, Report CEN/TC250/SC8

Feenstra, P.H. and de Borst, R., 1993, 'Aspects of Robust Computational Modeling for Plain and Reinforced Concrete', Heron, Vol. 38, No. 4, Delft University of Technology

Fenwick, R.C. and Paulay, T., 1968, 'Mechanisms of Shear Resistance of Concrete Beams', Journal of the Struct. Division, ASCE, Vol. 94, pp. 2325-2350

Frangou, M. and Pilakoutas, K., 1994, 'Strengthening of RC Columns by Lateral Tensioning', Proceedings of the Second Conference on Earthquake Resistant Construction and Design, DGEB-Publication No.8, Balkema, Rotterdam, pp. 841-848

Grob, J. and Thürlimann, B., 1976, 'Ultimate Strength and Design of Reinforced Concrete Beams under Bending and Shear', IABSE Mémoires, Vol. 36-II, pp. 105-120

Haas, M., 1993, 'Erdbebenberechnung von Stahlbeton-Tragwandsystemen nach verschiedenen Verfahren (Earthquake Resistant Design of RC Wall Systems according to Various Approaches)', Postgraduate Thesis, Swiss Federal Institute of Technology (ETH), Zurich

Haas, M. and Pilakoutas, K., 1994, 'Design of Reinforced Concrete Walls', Proceedings of the Second Conference on Earthquake Resistant Construction and Design, DGEB-Publication No.8, Balkema, Rotterdam, pp. 889-896

Haas, M. and Pilakoutas, K., 1995, 'Effect of Shear Deflections on the Ductility of RC Structures', Proceedings of the Fifth SECED Conference on European Seismic Design Practice, Balkema, Rotterdam, pp. 359-366

Hamadi, Y.D. and Regan, P.E., 1980, 'Behaviour in Shear of Beams with Flexural Cracks', Magazine of Concrete Research, Vol. 32, pp. 67-78

Hu, H. and Schnobrich, W.C., 1990, 'Non-Linear Analysis of Cracked Reinforced Concrete', ACI Struct. Journal, Vol. 87, pp. 199-207

Kani, G.N.J., 1964, 'The Riddle of Shear Failure and its Solution', ACI Journal, Vol. 61, pp. 441-467

Kani, G.N.J., 1967, 'How Safe are our Large Reinforced Concrete Beams?', ACI Journal, Vol. 64, pp. 128-141

Kirmair, H., 1987, 'Das Schubverhalten schlanker Stahlbetonbalken - Theoretische und experimentelle Untersuchungen für Leicht- und Normalbeton (Shear Behaviour of Slender RC Beams - Theoretical and Experimental Investigations on Normal and Light-Weight Concrete)', Deutscher Ausschuß für Stahlbeton, Heft 385, Berlin

Kirmair, H. and Mang, R., 1987, 'Das Tragverhalten der Schubzone schlanker Stahlbeton- und Spannbetonträger bei Biegung mit Längskraft (Response of the Shear Zone of Slender Reinforced and Prestressed Concrete Girders Subjected to Flexure and Axial Load)', Bauingenieur, Vol. 62, pp. 165-170

Kollegger, J. and Mehlhorn, G., 1990, 'Experimentelle Untersuchungen zur Bestimmung der Druckfestigkeit des gerissenen Stahlbetons bei einer Querbeanspruchung (Experimental Investigations on the Strength of Concrete Subjected to Lateral Load)', Deutscher Ausschuß für Stahlbeton, Heft 413, Berlin

Kotsovos, M.D., 1980, 'A Mathematical Model of the Deformational Behaviour of Concrete under Generalised Stress Based on Fundamental Material Properties', Materials and Structures/Research and Testing (RILEM, Paris), Vol.13, No.76, pp. 289-298

Kupfer, H.B. and Gerstle, K.H., 1973, 'Behaviour of Concrete under Biaxial Stresses', Journal of the Eng. Mechanics Division, ASCE, Vol. 99, pp. 852-866

Kupfer, H., Mang, R. and Karavesyroglou, M., 1983, 'Bruchzustand der Schubzone von Stahlbeton- und Spannbetonträgern - Eine Analyse unter Berücksichtigung der Rißverzahnung (Ultimate Limit State of the Shear Zone of Reinforced and Prestressed Concrete Girders - An Analysis Taking the Aggregate Interlock into account', Bauingenieur, Vol. 58, pp. 143-149

Leibengood, L.D., Darwin, D. and Dodds, R.H., 1986, 'Parameters Affecting FE Analysis of Concrete Structures', Journal of Struct. Engineering, ASCE, Vol 112, pp. 326-341

Leonhardt, F. and Walther, R., 1962, 'Versuche an Plattenbalken mit hoher Schubbeanspruchung (Tests on RC Girders subjected to High Shear)', Deutscher Ausschuß für Stahlbeton, Heft 152, Berlin

Leonhardt, F. and Walther, R., 1964, 'The Stuttgart Shear Tests, 1961', Translation 111, Cement and Concrete Association, London

Linde, P., 1993, 'Numerical Modelling and Capacity Design of Earthquake-Resistant Reinforced Concrete Walls', PhD Thesis, Swiss Federal Institute of Technology (ETH), Zurich

Ngo, D. and Scordelis, A.C., 1967, 'Finite Element Analysis of Reinforcement Concrete Beams', ACI Journal, Vol. 64, pp. 152-163

Nielsen, M.P., 1984, 'Limit Analysis and Concrete Plasticity', Prentice Hall, Englewood Cliffs, New Jersey

Nielsen, M.P., Braestrup, M.W. and Bach, F., 1978, 'Rational Analysis of Shear in Reinforced Concrete Beams', IABSE Proceedings, P-15/78, pp. 1-16

Nilson, A.H., 1968, 'Non-Linear Analysis of Reinforced Concrete by the Finite Element Method', ACI-Journal, pp. 757-766

Paulay, T. and Priestley, M.J.N., 1992, 'Seismic Design of Reinforced Concrete and Masonry Buildings', John Wiley and Sons, New York

Pilakoutas, K., 1990, 'Earthquake Resistant Design of Reinforced Concrete Walls', PhD Thesis, University of London

Pilakoutas, K. and Elnashai, A.S., 1991, 'Seismic Design of Ductile RC Members', International Conference on Earthquake, Blast and Impact, SECED, Manchester, pp. 510-519

Pilakoutas, K. and Haas, M., 1994, 'Ductility Design of Reinforced Concrete Members', Proceedings of the Second Conference on Earthquake Resistant Construction and Design, DGEB-Publication No.8, Balkema, Rotterdam, pp. 897-904

Placas, A. and Regan, P.E., 1971, 'Shear Failure of Reinforced Concrete Beams', ACI Journal, Vol. 68, pp. 763-773

Rashid, Y.R., 1968, 'Analysis of Prestressed Concrete Pressure Vessels', Nuclear Eng. and Design, pp. 334-344

Reinhardt, H.-W., 1981, 'Maßstabseinfluß bei Schubversuchen im Licht der Bruchmechanik (Size Effect in the Light of Fracture Mechanics)', Beton und Srahlbetonbau, Vol. 76, pp. 19-21

Reineck, K.-H., 1990, 'Ein Mechanisches Modell für den Querkraftbereich von Stahlbetonbauteilen (A Mechanical Model for the Shear Span of RC Members)', PhD Thesis, University of Stuttgart.

Reineck, K.-H., 1991. 'Ultimate Shear Force of Structural Members without Transverse Reinforcement Derived from a Mechanical Model', ACI Struct. Journal, pp. 592-602

Rots, J.G. and de Borst, R., 1987, 'Analysis of Mixed-Mode Fracture in Concrete', Journal of Eng. Mechanics, ASCE, Vol. 113, pp. 1739-1758

Rüsch, H. and Mayer, H., 1967, '5 Versuche zum Studium der Verformungen im Querkraftbereich eines Stahlbetonbalkens (5 Tests for the Investigation of Deformations in the Shear Span of RC Beams)', Deutscher Ausschuß für Stahlbeton, Heft 195, Berlin

Saenz, L.P., 1964, 'Equation for the Stress-Strain Curve of Concrete', ACI Journal, Vol. 61, pp. 1227-1239

Schlaich, J., Schäfer, K. and Jennewein, M., 1987, 'Toward a Consistent Design of Structural Concrete', PCI Journal, Vol. 32, No. 3, pp. 74-150

Schleeh, W., 1973, 'Die Ausbreitung der Einzellast in einem Biegeträger (The Influence of a Concentrated Load on a Beam under Flexure)', Beton und Stahlbetonbau, Vol. 68, pp. 39-43

Stempniewski, L. 1990, 'Flüssigkeitsgefüllte Stahlbetonbehälter unter Erdbebeneinwirkung (RC Containers Filled with Liquid Subjected to Seismic Loads)', PhD Thesis, University of Karlsruhe

Stevens, N.J., Uzumeri, S.M. and Collins, M.P., 1987, 'Analytical Modelling of Reinforced Concrete Subjected to Monotonic and Reversed Loadings', University of Toronto, Department of Civil Engineering, Publication No. 87-01

Stevens, N.J., Uzumeri, S.M., Collins, M.P. and Will, G.T., 1991, 'Constitutive Model for Reinforced Concrete Finite Element Analysis', ACI Struct. Journal, Vol. 88, pp. 49-59

Thürlimann, B., 1989, 'Design and Detailing of Reinforced Concrete Structures Using Stress Fields', Swiss Federal Institute of Technology, Zürich

Tassios, T.P., 1989, 'Specific Rules for Concrete Structures', Background Document for Eurocode 8, Part 1, Volume 2, Design Rules, Commission of European Communities, pp. 1-123

van Mier, J.G.M., 1987, 'Examples of Non-linear Analysis of RC Structures with DIANA', Heron, Vol. 32, No. 3, Delft University of Technology

Vecchio, F.J. and Collins, M.P., 1982, 'The Response of Reinforced Concrete to In-plane Shear and Normal Stresses', University of Toronto, Department of Civil Engineering, Publication No 82-03

Vecchio, F.J. and Collins, M.P., 1986, 'The Modified Compression Field Theory for Reinforced Concrete Elements Subjected to Shear', ACI Journal, Vol. 83, pp. 219-231

Vecchio, F.J. and Collins, M.P., 1988, 'Predicting the Response of Reinforced Concrete Beams Subjected to Shear Using Modified Compression Field Theory', ACI Struct. Journal, Vol. 85, pp. 258-268

Vintzeleou, E. and Tassios, T., 1986, 'Mathematical Models for Dowel Action under Monotonic Conditions', Magazine of Concrete Research, Vol. 38, pp. 13-22

Walther, R., 1964, 'Calculation of the Shear Strength of Reinforced and Prestressed Concrete Beams by the Shear Failure Theory', Translation 110, Cement and Concrete Association, London

Walraven, J.C., 1981, 'Fundamental Analysis of Aggregate Interlock', Journal of the Struct. Division, ASCE, Vol. 107, pp. 2245-2270

Walraven, J. and Lehwalter, N., 1990, 'Einfluß des Maßstabs in schubbeanspruchten Bauteilen ohne Schubbewehrung (Size Effect in Plain Concrete Members Subjected to Shear), Beton und Stahlbetonbau, Vol. 85, pp. 228-232

Wawrzynek, P. and Ingraffea, A.R., 1987, 'Interactive Finite Element Analysis of Fracture Processes: An Integrated Approach', Theoretical and Appl. Fracture Mech., Vol. 8, pp. 715-732

Zienkiewicz, O.C. and Taylor, R.L., 1991, 'The Finite Element Method', Volume 2, McGraw-Hill Europe, Maidenhead, England

Appendix A: Fortran Code for UMAT

```
      SUBROUTINE UMAT (STRESS, STATEV, DDSDDE, SE, SPD, SCD, RPL,
     & DDSDDT,DRPLDE, DRPLDT, STRAN, DSTRAN, TIME, DTIME, TEMP,
     & DTEMP, PREDEF, DPRED, CMNAME, NDI,NSHR, NTENS, NSTATV,
     & PROPS, NPROPS, COORDS, DROT, PNEWDT, CELENT, DFGRD0,
     & DFGRD1, NOEL, NPT, LAYER, KSPT, KSTEP, KINC)
C
      INCLUDE 'ABA_PARAM.INC'
C
      CHARACTER*8 CMNAME
C
      INTEGER*4 NTENS,NDI,K1,K2
C
      REAL*8 EMOD, ENU, EFAK, EG2, EG, A, B, C, A1, B1, C1, PHI, FC,
     & SIGCRACK, FACTOR, SIGCMAX, ECONCR, FACT2, MAXEPS,
     & PSIG, SIGSX, SIGSY, ESTEEL, EZERO, RHOX, RHOY, E1, E2, Z1, Z2,
     & N1, N2, N3, N4, EYIELDX, EYIELDY,
     & E11, E12, E13, E21, E22, E23, E31, E32, E33
C
      DIMENSION STRESS(NTENS), STATEV(NSTATV),
     & DDSDDE(NTENS,NTENS), DDSDDT(NTENS), DRPLDE(NTENS),
     & STRAN(NTENS), DSTRAN(NTENS), TIME(2), PREDEF(1), DPRED(1),
     & PROPS(NPROPS), COORDS(3), DROT(3,3), DFGRD0(3,3), DFGRD1(3,3)
C
C  LOCAL ARRAYS
C
      DIMENSION PEPS(2), PSIGC(3), ES(2), T(3,3), TT(3,3), TR(3,3),
     & STR(3), D(3,3),SIGC(3)
C
      PARAMETER (ZERO=0.D0, ONE=1.D0, TWO=2.D0, THREE=3.D0,
     & FOUR=4.D0, SIX=6.D0, PI=3.14159265359)
C
C  PROPERTIES
C
C  PROPS(1)      EMODUL CONCRETE (2*FC/EZERO)
C  PROPS(2)      EZERO (CONCRETE STRAIN AT PEAK COMPR. STRESS)
C  PROPS(3)      FC (CONCRETE STRENGTH)
C  PROPS(4)      SIGMA_CRACK
C  PROPS(5)      EMODUL STEEL
C  PROPS(6)      RHO_X (REINFORCEMENT RATIO)
C  PROPS(7)      RHO_Y (REINFORCEMENT RATIO)
C  PROPS(8)      FACTOR
C  PROPS(9)      EYIELDX (STEEL STRAIN AT YIELD ONSET, X-DIR.)
C  PROPS(10)     EYIELDY (STEEL STRAIN AT YIELD ONSET, Y-DIR.)
C  PROPS(11)     FACT2
```

```
C  TOTAL STRAIN INCREMENT
C
        DSTRAN(1)=DSTRAN(1)+STRAN(1)
        DSTRAN(2)=DSTRAN(2)+STRAN(2)
        DSTRAN(3)=DSTRAN(3)+STRAN(3)
C
C  ELASTIC PROPERTIES
C
        EMOD=PROPS(1)
        EZERO=PROPS(2)
        EFAK=EMOD/(ONE-ENU**TWO)
        EG2=EMOD/(ONE+ENU)
        EG=EG2/TWO
        EYIELDX=PROPS(9)
        EYIELDY=PROPS(10)
        FACT2=PROPS(11)
        PSIGC(3)=0.D0
        ENU=0.D0
C
C  STATE VARIABLES
C
        STATEV(16)=DSTRAN(1)
        STATEV(17)=DSTRAN(2)
        STATEV(18)=DSTRAN(3)
C
        STATEV(19)=STRAN(1)
        STATEV(20)=STRAN(2)
        STATEV(21)=STRAN(3)
C

C  ELASTIC STIFFNESS
C
        CALL ASET(DDSDDE, ZERO, NTENS*NTENS)
C
C
        DO K1=1,NDI
                DO K2=1,NDI
                        DDSDDE(K2,K1)=EFAK*ENU
                END DO
                DDSDDE(K1,K1)=EFAK
        END DO
        DO K1=NDI+1,NTENS
                DDSDDE(K1,K1)=EG
        END DO
C
```

```
C  PRINCIPAL VALUES FOR DSTRAN AND CRACK DIRECTION PHI
C
      IF(DSTRAN(1).EQ.ZERO.AND.DSTRAN(2).EQ.ZERO.
     &                  AND.DSTRAN(3).EQ.ZERO) THEN
            GOTO 10
      ELSE
C
            IF(DSTRAN(1).EQ.ZERO.AND.DSTRAN(2).EQ.ZERO) THEN
                  PEPS(1)= 0.5*DSTRAN(3)
                  PEPS(2)=-0.5*DSTRAN(3)
                  PHI=45.*PI/180.
            ELSE
C
                  A1=(DSTRAN(1)+DSTRAN(2))/TWO
                  B1=-DSTRAN(1)*DSTRAN(2)+
     &                  ONE/FOUR*DSTRAN(3)**TWO
C
                  IF(DSTRAN(1).EQ.DSTRAN(2)) THEN
                        PHI=45.*PI/180.
                  ELSE
                        C1=DSTRAN(3)/(DSTRAN(1)-DSTRAN(2))
                        PHI=ONE/TWO*ATAN(C1)
                  ENDIF
C
                  IF(A1**TWO+B1.LT.ZERO) THEN
                        WRITE(6,*)'A1**TWO+B1=NEG.',
     &                              A1**TWO+B1
                        PEPS(1)=A1
                        PEPS(2)=A1
                  ELSE
C
C
                        IF(DSTRAN(2).GT.DSTRAN(1)) THEN
                              PEPS(1)=A1-SQRT(A1**TWO+B1)
                              PEPS(2)=A1+SQRT(A1**TWO+B1)
                        ELSE
                              PEPS(1)=A1+SQRT(A1**TWO+B1)
                              PEPS(2)=A1-SQRT(A1**TWO+B1)
                        ENDIF
C
                              ENDIF
C
                  ENDIF
C
            STATEV(4)=PHI*180./PI
C
```

```
C   CALCULATE PRINCIPAL CONCRETE STRESSES
C
                FC=PROPS(3)
                SIGCRACK=PROPS(4)
                FACTOR=PROPS(8)
                SIGCMAX=FC
C
                IF(PEPS(1).LT.ZERO) THEN
                        SIGCMAX= FC/(0.8-FACT2*PEPS(2)/EZERO)
C
                        IF(SIGCMAX.LT.FC) THEN
                                SIGCMAX=FC
                        ENDIF
C
                        IF(PEPS(1).LT.TWO*EZERO) THEN
                                PSIGC(1)=ZERO
                        ELSE
                                PSIGC(1)=SIGCMAX*(2*PEPS(1)/EZERO-
     &                                  (PEPS(1)/EZERO)**TWO)
                        ENDIF
C
                ENDIF
C
                IF(PEPS(2).LT.ZERO) THEN
                        SIGCMAX= FC/(0.8-FACT2*PEPS(1)/EZERO)
C
                        IF(SIGCMAX.LT.FC) THEN
                                SIGCMAX=FC
                        ENDIF
C
                        IF(PEPS(2).LT.TWO*EZERO) THEN
                                PSIGC(2)=ZERO
                        ELSE
                                PSIGC(2)=SIGCMAX*(TWO*PEPS(2)/EZERO-
     &                                  (PEPS(2)/EZERO)**TWO)
                        ENDIF
C
                ENDIF
C
```

```
                IF(PEPS(1).GT.ZERO) THEN
C
                        ECONCR=TWO*FC/EZERO
                        EPSCRACK= SIGCRACK/ECONCR
C
C
                        IF(PEPS(1).LE.EPSCRACK) THEN
                                PSIGC(1)=PEPS(1)*ECONCR
                        ELSE
                                PSIGC(1)=SIGCRACK/(ONE+SQRT((PEPS(1)-
     &                                  EPSCRACK)*FACTOR))
                        ENDIF
C
                        IF(PEPS(1).GT.0.004) THEN
                                PSIGC(1)=0.D
                        ENDIF
C
                        PSIG=SIGCRACK/(ONE+SQRT((0.002-
     &                          EPSCRACK)*FACTOR))
C
                        IF(PEPS(1).GT.0.002.AND.PEPS(1).LE.0.004) THEN
                                PSIGC(1)=PSIG*(0.004-PEPS(1))/0.002
                        ENDIF
C
                ENDIF
C
                IF(PEPS(2).GT.ZERO) THEN
C
                        ECONCR=TWO*FC/EZERO
                        EPSCRACK= SIGCRACK/ECONCR
C
C
                        IF(PEPS(2).LE.EPSCRACK) THEN
                                PSIGC(2)=PEPS(2)*ECONCR
                        ELSE
                                PSIGC(2)=SIGCRACK/(ONE+SQRT((PEPS(2)-
     &                                  EPSCRACK)*FACTOR))
                        ENDIF
C
                        IF(PEPS(2).GT.0.004) THEN
                                PSIGC(2)=0.D
                        ENDIF
C
                        PSIG=SIGCRACK/(ONE+SQRT((0.002-
     &                          EPSCRACK)*FACTOR))
C
                        IF(PEPS(2).GT.0.002.AND.PEPS(2).LE.0.004) THEN
                                PSIGC(2)=PSIG*(0.004-PEPS(2))/0.002
                        ENDIF
C
                ENDIF
```

```
                STATEV(5)=PSIGC(1)
                STATEV(6)=PSIGC(2)
                STATEV(7)=SIGCMAX
C
C  ROTATE PRINCIPAL CONCRETE STRESSES IN XY-DIRECTIONS
C
                TR(1,1)=COS(-PHI)**TWO
                TR(1,2)=SIN(-PHI)**TWO
                TR(1,3)=TWO*COS(-PHI)*SIN(-PHI)
                TR(2,1)=SIN(-PHI)**TWO
                TR(2,2)=COS(-PHI)**TWO
                TR(2,3)=-TWO*COS(-PHI)*SIN(-PHI)
                TR(3,1)=-COS(-PHI)*SIN(-PHI)
                TR(3,2)=COS(-PHI)*SIN(-PHI)
                TR(3,3)=COS(-PHI)**TWO-SIN(-PHI)**TWO
C
                DO K1=1,NTENS
                        R=ZERO
                        DO K2=1,NTENS
                                R=R+TR(K1,K2)*PSIGC(K2)
                        ENDDO
                        SIGC(K1)=R
                ENDDO
C
                STATEV(8)=SIGC(1)
                STATEV(9)=SIGC(2)
                STATEV(10)=SIGC(3)
C
C  CALCULATE STEEL STRESSES
C
                ESTEEL=PROPS(5)
C
                SIGSX=ESTEEL*DSTRAN(1)
                SIGSY=ESTEEL*DSTRAN(2)
C
                IF(SIGSX.GT.EYIELDX*ESTEEL) THEN
                        SIGSX=EYIELDX*ESTEEL
                ENDIF
C
                IF(SIGSY.GT.EYIELDY*ESTEEL) THEN
                        SIGSY=EYIELDY*ESTEEL
                ENDIF
C
                IF(SIGSX.LT.-EYIELDX*ESTEEL) THEN
                        SIGSX=-EYIELDX*ESTEEL
                ENDIF
C
                IF(SIGSY.LT.-EYIELDY*ESTEEL) THEN
                        SIGSY=-EYIELDY*ESTEEL
                ENDIF
C
```

```
            STATEV(11)=SIGSX
            STATEV(12)=SIGSY
C
C  CALCULATE RC STRESSES
C
            RHOX=PROPS(6)
            RHOY=PROPS(7)
C
            STRESS(1)=SIGC(1)+RHOX*SIGSX
            STRESS(2)=SIGC(2)+RHOY*SIGSY
            STRESS(3)=SIGC(3)
C
              STATEV(13)=STRESS(1)
              STATEV(14)=STRESS(2)
              STATEV(15)=STRESS(3)
              STATEV(16)=EPSCRACK
C
C  CALCULATION OF STRESS ENERGY AT EACH INTEGRATION POINT
C
              DO K1=1,NTENS
                    STATEV(K1)=DSTRAN(K1)*STRESS(K1)
              ENDDO
C
C  CALCULATE JACOBIAN FOR CONCRETE IN PRINCIPAL DIRECTIONS
C
C       CASE NR 1 :  THE PRINCIPAL CONCRETE STRESSES PSIGC(I) ARE
C                    BOTH NEGATIVE=COMPRESSION.
C
                IF(PEPS(1).LT.ZERO.AND.PEPS(2).LT.ZERO) THEN
C
                      E11=2*FC/EZERO-2*FC*PEPS(1)/EZERO**2
                      E12=0.0D
                      E13=0.0D
                      E21=0.0D
                      E22=2*FC/EZERO-2*FC*PEPS(2)/EZERO**2
                      E23=0.0D
                      E31=0.0D
                      E32=0.0D
                      E33=(PSIGC(1)-PSIGC(2))/(2*(PEPS(1)-PEPS(2)))
C
                ENDIF
C
```

```
C       CASE NR 2A:THE PRINCIPAL CONCRETE STRESS PSIGC(1) IS
C                  POSITIVE=TENSION BUT THE PRINCIPAL CONCRETE
C                  STRESS PSIGC(2) IS NEGATIVE=COMPRESSION.
C                  HOWEVER,THE PRINCIPAL TENSION STRAIN PEPS(1) IS
C                  LESS THAN THE CRACKING STRAIN EPSCRACK
C
            IF(PEPS(1).GT.ZERO.AND.PEPS(2).LT.ZERO.AND.
     &                  PEPS(1).LT.EPSCRACK) THEN
C
                  E11=2*FC/EZERO
                  E12=0.0D
                  E13=0.0D
                  E21=0.0D
                  E22=2*FC/EZERO-2*FC*PEPS(2)/EZERO**2
                  E23=0.0D
                  E31=0.0D
                  E32=0.0D
                  E33=(PSIGC(1)-PSIGC(2))/(2*(PEPS(1)-PEPS(2)))
C
            ENDIF
C
C       CASE NR 2B:THE PRINCIPAL CONCRETE STRESS PSIGC(2) IS
C                  POSITIVE=TENSION BUT THE PRINCIPAL CONCRETE
C                  STRESS PSIGC(1) IS NEGATIVE=COMPRESSION.
C                  HOWEVER,THE PRINCIPAL TENSION STRAIN PEPS(2) IS
C                  LESS THAN THE CRACKING STRAIN EPSCRACK
C
            IF(PEPS(1).LT.ZERO.AND.PEPS(2).GT.ZERO.AND.
     &                  PEPS(2).LT.EPSCRACK) THEN
C
                  E11=2*FC/EZERO-2*FC*PEPS(1)/EZERO**2
                  E12=0.0D
                  E13=0.0D
                  E21=0.0D
                  E22=2*FC/EZERO
                  E23=0.0D
                  E31=0.0D
                  E32=0.0D
                  E33=(PSIGC(1)-PSIGC(2))/(2*(PEPS(1)-PEPS(2)))
C
            ENDIF
C
```

```
C       CASE NR 3A:THE PRINCIPAL CONCRETE STRESS PSIGC(2) IS
C                  NEGATIVE=COMPRESSION BUT THE PRINCIPAL
C                  CONCRETE STRESS PSIGC(1) IS POSITIVE=TENSION
C                  AND THE PRINCIPAL TENSION STRAIN PEPS(1) IS MORE
C                  THAN THE CRACKING STRAIN EPSCRACK
C
              IF(PEPS(1).GT.EPSCRACK.AND.PEPS(2).LT.ZERO) THEN
C
                  N1=1.0+SQRT(FACTOR*(PEPS(1)-EPSCRACK))
                  Z1=SIGCRACK*FACTOR/(2*SQRT(FACTOR*(PEPS(1)-
     &                                EPSCRACK)))
                 N3=0.8-FACT2*PEPS(1)/EZERO
C
                  E11=-Z1/N1**2
                  E12=0.0D
                  E13=0.0D
                  E21=2*FC*PEPS(2)   *FACT2/(N3**2*EZERO**2)-
     &                 FC*PEPS(2)**2*FACT2/(N3**2*EZERO**3)
                  E22=2*FC/(N3*EZERO)-2*FC*PEPS(2)/(N3*EZERO**2)
                  E23=0.0D
                  E31=0.0D
                  E32=0.0D
                  E33=(PSIGC(1)-PSIGC(2))/(2*(PEPS(1)-PEPS(2)))
C
              ENDIF
C
C       CASE NR 3B: THE PRINCIPAL CONCRETE STRESS PSIGC(1) IS
C                  NEGATIVE=COMPRESSION BUT THE PRINCIPAL
C                  CONCRETE STRESS PSIGC(2) IS POSITIVE=TENSION
C                  AND THE PRINCIPAL TENSION STRAIN PEPS(2) IS MORE
C                  THAN THE CRACKING STRAIN EPSCRACK
C
              IF(PEPS(1).LT.ZERO.AND.PEPS(2).GT.EPSCRACK) THEN
C
                  N2=1.0+SQRT(FACTOR*(PEPS(2)-EPSCRACK))
                  Z2=SIGCRACK*FACTOR/(2*SQRT(FACTOR*(PEPS(2)-
     &                                EPSCRACK)))
                 N4=0.8-FACT2*PEPS(2)/EZERO
C
                  E11=2*FC/(N4*EZERO)-2*FC*PEPS(1)/(N4*EZERO**2)
                  E12=2*FC*PEPS(1)*FACT2/(N4*EZERO)**2-
     &                 FC*PEPS(1)**2*FACT2/(N4**2*EZERO**3)
                  E13=0.0D
                  E21=0.0D
                  E22=-Z2/N2**2
                  E23=0.0D
                  E31=0.0D
                  E32=0.0D
                  E33=(PSIGC(1)-PSIGC(2))/(2*(PEPS(1)-PEPS(2)))
C
              ENDIF
```

```
C       CASE NR 4 :  THE PRINCIPAL CONCRETE STRESSES PSIGC(I) ARE
C                    POSITIVE=TENSION AND BOTH ARE LESS
C                    THAN EPSCRACK.
C
              IF(PEPS(1).GT.ZERO.AND.PEPS(2).GT.ZERO.AND.PEPS(1).LT.
     &                       EPSCRACK.AND.PEPS(2).LT.EPSCRACK) THEN
C
                    E11=2*FC/EZERO
                    E12=0.0D
                    E13=0.0D
                    E21=0.0D
                    E22=2*FC/EZERO
                    E23=0.0D
                    E31=0.0D
                    E32=0.0D
                    E33=(PSIGC(1)-PSIGC(2))/(2*(PEPS(1)-PEPS(2)))
C
              ENDIF
C
C       CASE NR 5A:THE PRINCIPAL CONCRETE STRESSES PSIGC(I) ARE
C                  POSITIVE=TENSION AND PEPS(2) IS LESS
C                  THAN EPSCRACK WHILE PEPS(1) IS MORE THAN
C                  EPSCRACK
C
            IF(PEPS(2).GT.ZERO.AND.PEPS(1).GT.EPSCRACK.AND.PEPS(2).LT.
     &                EPSCRACK) THEN
C
                    N1=1.0+SQRT(FACTOR*(PEPS(1)-EPSCRACK))
                    Z1=SIGCRACK*FACTOR/(2*SQRT(FACTOR*(PEPS(1)-
     &                                EPSCRACK)))
C
                    E11=-Z1/N1**2
                    E12=0.0D
                    E13=0.0D
                    E21=0.0D
                    E22=2*FC/EZERO
                    E23=0.0D
                    E31=0.0D
                    E32=0.0D
                    E33=(PSIGC(1)-PSIGC(2))/(2*(PEPS(1)-PEPS(2)))
C
              ENDIF
C
```

```
C       CASE NR 5B:THE PRINCIPAL CONCRETE STRESSES PSIGC(I) ARE
C                  POSITIVE=TENSION AND PEPS(1) IS LESS
C                  THAN EPSCRACK WHILE PEPS(2) IS MORE THAN
C                  EPSCRACK
C
C
        IF(PEPS(1).GT.ZERO.AND.PEPS(2).GT.EPSCRACK.AND.PEPS(1).LT.
     &                EPSCRACK) THEN
C
                  N2=1.0+SQRT(FACTOR*(PEPS(2)-EPSCRACK))
                  Z2=SIGCRACK*FACTOR/(2*SQRT(FACTOR*(PEPS(2)-
     &                        EPSCRACK)))
C
                  E11=2*FC/EZERO
                  E12=0.0D
                  E13=0.0D
                  E21=0.0D
                  E22=-Z2/N2**2
                  E23=0.0D
                  E31=0.0D
                  E32=0.0D
                  E33=(PSIGC(1)-PSIGC(2))/(2*(PEPS(1)-PEPS(2)))
C
        ENDIF
C
C       CASE NR 6 :  THE PRINCIPAL CONCRETE STRESSES PSIGC(I) ARE
C                    POSITIVE=TENSION AND PEPS(I) BOTH ARE MORE
C                    THAN EPSCRACK.
C
        IF(PEPS(1).GT.EPSCRACK.AND.PEPS(2).GT.EPSCRACK) THEN
C
                  N1=1.0+SQRT(FACTOR*(PEPS(1)-EPSCRACK))
                  Z1=SIGCRACK*FACTOR/(2*SQRT(FACTOR*(PEPS(1)-
     &                        EPSCRACK)))
                  N2=1.0+SQRT(FACTOR*(PEPS(2)-EPSCRACK))
                  Z2=SIGCRACK*FACTOR/(2*SQRT(FACTOR*(PEPS(2)-
     &                        EPSCRACK)))
C
                  E11=-Z1/N1**2
                  E12=0.0D
                  E13=0.0D
                  E21=0.0D
                  E22=-Z2/N2**2
                  E23=0.0D
                  E31=0.0D
                  E32=0.0D
                  E33=(PSIGC(1)-PSIGC(2))/(2*(PEPS(1)-PEPS(2)))
C
        ENDIF
C
```

```
      DO K1=1,NTENS
            DO K2=1,NTENS
            DDSDDE(K1,K2)=ZERO
            END DO
      END DO
C
      DDSDDE(1,1)=E11
      DDSDDE(1,2)=E12
      DDSDDE(1,3)=E13
      DDSDDE(2,1)=E21
      DDSDDE(2,2)=E22
      DDSDDE(2,3)=E23
      DDSDDE(3,1)=E31
      DDSDDE(3,2)=E32
      DDSDDE(3,3)=E33
C
C  ROTATE CONCRETE JACOBIAN IN XY-DIRECTION
C  FIRST ESTABLISH TRANFORMATION MATRIX [T] AND ITS TRANSPOSE
C
            T(1,1)=COS(PHI)**TWO
            T(1,2)=SIN(PHI)**TWO
            T(1,3)=COS(PHI)*SIN(PHI)
            T(2,1)=SIN(PHI)**TWO
            T(2,2)=COS(PHI)**TWO
            T(2,3)=-COS(PHI)*SIN(PHI)
            T(3,1)=-TWO*COS(PHI)*SIN(PHI)
            T(3,2)=TWO*COS(PHI)*SIN(PHI)
            T(3,3)=COS(PHI)**TWO-SIN(PHI)**TWO
C
            TT(1,1)=COS(PHI)**TWO
            TT(1,2)=SIN(PHI)**TWO
            TT(1,3)=-TWO*COS(PHI)*SIN(PHI)
            TT(2,1)=SIN(PHI)**TWO
            TT(2,2)=COS(PHI)**TWO
            TT(2,3)=TWO*COS(PHI)*SIN(PHI)
            TT(3,1)=COS(PHI)*SIN(PHI)
            TT(3,2)=-COS(PHI)*SIN(PHI)
            TT(3,3)=COS(PHI)**TWO-SIN(PHI)**TWO
C
            DO K1=1,NTENS
                  DO K2=1,NTENS
                        R=ZERO
                        DO K3=1,NTENS
                              R=R+TT(K1,K3)*DDSDDE(K3,K2)
                        ENDDO
                        D(K1,K2)=R
                  ENDDO
            ENDDO
C
```

```
                DO K1=1,NTENS
                      DO K2=1,NTENS
                            DDSDDE(K1,K2)=D(K1,K2)
                      END DO
                END DO
C
                DO K1=1,NTENS
                      DO K2=1,NTENS
                            R=ZERO
                            DO K3=1,NTENS
                                  R=R+DDSDDE(K1,K3)*T(K3,K2)
                            ENDDO
                            D(K1,K2)=R
                      ENDDO
                ENDDO
C
                DO K1=1,NTENS
                      DO K2=1,NTENS
                            DDSDDE(K1,K2)=D(K1,K2)
                      END DO
                END DO
C
C  CALCULATE JACOBIAN FOR STEEL
C
                IF(SIGSX.GT.ZERO.AND.DSTRAN(1).LT.EYIELDX) THEN
                      E1=RHOX*ESTEEL
                ENDIF
C
                IF(SIGSX.GT.ZERO.AND.DSTRAN(1).GT.EYIELDX) THEN
                      E1=ZERO
                ENDIF
C
                IF(SIGSX.LT.ZERO.AND.DSTRAN(1).GT.-EYIELDX) THEN
                      E1=RHOX*ESTEEL
                ENDIF
C
                IF(SIGSX.LT.ZERO.AND.DSTRAN(1).LT.-EYIELDX) THEN
                      E1=ZERO
                ENDIF
C
```

```
            IF(SIGSY.GT.ZERO.AND.DSTRAN(2).LT.EYIELDY) THEN
                  E2=RHOY*ESTEEL
            ENDIF
C
            IF(SIGSY.GT.ZERO.AND.DSTRAN(2).GT.EYIELDY) THEN
                  E2=ZERO
            ENDIF
C
            IF(SIGSY.LT.ZERO.AND.DSTRAN(2).GT.-EYIELDY) THEN
                  E2=RHOY*ESTEEL
            ENDIF
C
            IF(SIGSY.LT.ZERO.AND.DSTRAN(2).LT.-EYIELDY) THEN
                  E2=ZERO
            ENDIF
C
C  JACOBIAN FOR REINFORCED CONCRETE
C
            DDSDDE(1,1)=DDSDDE(1,1)+E1
            DDSDDE(2,2)=DDSDDE(2,2)+E2
C
      ENDIF
10    RETURN
      END
```

Appendix B: Input File for ABAQUS with UMAT

*HEADING, UNSYMM
2D Solid with UMAT (according to the MCFT)
Analysis of a 4-Storey Wall, 96 Elements
Ductility 3.4, EC8
*NODE
1, 0.0, 0.0
7, 6.0, 0.0
8, 0.0, 1.0
14, 6.0, 1.0
15, 0.0, 2.0
21, 6.0, 2.0
22, 0.0, 3.0
28, 6.0, 3.0
29, 0.0, 4.0
35, 6.0, 4.0
36, 0.0, 5.0
42, 6.0, 5.0
43, 0.0, 6.0
49, 6.0, 6.0
50, 0.0, 7.0
56, 6.0, 7.0
57, 0.0, 8.0
63, 6.0, 8.0
64, 0.0, 9.0
70, 6.0, 9.0
71, 0.0, 10.0
77, 6.0, 10.0
78, 0.0, 11.0
84, 6.0, 11.0
85, 0.0, 12.0
91, 6.0, 12.0
92, 0.0, 13.0
98, 6.0, 13.0
99, 0.0, 14.0
105, 6.0, 14.0
106, 0.0, 15.0
112, 6.0, 15.0
113, 0.0, 16.0
119, 6.0, 16.0

```
*NGEN
1,    7
8,    14
15,   21
22,   28
29,   35
36,   42
43,   49
50,   56
57,   63
64,   70
71,   77
78,   84
85,   91
92,   98
99,   105
106,  112
113,  119
*NSET, NSET=S1, GENERATE
1,    7,    1
*NSET, NSET=S2, GENERATE
29,   35,   1
*NSET, NSET=S3, GENERATE
57,   63,   1
*NSET, NSET=S4, GENERATE
85,   91,   1
*NSET, NSET=S5, GENERATE
113,  119,  1
*ELEMENT, TYPE=CPS4
1, 1, 2, 9, 8
*ELGEN
1, 6, 1, 1, 16,   7, 6
*ELSET, ELSET=SET1, GENERATE
1,    19,   6
6,    24,   6
*ELSET, ELSET=SET2, GENERATE
25,   43,   6
30,   48,   6
*ELSET, ELSET=SET3, GENERATE
49,   67,   6
54,   72,   6
*ELSET, ELSET=SET4, GENERATE
73,   91,   6
78,   96,   6
*ELSET, ELSET=SET5, GENERATE
2,    20,   6
3,    21,   6
4,    22,   6
5,    23,   6
```

```
*ELSET, ELSET=SET5, GENERATE
26,  92,  6
27,  93,  6
28,  94,  6
29,  95,  6
*SOLID SECTION, ELSET=SET1, MATERIAL=MAT1
0.3
*MATERIAL, NAME=MAT1
*USER MATERIAL, CONSTANTS=11, UNSYMM
20000.0,  -0.0031,  -31.0,  2.0,  210000.0,  0.0104,  0.0067,  200.0
0.00228,  0.00228,  0.24
*DEPVAR
21
*SOLID SECTION, ELSET=SET2, MATERIAL=MAT2
0.3
*MATERIAL, NAME=MAT2
*USER MATERIAL, CONSTANTS=11, UNSYMM
20000.0,  -0.0026,  -25.5,  2.0,  210000.0,  0.0052,  0.0067,  200.0
0.00228,  0.00228,  0.24
*DEPVAR
21
*SOLID SECTION, ELSET=SET3, MATERIAL=MAT3
0.3
*MATERIAL, NAME=MAT3
*USER MATERIAL, CONSTANTS=11, UNSYMM
20000.0,  -0.002,  -20.0,  2.0,  210000.0,  0.00223,  0.0052,  200.0
0.00228,  0.00228,  0.24
*DEPVAR
21
*SOLID SECTION, ELSET=SET4, MATERIAL=MAT4
0.3
*MATERIAL, NAME=MAT4
*USER MATERIAL, CONSTANTS=11, UNSYMM
20000.0,  -0.002,  -20.0,  2.0,  210000.0,  0.00223,  0.0028,  200.0
0.00228,  0.00228,  0.24
*DEPVAR
21
*SOLID SECTION, ELSET=SET5, MATERIAL=MAT5
0.3
*MATERIAL, NAME=MAT5
*USER MATERIAL, CONSTANTS=11, UNSYMM
20000.0,  -0.002,  -20.0,  2.0,  210000.0,  0.0026,  0.00268,  200.0
0.00228,  0.00228,  0.24
*DEPVAR
21
```

```
*SOLID SECTION, ELSET=SET6, MATERIAL=MAT6
0.3
*MATERIAL, NAME=MAT6
*USER MATERIAL, CONSTANTS=11, UNSYMM
20000.0,   -0.002,     -20.0,   2.0,   210000.0,  0.00223,   0.00268,   200.0
0.00228,   0.00228,    0.24
*DEPVAR
21
*BOUNDARY
S1,   1, 3
*STEP
*STATIC
*CLOAD
S2,   2, -0.1
S3,   2, -0.1
S4,   2, -0.1
S5,   2, -0.08
*NODE PRINT, FREQ=0
*EL PRINT,      FREQ=0
*END STEP
*STEP, INC=1000
*STATIC, RIKS
*CLOAD
29,   1, 0.22
57,   1, 0.33
85,   1, 0.43
113,  1, 0.465
*NODE PRINT, FREQ=2
U
*EL PRINT,      FREQ=2
SDV1
SDV2
SDV3
*END STEP
```